SKI Report 2005:55

Research

Application of Master Curve Methodology for Structural Integrity Assessments of Nuclear Components

Iradj Sattari-Far
Kim Wallin

October 2005

ISSN 1104–1374
ISRN SKI-R-05/55-SE

SKI perspective

Background

Ferritic steels are widely used in different kinds of constructions. One problem with this material is that in the transition region the fracture toughness decreases drastically as the temperature drops. In this region the final failure is often occurred by cleavage preceded by some ductile crack growth. A procedure for mechanical testing and statistical analysis of fracture toughness of this type of materials is describing in the ASTM E 1921-03 standard.

The above mentioned standard is accounting for temperature dependence of fracture toughness through an approach developed by Kim Wallin, widely known as Master Curve method. Wallin has observed that a wide range of this type of material has a characteristic shape of the fracture toughness-temperature curve, and the only difference between different steels is the absolute position of the curve with respect to temperature. The temperature dependence of fracture toughness can be determined by performing a certain amount of fracture toughness tests at a given temperature.

Results of the application of Master Curve method for evaluation of fracture toughness in the transition region have shown that this method relaxes some of the over-conservatism which has been observed in using the ASME method, generally known as ASME K_{IC} reference curve.

At this time, several countries have adopted or are in the process of adopting the Master Curve method into their brittle fracture safety assessment procedures (Finland, Germany, USA etc.). In Sweden, the ASME K_{IC} reference curve is still used as the only approved method in safety evaluations.

Objective

The objective was to perform an in-depth investigation of the Master Curve methodology and also based on this method develop a procedure for fracture assessments of nuclear components. The results of this study will be used for the SKI´s position on whether the Master curve methodology will be adopted into our brittle fracture assessment procedures.

Results

The project has sufficiently illustrated the capabilities of the Master Curve methodology for fracture assessments of nuclear components. Within the scope of this work, the theoretical background of the methodology and its validation on small and large specimens has been studied and presented to a sufficiently large extent, as well as the correlations between the charpy-V data and the Master Curve T_0 reference temperature in the evaluation of fracture toughness. The work gives a comprehensive report of the background theory and the different applications of the Master Curve methodology.

The main results of the work have shown that the cleavage fracture toughness is characterized by a large amount of statistical scatter in the transition region, it is specimen size dependent and it should be treated statistically rather than deterministically. The Master Curve methodology is able to make use of statistical data in a consistent way.

Furthermore, the Master Curve methodology provides a more precise prediction of the fracture toughness of embrittled materials in comparison with the ASME K_{IC} reference curve, which often gives over-conservative results.

The suggested procedure in this study, concerning the application of the Master Curve method in fracture assessments of ferritic steels in the transition region and the low shelf regions, is valid for the temperatures range $T_0-50 \leq T \leq T_0+50$ ^{0}C. If only approximate information is required, the Master Curve may well be extrapolated outside this temperature range. The suggested procedure has also been illustrated for some examples.

The primary objective to provide sufficient information about the Master Curve methodology is now considered to be fulfilled. The SKI assessment is that for the time being there is no immediate need for further studies.

Project Information

SKI´s project leader: Konstantinos Xanthopoulos.
Project Number: 14.42-031047/23131.
Project Organisation: Det Norske Veritas AB Consulting (DNV) has been managing the project and has also worked as the principal investigator, with Iradj Sattari-Far as project leader. Peter Dillström at DNV and Kim Wallin at VTT in Finland have assisted this work.

SKI Report 2005:55

Research

Application of Master Curve Methodology for Structural Integrity Assessments of Nuclear Components

Iradj Sattari-Far[1]
Kim Wallin[2]

[1]Det Norske Veritas
Box 30234
SE-104 25 Stockholm
Sweden

[2]VTT
P.O. Box 1000
FI-02044 VTT
Finland

October 2005

Table of Content — *Page*

ACKNOWLEDGEMENT ... 3

1. INTRODUCTION ... 5

2. BACKGROUND ... 7
  2.1. Brittle fracture ... 8
  2.2. LEFM K_{IC} versus EPFM K_{JC} ... 12

3. THEORETICAL BASIS OF THE MASTER CURVE METHOD ... 15
  3.1. Mechanism of cleavage fracture ... 15
  3.2. Probability of cleavage initiation ... 20
  3.3. Conditional cleavage propagation ... 24

4. DETERMINATION OF MASTER CURVES ... 35
  4.1. Comparison of Master Curve K_{JC} and ASME K_{Ic} ... 39

5. MASTER CURVE ANALYSIS OF SMALL SPECIMENS ... 41
  5.1. Master Curve analysis of miniature specimens ... 42
  5.2. Test results of other small specimens ... 52
  5.3. Comparison of CT- and 3PB-specimens ... 61

6. MASTER CURVE ANALYSIS OF LARGE SCALE EXPERIMENTS ... 65
  6.1. Experiment TSE-2 at ORNL ... 66
  6.2. Experiment TSE-3 at ORNL ... 69
  6.3. Experiments TSE-5 and TSE-6 at ORNL ... 70
  6.4. Experiment TSE-7 at ORNL ... 73
  6.5. Experiment TSE-FR at Framatome ... 75
  6.6. Experiment NESC-I at AEA ... 78
  6.7. Experiment NESC-II at MPA ... 79
  6.8. Experiment O1 at KTH ... 82
  6.9. Experiment NESC-IV at ORNL ... 84
  6.10. Experiments PTSE-1 and PTSE-2 at ORNL ... 88

7. CONSTRAINT EFFECTS ... 90
  7.1. Stress field around a crack tip ... 91
  7.2. Constraint parameters ... 94
  7.3. Constraint considerations in the Master Curve Methodology ... 100
    7.3.1. Constraint considerations of small specimens ... 100
    7.3.2. Constraint considerations of large scale experiments ... 111

7.4. Constraint correction for surface cracks 116

8. CORRELATION BETWEEN CHARPY IMPACT CVN AND T0 119
8.1. Charpy-V – T_0 correlations for nuclear grade pressure vessel steels 120
8.2. Relation between T_{28J} and T_{41J} 125
8.3. Analysis of complete CVN transition curves 125
8.4. Analysis of incomplete CVN transition curves 133
8.5. CVN-T_o relationships 137
8.6. Significance of ASME Code Cases N-629 and N-631 137

9. APPLICATION OF THE MC METHOD IN OTHER COUNTRIES 145

10. ASSESSMENT PROCEDURE BASED ON THE MC METHOD 147
10.1. Simplified assessment procedure 147
10.2. Advanced assessment procedure 150

11. CONCLUSIONS AND RECOMMENDATIONS 154

REFERENCES 156

APPENDIX: EXAMPLE PROBLEMS 162

ACKNOWLEDGEMENT

This research project is sponsored by the Swedish Nuclear Power Inspection (SKI) under contract: SKI-14.42-031047/23131. This support is greatly appreciated. The authors are delighted to thank Björn Brickstad and Kostas Xanthopoulos (SKI) for their support and encouragement over the course of this project.

1. INTRODUCTION

Integrity assessment of structures containing planar flaws (real or postulated) requires the use of fracture mechanics. Fracture mechanics compares, in principle, two different crack growth parameters: the driving force and the material resistance. The driving force is a combination of the flaw size (geometry) and the loading conditions, whereas the material resistance describes the materials capability to resist a crack from propagating. Up to date, there exist several different testing standards (and non-standardised procedures) by which it is possible to determine some parameters describing the materials fracture resistance (ASTM E 399, ASTM E 1820, BS 7448, ESIS P2 etc.). Unfortunately, this has led to a myriad of different parameter definitions and their proper use in fracture assessment may be unclear.

Historically, fracture mechanics evolved from a continuum mechanics understanding of the fracture problem. It was assumed that there existed a single fracture toughness value controlling the materials fracture. If the driving force was less than this fracture toughness, the crack would not propagate and if it exceeded the fracture toughness the crack would propagate. Thus, crack initiation and growth were assumed to occur at a constant driving force value. The only thing assumed to affect this critical value was the constraint (crack-tip stress triaxiality) of the specimen (or structure). Since, at that time, there were no means to quantitatively assess the effect of constraint on the fracture toughness, the fracture toughness had to be determined with a specimen showing as high a constraint as possible. This leads to the use of, deeply cracked, bend specimens for the fracture toughness determination. It was assumed that the stress state assumption of the continuum mechanics analysis were valid for fracture toughness as well, regardless of fracture micro-mechanism. This statement has later been proven to be wrong. Different fracture micro-mechanisms exhibit different physical features that affect the validity of a specific fracture toughness parameter to describe that fracture micro-mechanism.

The ASTM E 1921-03 standard [2003] describes a procedure for the mechanical testing and statistical analysis of fracture toughness of ferritic steels in the transition region. This ASTM standard accounts for temperature dependence of fracture toughness through a Master Curve approach developed by Wallin [1991]. Wallin observed that a wide range of ferritic steels have a characteristic fracture toughness-temperature curve, and the only difference between different steels was the absolute position of the curve with respect to temperature. The temperature dependence of the fracture toughness can be determined by performing a certain amount of fracture toughness test at a given temperature. Using the Master curve for evaluation of the fracture toughness in the transition region releases the over-conservatism that has been observed in using the ASME K_{IC} curve. The application of the Master Curve methodology in prediction of the fracture events in nuclear components has shown promising results, see for instance Bass *et al* [2000], Sattari-Far [2000 and 2004] and Wallin [2004c].

The primary objective of this report is to establish a straight forward procedure in application of the Master Curve methodology in fracture assessments of the nuclear components. In performing this task, the background of the methodology and its validation are studied.

Chapters 2 and 3 give background and theoretical aspects of the methodology, emphasizing the probabilistic handling of fracture toughness data. Chapter 4 briefly describes the procedure for performing fracture toughness testing and determination of the Master Curves according to the ASTM E1921 standard. Chapter 5 gives results of application of the Master Curve methodology in determination of validated fracture toughness from miniature sized test specimens. The validation of the methodology in predictions of fracture events in large scale experiments are investigated in Chapter 6. The capability of the methodology in considering the constraint effects are examined in Chapter 7. As in the cases of existing nuclear power plants, fracture toughness data are often not available and the available material information is often limited to Charpy-V test results, correlations between the impact energy and the Master Curve fracture toughness are therefore given in Chapter 8. Chapter 9 gives information on application of this methodology in different countries.

Based on the results presented in Chapters 1-9, a procedure on how to apply this methodology is developed and presented in Chapter 10. The use of this procedure is demonstrated in Appendix of this report, using some realistic examples. Finally, Chapter 11 concludes this report and gives recommendations on how to use this methodology.

2. BACKGROUND

Fracture mechanics, based on a continuum mechanics, gives means in understanding of fracture behaviour in cracked bodies. It is commonly assumed that there exists a single fracture toughness value controlling the materials fracture. If the crack driving force in the body is less than this value, the crack will not propagate and if it exceeds this value the crack will propagate.

The concept of linear elastic fracture mechanics (LEFM) that was derived prior to 1960 is applicable only to structures whose global behaviour are linear. In application of LEFM, the crack-tip field in a cracked body is described by the stress intensity factor, *K*, provided that certain conditions are satisfied. LEFM is valid for the cases in which the nonlinear material behaviour is confined to a small region surrounding the crack tip. In other cases, it is virtually impossible to characterize the fracture behaviour with LEFM, and an alternative fracture mechanics model is required. Since 1960, fracture mechanics theories have been developed to account for various types of non-linear material behaviour and loading condition. Elastic-plastic fracture mechanics (EPFM) approaches based on elastic-plastic parameters, the *J*-integral or the crack-tip opening displacement (*CTOD*), extend the limitations of LEFM. Both parameters describe crack-tip conditions in elastic-plastic materials, and each can be used as a fracture criterion. There are, however, limits to the applicability of *J* or *CTOD*, but these limits are much less restrictive than the validity requirements of LEFM.

The crack-tip field and the fracture toughness are only geometry independent within a limited range of loading and geometric conditions, which ensures similar crack-tip stress triaxiality (constraint). The size and geometry requirements restrict the application of different fracture mechanics disciplines. Under small scale yielding (SSY) conditions, a single parameter (e.g. *K*, *J* or *CTOD*) characterizes crack-tip conditions and thus can be used as a geometry-independent fracture criterion. At increasing loads in finite cracked bodies, the initially SSY field gradually diminishes as the plastic zone senses nearby traction free boundaries. Consequently, the single-parameter fracture mechanics disciplines break down, and the fracture toughness depends on the size and geometry and type of loading of the fractured body. A number of approaches have been proposed to extend fracture mechanics applications beyond the limits of the single-parameter assumptions. Most of these new approaches involve the introduction of a second parameter to characterize the crack-tip conditions, so called two-parameter fracture mechanics approaches.

2.1. Brittle fracture

Two models claiming to predict the temperature dependence of cleavage fracture toughness are the RKR-model (Ritchie, Knott & Rice) and the Beremin model (known as the local approach). Both models essentially assume a constant cleavage fracture stress (σ_c, σ_u) and end up with similar results for the temperature dependence. It may be somewhat misleading to talk about temperature dependence, since the models actually predict an inverse dependence between fracture toughness and yield strength:

$$K_{IC} \sim \sigma_y^{-c} \tag{2-1}$$

Both models yield for a moderately strain hardening material (n = 10) having the "standard" Weibull slope (m = 22) c = 4.5.

The models were originally verified for materials with the ductile to brittle transition occurring at low temperatures, where the change in yield strength with temperature was considerable. However, for more brittle materials, where the ductile to brittle transition occurs above room temperature, the models are unable to predict the temperature dependence correctly [Merkle, Wallin and McCabe, 1998]. Wallin [2004] studied fracture toughness data of A533B Cl.1 in both unirradiated and irradiated conditions. He came to the following postulate:

- The temperature dependence of cleavage fracture toughness is mainly controlled by the thermal part of the materials yield strength, whereas the location on the temperature scale is more controlled by the athermal part of the yield strength.

Based on this postulate, a unified description of the fracture toughness temperature dependence for ferritic steels may be possible.

Even though materials failing by cleavage fracture were not part of the development of the K_{IC} standards, it soon became applied to testing of nuclear pressure vessel steels. Actually, today, the common assumption is that ASTM E399 and other K_{IC} standards are especially suited for brittle fracture. This is a misconception, coming from the erroneous interpretation of plane-strain coming from the Irwin investigation. Also in the case of brittle fracture, the original continuum mechanics based interpretation was assumed, i.e. that valid K_{IC} results are lower bound specimen size insensitive material values showing only little scatter. Based on the present understanding of the physics of the cleavage fracture micro-mechanism, this assumption is known to be incorrect, [Wallin, 2004].

Based on an interpretation of the physics, the Master Curve method was developed at VTT. The method adjusts for size effects in brittle fracture toughness. Physically, the fracture toughness in temperature space can be divided into three regions, brittle fracture region, transition region and upper shelf. The brittle fracture region is further divided into two separate regions, depending on the way specimen size affects the fracture toughness. In the lower shelf region, size effects are negligible, but at higher toughness values, the brittle fracture toughness will be affected by a statistical size effect. The transition region is defined as the temperature region, where cleavage fracture occurs after some amount of ductile tearing. This region will be specimen size dependent due to the statistical size effect. Finally, the upper shelf is defined as the temperature region where the fracture mechanism is fully ductile. Also the temperature for the onset of upper shelf is specimen size dependent due to the statistical size effect. Besides, statistical size effects, the fracture toughness can be affected by specimen constraint. The basic Master Curve has been standardised by ASTM in ASTM E 1921-03, [ASTM, 2003].

The statistical size effect, due to the weakest link nature of cleavage fracture initiation, is active also for valid K_{IC} results, provided they are above the lower shelf. A good example of this is given by the HSST 02 plate data used originally to develop the ASME K_{IC} reference curve shown in Fig. 2.1, [Marston, 1978]. The data, originally known as the "million dollar curve", constituted the first large fracture toughness data set generated for a single material. Normally, only the valid K_{IC} results are reported, but for clarity, here also the invalid results are included. It is evident that there is a difference between the smaller 1T & 2T specimens and the larger 4T & 6T specimens. This size effect, shown in Fig. 2.2, is fully in line with the theoretical statistical size effect as used by the Master Curve methodology.

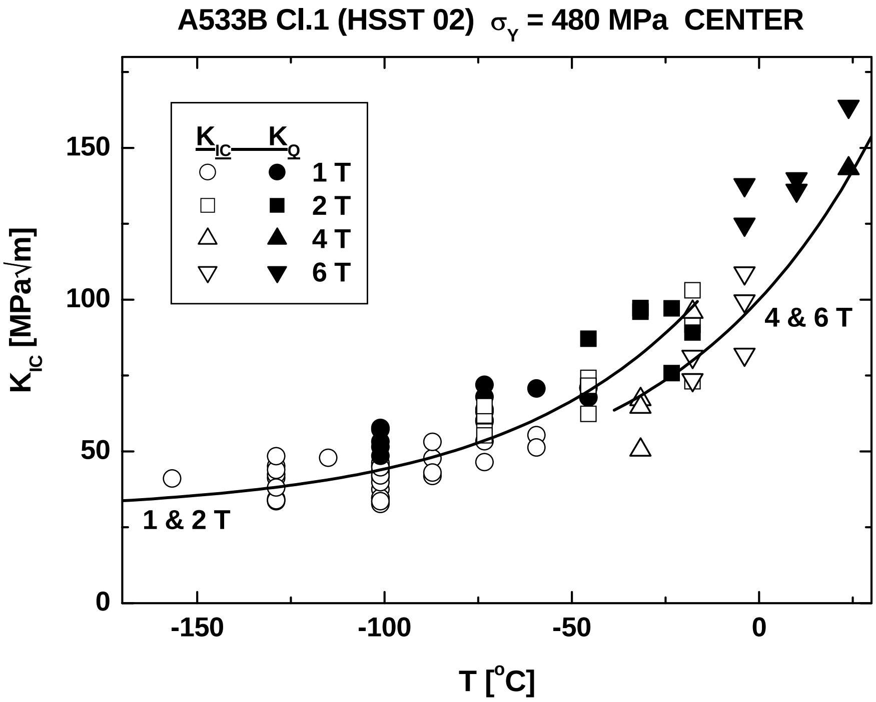

Fig. 2.1. Valid brittle fracture K_{IC} data for the HSST 02 plate indicating decreasing fracture toughness with increasing specimen size, [Marston, 1978].

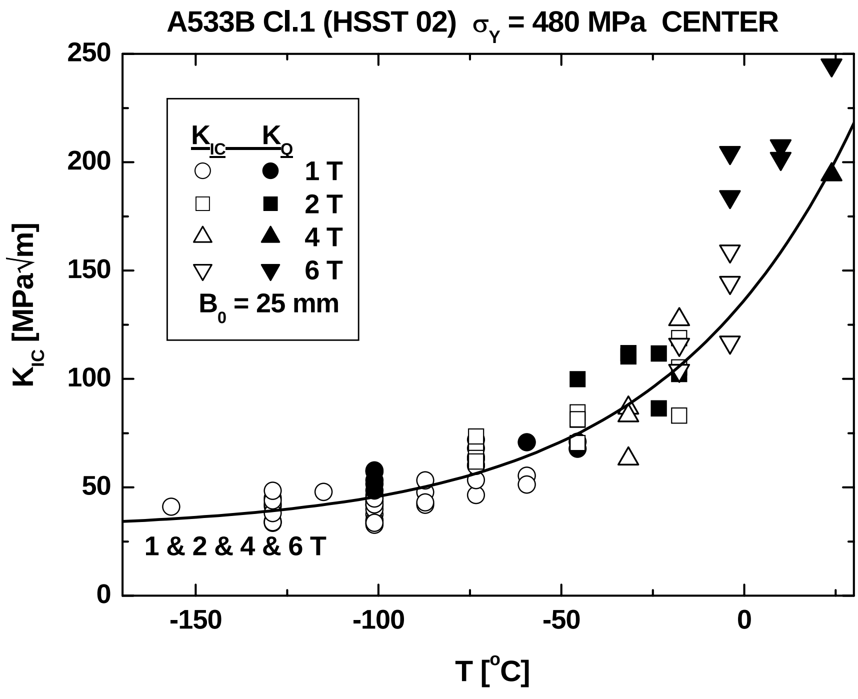

Fig. 2.2: Size effect in valid brittle fracture K_{IC} data for the HSST 02 plate is correctly described with the Master Curve.

Another example showing the decrease in K_{IC} with increasing specimen size has been presented by MPA, shown in Fig. 2.3, [Issler, 1979]. Even though the data are limited in number, it clearly indicates decreasing fracture toughness with increasing specimen size, for all valid K_{IC} values. Also in this case, the size effect is in line with the theoretical prediction of the Master Curve. Numerous similar data sets can easily be found in the open literature.

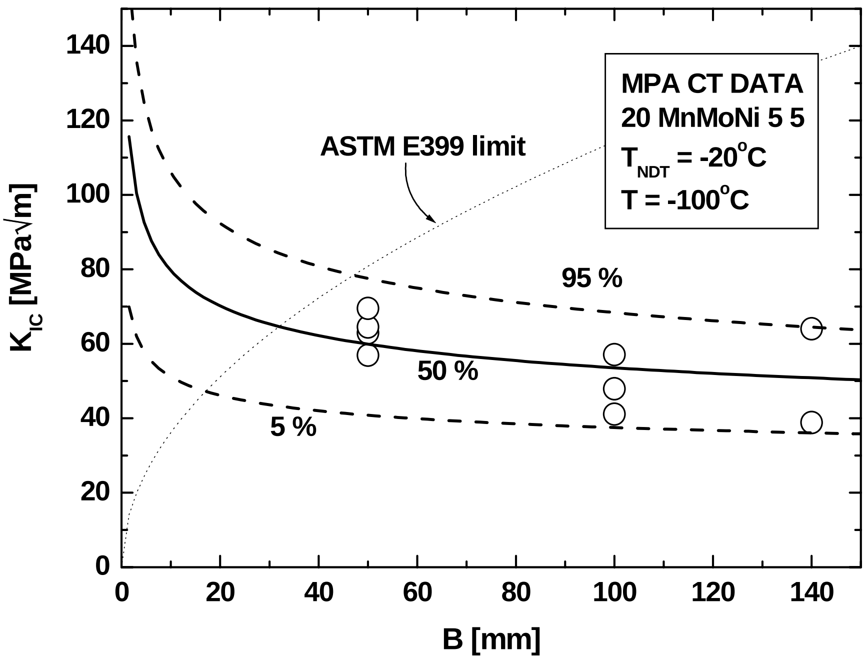

Fig. 2.3: MPA brittle fracture K_{IC} data, for KS13, showing size effect in accordance with the Master Curve, [Issler, 1979].

Within the same nuclear safety research programme, MPA has also tested three "gigantic" CT specimens with 500 mm thickness, [Kussmaul et al, 1986]. One specimen corresponded to material KS05 and two to KS15. The results, together with smaller specimen valid K_{IC} results are presented in Fig. 2.4. A clear size effect can be seen. The very large specimens provide clearly lower fracture toughness values than predicted based on the smaller specimen behaviour.

If the data is analysed and size adjusted with the Master Curve, the different specimen sizes are in much better agreement, shown in Fig. 2.5. It should be pointed out that the specimens in question have been produced from different forgings, and slightly different NDT values have been reported for the small and large specimen materials, [Kussmaul et al, 1986]. Overall, the evidence is however clear. K_{IC} in the case of brittle fracture is not a deterministic limiting lower bound value. It has the same kind of size effect as K_{JC} values corresponding to cleavage fracture and they need to be analysed by the Master Curve.

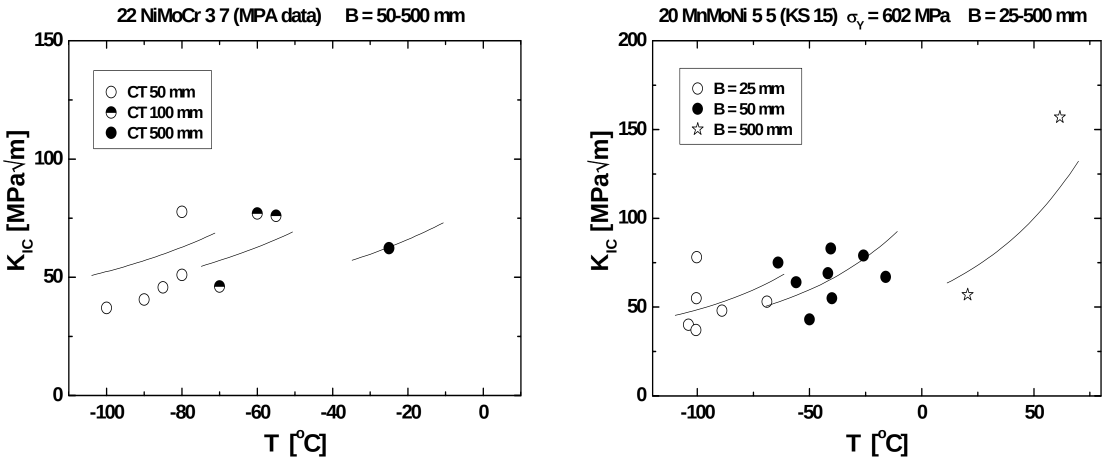

Fig. 2.4: MPA brittle fracture K_{IC} data, for KS05 and KS15, showing size effect for valid K_{IC} values, [Kussmaul et al, 1986].

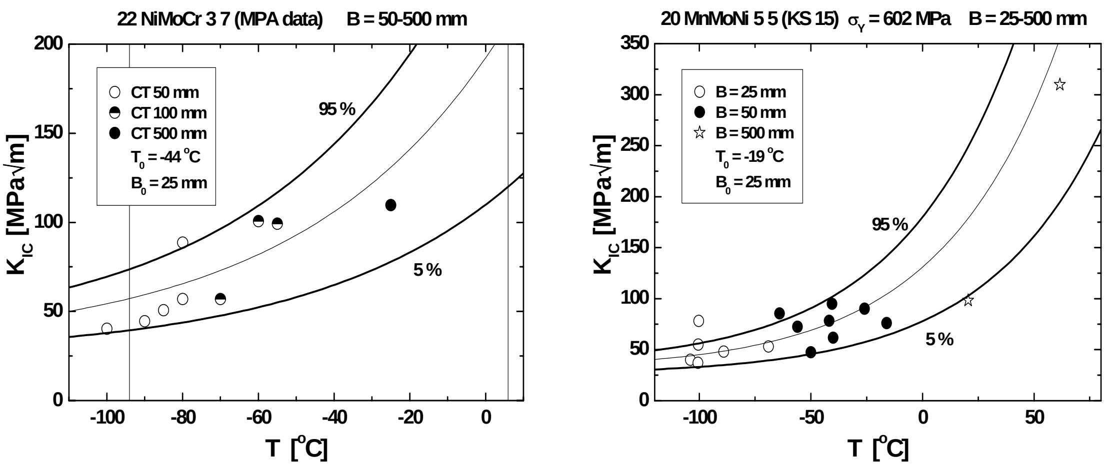

Fig. 2.5: MPA brittle fracture K_{IC} data, for KS05 and KS15, showing size effect to be in accordance with the Master Curve.

2.2. LEFM K_{IC} versus EPFM K_{JC}

The common misconception, originating from the erroneous interpretation of conditions required for plane-strain fracture toughness, is to assume that only valid K_{IC} results correspond to plane-strain. The size requirements given in ASTM E399, have been assumed to be a criteria for plane-strain. In reality, the requirements are intended to ensure the applicability of linear-elastic fracture mechanics, so that the fracture toughness can simply be estimated from load information. The requirements have nothing to do with the limiting conditions for plane-strain stress state in front of the crack. Modern finite element analyses have shown that the specimen thickness can be reduced by more than a factor of 10, from the ASTM E399 criterion, without loss of the plane-strain stress state. The main difference between K_{IC} and K_{JC} is that, K_{JC} has to be estimated via the elastic-plastic parameter J, which requires the measurement of both load and load-point displacement. As long as the K_{JC} values fulfil the size requirements given in ASTM E1921, they are of equal significance as valid K_{IC} values for cleavage fracture. In both cases, the fracture toughness is affected by the statistical size effect. This means that both K_{IC} and K_{JC} values, in the case of cleavage fracture, have to be analysed using the Master Curve method.

Fig. 2.6 presents data from McCabe [1993], showing the effect of specimen thickness on the median fracture toughness. The error bars indicate the 90 % confidence bounds of the median estimate. The smaller specimens correspond to elastic-plastic K_{JC} values whereas the 100 mm thick specimens yield valid linear-elastic K_{IC} values. Regardless of parameter type, all specimens follow the same size dependence as predicted by the Master Curve. Thus, the size effect is identical to the one seen for valid K_{IC} results, shown e.g. in Fig. 2.3. This shows that the specimens are not affected by changes in the stress state, only the statistical size effect.

Also the HSST 02 plate shows the similarity between K_{IC} and K_{JC}. Fig. 2.7a shows the original HSST 02 K_{IC} data analysed by the ASTM E1921 Master Curve method. Fig. 2.7b shows elastic plastic results for the same plate, tested by EPRI and ORNL [Solokov et al, 1997], also analysed by the ASTM E1921 Master Curve method. The K_{IC} data yield a T_0 estimate of -28ºC and the K_{JC} yield a T_0 estimate of -23ºC. The difference between the two estimates is only 5ºC. This is very little, since it includes both the statistical uncertainty connected to T_0 estimation, as well as the effect of possible material in-homogeneity.

Above only a couple examples of the similarity between K_{IC} and K_{JC} have been given. In the literature it would be quite easy to find more examples showing the same similarity. However, in order to avoid repetition and since the HSST 02 K_{IC} data forms the basis for the ASME K_{IC} reference curve, which also is used in the German KTA code, it was felt that the example constituted by HSST 02 provides the best demonstration of the similarity between K_{IC} and K_{JC}.

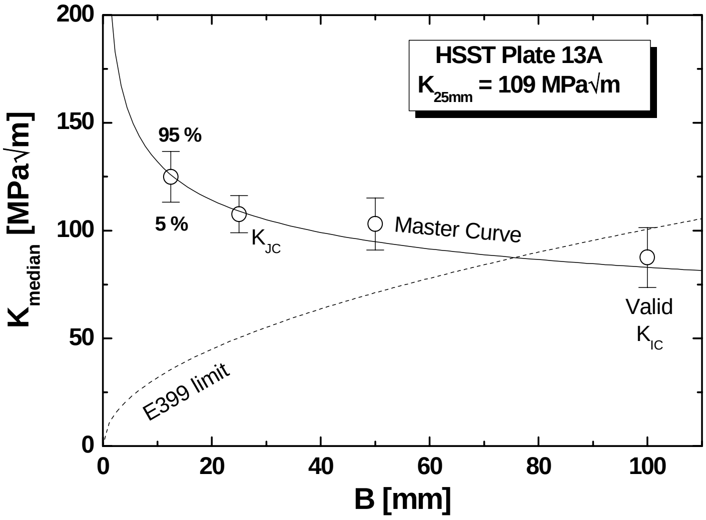

Fig. 2.6: Effect of specimen thickness on K_{JC} and K_{IC} fracture toughness explained by the statistical size effect, [McCabe, 1993].

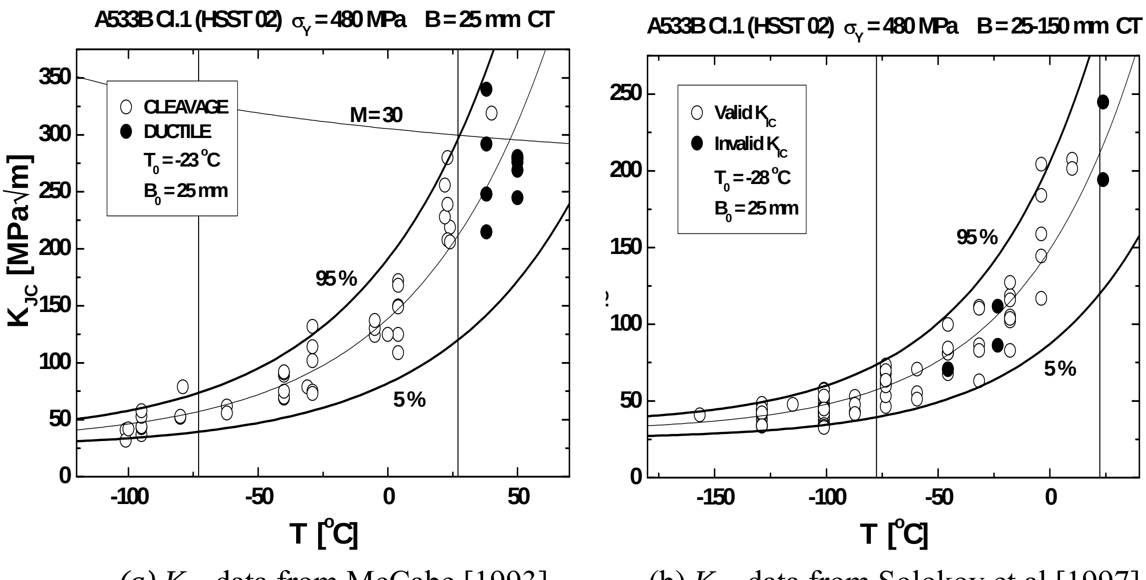

(a) K_{IC} data from McCabe [1993] (b) K_{JC} data from Solokov et al [1997]

Fig. 2.7: Application of the ASTM E1921 Master Curve analysis to KIC and KJC results of the HSST 02 tests.

3. THEORETICAL BASIS OF THE MASTER CURVE METHOD

The micromechanism of cleavage fracture exhibits a strong sensitivity to the stress field at the crack tip. Moreover, the highly localized phenomenon of cleavage fracture also demonstrates high sensitivity to the random inhomogeneities in the material along the crack front. Consequently, cleavage fracture toughness values which meet the specified size requirements nevertheless display large amount of statistical scatter, especially for temperatures corresponding to the transition region. Because of this substantial scatter, cleavage toughness data should be treated statistically rather than deterministically. It means that a given steel does not have a single value of toughness at a particular temperature in the transition region; rather, the material has a toughness distribution. Testing of numerous specimens to obtain a statistical distribution of the fracture toughness can be expensive and time-consuming. In addition, there has been an interest to utilize small fracture specimens, e.g. of Charpy size, to obtain fracture toughness data when severe limitations exist on material availability, for instance when considering irradiation embrittlement for ferritic materials. To reduce these problems, a methodology has been developed that greatly simplifies the process of determination of fracture toughness in the transition region. The ASTM E 1921-03 standard [2003] describes the procedure for the mechanical testing and statistical data analysis of ferritic steels in the transition region. This ASTM standard accounts for temperature dependence of toughness through a Fracture Toughness Master Curve approach developed by Wallin [1991]. Wallin observed that a wide range of ferritic steels have a characteristic fracture toughness-temperature curve, and the only difference between different steels was the absolute position of the curve with respect to temperature. The temperature dependence of the fracture toughness can be determined by performing a certain amount of fracture toughness tests at a given temperature. A brief description of the theoretical basis of the Master Curve methodology is given below based on NUREG/CR-5504 [Merkle, Wallin and McCabe, 1998].

3.1. Mechanism of cleavage fracture

The different possible mechanisms of cleavage fracture initiation are qualitatively rather well known. Primarily the initiation is a critical stress controlled process, where stresses and strains acting on the material produce a local failure, which develops into a dynamically propagating cleavage crack. The local “initiators” may be precipitates, inclusions or grain boundaries, acting alone or in combination. An example of a typical cleavage fracture initiation process is presented schematically in Fig. 3.1. The critical steps for cleavage fracture are:

(I) Initiation of a microcrack e.g. fracturing of a second phase particle or grain boundary.

(II) Propagation of this microcrack into the surrounding grains.

(III) Further propagation of the propagating microcrack into other adjacent grains.

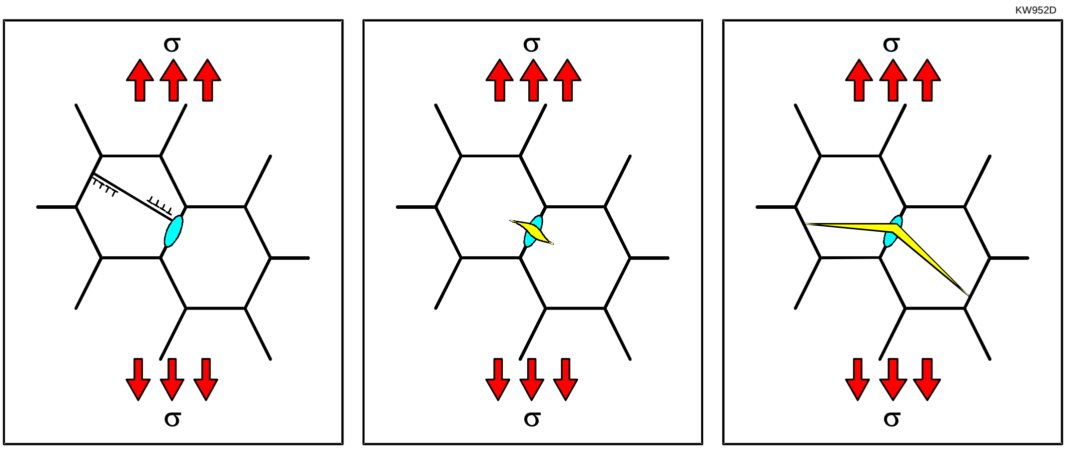

Local stress produces a dislocation pile-up which impinges on a grain boundary carbide.

Cracking of the carbide introduces a microcrack which propagates into the matrix.

Advancing microcrack encounters the first large angle boundary.

Fig. 3.1: An example of a cleavage fracture initiation process.

Depending on loading geometry, temperature, loading rate and material, different steps are more likely to be most critical. For structural steels at lower shelf temperatures and ceramics, in the case of cracks where the stress distribution is very steep, steps II and III are more difficult than initiation and they tend to control the fracture toughness. At higher temperatures, where the steepness of the stress distribution is smaller, propagation becomes easier in relation to initiation and step I becomes more and more dominant for the fracture process. The temperature region where step I dominates is usually referred to as the transition region. On the fracture surface of a specimen with a fatigue crack this is usually seen as a difference in the number of initiation sites visible on the fracture surface, as shown in Fig. 3.2. At lower shelf temperatures, numerous initiation sites are visible, whereas at higher temperatures, corresponding to the transition region, only one or two initiation sites are seen. In the case of notched or plain specimens, only a few initiation sites are seen even on the lower shelf. This is due to that, for cracks, the peak stresses are very high virtually from the beginning of loading, whereas for notched and plain specimens, the peak stresses increase gradually during loading. Because no materials are fully uniform on a microscale, cleavage fracture initiation is a statistical event, which have implications upon the macroscopic nature of brittle fracture. A statistical model is thus needed to describe the probability of cleavage fracture, [Merkle, Wallin and McCabe, 1998].

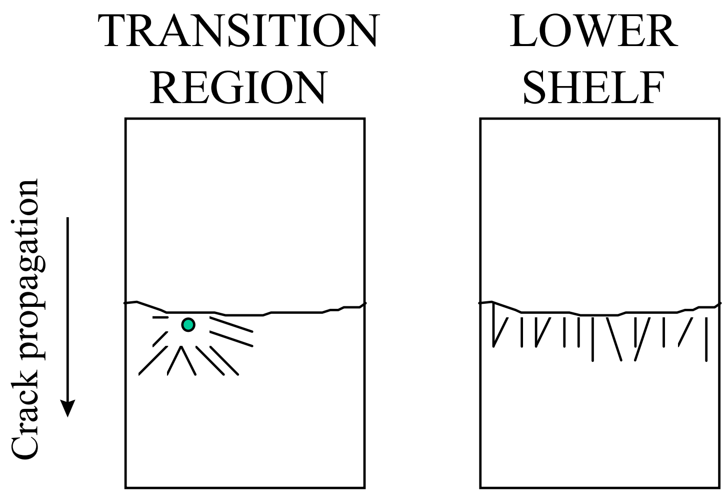

Fig. 3.2: Typical cleavage fracture surfaces for specimens with cracks. Lower shelf conditions produce numerous initiation sites, whereas in the transition region, only one or two initiation sites are visible.

The basis of a general statistical model is presented in Fig. 3.3. It is assumed that the material in front of the crack contains a distribution of possible cleavage fracture initiation sites i.e. cleavage initiators. The cumulative probability distribution for a single initiator being critical can be expressed as $\Pr\{I\}$ and it is a complex function of the initiator size distribution, stress, strain, grain size, temperature, stress and strain rate etc. The shape and origin of the initiator distribution is not important in the case of a "sharp" crack. The only necessary assumption is that no global interaction between initiators exists. This means that interactions on a local scale are permitted. Thus a cluster of cleavage initiations may be required for macroscopic initiation. As long as the cluster is local in nature, it can be interpreted as being a single initiator. All the above factors can be implemented into the initiator distribution and they are not significant as long as no attempt is made to determine the shape and specific nature of the distribution.

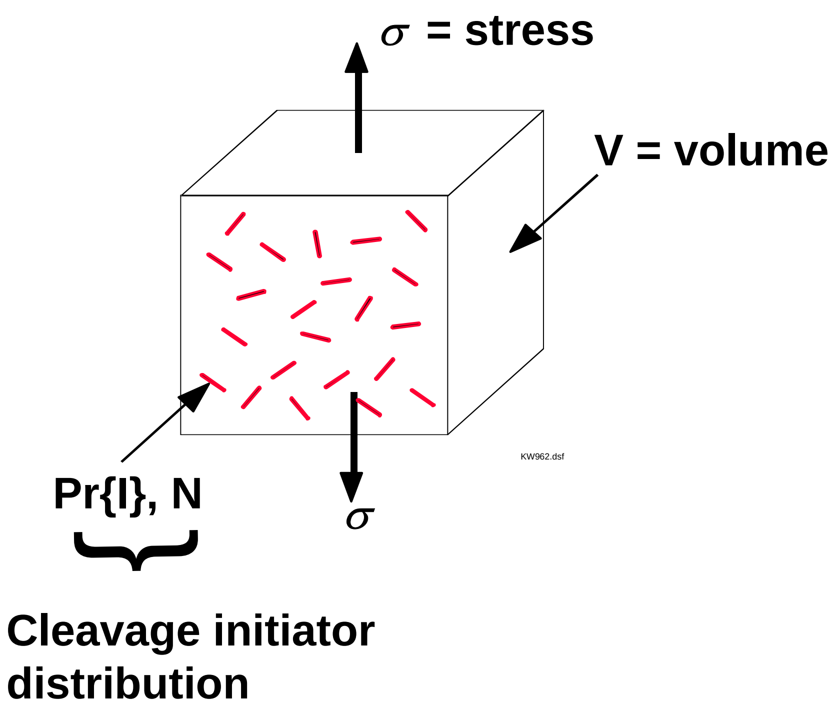

Fig. 3.3: Basis of the general statistical model.

If a particle (or grain boundary) fails, but the broken particle is not capable of initiating cleavage fracture in the matrix, the particle sized microcrack will blunt and a void will form. Such a void is not considered able to initiate cleavage fracture. Thus, the cleavage fracture initiator distribution is affected by the void formation, leading to a conditional probability for cleavage initiation (Pr{I/O}).The condition being that the cleavage initiator must not have become a void. The cleavage fracture process contains also an other conditional event, i.e. that of propagation. An initiated cleavage crack must be able to propagate through the matrix in order to produce failure. Thus the conditional probability will be that of propagation after initiation (Pr{P/I}).

The cleavage fracture initiation process can be expressed in the form of a probability tree as shown in Fig. 3.4.

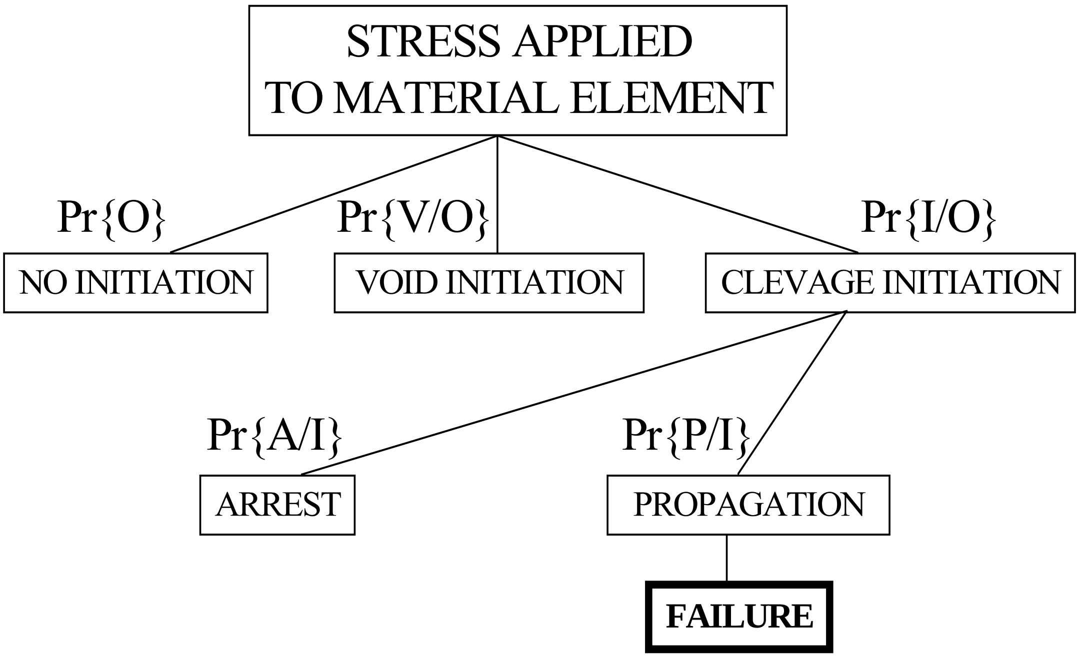

Fig. 3.4: Probability tree for cleavage fracture.

Here, the probabilities of the different events are defined as:

Pr{I} = probability of cleavage initiation

Pr{V} = probability of void initiation

Pr{O} = probability of "no event"

Pr{I/O} = conditional probability of cleavage initiation (no prior void initiation)

Pr{V/O} = conditional probability of void initiation (no prior cleavage initiation)

Pr{P/I} = conditional probability of propagation (in the event of cleavage initiation)

Pr{A/I} = conditional probability of arrest (in the event of cleavage initiation)

The following relations are clear from the probability tree:

Pr{O} + Pr{V/O} + Pr{I/O} = 1 (the sum of probabilities is unity)

and

Pr{A/I} + Pr{P/I} = Pr{I/O} (the sum of propagation and arrest equals the conditional initiation probability)

3.2. Probability of cleavage initiation

To simplify derivation it is advisable first to evaluate only the cumulative failure probability of cleavage initiation, leaving propagation to a later stage. Since initiation is controlled by a single local initiator being critical, weakest link statistics is applicable for the process.

Weakest link statistics indicates that at least one initiation is required for failure, which is equal to $P_f=1-S_r$, where S_r is the survival probability, i.e. the probability of no initiation. The cumulative failure probability of a volume element, with an uniform stress state, can thus be expressed as

$$P_f = 1 - \left[1 - \Pr\{I/O\}\right]^N \qquad (3\text{-}1)$$

where N is the number of initiators in the volume element.

The relation between the cleavage initiation probability Pr{I} and the conditional cleavage initiation probability Pr{I/O} is

$$\Pr\{I/O\} = \Pr\{I\}\cdot(1 - \Pr\{V/O\}) \qquad (3\text{-}2)$$

i.e. the probability of cleavage initiation times the probability of not having void initiation. Eq. (3-2) apparently makes a reliable estimation of the overall cleavage initiation probability more difficult. However, it will subsequently be shown that the problem is resolved for a sharp crack in small scale yielding.

Normally the exact number of initiators in a volume element is not known. If, however, the initiators are assumed to be randomly distributed in the material, the number of initiators in a randomly selected volume element will be Poisson distributed. The Poisson distribution has the form:

$$P_N = \frac{\overline{N}^N \cdot \exp\left(-\overline{N}\right)}{N!} \qquad (3.3)$$

where $\overline{N}$ is the mean number of initiators, related to the mean number of initiators per unit volume ($\overline{N}_V$) by $\overline{N} = \overline{N}_V \cdot V$.

The cumulative cleavage initiation probability, in terms of the mean number of initiators, becomes:

$$P_f = 1 - \sum_{N=0}^{\infty} [1 - \Pr\{I\} \cdot (1 - \Pr\{V/O\})]^N \cdot P_N \tag{3-4a}$$

or

$$P_f = 1 - \sum_{N=0}^{\infty} \frac{\{\overline{N} \cdot [1 - \Pr\{I\} \cdot (1 - \Pr\{V/O\})]\}^N \cdot e^{-\overline{N}}}{N!} \tag{3-4b}$$

Eq. (3-4b) looks complicated, but it can be simplified by making use of the exponential equation. By definition, the exponential equation can be expressed as

$$e^x = \sum_{N=0}^{\infty} \frac{x^N}{N!} \tag{3-5}$$

Inserting Eq. (3-5) into Eq. (3-4b) yields the simple form

$$P_f = 1 - \exp\{-\overline{N} \cdot \Pr\{I\} \cdot (1 - \Pr\{V/O\})\} \tag{3-6a}$$

or

$$P_f = 1 - \exp\{-\overline{N}_V \cdot V \cdot \Pr\{I\} \cdot (1 - \Pr\{V/O\})\} \tag{3-6b}$$

The previous derivation was for one volume element, but in the case of several (n) independent volume elements with varying sizes and stresses (Fig. 3.5), the cumulative cleavage initiation probability is obtained by summation

$$P_f = 1 - \exp \sum_{i=1}^{n} \{-\overline{N}_V \cdot V_i \cdot \Pr_i\{I\} \cdot (1 - \Pr_i\{V/O\})\} \tag{3-7}$$

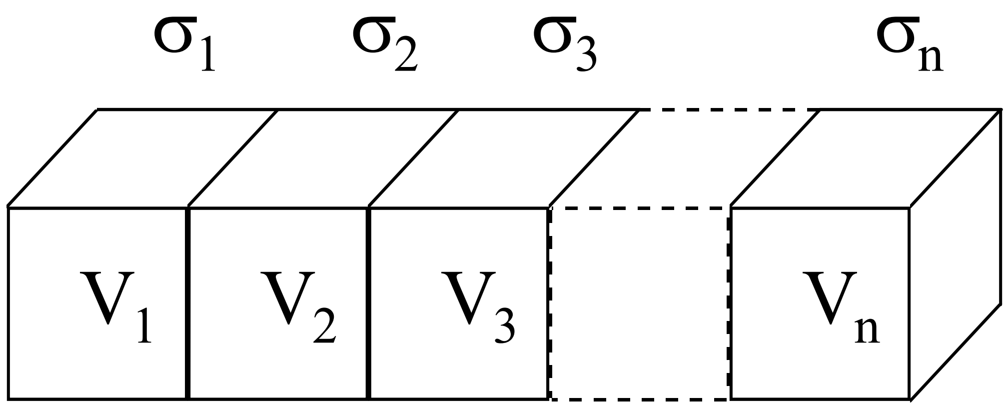

Fig. 3.5: Several independent volume elements.

For a "sharp" crack in small scale yielding the stresses and strains are described by the HRR field. One property of the HRR field is that the stress distribution is self similar and another that the stresses have an angular dependence. The term “small scale yielding” is in this derivation used to describe the loading situation where the self similarity of the stress field remains unaffected by loading. Thus the stress field can be divided into small fan like elements with an angle increment $\Delta\theta$ (Fig. 3.6). In this case the cumulative cleavage initiation probability is written as:

$$P_f = 1 - \exp \sum_{\theta=0}^{2\pi} \left[\sum_{x=0}^{x_p} \left\{ -\overline{N}_V \cdot B \cdot \Delta x \cdot x \cdot \sin(\Delta\theta) \cdot \Pr_{x,\theta}\{I\} \cdot \left(1 - \Pr_{x,\theta}\{V/O\} \right) \right\} \right] \quad (3\text{-}8)$$

where the volume element in the x-direction, described by Δx must be clearly larger than the initiator size ($\Delta x > \sim 10$ µm). The double summation indicates that the summation is performed over the whole cleavage fracture process zone. The cleavage fracture process zone is essentially restricted to the region of high tensile stresses and plastic strains. For simplicity, the stress distribution is assumed to be uniform over the specimen thickness B (crack front length). Accounting for the thickness dependence of the stress distribution would only lead to the addition of a third summation over the thickness in slices ΔB. As long as the thickness dependence of the stress distribution is independent of K_I (small scale yielding), the overall effect of the third summation does not affect the outcome of the derivation.

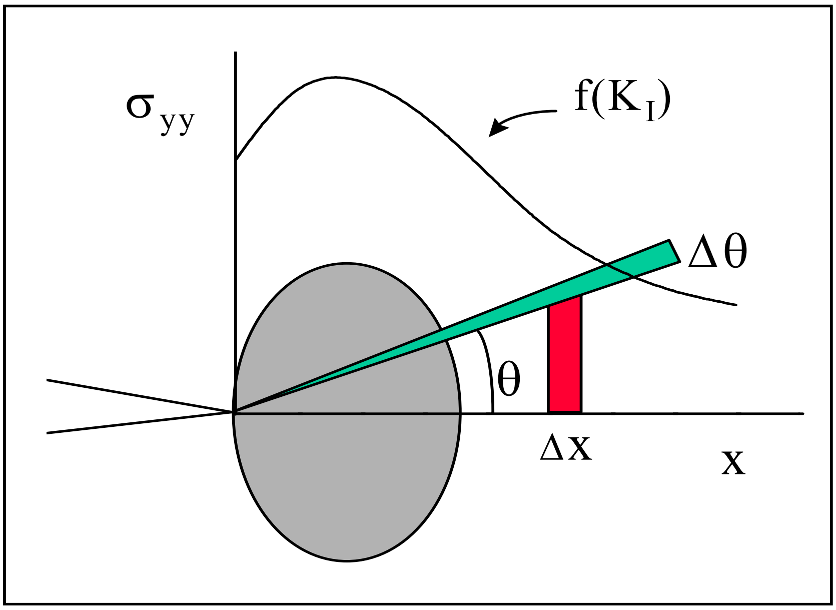

Fig. 3.6: Stress distribution in front of a crack showing definitions of Δθ, θ, x and Δx.

Due to the self similar properties of the sharp crack stress field it is possible to normalize the distance with the stress intensity factor to produce a uniqueness description of the stress distribution:

$$U = \frac{x}{\left(K_I/\sigma_y\right)^2} \tag{3-9}$$

When Eq. (3-9) is substituted into Eq. (3-8), the probability of cleavage initiation can be expressed in terms of K_I and U, as expressed in Eq. (3-10).

$$P_f = 1 - \exp\left\{B \cdot \frac{K_I^4}{\sigma_y^4} \cdot \sum_{\theta=0}^{2\pi} \left[\sum_{U=0}^{U_p} \left\{ -\overline{N}_V \cdot \Delta U \cdot U \cdot \sin(\Delta\theta) \cdot Pr_{U,\theta}\{I\} \cdot \left(1 - Pr_{U,\theta}\{V/O\}\right) \right\} \right] \right\} \tag{3-10}$$

The value of the double summation in Eq. (3-10) is always negative and independent of K_I. Thus the expression can be simply written as:

$$P_f = 1 - \exp\left\{ -B \cdot K_I^4 \cdot \text{constant} \right\} \tag{3-11a}$$

or

$$P_f = 1 - \exp\left\{ -\frac{B}{B_0} \cdot \left(\frac{K_I}{K_0} \right)^4 \right\} \tag{3-11b}$$

where B_0 is a freely definable normalisation crack front length and K_0 corresponds to a cumulative initiation probability of 63.2 %.

The remarkable feature of the cumulative cleavage initiation probability distribution is that it is really independent of the local cleavage initiator distribution. The result contains no approximations. The only assumption is that the initiators are independent on a global scale. In other words, it is assumed that the volume elements are independent for a constant K_I. Only, if it is assumed that a certain fraction of the crack front must experience critical initiations to cause macroscopic failure, then the result will differ from that of Eq. (3-11). The result is valid as long as the stresses inside the process zone are self similar in nature, so that they can be described by a single parameter (e.g. K_I). The result is also applicable for other than SSY (small scale yielding) conditions, provided it is possible to transform the stress distribution to correspond to the SSY situation ($K_{ISSY} = f\{K_J\}$). Such a SSY correction is usually possible for cracks with a strong bending component. If the stress distributions inside the process zone are not self similar, Eq. (3-11) will not be correct. For such cases, Eq. (3-8) must be used and subsequently, some quite far going assumptions regarding the local cleavage initiation probability must be made.

3.3. Conditional cleavage propagation

Eq. (3-11) would imply that an infinitesimal K_I value might lead to a finite failure probability. This is not true in reality. For very small K_I values the stress gradient becomes so steep that even if cleavage fracture can initiate, it cannot propagate into the surrounding and other adjacent grains, thus causing a zone of microcracks in front of the main crack. If propagation in relation to initiation is very difficult, a stable type of fracture may evolve. This is an effect often seen with ceramics. The need for propagation leads to a conditional crack propagation criteria, causing a lower limiting K_{min} value, below which cleavage fracture is impossible. For structural steels in the lower shelf temperature range, the fracture toughness is likely to be controlled by the instability of propagation.

The question regarding propagation alters the above pure weakest link type argument somewhat. It means that initiation is not the only requirement for cleavage fracture, but additionally a conditional propagation requirement must be fulfilled.

Fig. 3.4 reveals that the probability of failure is governed by the probability of propagation, and prior initiation at the same load. Thus one must examine the probability of cleavage initiation during a very small load increment, assuming that no initiation has occurred before. Such a probability constitutes a conditional event and the resulting function is known as the hazard function and is defined as:

$$h(K_I)=\frac{1}{1-P_f}\cdot\frac{d}{dK_I}(P_f) \tag{3-12}$$

For the cumulative cleavage initiation probability, Eq. (3-11b), the hazard function is simply

$$h_i(K_I)=\frac{4\cdot K_I^3}{K_0^4}\cdot\frac{B}{B_0}\ \text{(initiation)} \tag{3-13}$$

When the hazard function for initiation is multiplied by the conditional probability of propagation (P{P/I}), the hazard function for failure is obtained as

$$h_f(K_I)=P\{P/I\}\cdot\frac{4\cdot K_I^3}{K_0^4}\cdot\frac{B}{B_0}\ \text{(failure)} \tag{3-14}$$

and the cumulative failure probability including propagation becomes

$$P_f=1-\exp-\int_{K_{min}}^{K_I} P\{P/I\}\cdot\frac{B}{B_0}\cdot\frac{4\cdot K_I^3}{K_0^4}\cdot dK_I \tag{3-15}$$

The conditional probability of propagation (P{P/I}) indicates the instantaneous probability of propagation and as such it is similar to the hazard function for propagation alone.

In order to solve Eq. (3-15), the conditional probability of propagation (P{P/I}) must be known in a functional form. Presently it is not possible to define a single specific function for P{P/I}, but some possible forms can be deduced from the stress distribution. If the probability of propagation is controlled by the steepness of the stress distribution, it will essentially be a function of the derivative of the HRR field, as shown in Fig. 3.7.

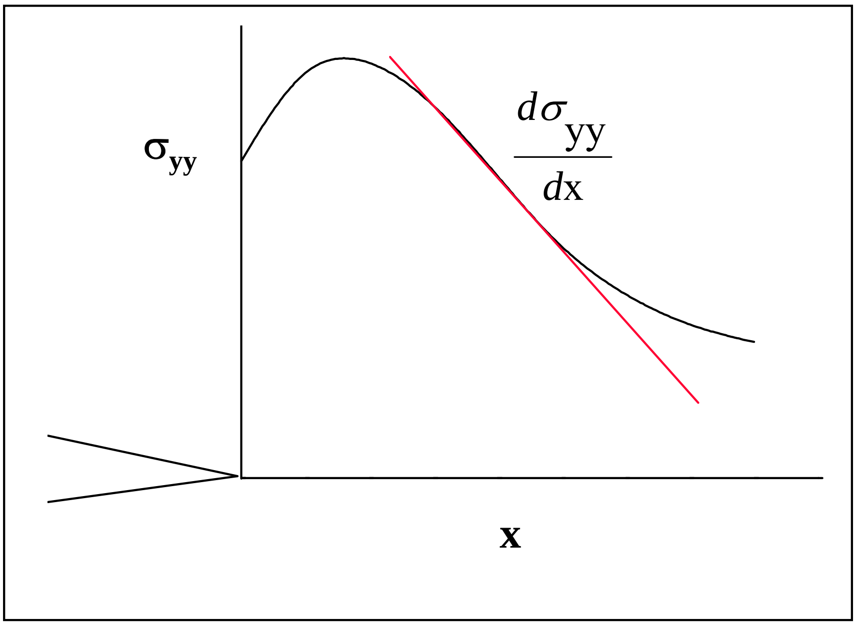

Fig. 3.7: Steepness of stress distribution in front of crack.

The stress distribution can be expressed as:

$$\sigma_{yy} = \left(\frac{K_I^2}{x} \right)^{\frac{1}{N+1}} \cdot f(\theta) \tag{3-16}$$

where N is the strain hardening exponent.

The derivative of the stress distribution becomes thus:

$$\frac{\partial\sigma_{yy}}{\partial x} = -\left(\frac{1}{N+1}\right)\cdot\frac{\sigma_{yy}^{N+2}}{K_I^2\cdot f(\theta)^{N+1}} \tag{3-17}$$

It is seen from Eq. (3-17) that the steepness of the stress distribution is a combined function of the stress, angular location and the stress intensity factor. The stress and angular dependence are random parameters (independent of K_I) thus causing the probability of propagation to be a simple function of K_I. If P{P/I} is only controlled by the steepness of the stress distribution, two possible forms are evident as expressed in Eq. (3-18a) and (3-18b):

$$P_1(P/I) = A_1\cdot\left[1-\left(\frac{K_{min1}}{K_I}\right)^2\right] \tag{3-18a}$$

and

$$P_2(P/I) = A_2\cdot\left(1-\frac{K_{min2}}{K_I}\right)^2 \tag{3-18b}$$

However, since P{P/I} is a measure of an instantaneous propagation rate, it is possible that it is controlled by the change rate of the steepness of the stress distribution (Eq. 3-19).

$$\frac{\partial}{\partial K_I}\left(\frac{\partial\sigma_{yy}}{\partial x}\right) = \left(\frac{2}{N+1}\right)\cdot\frac{\sigma_{yy}^{N+2}}{K_I^3\cdot f(\theta)^{N+1}} \tag{19}$$

Eq. (3-19) implies two additional possible forms for P{P/I}, Eq. (3-20a) and (3-20b)

$$P_3(P/I) = A_3\cdot\left[1-\left(\frac{K_{min3}}{K_I}\right)^3\right] \tag{3-20a}$$

and

$$P_4(P/I) = A_4\cdot\left(1-\frac{K_{min4}}{K_I}\right)^3 \tag{3-20b}$$

The possible forms are presented graphically in Fig. 3.8. All the equations are functions growing from 0 to A, where A is a number smaller than 1. The constant A reflects the finite probability of crack arrest even in a uniform stress field, being due to a possible misorientation between the microcrack and the possible cleavage crack planes and the need to cross a grain boundary.

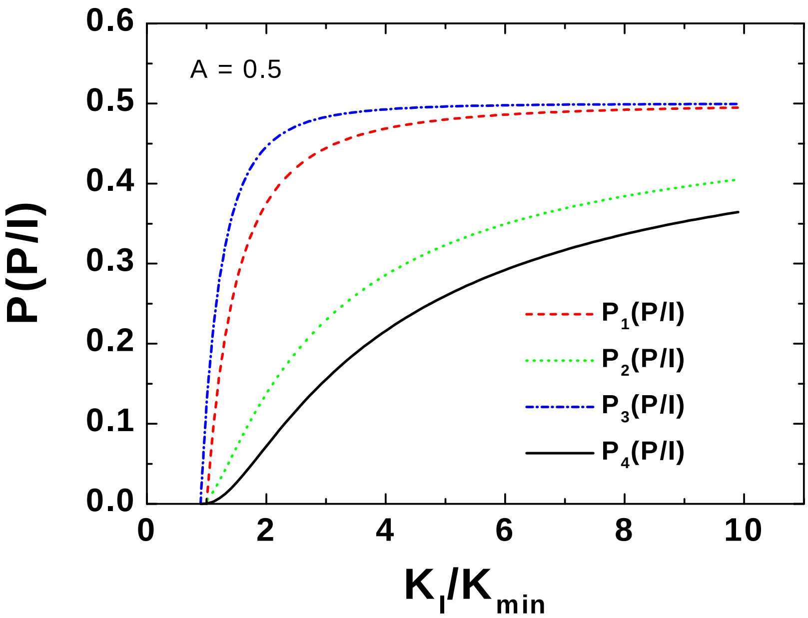

Fig. 3.8: Comparison of the different conditional propagation probability functions in Eqs. (3-18) and (3-20) using A = 0.5 as the limiting propagation probability.

When Eqs. (3-18) and (3-20) are inserted into Eq. (3-15), the following possible forms for the total cumulative failure probability are obtained

$$P_{f1} = 1 - \exp\left\{ -\frac{B}{B_0} \cdot \frac{A_1}{K_0^4} \cdot \left(K_I^2 - K_{min1}^2 \right)^2 \right\} \tag{3-21a}$$

$$P_{f2} = 1 - \exp\left\{ -\frac{B}{B_0} \cdot \frac{A_2}{K_0^4} \cdot \left(K_I - K_{min2} \right)^3 \cdot \left(K_I + K_{min2} \right)^3 \right\} \tag{3-21b)s}$$

$$P_{f3} = 1 - \exp\left\{ -\frac{B}{B_0} \cdot \frac{A_3}{K_0^4} \cdot \left(K_I^4 - 4 \cdot K_{min3}^3 \cdot K_I + 3 \cdot K_{min3}^4 \right) \right\} \tag{3-21c}$$

$$P_{f4} = 1 - \exp\left\{ -\frac{B}{B_0} \cdot \frac{A_4}{K_0^4} \cdot \left(K_I - K_{min4} \right)^4 \right\} \tag{3-21d}$$

The equations are compared graphically in Fig. 3.9, where K_{min} refers to K_{min4}. Experimentally it is virtually impossible (would require more than 1000 tests) to tell the four expressions apart. They start clearly to deviate from each other only at very low cumulative probability values. The expression producing the most conservative estimate for the minimum fracture toughness is P_{f4}.

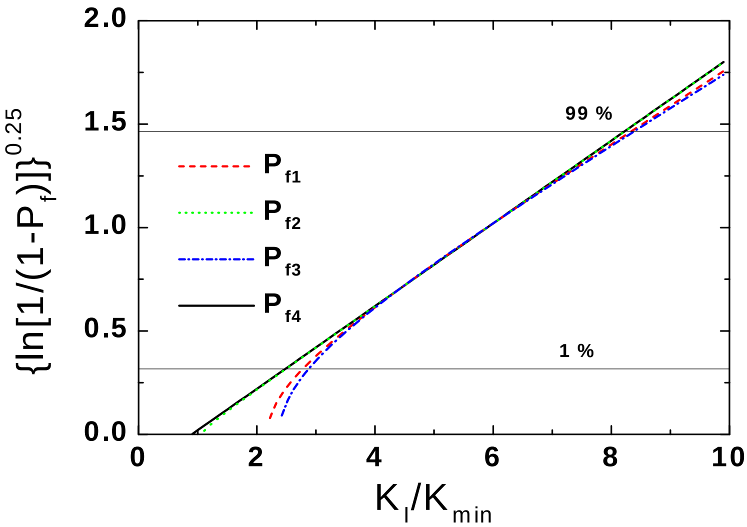

Fig. 3.9: Comparison of different cumulative failure probability expressions, Eq. (3-21a-d). The expressions are plotted against a normalised form of P_{f4}, using $K_0/K_{min4} = 5$.

The individual parameter values used in Fig. 3.9 are presented in Table 3.1, which essentially confirms the trends seen in Fig. 3.9. The expression P_{f1} is essentially identical with P_{f3} and P_{f2} is essentially identical with P_{f4} and P_{f4} yields the most conservative estimate of K_{min}. For engineering safety assessment purposes it is clearly advisable to use P_{f4} to describe the cumulative failure probability.

Table 3.1: Relation between different possible cumulative failure probability parameters.

P_{f1}	$A_1/A_4 = 0.66$	$K_{min1}/K_{min4} = 2.28$
P_{f2}	$A_2/A_4 = 0.90$	$K_{min2}/K_{min4} = 1.20$
P_{f3}	$A_3/A_4 = 0.60$	$K_{min3}/K_{min4} = 2.48$
P_{f4}	$A_4/A_4 = 1$	$K_{min4}/K_{min4} = 1$

The above derivations are based on the assumption that the probability of cleavage initiation is less than unity. This is normal for configurations like plain and notched specimens and cracked specimens in cases where initiation is sufficiently difficult. For material conditions where initiation is simple, the probability of cleavage initiation in the case of a crack may become unity. This can occur on the so called "lower shelf" of the material. Essentially it means that all possible initiation sites are activated and initiation occurs as soon as the crack is loaded, making the initiation event independent of the load level (and subsequently independent of specimen thickness). Thus, in the case of a crack, the lower shelf toughness may be controlled purely by the probability of propagation. For plain and notched configurations, however, the probability of initiation will still be a function of load level even on the lower shelf. Therefore, a simple correlation between notched and cracked configurations may not be possible for the lower shelf material conditions.

As previously stated, the conditional probability of propagation (P{P/I}) indicates the instantaneous probability of propagation and as such it is similar to the hazard function for propagation alone. However P{P/I} does not as such constitute a hazard function, because the hazard function (like the incremental distribution) must have the units of $1/K_I$. Therefore, substitution of the normalisation parameter K_e in the place of the constant A yield, corollary to Eqs. (3-18 and 3-20), logical forms for the hazard function of propagation alone:

$$h_{P1}(K_I) = \frac{1}{K_{e1}} \cdot \left[1 - \left(\frac{K_{min1}}{K_I}\right)^2\right] \tag{3-22a}$$

$$h_{P2}(K_I) = \frac{1}{K_{e2}} \cdot \left(1 - \frac{K_{min2}}{K_I}\right)^2 \tag{3-22b}$$

$$h_{P3}(K_I) = \frac{1}{K_{e3}} \cdot \left[1 - \left(\frac{K_{min3}}{K_I}\right)^3\right] \tag{3-22c}$$

$$h_{P4}(K_I) = \frac{1}{K_{e4}} \cdot \left(1 - \frac{K_{min4}}{K_I}\right)^3 \tag{3-22d}$$

The corresponding cumulative failure probabilities are:

$$P_{f1LS} = 1 - \exp\left\{-\frac{K_{min1}}{K_{e1}} \cdot \left[\frac{K_I}{K_{min1}} + \frac{K_{min1}}{K_1} - 2\right]\right\} \tag{3-23a}$$

$$P_{f2LS} = 1 - \exp\left\{-\frac{K_{min2}}{K_{e2}} \cdot \left[2 \cdot \ln\left(\frac{K_{min2}}{K_I}\right) + \frac{K_I}{K_{min2}} - \frac{K_{min2}}{K_1}\right]\right\} \tag{3-23b}$$

$$P_{f3LS} = 1 - \exp\left\{-\frac{K_{min3}}{K_{e3}} \cdot \left[\frac{K_I}{K_{min3}} + \frac{1}{2} \cdot \left(\frac{K_{min3}}{K_1}\right)^2 - \frac{3}{2}\right]\right\} \tag{23c}$$

$$P_{f4LS} = 1 - \exp\left\{-\frac{K_{min4}}{K_{e4}} \cdot \left[\frac{K_I}{K_{min4}} - 3 \cdot \ln\left(\frac{K_I}{K_{min4}}\right) - 3 \cdot \frac{K_{min4}}{K_1} + \frac{1}{2}\left(\frac{K_{min4}}{K_I}\right)^2 + \frac{3}{2}\right]\right\} \tag{3-23d}$$

Eqs. (3-23a-d) are compared in graphic form in Fig. 3.10 for an imaginary lower shelf data set with a median fracture toughness of approximately 40 (units not specified). The same trend as before for the initiation plus propagation case is seen. The expression P_{f1LS} is essentially identical with P_{f3LS} and P_{f2LS} is essentially identical with P_{f4LS} and P_{f4LS} yields the most conservative estimate of K_{min}. The expressions P_{f1LS} and P_{f3LS} appear unrealistic in shape compared to existing lower shelf data. Expression P_{f2LS} appears, intuitively, from the stress distribution point of view to be most likely the correct one, but the expression P_{f4LS} is almost identical in shape and slightly more conservative. Additionally, the form of P_{f4} (for initiation + propagation) is very suitable for statistical estimation, because it is identical to a simple three parameter Weibull distribution with a fixed shape (exponent = 4). Thus, P_{f4} and P_{f4LS} are selected as the basis for the Master Curve scatter and size effect.

The Master Curve scatter in the case of initiation plus propagation is described optimally by Eq. (3-21d), which can be reformulated in the convenient form of a three parameter Weibull expression with the exponent fixed to 4:

$$P_f = 1 - \exp\left\{ -\frac{B}{B_0} \cdot \left(\frac{K_I - K_{min}}{K_0 - K_{min}} \right)^4 \right\} \qquad (3\text{-}24)$$

Here, K_0 equals the load level corresponding to a 63.2 % cumulative failure probability, B_0 is a freely selected normalising thickness, e.g. 25 mm and K_{min} is the lower limiting fracture toughness corresponding to zero probability of failure.

The size effect, implied by Eq. (3-24), has the form:

$$K_{IC}^{(2)} = K_{min} + (K_{IC}^{(1)} - K_{min}) \cdot \left(\frac{B_1}{B_2} \right)^{1/4} \qquad (3\text{-}25)$$

The theory predicts that the size effect disappears in the lower shelf toughness range and also the scatter changes somewhat, compare Figs. 3.9 and 3.10. On the lower shelf the cumulative failure probability is described by Eq. (3-23d) which is of a somewhat more complex form than Eq. (3-24). Unfortunately, the derivation is incapable of predicting when lower shelf conditions are prevailing, thus making it difficult to decide when to use Eq. (3-24) and when to use Eq. (3-23d). Experimentally the problem can easily be solved by performing tests in both regions. From an engineering assessment point of view, however, a conservative estimate is obtained with Eq. (3-24) also on the lower shelf.

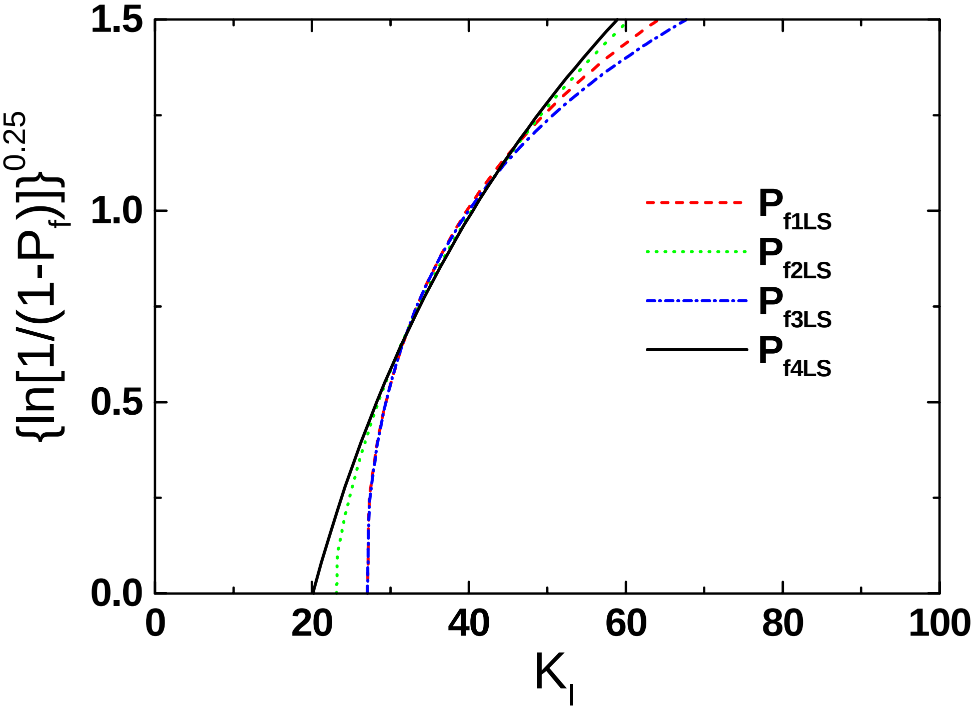

Fig. 3.10: Comparison of different possible cumulative failure probability expressions for lower shelf behaviour in Eq. (3-23a-d).

In the case of initiation, the resulting equations contain no approximations. The only assumption is that the initiators are independent on a global scale. In other words, it is assumed that the volume elements are independent for a constant K_I. Only, if it is assumed that a certain fraction of the crack front must experience critical initiations to cause macroscopic failure, then the result will differ from what is presented here. The only other restriction comes from the requirement that the volume elements in the x-direction must be clearly larger than the initiator size, but this requirement is effective only for the transition region where it is easily fulfilled. On the lower shelf, initiation is automatic and does not depend on the volume element size.

In the case of propagation, the resulting equations contain more uncertainties, but in this case, a conservative result has been chosen.

In the derivation of the above equations, the cleavage fracture process zone was assumed to be equal to the region of high stresses and plastic strain. The result is, however, not sensitive to the definition of the process zone as long as it is assumed that the stress and strain distributions inside the process zone correlate with K_I, CTOD or J. This aspect becomes important when examining the effect of large scale yielding and ductile tearing.

4. DETERMINATION OF MASTER CURVES

The ASTM E1921-03 standard describes the determination of a reference temperature, T_0 in ^{o}C, which characterizes the fracture toughness of ferritic steels that experience onset of cleavage cracking at elastic, or elastic-plastic K_{Jc} instability, or both. By definition, T_0 is a temperature at which the median of the K_{Jc} distribution from 1T size specimens will be equal to 100 MPa√m. Static elastic-plastic fracture tests are performed on standard SEN(B) or CT specimens having deep notches (a/W= 0.5) to measure the J-integral values at cleavage fracture (denoted J_c). The test temperature (T) and configuration of all specimens must be identified. The test temperature should be selected in the lower part of the ductile-to-brittle region as close as possible to the eventual T_0. The standard requires a minimum of six replicate tests which meet the crack front straightness tolerances, the limits on ductile tearing prior to cleavage, the size/deformation limits, etc. It is also possible to use miniature specimen sizes in the fracture toughness test. For example, using test specimens of section 5x5 mm^2 needs 12 validated tests (Table 5-3). The J-integral values at fracture are converted to their equivalent units of stress intensity factor using:

$$K_{Jc} = \sqrt{\frac{EJ_c}{1-\nu^2}} \qquad \mathrm{MPa}\sqrt{\mathrm{m}}\,, \tag{4-1}$$

where E denotes the elastic modulus and ν the Poisson’s ratio of the material. The maximum K_{Jc} capacity of a specimen is restricted to:

$$K_{Jc(\mathrm{limit})} = \sqrt{\frac{Eb_0\sigma_Y}{M(1-\nu^2)}}\,, \tag{4-2}$$

where σ_Y is the material yield strength at the test temperature and b_0 the specimen remaining ligament. The standard sets M = 30 in order to assure that the SSY condition prevails in the test specimen. K_{Jc} data that exceed this requirement may be used in a data censoring procedure described in the standard, including additional restrictions. For test program conducted on other than 1T specimens, the measured toughness data should be size-corrected to their 1T equivalent according to

$$K_{Jc(1T)} = 20 + \left[K_{Jc(x)} - 20\right]\left(\frac{B_{x}}{B_{1T}}\right)^{1/4}, \tag{4-3}$$

where B_{1T} is the 1T specimen size (25 mm) and B_x the corresponding dimension of the test specimen. In Eq. (4-3), 20 MPa√m represents the minimum (threshold) fracture toughness adopted for ferritic steels addressed by the standard.

The ASTM E1921-03 standard adopts a three-parameter Weibull model to define the relationship between K_{Jc} and the cumulative failure probability, P_f. The term P_f is the probability for failure at or before K_{Jc} for an arbitrarily chosen specimen taken from a large population of specimens. By specifying two of the three Weibull parameters, the failure probability has the form:

$$P_f = 1 - \exp\left(-\left[\frac{K_{Jc} - K_{\min}}{K_0 - K_{\min}}\right]^4\right). \tag{4-4}$$

Here, the Weibull distribution shape has been assigned a value of 4 derived from theoretical arguments. For ferritic steels with yield strengths ranging from 275 to 825 MPa, the cumulative probability distribution of the fracture toughness is independent of specimen size and test temperature, when K_{min} is set as 20 MPa√m. The scale parameter K_0 is the data-fitting parameter. K_0 corresponds to 63% cumulative probability. When using the maximum likelihood statistical method of data fitting, K_{Jc} and K_0 are equal, and p_f is 0.632. The following equation can be used for a sample that consists of six or more valid K_{Jc} values in order to evaluated K_0.

$$K_0 = \left[\sum_{i=1}^{N} \frac{(K_{Jc(i)} - 20)^4}{N}\right]^{1/4} + 20, \tag{4-5}$$

where N denotes the number of valid tests (six minimum). Note that K_0 can also be evaluated using both valid and censored test data. The procedure for this is given in the ASTM E1921-03 standard.

The estimated median (50% probability) K_{Jc} value, assuming p_f = 0.50 in Eq. (4-4), of the population at the tested temperature can be obtained from K_0 as expressed in Eq. (4-6):

$$K_{Jc(\mathrm{med})} = 0.9124(K_0 - 20) + 20. \qquad (4\text{-}6)$$

The Master Curve is defined as the median (50% probability) toughness for the 1T specimen over the transition range for the material. Based on fitting to test results, the shape of the Master Curve for the 1T specimen is described by Eq. (4-7):

$$K_{Jc(50\%)} = 30 + 70\exp\left[0.019(T\text{-}T_0)\right]. \qquad (4\text{-}7)$$

The lower-bound (5% probability) and upper-bound (95% probability) curves can also be set up. These three curves are given by the following expressions:

$$K_{Jc(5\%)} = 25.4 + 37.8\exp\left[0.019(T\text{-}T_0)\right]. \qquad (4\text{-}8)$$

$$K_{Jc(95\%)} = 34.6 + 102.2\exp\left[0.019(T\text{-}T_0)\right]. \qquad (4\text{-}9)$$

Where, K_{Jc} is in MPa√m and T and T_0 in ^{o}C.

Finally, the reference temperature T_0 (^{o}C), for which K_{Jc} is 100 MPa√m, is obtained from the following expression:

$$T_0 = T - \frac{1}{0.019}\ln\left[\frac{K_{Jc(\mathrm{med})} - 30}{70}\right]. \qquad (4\text{-}10)$$

The reference temperature T_0 should be relatively independent of the test temperature that has been selected. Hence, data that are distributed over a restricted temperature range, namely T_0 ± 50 ^{o}C, can be used to determine T_0. This temperature range together with the specimen size requirement, Eq. (4-2), provides a validity window, where test results can be obtained, as shown in Fig. 4.1.

Note that the Master Curve methodology describes the cleavage fracture toughness of the material under high constraint conditions for which the single parameter characterization of the material toughness (K_{Jc}) holds. Indeed, adoption of a three parameter Weibull distribution to describe measured K_{Jc}-values, with a geometry independent value of K_0, theoretically requires that SSY conditions prevail at fracture in each of replicate test specimens used to compute the statistical estimate for K_0 and thereafter T_0. Moreover, the ASTM E1921 standard does not require testing of 1T size specimens. It is allowed to use Charpy size fracture specimens (W= B= 10 mm, a/W= 0.5) and convert the results to 1T equivalent values using Eq. (4-3). This is a major advantage of the MC methodology, having in mind the severe limitations which exist on material availability in nuclear irradiation embrittlement studies. The ASTM procedure includes limits relative to specimen size and K_{Jc}-values through Eq. (4-2). Indeed, the M= 30 value has been selected largely on the basis of experimental data sets to ensure the existence of the SSY condition at fracture of the replicate test specimens. The connection between T_0 and the crack-tip constraint become exceedingly complex once SSY conditions begin to breakdown under increasing load. This issue will be discussed in section eight of this report.

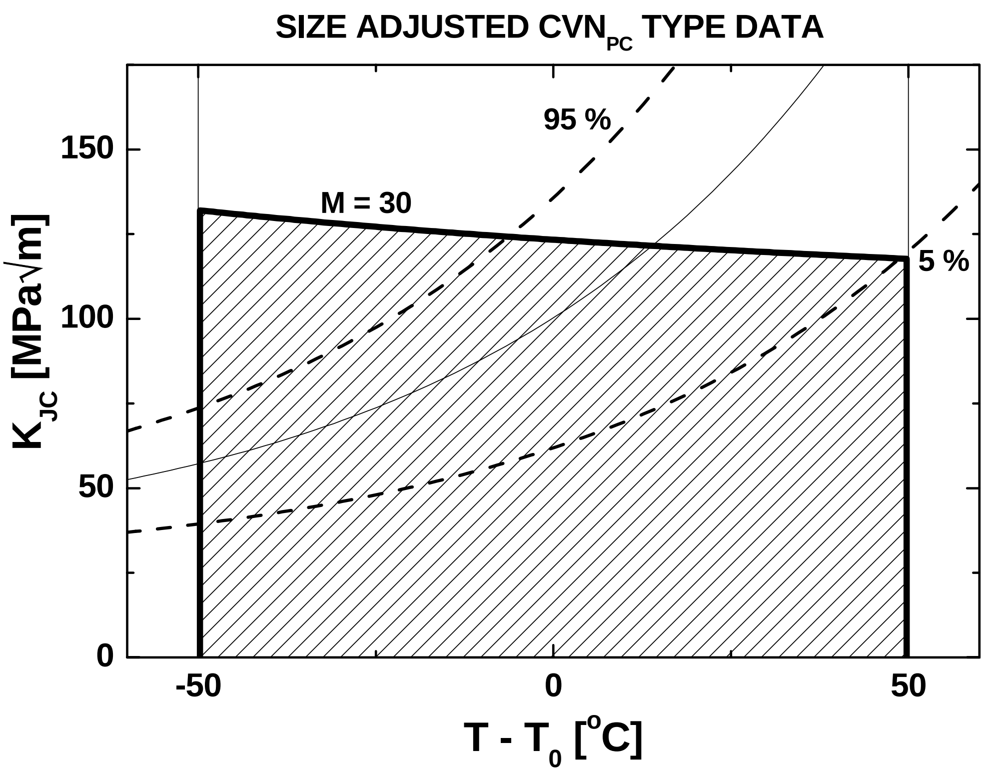

Fig. 4.1: Validation window in application of the Master Curves for the ferritic materials.

4.1. Comparison of Master Curve K_{JC} and ASME K_{Ic}

It is illustrative to compare the master K_{Jc} curves with the ASME K_{Ic} curves. The ASME Section XI Code includes two reference curves, K_{Ic} and K_{Ia}, that give conservative estimates of fracture toughness versus temperature. The K_{Ia}–curve is based on the lower bound of crack arrest data and the K_{Ic}–curve is based on the lower bound of static initiation critical K_I values as a function of temperature. These curves are given in the Code as a function of a reference temperature, RT_{NDT}, which is determined through drop weight and Charpy test results. According to the Code, RT_{NDT} is defined as the higher of the following two cases

(i) The drop weight NDT.

(ii) 33°C below the minimum temperature at which the lowest of three Charpy results is at least 68 J.

The ASME reference curves have the following forms as a function of RT_{NDT}

$$K_{Ia} = 29.4 + 1.355\exp\left[0.026(T\text{-}RT_{NDT} + 89)\right], \tag{4-11}$$

$$K_{Ic} = 36.5 + 3.084\exp\left[0.036(T\text{-}RT_{NDT} + 56)\right], \tag{4-12}$$

where K in MPa√m and RT_{NDT} in °C.

It should be noted that RT_{NDT} is not determined directly from fracture toughness tests, but from Pellini and Charpy test (which are conducted on notched specimens under dynamic loading). On the contrary, the reference temperature T_0 in the Master Curve methodology is determined directly from fracture tests on standard cracked specimens.

A comparison between the Master Curves and the ASME K_{IC} reference curve is shown in Fig. 4.2. The material is a specially heat treated A533 GB to study fracture behaviour of an aged reactor pressure vessel under a cold over-pressurization scenario, [Sattari-Far, 2004a]. The T_0 and RT_{NDT} values were 30 °C and 72 °C, respectively.

A Master Curve analysis of the original data of the ASME K_{IC} reference curve shows that the ASME K_{IC} curve corresponds practically to the same degree of confidence as a 5 % Master Curve for low temperatures. This comparison is also shown in Figs. 8.18 and 8.21 and will be discussed in section 8.6 of this report.

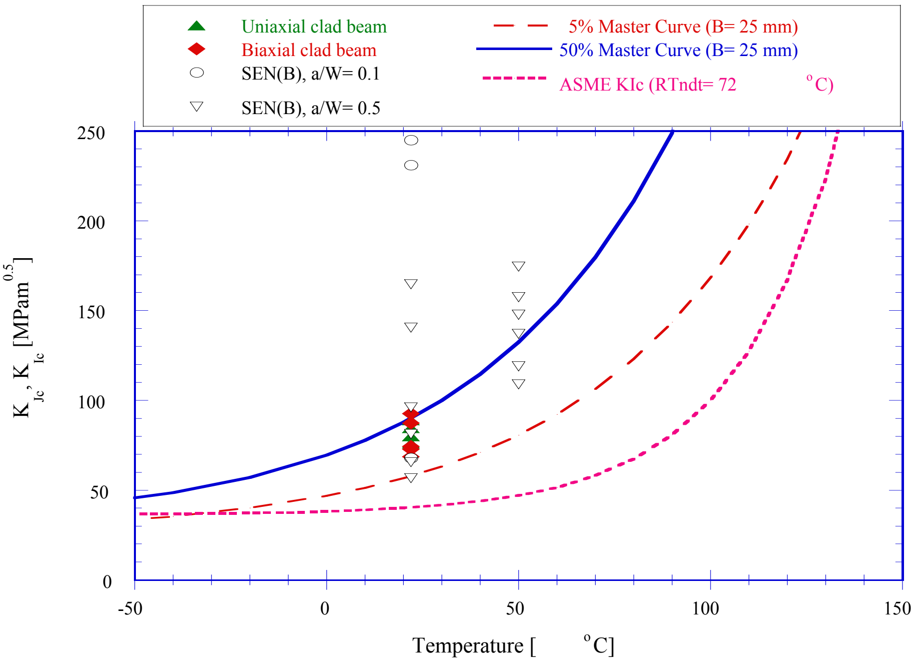

Fig. 4.2: Cleavage fracture toughness based on the Master Curves and ASME KIc curve for a specially heat treated A533 GB steel, [Sattari-Far, 2004a].

5. MASTER CURVE ANALYSIS OF SMALL SPECIMENS

One important feature of the Master Curve method is that it can be used to determine the brittle fracture toughness using only a few relatively small specimens. Classically, the specimen thickness has been assumed to be of greater importance than the remaining ligament size, but for deeply cracked bend specimens with $b \leq B$, the ligament size is really the primary dimension controlling the measuring capacity of the specimen. The significance of the specimen thickness with regard to loss of constraint is further lowered when side-grooving the specimen. Side-grooving reduces the length of the crack front, but also raises the stress triaxiality in the near-surface region. The overall effect of side-grooving tends to be insignificant for "normal size" specimens. For very small specimens it helps to maintain the constraint in the thickness direction.

The lower shelf of fracture toughness is not covered by the basic Master Curve method. The model used in the basic Master Curve method is based upon the assumption that brittle fracture is primarily initiation-controlled, even though it contains a conditional crack propagation criterion, which is one reason for the lower bound fracture toughness K_{min}. On the lower shelf, for the case of cracks, the initiation criterion is no longer dominant, but the fracture is completely propagation-controlled. In this case there is no statistical specimen size effect (as prescribed in the basic method) and also the toughness distribution differs from the basic Master Curve assumption. Due to this problem of the description of the lower shelf and to avoid the effect of significant ductile tearing, the new version of the ASTM E1921-03 testing standard limits the temperature range suitable for T_0 determination to -50ºC $\leq T-T_0 \leq$ +50ºC.

The temperature range, together with the specimen size requirement given in Eq. (4-2), provides a validity window, within which valid test results can be obtained as shown schematically in Fig. 4.1. The specimen size influences the size of this validity window, by shifting the M = 30 curve. Since most test results are expected to lie within the 5 % and 95 % scatter bounds, it is more difficult to obtain valid test results with smaller specimens. This means that the miniature specimens require more tests than larger specimens to obtain the same success level (reliability).

In this Chapter, the applicability of the miniature and larger laboratory specimens to determine the Master Curve T_0 transition temperature is studied. Also studied is the comparison of the T_0 estimates from 3PB- and CT-specimen tests to find any possible differences.

5.1. Master Curve analysis of miniature specimens

Materials and geometries

The results presented here are mainly selected from a comprehensive study performed at VTT [Wallin et al at, 2004b]. Four different specimen geometries were selected for the primary part of the study, as shown in Fig. 5.1. The normal 10x10 mm Charpy-V specimen geometry acted as a reference, the 5x5 and 5x10 mm 3PB-specimens were used to investigate the effect of the ligament size for a constant thickness, and the 3x4 mm specimens were used to investigate a "lower limit" specimen size. All specimens were tested in three point bending with a span to width ratio of 4, crack length to specimen width ratio of 0.5 and 10 % + 10 % side-grooves with a 45º included angle and 0.25 mm radius. The K_{max} during fatigue pre-cracking was for all specimens held at 10 MPa√m. The testing and J-analysis were mainly performed in accordance with the testing standard ASTM E1820-99. Some of the old 10x10 mm specimens were tested in accordance with the testing standard ASTM E813-86. All 10x10 and 5x10 mm specimens were tested using the unloading compliance method to monitor crack growth, whereas the smaller specimens were loaded directly to fracture. After the test, the amount of ductile crack growth (if any) in each specimen was measured optically. This enabled the construction of multi-specimen J-R curves.

The tested materials given in this report are listed in Table 5.1. Three materials were tested both in irradiated and non-irradiated condition. The neutron fluence of the three irradiated materials was approximately 1.5×10^{19} n/cm^2 (E > 1 MeV) and the irradiation temperature T_{irr} = 265ºC. The irradiation was performed 15 years ago and the original irradiated 10x10 mm specimens were tested 13 years ago. The smaller specimens were tested within the last 5 years. Steel A533B Cl.1 (HSST 03) is the American correlation monitor material and A533B Cl.1 (JRQ) is the Japanese correlation monitor material used by IAEA in the coordinated research programmes on irradiation embrittlement (IAEA CRP 3) [Brumovsky et al, 1995].

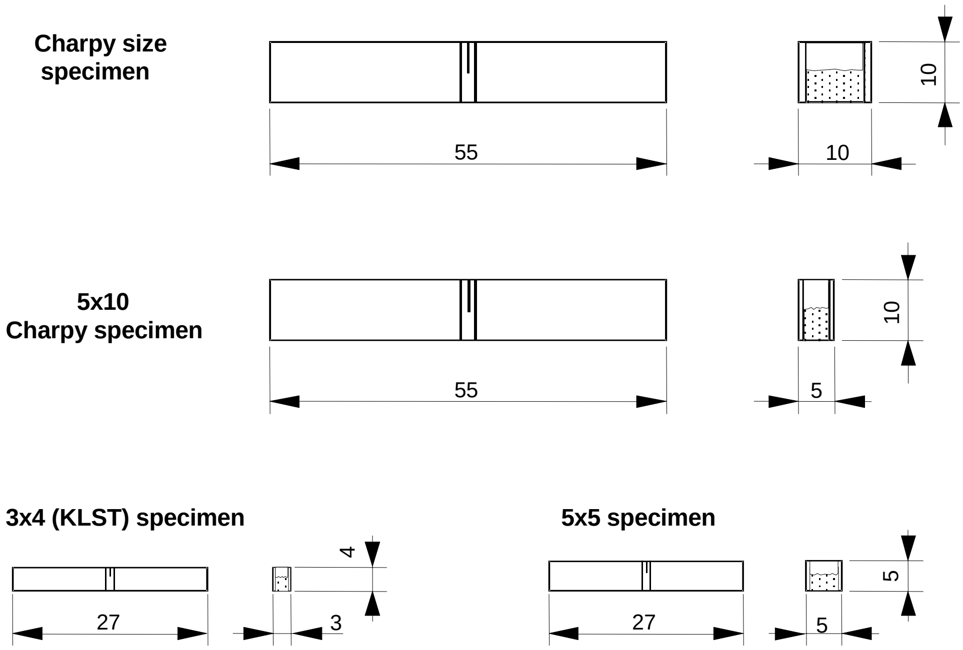

Fig. 5.1: Specimen geometries studied for applicability of small specimens, [Wallin et al, 2004b].

The specimens from the HSST 03 plate and the irradiated JRQ were taken in the L-T orientation, whereas the reference state JRQ specimens were taken in the T-L orientation. The irradiated JRQ specimens were taken from different thickness locations of the plate, whereas the other specimens were taken from the quarter depth location. The A508 Cl.3 forgings corresponded to the French (FFA) and Japanese (JFL) forgings included in the IAEA CRP 3 programs. The specimens were taken from the quarter thickness location in the L-T orientation. Weld 502 is a corresponding Russian submerged arc weld used in an IAEA coordinated research programme on VVER materials [Valo et al, 1999], where the specimens were taken in the T-W (transverse-weld) orientation.

Master Curve analysis

The Master Curve analysis followed the ASTM E1921-03 standard [ASTM, 2003]. Two levels of censoring were applied. First, for all data referring to "non-cleavage" (ductile end of test) it was prescribed that $\delta_i = 0$ in Eq. (5-1). Secondly, all data violating the specimen size validity criterion of Eq. (4-2) were assigned the toughness value corresponding to the validity criterion with $\delta_i = 0$.

In accordance with ASTM E1921-03, a plane strain stress state was assumed for all data sets, since this is more in line with the original assumptions made in the development of the Master Curve method and specifically the temperature dependence expression. A plastic η-factor of 2 was used instead of 1.9 as prescribed in the ASTM E1921-03 standard. The reason for this was that the testing and J-analysis followed the testing standard ASTM E1820-99. The effect of using the η-factor of 2 instead of 1.9 is a 1-2ºC bias of the T_0 values towards lower temperatures. This is of importance when comparing the 3PB-results with CT-results.

Table 5-1: Materials used in the MC analysis of small specimens, [Wallin et al, 2004b].

Material	σ_Y [MPa]	σ_U (MPa)	T_{28J} (ºC)	CV_{US} (J)
A533B Cl.1 (HSST 03) L-T	450	640	-22	150
A533B Cl.1 (JRQ) T-L	486	620	-29	210
A533B Cl.1 (JRQ-irr.) L-T	687	815	+84	129
A508 Cl.3 (FFA) L-T	434	570	-64	204
A508 Cl.3 (FFA-irr.) L-T	509	635	-28	200
A508 Cl.3 (JFL) L-T	450	593	-58	210
A508 Cl.3 (JFL-irr.) L-T	516	641	-25	210
Weld 502 T-W	472	607	-24	123

σ_Y, σ_U = yield and ultimate stress.

T_{28J}, CV_{US} = CVN 28J transition temperature and upper shelf energy.

For the comparison of different size specimen data, and for the calculation of the Master Curve transition temperature T_0, all data were thickness-adjusted to the reference flaw length (thickness) B_0 = 25 mm using Eq. (4-3).

For all data sets, T_0 was estimated from the size-adjusted K_{Jc} data using a multi-temperature randomly censored maximum likelihood expression according to ASTM E1921-03 as given in Eq. (5-1).

$$\sum_{i=1}^{n} \frac{\delta_i \cdot \exp\{0.019[T_i - T_0]\}}{11 + 77 \cdot \exp\{0.019[T_i - T_0]\}} - \sum_{i=1}^{n} \frac{\left(K_{IC_i} - 20\right)^4 \cdot \exp\{0.019[T_i - T_0]\}}{\left(11 + 77 \cdot \exp\{0.019[T_i - T_0]\}\right)^5} = 0 \qquad (5\text{-}1)$$

Where, Kroneckers delta $\delta_i = 1$ when K_{IC} corresponds to failure by brittle fracture (a valid test datum), and $\delta_i = 0$ when K_{IC} corresponds to a non-failure test (violating the size requirement of the ASTM E 1921 standard). The transition temperature, T_0, was solved by iteration using Eq. (5-1).

Ideally, the Master Curve should not be fitted to data below T_0 - 50ºC, i.e. data close to or on the lower shelf, where a temperature fit becomes highly inaccurate and where deviation in the lower shelf toughness from the Master Curve assumption may bias the results. Therefore, in the determination of T_0 the data was limited to -50ºC<T- T_0<+50ºC. The results for the individual data sets are presented in Figs. 5.2 to 5.9.

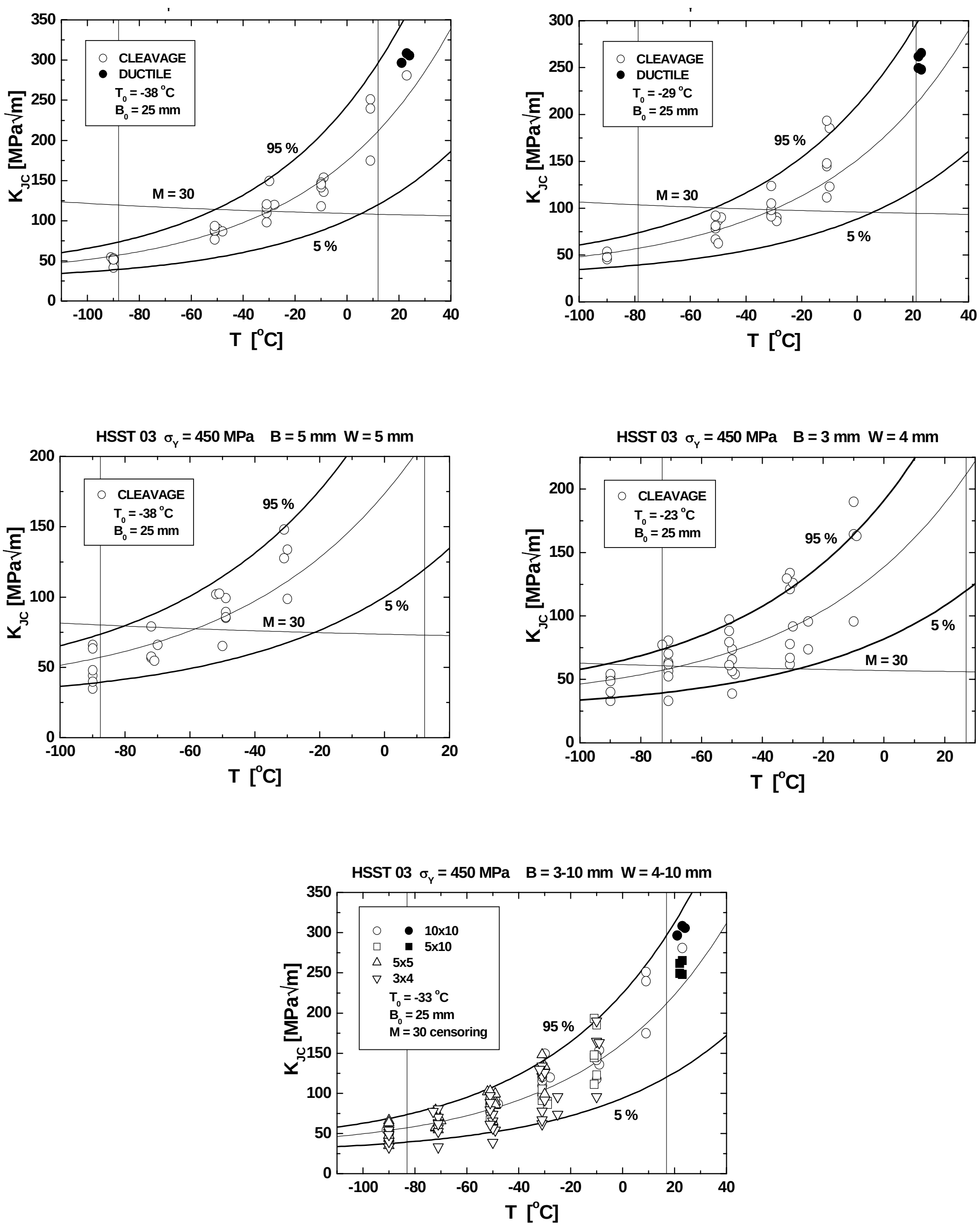

Fig. 5.2: Master Curve analysis of the HSST 03 material, [Wallin et al, 2004b].

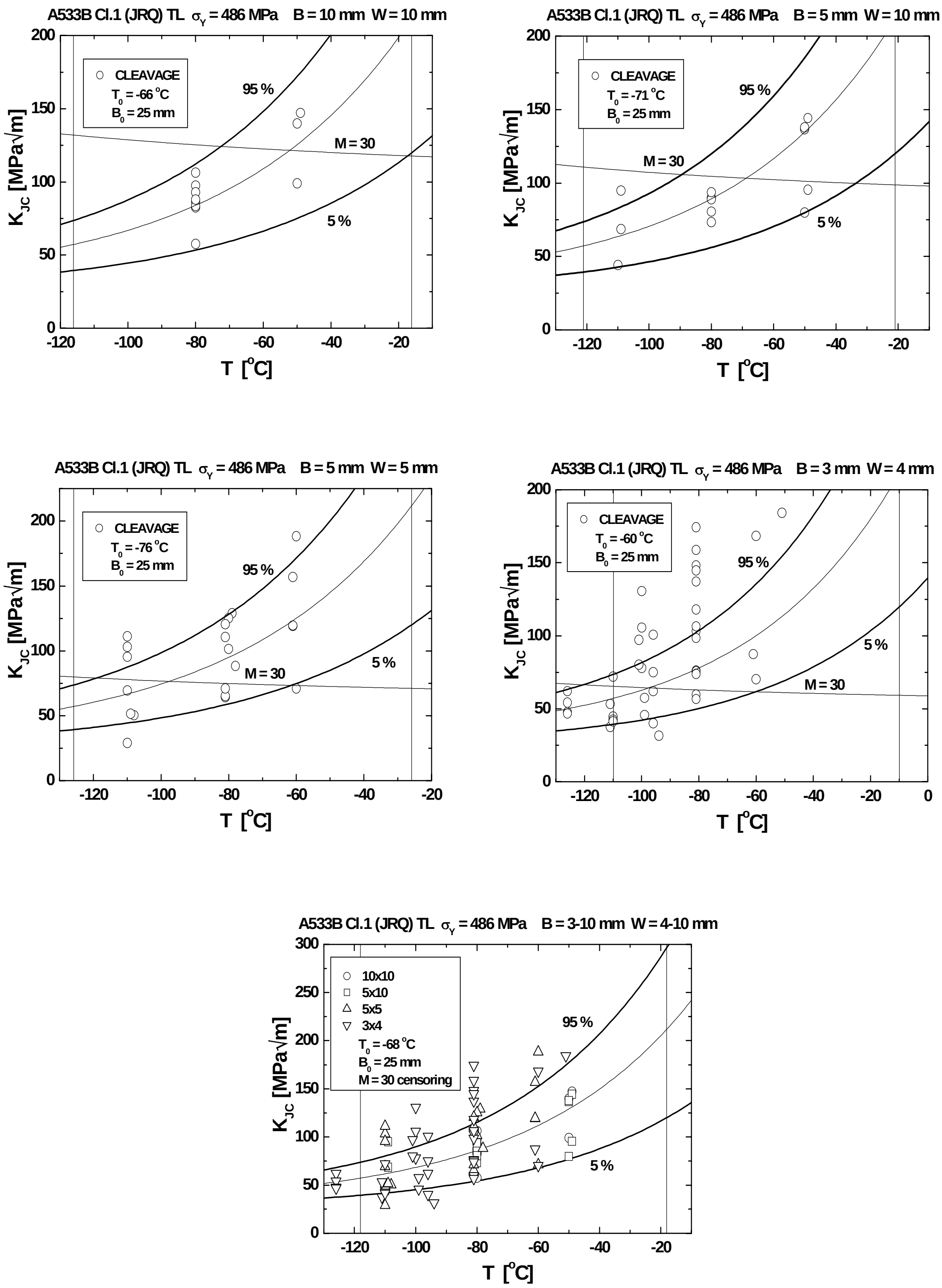

Fig. 5.3: Master Curve analysis of the A533B Cl1 material, [Wallin et al, 2004b].

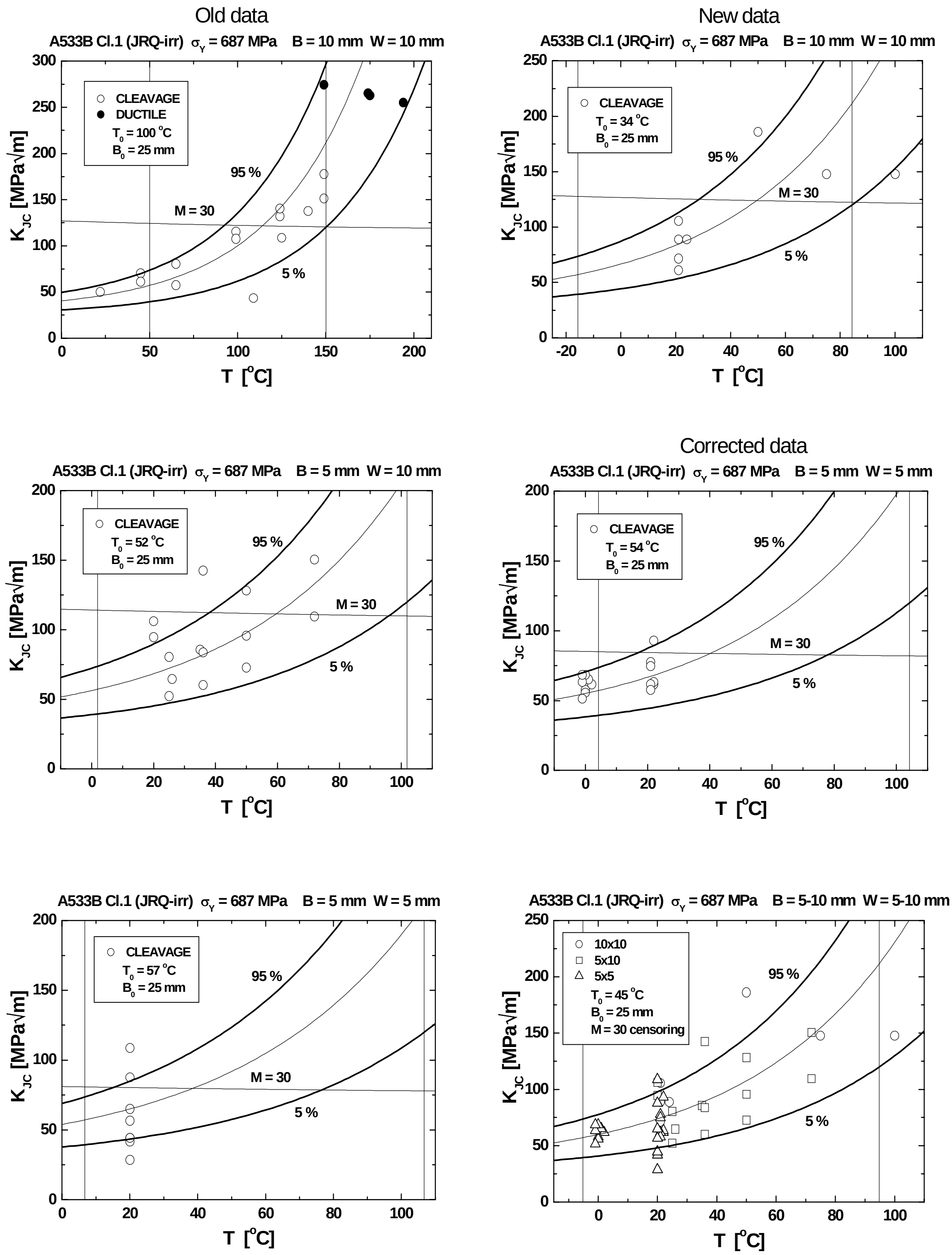

Fig. 5.4: Master Curve analysis of the irradiated A533B Cl1 material, [Wallin et al, 2004b].

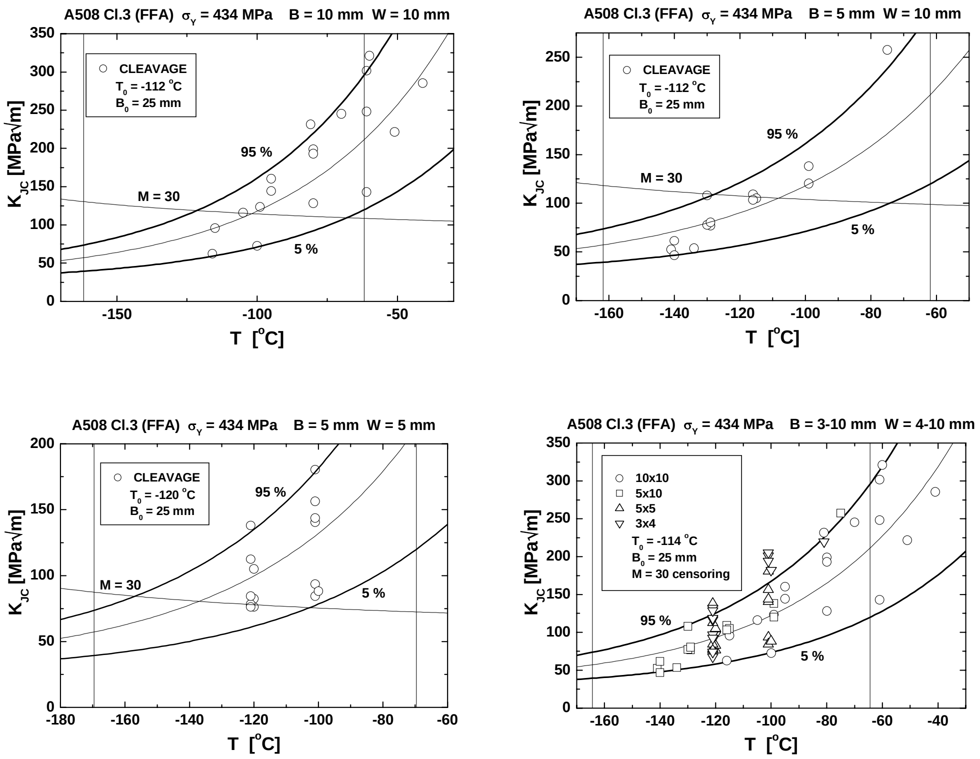

Fig. 5.5: Master Curve analysis of French A508 Cl3 material, [Wallin et al, 2004b].

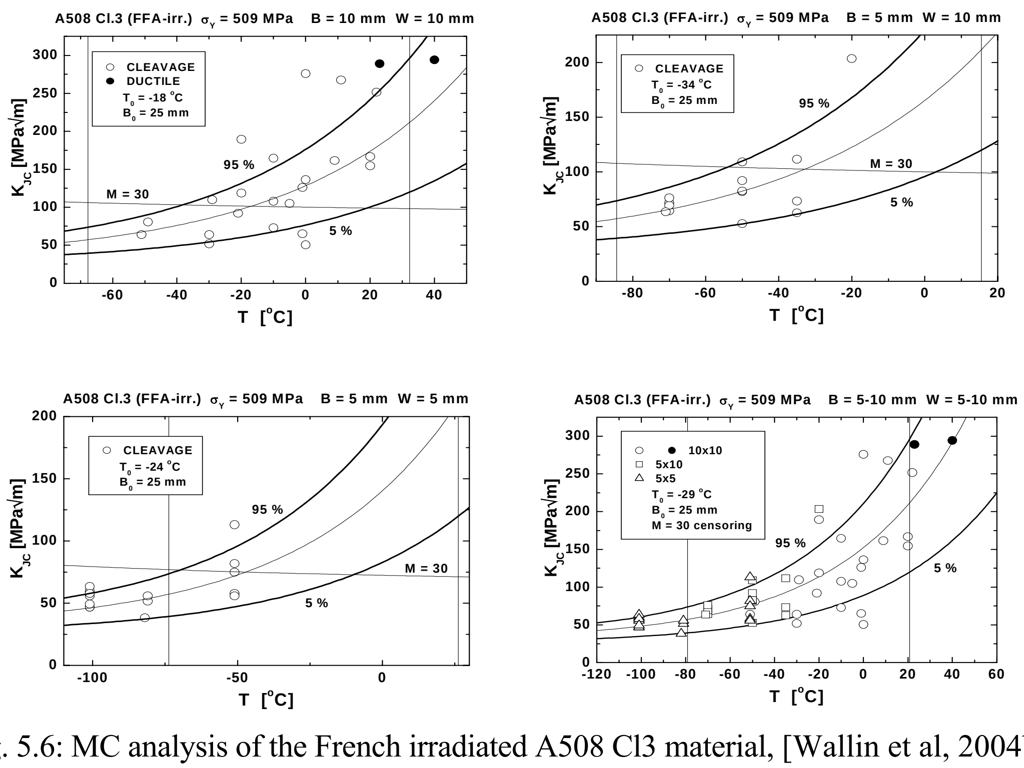

Fig. 5.6: MC analysis of the French irradiated A508 Cl3 material, [Wallin et al, 2004b].

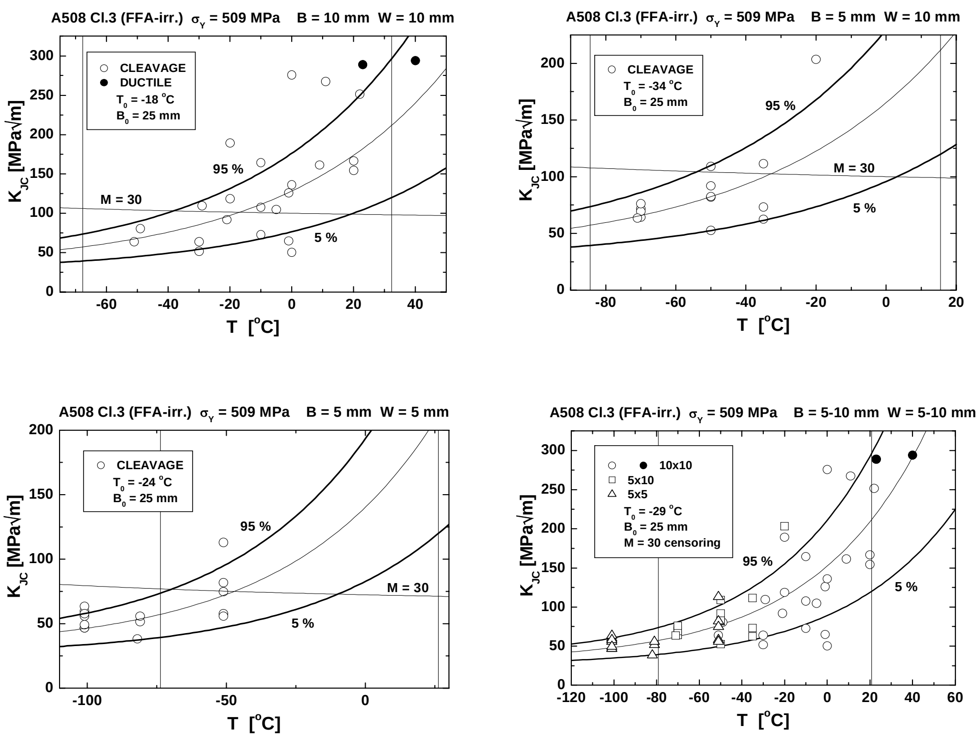

Fig. 5.7: Master Curve analysis of the Japanese A508 Cl3 material, [Wallin et al, 2004b].

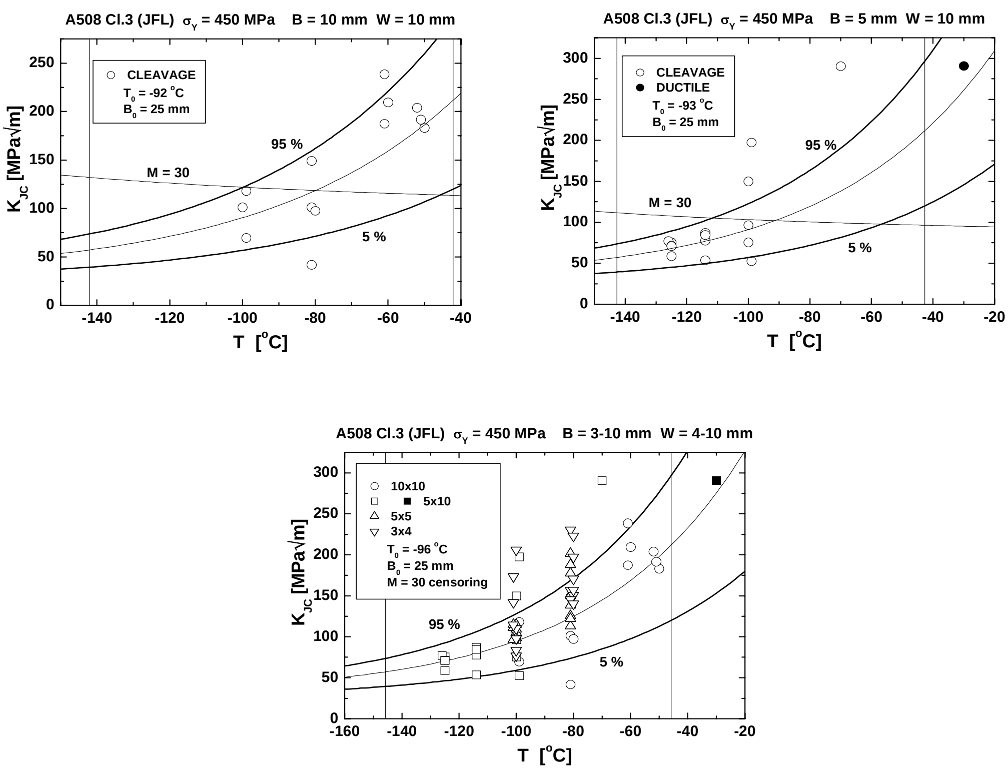

Fig. 5.8: MC analysis of the Japanese irradiated A508 Cl3 material, [Wallin et al, 2004b].

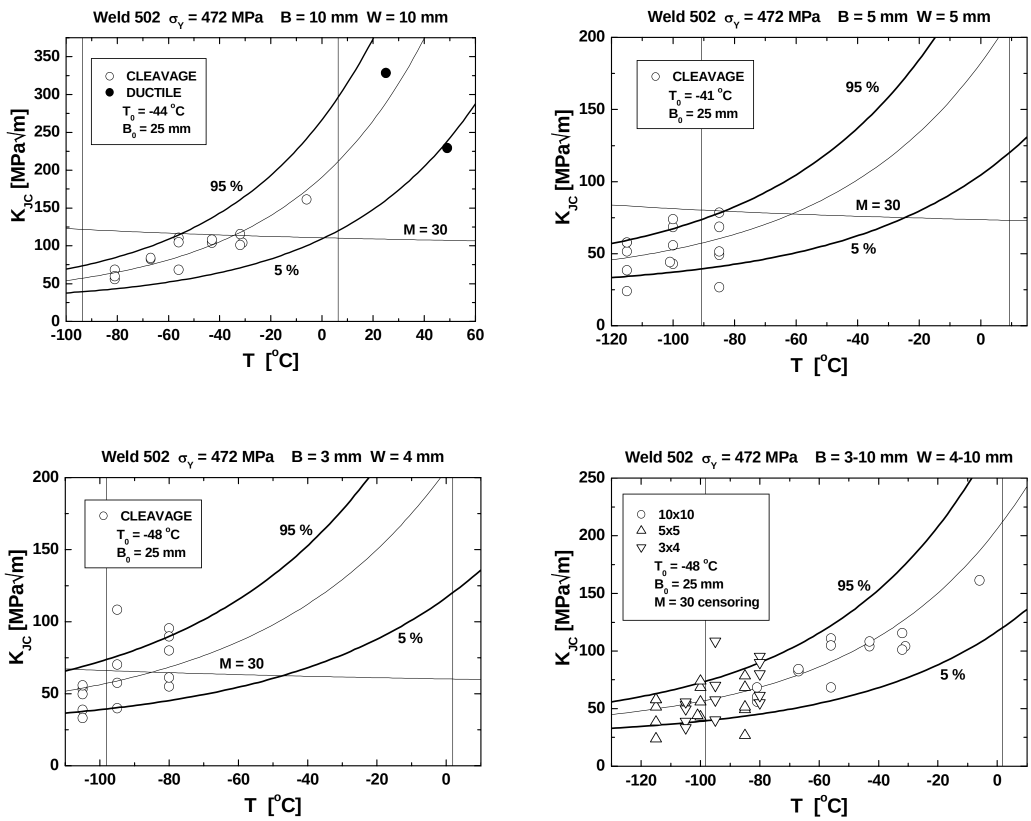

Fig. 5.9: Master Curve analysis of the weld 502 material, [Wallin et al, 2004b].

With the exception of 4 miniature data sets, all the individual sets produced a T_0 estimate (i.e. at least one valid test result) and in 61 % of the sets the number of valid results was sufficient to also produce a valid T_0 estimate. The four data sets with no valid data were included in the calculation of the combined T_0 estimate, thus guaranteeing that the miniature specimen behaviour was accounted also for these materials. For some data sets, with decreasing specimen size there seems to be an increase in scatter, for the 1T-adjusted data. This indicates that the miniature specimens no longer represent a macroscopically homogeneous material. This is, however, not a clear trend. A part of the increased scatter is of course also related to a loss of constraint with the small specimens. However, the lowest fracture toughness values are often measured with the smallest specimens. Thus, it appears that the loss of constraint for the miniature specimens does not begin before the specimen size criterion is violated. Overall, the different specimen sizes produce overlapping scatter bands with only one clear exception, as seen from the combined analysis figures.

The original 13 year old irradiated 10x10 mm specimens of JRQ material (Fig. 5.4) show a very different behaviour than the new 10x10 mm specimens and smaller specimens. The new 10x10 and 5x10 mm specimens and both sets of 5x5 mm specimens behave approximately in the same manner, but the old 10x10 mm specimens showed a more than 50ºC higher T_0 temperature. The reason for this behaviour is not known. The difference is so large, and the fracture toughness values are so low, that it cannot be attributed to constraint effects. This is also verified by the new 10x10 mm specimens. Also, since the different size specimens do not produce overlapping scatter bands, the difference cannot be explained with the fracture toughness temperature dependence. The only difference in the material of the original 10x10 mm specimens and the newer specimens is that the new specimens were tested 10-13 years later than the original 10x10 mm specimens. There is, however, no reason to assume that even such a long storage time at room temperature would improve the fracture toughness of a severely irradiation embrittled material. Experimental errors cannot be ruled out but, based on the performed quality assurance analysis they are unlikely. It is however clear that the original 10x10 mm specimens do not correspond to the same material state as the newer specimens. Therefore, the original 10x10 mm specimen data were not included in the combined estimate of fracture toughness nor in the further comparison of the different specimen sizes. The reason for the improved toughness of the irradiated JRQ material after the long time of room temperature storage requires a further investigation, but this is not included in the present study.

5.2. Test results of other small specimens

To study the use of small specimens in determination of Master Curves, besides VTT's own test results, some data taken from literature were also evaluated. Data related to the high-copper weld 73W (Linde 124) tested by SCK•CSN [Chaouadi, 1998], the HSST 02 plate (A533B Cl.1) tested by ORNL [Sokolov et al, 1998] and four pressure vessel steels, JRQ (A533B Cl.1), KFY5 (A508 Cl.3), KFU4 (A508 Cl.3) and JFL (A508 Cl.3) tested by KAERI [Lee et al, 1999] were analysed by Wallin et al [2004b] using the present method. SCK•CSN tested 10x10, 10x8, 8x8 and 5x8 mm specimens. All specimens were side-grooved. In addition to the SCK•CSN data, also a set of 10x10 mm side-grooved specimens tested at VTT were included in the analysis. The 10x10, 10x8 and 8x8 mm specimens were analysed together as representing only one geometry. ORNL tested 10x10, 5x10 and 5x5 mm specimens. All 5-mm thick specimens were side-grooved, but the 10-mm thick specimens were not side-grooved. KAERI tested 10x10 and 3.3x3.3 mm specimens. The specimens were taken from the 1/4-thickness location in the T-L orientation. None of the specimens were side-grooved. Since the raw data were not available, no quality assurance could be performed on the data. However, the laboratories are very experienced and considered to demonstrate a high level of expertise. The results from this MC analysis are presented in Figs. 5.10 to 5.15. The KAERI T_0 values for 10x10 mm JRQ and JFL are -67ºC and -97ºC, respectively. These values are practically identical with the VTT values of -66ºC and -96ºC. This renders trust in the quality of the results.

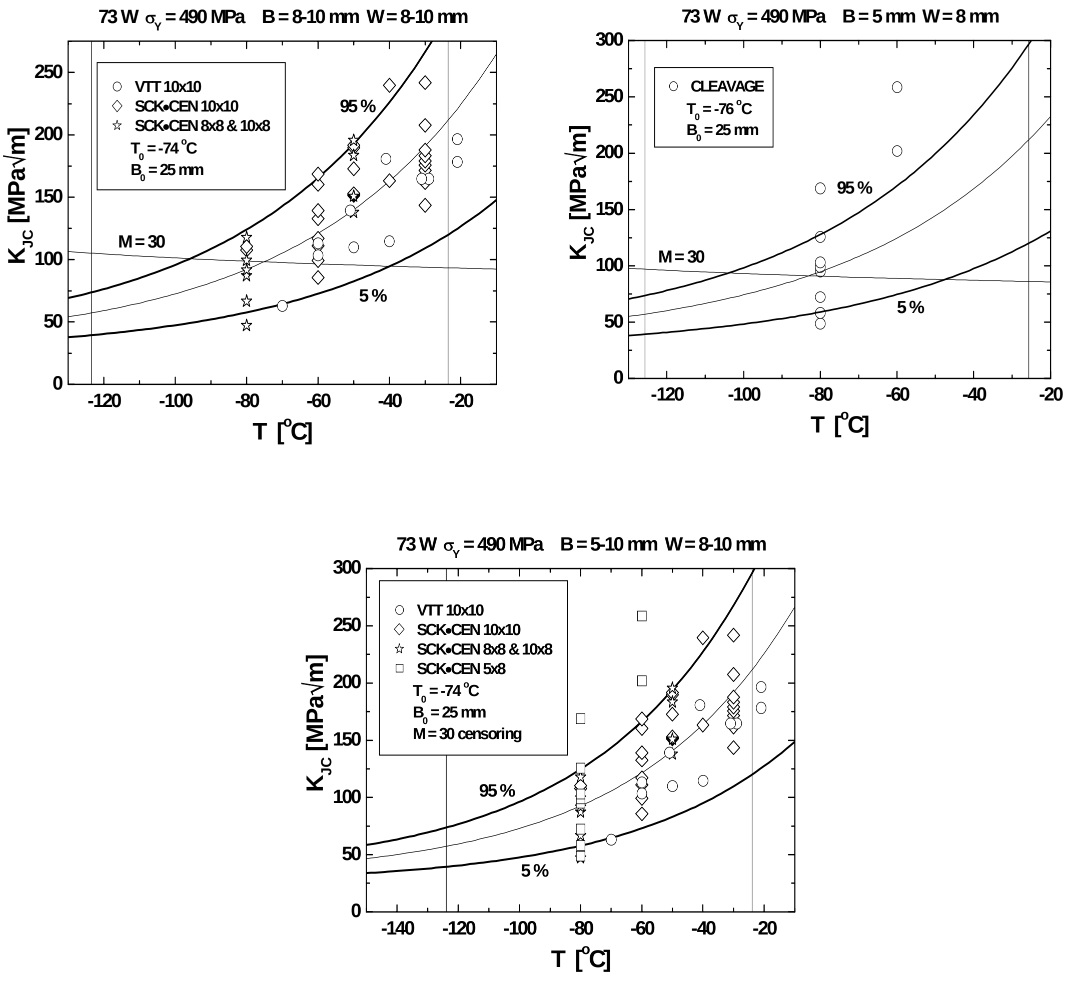

Fig. 5.10: Master Curve analysis of the weld 73 material, [Wallin et al, 2004b].

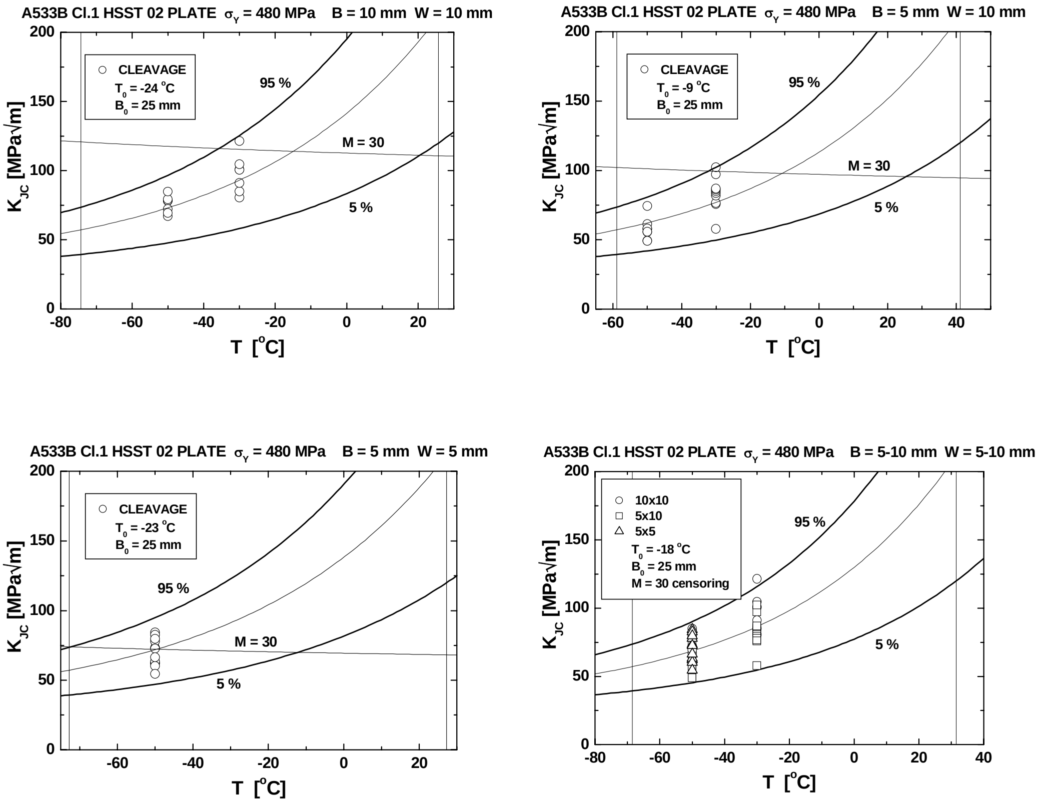

Fig. 5.11: Master Curve analysis of the A533B Cl1 HSST 02 material, [Wallin et al, 2004b].

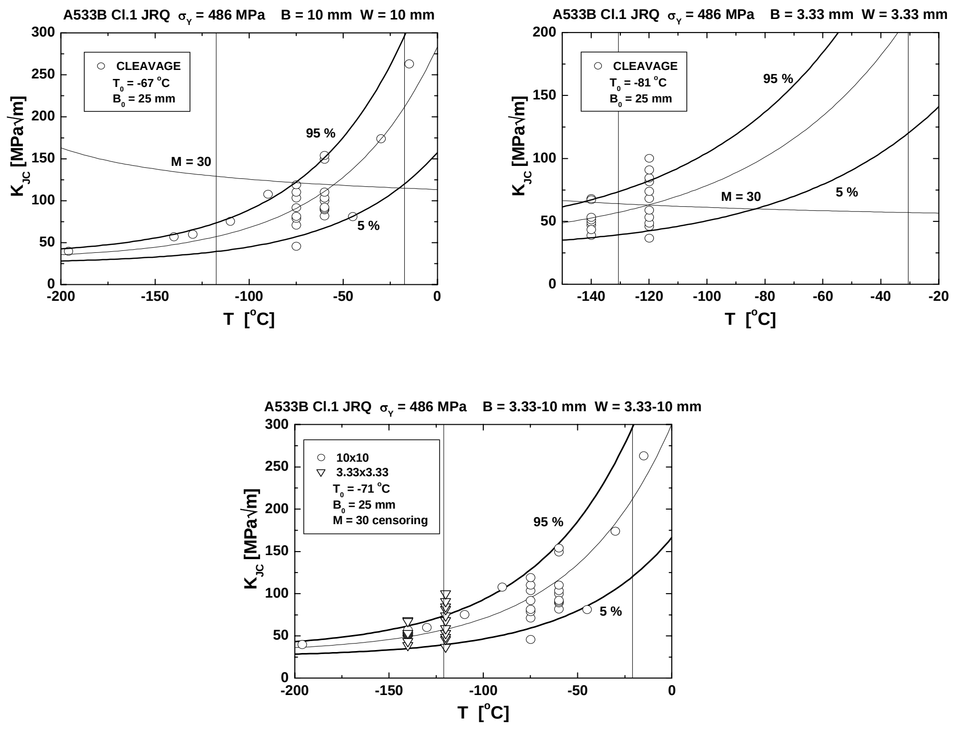

Fig. 5.12: Master Curve analysis of the A533B Cl1 JRQ material, [Wallin et al, 2004b].

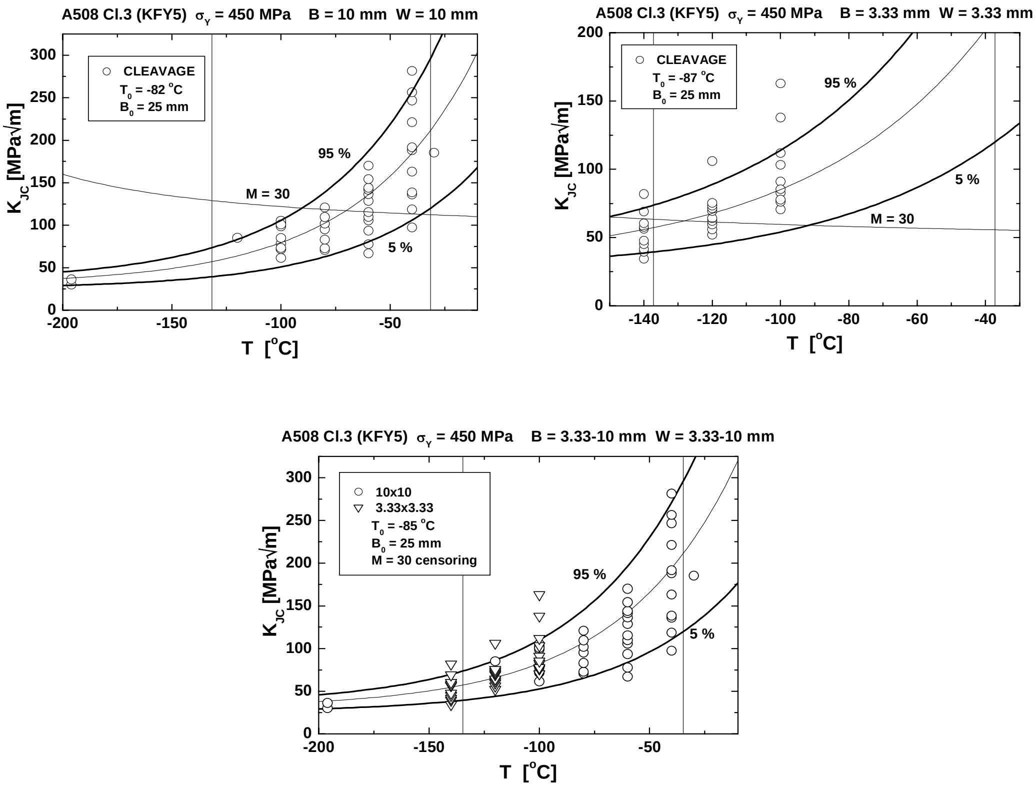

Fig. 5.13: Master Curve analysis of the A508 Cl3 KFY5 material, [Wallin et al, 2004b].

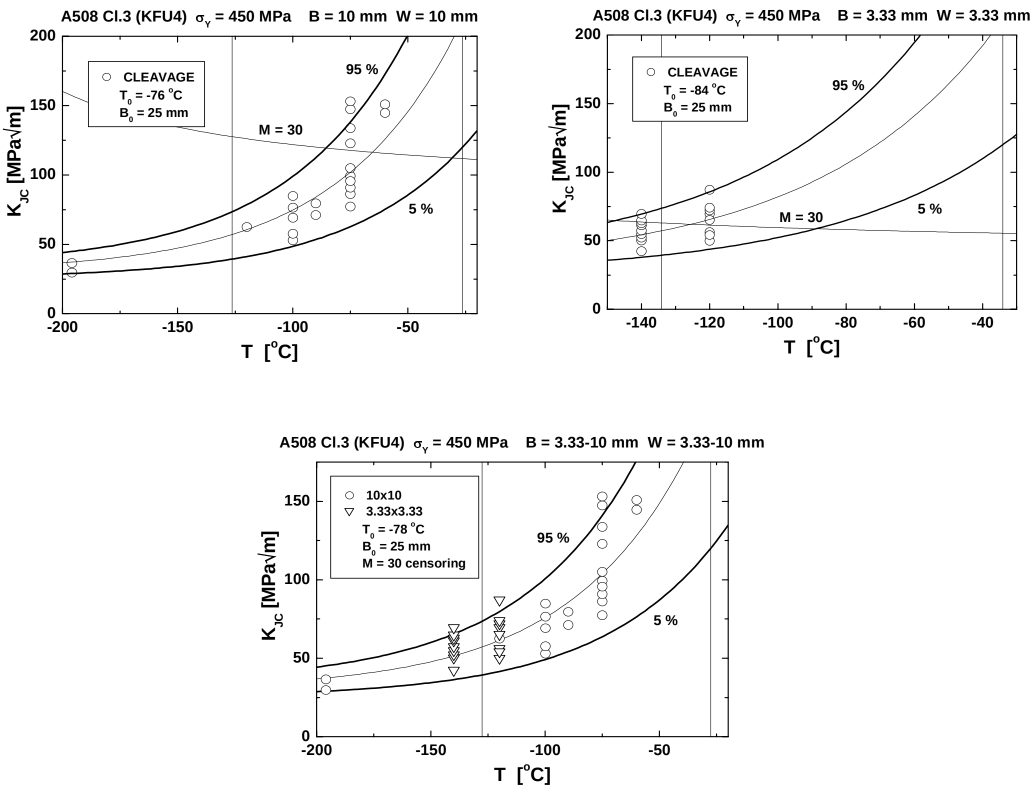

Fig. 5.14: Master Curve analysis of the A508 Cl3 KFU4 material, [Wallin et al, 2004b].

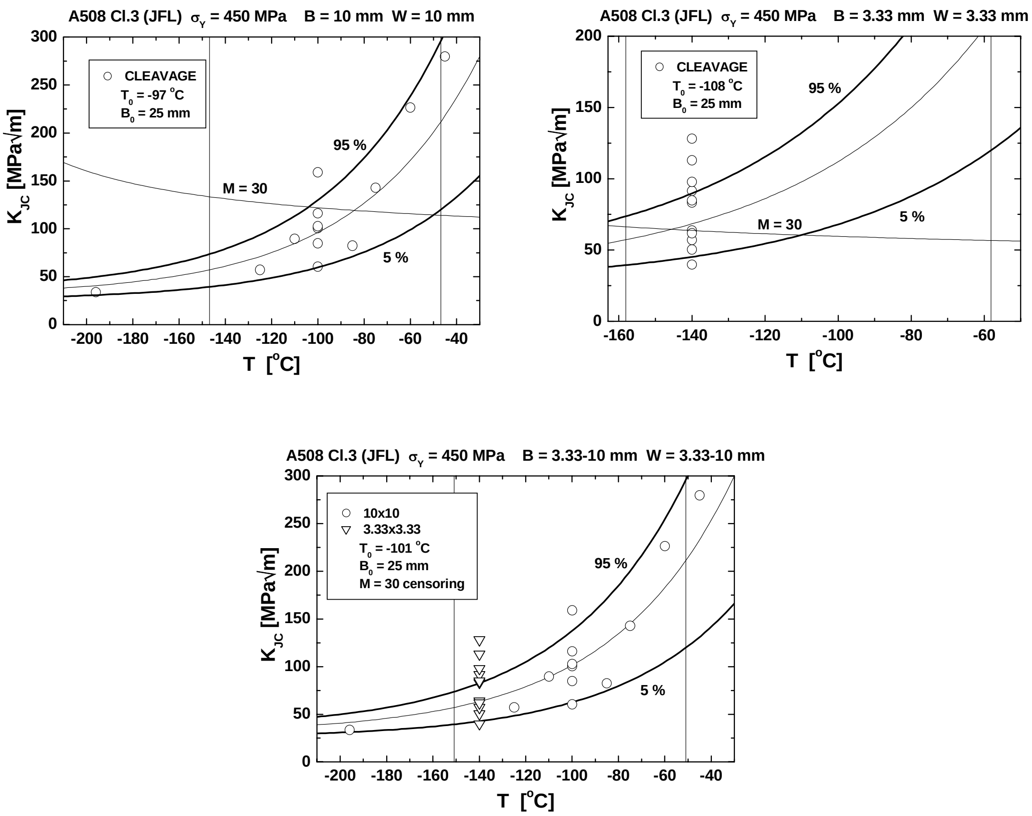

Fig. 5.15: Master Curve analysis of the A508 Cl3 JFL material, [Wallin et al, 2004b].

The applicability of the different specimen sizes was investigated by comparing the individual results to the overall behaviour of the different materials. Generally, the estimates actually fall within ±10ºC scatter bands, practically regardless of the number of valid results. Table 5.2 contains a compilation of the offset behaviour of the different specimens. Almost the same result is obtained for the 10x10, 5x10 and 5x5 mm specimens. The scatter for the 5x5 mm specimens is larger than for the 5x10 mm specimens, but the number of valid results is on the average fewer than for the 5x5 mm specimens. There seems to be a systematic difference between the 3x4 and 3.3x3.3 mm specimens. This difference is likely to be attributed to the side-grooves. The 3.3x3.3 mm specimens, which were tested without side-grooves, had a tendency to produce somewhat lower T_0 estimates. It seems that side-grooving is needed for such a small specimen thickness. An interesting detail is that the 3x4 mm specimens actually have a tendency to yield higher T_0 estimates. This is attributed to the fact that the T_0 estimate for these specimens is based on the lower tail of the fracture toughness distribution (the upper tail is censored). Therefore these specimens reflect the most brittle material being tested. Besides material inhomogeneity, also statistical outliers will cause the T_0 estimates for these small specimens to show a trend of higher values than measured with larger specimens, since high toughness outliers will be censored.

Table 5-2: Comparison of T_0 estimates from different specimen sizes.

Specimen type	Average offset T_0-T_{0All} ºC	Standard deviation of T_0-T_{0All}	Average number of valid data in sets (r)
10x10	-0.8	6.9	9.8
5x10	+0.9	4.7	10.2
5x5	+3.1	7.6	5.6
3x4 (3.3x3.3)	+1.9	10.7	4.2

The accuracy of the T_0 estimate should be dependent upon the number of valid results. This is presented in Fig. 5.16, where the experimental offset is plotted as a function of r (number of valid tests). Also included in the figure are the theoretical 5 % and 95 % confidence bounds for a homogeneous material. Generally the experimental results scatter as predicted. Interestingly, even data sets with $r < 6$ actually fall within the ±10ºC scatter bounds.

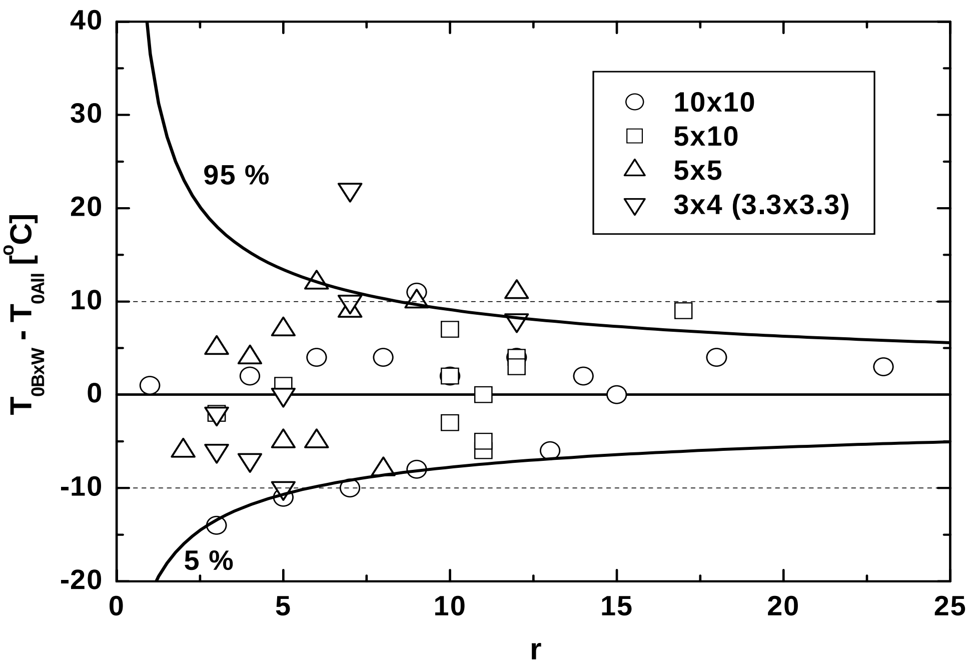

Fig. 5.16: The accuracy of T_0 estimate related to the number of valid tests, [Wallin et al, 2004b].

Based on this study, it is clear that the miniature bend specimens studied are applicable to determine the Master Curve T_0. For this data set, the optimal testing temperature is in the range -50ºC ≤ T- T_0 ≤ -20ºC. More specimens must be tested as their size decreases, but the overall material needed is reduced. Table 5.3 gives an estimate of the number of specimens needed to obtain a valid T_0 estimate for a steel with a yield strength of 500 MPa. It turns out that, based on material needed, the most efficient specimen size is 5x5 mm. With this specimen size the amount of material needed corresponds to 1.5 times a normal Charpy specimen. This is sufficient to give a valid T_0 estimate, having the same degree of accuracy as determined by 7 normal Charpy specimens.

Table 5-3: Number of specimens needed to produce a valid T_0 estimate.

Specimen type	Number of specimens needed	Amount of material as CVN equivalent
10x10	7	7
5x10	7	3.5
5x5	12	1.5
3x4	28	2.5
3.3x3.3	40	2.5

In addition to study miniature size specimens in development of Master Curve, a comprehensive study on larger laboratory specimens has been performed by Wallin [1998], where a nuclear grade pressure vessel forging of type 22NiMoCr37 (A508 Cl.3) has undergone extensive fracture toughness testing. The tests were performed on standard geometry CT-specimens having thickness of 12.5 mm, 25 mm, 50 mm and 100 mm. The *a/W*-ratio was close to 0.6 for all specimens. One set of specimens was 20% side-grooved. A total of 757 results fulfilling the ESIS-P2 test method validity requirements with respect to pre-fatigue crack shape and the ASTM E-1921 pre-fatigue load, were obtained. The master curve statistical analysis method was applied extensively on the data, in order to verify the validity of the method. The summary results of this study are presented in Fig. 5.17. Some of the main conclusions of this study regarding the validity of the master curve method for the studied reactor pressure vessel steel are as below:

- The Master Curve assumptions on data scatter, size effect, minimum fracture toughness and temperature dependence are valid.
- Testing should include several test temperatures, in order to minimise any effects from a possible small deviation from the master curve temperature dependence.
- The master curve specimen size requirement in E1921-03 is valid.
- Determination of T_0 should be based on test results in the temperature range -50°C $\leq T - T_0 \leq$ +50°C.
- If only approximate (lower bound type) information regarding the fracture toughness is required, the master curve can well be extrapolated outside the range -50°C $\leq T - T_0 \leq$ +50°C.
- If an accurate description of the fracture toughness outside this temperature range is required, tests should preferably be performed at the specific temperature of interest. The master curve analysis method (excluding the temperature extrapolation) can be used also in this case for the description of scatter and size effects.

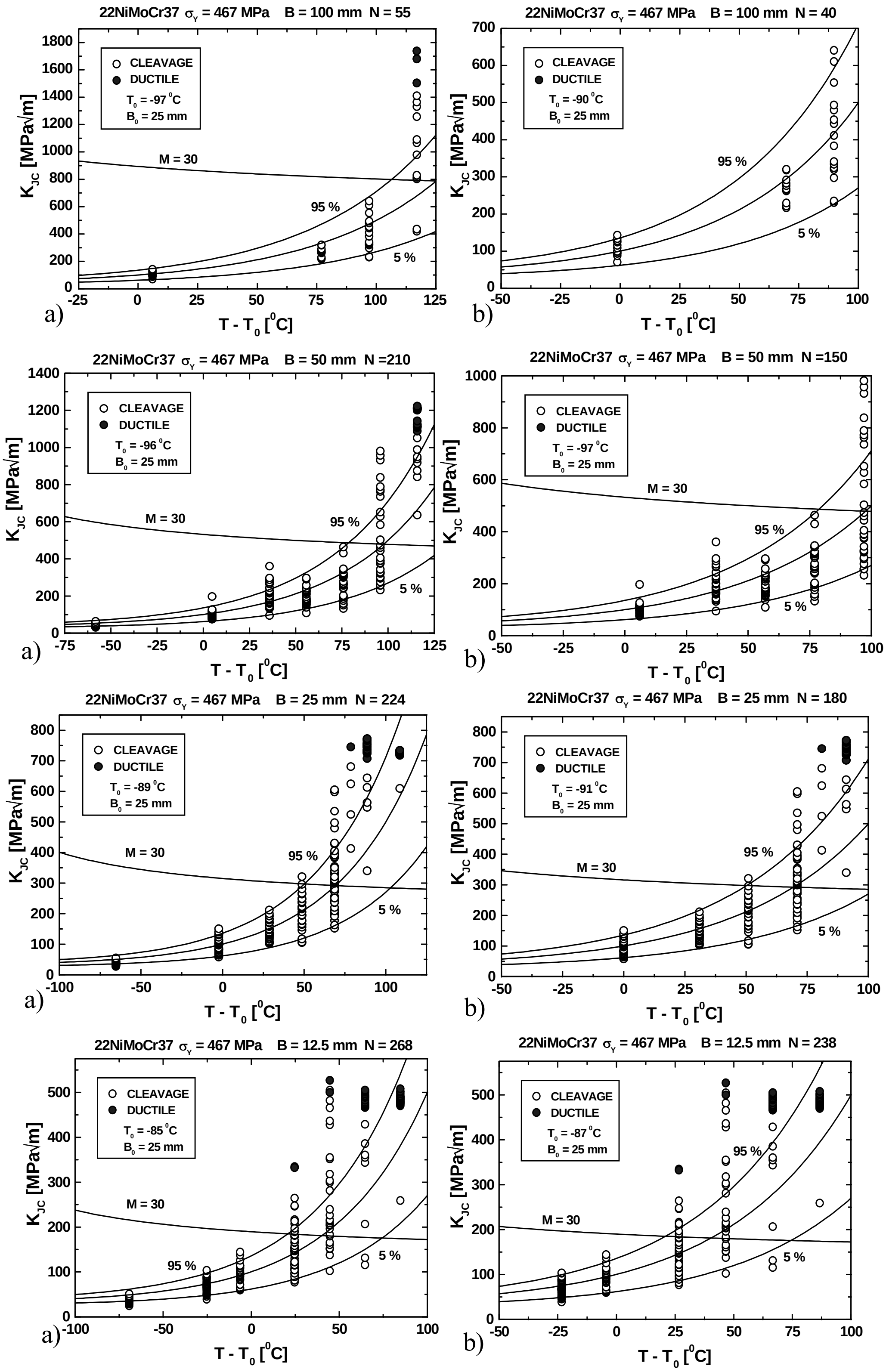

Fig. 5.17: MC analysis of a A508 Cl.3 material using specimen thickness of: (a) 100 mm, (b) 50 mm, (c) 25 mm and (d) 12.5 mm, [Wallin, 1998]. Using all data are presented in the left figures and using data in the range -50°C ≤ T_0 ≤ +100°C in the right figures, respectively

5.3. Comparison of CT- and 3PB-specimens

There has been a discussion related to the possible difference between three-point-bend (3PB-) and compact tension (CT-) specimens. The CT-specimens have a higher positive T_{stress} than the 3PB-specimens (Sherry et al, 1995]. If a positive T_{stress} influenced the fracture toughness similarly to negative ones, CT-specimens could be predicted to produce higher T_0 values than 3PB-specimens. Any systematic comparison on the effects of geometries has not been published to date.

Data from the literature, combined with VTT's own data, were used for this comparison. The Master Curve analysis of the data was performed as described earlier for the miniature size bend specimens. The data sets are identified in Table 5.4 together with the results of the Master Curve analyses. For the analysis of the T_0 difference between the two specimen geometries, the individual sample sizes had to be accounted for. This was done by defining an effective number of valid results (r_{eff}) for each material depending on the combined number of valid results. The equation for r_{eff} is as given by Eq. (5-2).

$$r_{eff_i} = \frac{r_{3PB_i} \cdot r_{CT_i}}{r_{3PB_i} + r_{CT_i}} \tag{5-2}$$

The mean temperature difference , $\Delta\overline{T}_0$, is then obtained from Eq. (5-3):

$$\Delta\overline{T}_0 = \frac{\sum_{i=1}^{N} \Delta T_{0i} \cdot r_{eff_i}}{\sum_{i=1}^{N} r_{eff_i}} \tag{5-3}$$

It follows that the theoretical standard deviation of the temperature difference, at a toughness level close to T0, is of the form Eq. (5-4):

$$\sigma_{\Delta\overline{T}_0} \approx \frac{18°C}{\sqrt{\sum_{i=1}^{n} r_{eff_i}}} \tag{5-4}$$

The resulting offset for the data in Table 5.4 is 8.1ºC. This means that the CT specimen geometry produces on the average 8ºC higher T_0 values than 3PB specimens. 1-2ºC of this offset can be explained by the fact that a plastic η-factor of 2 has generally been used with the bend specimens. ASTM E1921 use a value of 1.9 which produces slightly higher T_0 estimates. Even then there still remains an offset of about 6-7ºC between the two specimen geometries. The information in Table 5.4 is visualised in Fig. 5.18.

The theoretical standard deviation (based on r_{eff}) for ΔT_0 is 6.1ºC. The experimental standard deviation is 8.0ºC, which indicates that the uncertainty in the offset is 5.2ºC. This value includes the uncertainties related to test performance, material and the offset itself. Overall, the offset appears to be rather well defined. The ratio of valid results to all results does not have a noticeable effect on the offset, indicating that specimen size, or loading level, does not have a significant effect on the result.

Wallin [15] developed an experimental T_{stress} correction for the Master Curve for shallow cracked bend specimens. He established an approximate relation of the form given in Eq. (5-5):

$$T_0 \approx T_{0deep} + \frac{T_{stress}}{10\,MPa/°C} \quad : \text{for } T_{stress} < 0 \qquad (5\text{-}5)$$

From an engineering assessment point of view, both the CT- and 3PB-specimens should be taken to represent a $T_{stress} = 0$ constraint level. Based on the present state of knowledge any additional corrections (e.g. correcting the 3PB-results to correspond to CT geometry) are not considered necessary, since this might just lead to new non-quantifiable uncertainties. In the future, when the effect of T_{stress} on the fracture toughness is better quantified, such a correction should be pursued.

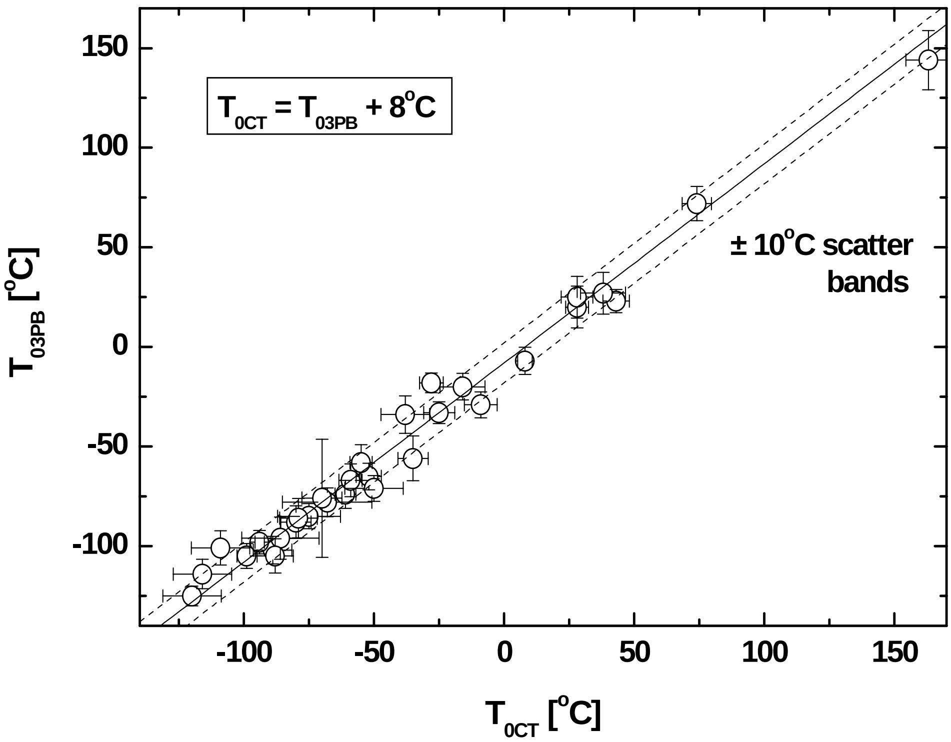

Fig. 5.18: Comparison of T_0 estimates from CT and 3PB specimens, [Wallin et al, 2004b].

Table 5-4: Materials for comparison of CT- and 3PB-specimen results.

			CT specimens				**3PB specimens**			
Material	Ref.	σ_Y MPa	B mm	T_0 ºC	r	n	B mm	T_0 ºC	r	n
A515	28	295	25	-16	12	24	10	-20	20	37
A533B Cl.1	28	617	12.5-25	-52	38	39	10	-65	20	23
A533B Cl.1	28	488	25	-80	26	26	10	-88	13	16
A533B Cl.1	25	462	12.5-50	8	111	111	10	-7	19	40
A508 Cl.3	29	414	12.5	-89	16	27	10-200	-102	18	129
A508 Cl.3	27	450	12.5	-109	7	8	3-10	-101	12	24
A508 Cl.3	27	450	25	-68[1]	3	3	3-10	-78	17	39
A508 Cl.3	27	450	25	-75	6	6	3-10	-85	22	73
A533B Cl.1	27	486	12.5	-50	7	7	3-10	-71	21	44
A533B Cl.1	30-33	450	12.5-150	-25	25	44	3-10	-33	30	115
73 W	25,34	490	25-200	-61	54	78	10	-74	18	58
A533B Cl.1	30,31,35	480	25-150	-28	42	83	10	-18	36	44
10MnMoNi 5	36	630	25-100	-79	17	27	25	-86	9	17
2¼Cr-1Mo	37,38	280	25	28	45	58	10	20	8	18
A508 Cl.3	39	434	12.5-100	-116	7	38	3-10	-114	16	63
A508 Cl.3 Irr.	39	509	12.5	-9	22	27	5-10	-29	21	54
WF70 Weld	40	512	12.5-100	-55	49	65	10	-58	11	14
WF70 Noz. W.	40	545	12.5-25	-35	26	32	10	-56	7	7
WF70 W. Irr.	41	646	12.5-25	28	24	35	10	25	8	10
A533B Cl.1	42,43	480	12.5-25	-99	65	124	10-230	-105	23	223
A302B	13	534	12.5-25	74	28	28	10	72	12	12
A508 Cl.2	44	467	12.5-100	-94	273	757	10	-98	26	59
73 W Irr.	34,45	660	25-100	43	34	46	10	23	26	30
72 W	34,46	505	25-200	-59	44	76	10	-67	13	22
15X2MϕA	46	590	25	-120	7	15	3-10	-125	36	90
15X2MϕA LT	46	600	25-75	-86[1]	4	6	10-25	-96	8	14
15X2MϕA SL	46	600	12.5-100	-70	15	30	10-25	-76[1]	1	8
15X2MϕA	46	880	25	163	12	14	10	144[1]	4	5
Cb10XMFT	46	400	12.5-100	-38	10	15	10-150	-34	10	17
Cb10XMFT Irr.	46	600	12.5	38	12	15	10	27	8	10
A533B Cl. 1	47	488	25	-88	18	18	10	-105	12	18

[1]Defined as T_Q by E1921

6. MASTER CURVE ANALYSIS OF LARGE SCALE EXPERIMENTS

The validity of the Master Curve methodology is examined here by applying the methodology for prediction of fracture events in different large scale experiments. There are limited experiments, which are conducted with good quality and also documented with enough details available in the open literature. Ten experiments are chosen for this validation exercise. It covers thermal shock experiments (TSE) performed at Oak Ridge National Laboratory (ORNL) in USA and at Framatome in France, experiments conducted within the NESC projects and also the experiment related to study on the fracture behaviour of the Swedish Oskarshamn 1 reactor. These selected experiments are:

Experiments TSE-2, TSE-3, TSE-5, TSE-6 and TSE-7: These are experiments chosen from the eight thermal shock experiments of pressure vessels conducted at ORNL within the Heavy-Section Steel Technology (HSST) program.

Experiment TSE-Fr: This is a thermal shock experiment conducted at Framatome.

Experiments NESC-I, NESC-II and NESC-IV: These are experiments chosen from the NESC research activities coordinated by JRC in the Netherlands related to structural integrity of nuclear components.

Experiment O1: This is an experiment related to the study on the fracture behaviour of the Swedish Oskarshamn 1 reactor under cold pressurization.

The main objective of all these experiments has been to study the cleavage fracture events in the transition region. With exception of tests O1 and NESC-IV, all other tests are pressurized-thermal shock experiments on thick-walled cylinders. Tests O1 and NESC-IV are conducted on large beams under mechanical uniaxial and biaxial loading.

The main information of these experiments is summarized in Table 6.1. Here, $T_{0(25)}$ is the Master Curve T_0 evaluated from the standard 25-mm specimens. In general, the crack growth initiation event is chosen as the failure event in the analysis of these experiments based on the Master Curve methodology. The main outcomes of these experiments and the assessment results are briefly described in the following.

Table 6.1: Main data of the experiments used in the validation of the MC methodology.

Test	Material	*a/t* [mm/mm]	*2c* [mm]	RT_{NDT} [°C]	$T_{0(25)}$ [°C]
TSE-2	A508Cl2	19/152	38	75	56
TSE-3	A508Cl2	11/152	914	75	101
TSE-5	A508Cl2	16/152	1220	66	27
TSE-6	A508Cl2	7/76	1220	66	27
TSE-7	A508Cl2	14/152	37	-1	-27
TSE-Fr	A508Cl3	17/230	1000	-7	17
NESC-I	A508Cl3	76/170	205	134	68
NESC-II	17MoV84	20/189	59	140	60
O1	A508Cl3	20/80	60	72	30
NESC-IV	A533GB	19/102	53	-35	-83

6.1. Experiment TSE-2 at ORNL

TSE-2 is a thermal shock experiment on a thick-walled pressure vessel with a wall thickness of 152 mm, [Cheverton, 1976]. The fracture mechanical material characterization of TSE-2 was based on small specimen K_{IC} and K_Q results. The specimens used were Charpy-V-sized bend specimens (CVN_{pc}) and 10, 25 and 50 mm compact tension specimens (CT). No separation was made between valid K_{IC} results corresponding to brittle fracture and K_Q results corresponding to yielding or ductile tearing. Thus, it was impossible to perform a detailed statistical analysis on the whole data set. An approximate analysis was performed applying only temperatures where the data clearly correspond to brittle fracture.

After 36 s into the transient, the crack propagated at the upper end. A second initiation, at the lower end occurred after 86 s into the transient. The first initiation grew the crack essentially in the axial direction. The resulting ”intermediate” crack had a clearly non-symmetrical profile that was not modelled in the analysis. Therefore, only the first initiation has been included in the re-evaluation. Because it was a semicircular crack, the stress intensity factor (K_I) distribution and the temperature (T) distribution varied strongly along the crack front. The combination of maximum K_I and minimum T occurred at the edge of the crack. This is the reason for the axial propagation. At the time of initiation (36 s) WPS is not yet active. The actual un-corrected test data is presented in Fig. 6.1a. The TSE-2 result refer to maximum K_I and minimum T occurring along the crack front at the time of initiation. The TSE-2 result appear to be described by the mean behaviour of the CVN_{pc} specimens, but it is higher than predicted by the larger CT specimens. The test result could be explained with constraint arguments, but the statistical size effect argument is equally applicable. The portion of the crack front experiencing maximum K_I and minimum T is obviously only a small portion of the whole crack front. The effective crack front length for TSE-2 is likely to be closer to 10 mm than to $19 \cdot \pi$ mm which is the total crack front length.

For surface cracks, it may be difficult to visualize the total crack front length. A more simple measure for the crack front length is $2 \cdot c$, i.e. the projection of the true crack front length. For normal loading cases where the temperature along the crack front is constant, a combination of $2 \cdot c$ and the maximum K_I is from a statistical stand point accurate to within 10 % compared to a more detailed analysis of the crack front. However, in the case of a thermal shock, one must also account for the temperature distribution along the crack front. For the re-evaluation of TSE-2, the effective thickness was fixed to $2 \cdot c$, but instead of using the maximum K_I and the minimum T, effective average values were used. The effective average values were estimated with respect to K_I^4 and $\exp\{-0.019 \cdot T\}$ in order to achieve an averaging in terms of the statistical model and the Master Curve.

The outcomes of this test are re-evaluated by Wallin [1995] based on the Master Curve methodology. The size corrected ($2 \cdot c$) TSE-2 data is presented in Fig. 6.1b. Again, the statistical size correction brings the material characterization data more closely together. The re-evaluated TSE-2 result is slightly below the mean Master Curve, but it still corresponds to more than a 30 % failure probability. Thus, the application of the statistical brittle fracture model together with the Master Curve would yield a fully satisfactory description of TSE-2.

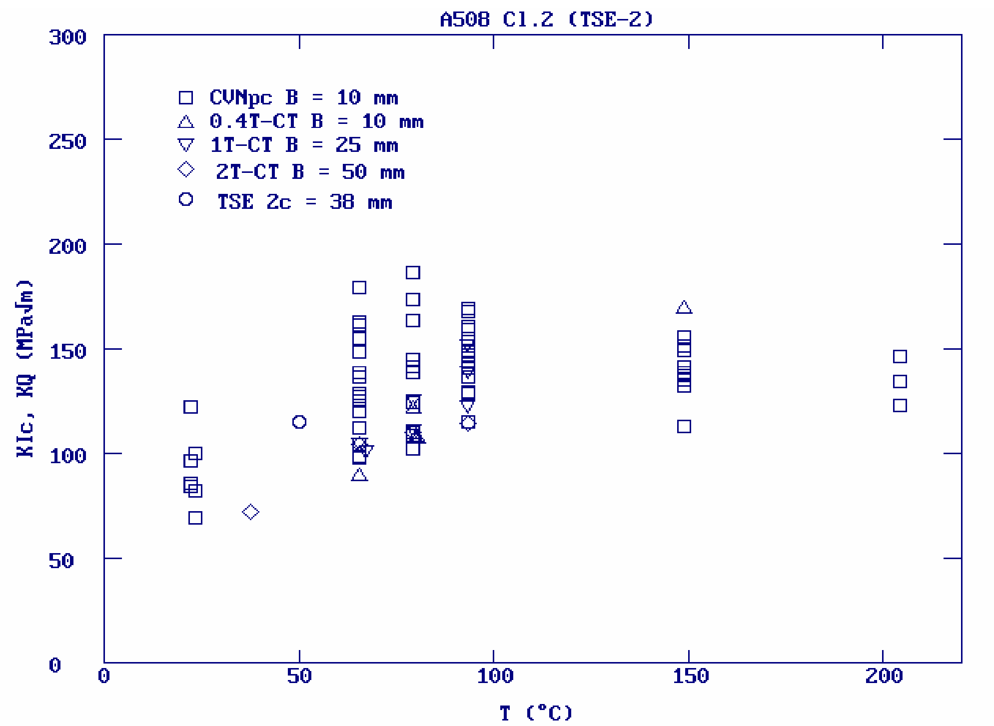

(a) Un-corrected TSE-2 data.
(a)
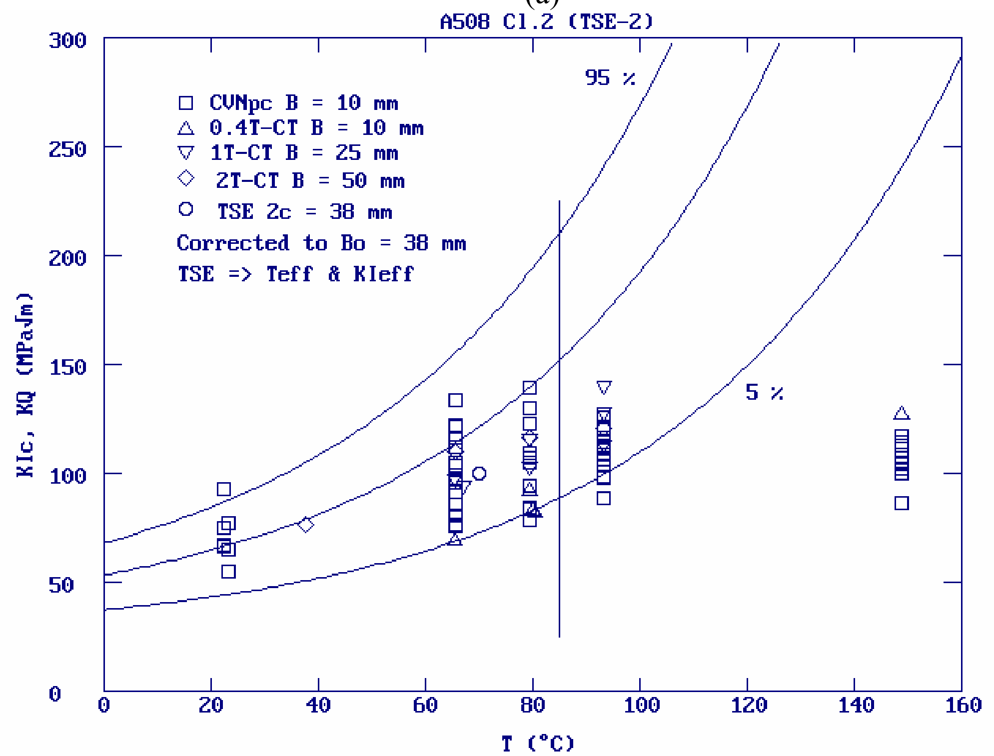

(b) Size corrected TSE-2 data.

Fig. 6.1: Un-corrected and size-corrected data of the TSE-2 test. The test results correspond to average K_I and average temperature.

6.2. Experiment TSE-3 at ORNL

TSE-3 is a thermal shock experiment on a thick-walled pressure vessel with a wall thickness of 152 mm [Cheverton and Bolt, 1977]. TSE-3 was a repetition of TSE-1, using the same crack but applying a stronger thermal shock transient. In connection with the analysis of TSE-1, two core holes were born from the flaw zone. The holes were plugged with snug fitting bars that were seal-welded at the outer surface. The possible effect of the holes on the stress intensity factor was not estimated quantitatively. They were however expected to cause ”premature” crack initiation during the test. The analysis of the test proved difficult. All four operational crack opening displacement (COD) gages gave different indications as to the time of crack initiation. No attempt to define the likely initiation K_I and T was made. It was only concluded that it seemed reasonable that the presence of the core holes had a significant effect on crack propagation, and it is not possible to determine whether the flaw would have initiated in the absence of the core holes. However, the fractography revealed that the crack did not propagate at the edges of the holes. This was attributed to a free surface effect that more than compensate for the stress concentration around the holes. This is somewhat contradicting to the earlier conclusion regarding the effect of the holes. A re-evaluation of the test indicate that, from the point of crack growth initiation the core holes have not played a significant role and therefore an attempt to estimate the likely initiation K_I and T can be made.

Gage XE-31 indicated a relatively large crack opening very early (24 s) in the transient. At this time, the temperature at the crack tip was above 200 °C, making brittle fracture quite unlikely. None of the other gages reacted at this time. Also, the acoustic emission (AE) data do not indicate significant crack growth at this time. A comparison of the fracture surface corresponding to the flaw region in the vicinity of XE-31 with fracture surfaces form Charpy-V specimens indicated that the temperature at fracture has been close to 100 °C. Thus, the first indication of crack initiation is ruled as non-significant.

Gage XE-32 opened at 110 s into the transient. Approximately at the same time there was a reaction also in the other operational gages and the AE data indicated major crack growth. The time 110 s appear to be the likely time of crack initiation. At this time WPS is not yet active. The actual un-corrected test data are presented in Fig. 6.2a. There was a later indication with gage XE-34 at 178 s, but this is unlikely to correspond to first initiation. Since the propagation of the crack was not monitored more accurately, it is not possible to conclude whether the crack at the location of XE-34 had grown prior to 178 s. Therefore this latter indication was not included in the re-analysis.

The outcome of this test are analysed by Wallin [1995] based on the Master Curve methodology. Fig. 6.2a indicates that the material characterization data overestimate the behaviour of TSE-3. However, performing a statistical size correction (2·c) and applying the Master Curve yield a fully satisfactory description of TSE-3, Fig. 6.2b. The likely first initiation corresponds very close to a 50 % failure probability.

6.3. Experiments TSE-5 and TSE-6 at ORNL

TSE-5 and TSE-6 are thermal shock experiments on two thick-walled pressure vessels [Cheverton et al, 1985]. These experiments utilized essentially identical material and flaw lengths. Their main difference is the plate thickness, which for TSE-5 is 152 mm and for TSE-6 is 76 mm. The fracture mechanical material characterization was more advanced, than for the earlier tests, in that the elastic plastic K_J parameter was used. However, no separation was made between tests ending in cleavage fracture or tests corresponding to ductile load maximum. The specimens used were Charpy-V sized bend specimens (CVN_{pc}) and 25 and 50 mm compact tension specimens (CT). Due to the lack of separation between cleavage fracture and load maximum data, it was impossible to perform a detailed statistical analysis to the whole data set. An approximate analysis was performed applying only temperatures where the data clearly correspond to brittle fracture.

The raw data, including the TSE results, is presented in Fig. 6.3a. The two TSE results corresponding to the lowest temperatures refer to TSE-6 and the remaining results refer to TSE-5. The yield stress of the material is 710 MPa and the stress intensity factor yielding a plastic zone of 0.5 mm is approximately 69 MPa√m. For the second lowest temperature there appear to be no size effects, but for the lowest temperature there appear to be a clear size effect.

The outcomes of these tests are analysed by Wallin [1995] based on the Master Curve methodology. Fig. 6.3b gives the size corrected data together with the Master Curve. The results reveal a specific trend, i.e. successive initiations correspond always to a higher KI value than previous initiations. This is true even in the case of decreasing temperature (TSE-6). The reason for this is somewhat unclear, but is likely to be caused by some kind of combination of ductile ligaments and warm prestress connected to the crack arrest event. When a crack propagates by cleavage within an increasing temperature gradient, usually ductile ligaments are formed (isolated bands where the crack does not propagate). These ligaments have a tendency to carry part of the load, thus decreasing to some extent the effective K_I. The crack arrest event itself, is essentially a form of warm prestress event. The crack cannot reinitiate until the warm prestress effect is overcome. For the TSE:s the warm prestress effect appear the most likely reason for the increasing toughness for successive initiations.

It appears that the first initiation values are the most reliable and therefore the present analysis focuses on them. Fig. 6.3b reveal the statistical size correction, combined with the MC is very capable of describing the first initiation behaviour of the TSE:s. Even basing the analysis only on the CVN_{pc} results, would yield the same result, i.e. the statistical size correction is capable of describing a 122 times difference in crack front length.

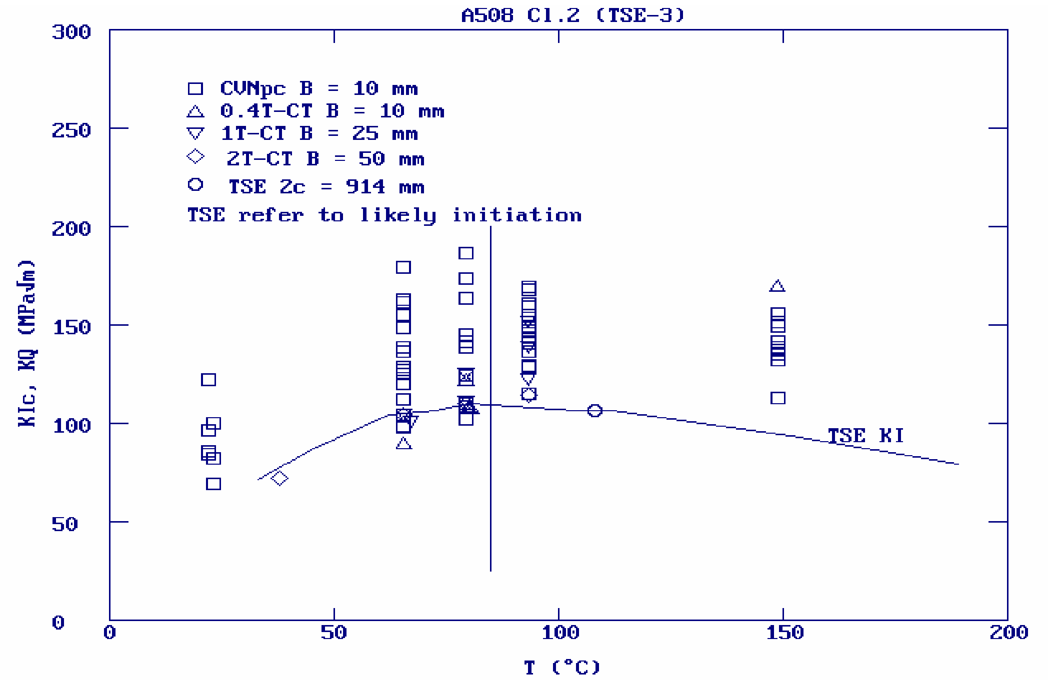

(a) Un-corrected TSE-3 data.

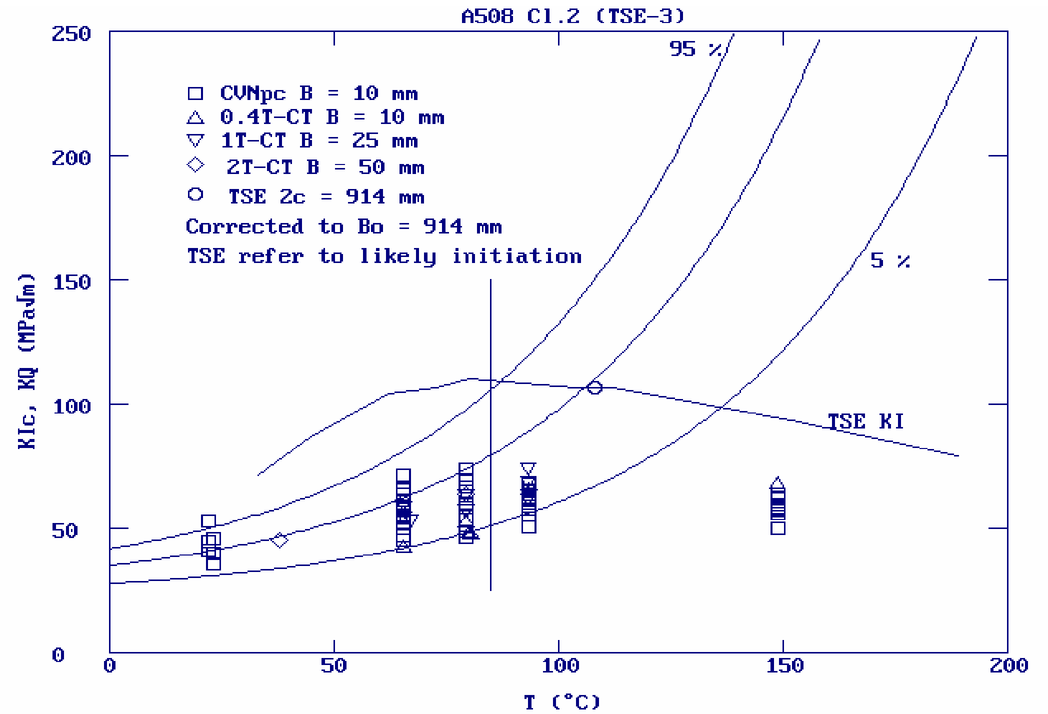

(b) Size corrected TSE-3 data.

Fig. 6.2: Un-corrected and size-corrected data of the TSE-3 test. The test results correspond to likely first initiation.

6.4. Experiment TSE-7 at ORNL

TSE-7 is a thermal shock experiment on a thick-walled pressure vessel with a wall thickness of 152 mm [Cheverton et al, 1985b]. This experiment was the second experiment involving a semi-elliptical surface flaw. The material characterization was based on the elastic plastic K_J parameter and this time there was also a distinction made between brittle fracture and brittle fracture after ductile tearing. However, it is unclear if specimens not failing by cleavage at all have been included in the data listing. The semi-elliptical crack was after testing found to have been highly irregular in shape. This irregularity was disregarded in the original analysis. The shape of the crack was such that the K_I value estimated by the original analysis is likely to underestimate the actual situation in the test. Similar to TSE-2, the interpretation of the test is disturbed by the fact that neither K_I nor T is constant along the crack front. Since the K_I analysis of the crack was inaccurate, it was decided only to take the apparent maximum K_I (combined with the local temperature) and to use $2 \cdot c$ as the effective crack length. After the first initiation, two additional initiations occurred. The problem is that strong bifurcation occurred all along the cylinder surface, making an accurate estimation of both actual K_I as well as effective crack front length, practically impossible. Therefore, only the first initiation was included in the re-evaluation.

The outcomes of this test are analysed by Wallin [1995] based on the Master Curve methodology. The uncorrected test data is presented in Fig. 6.4a and the size corrected data together with the Master Curve is presented in Fig. 6.4b. Considering the inaccuracy of the analysis of TSE-7, the result complies surprisingly well with the size corrected material characterization data.

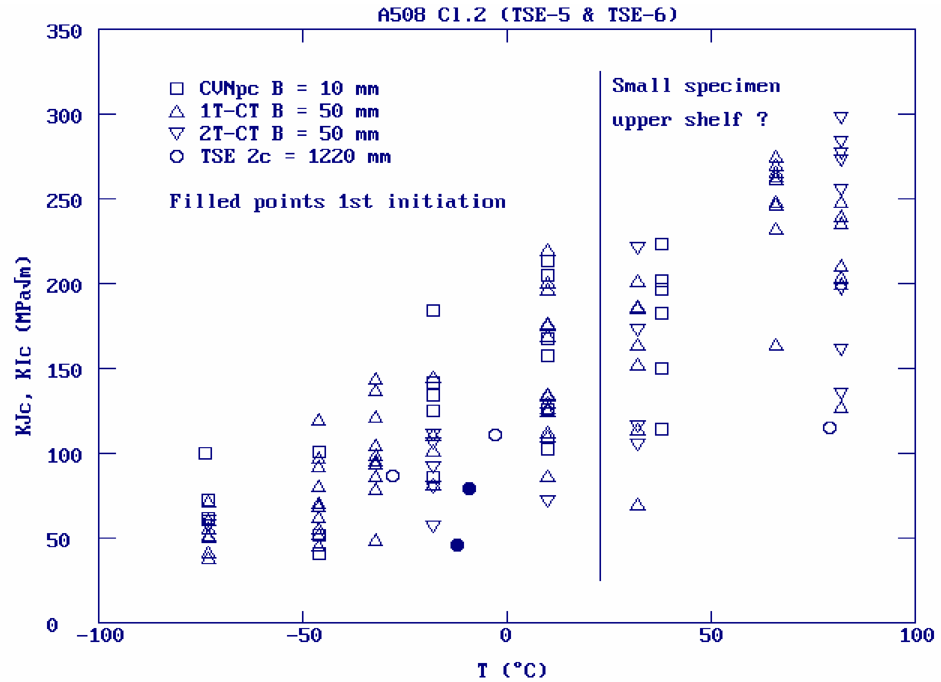

(a) Un-corrected TSE-5 and TSE-6 data.

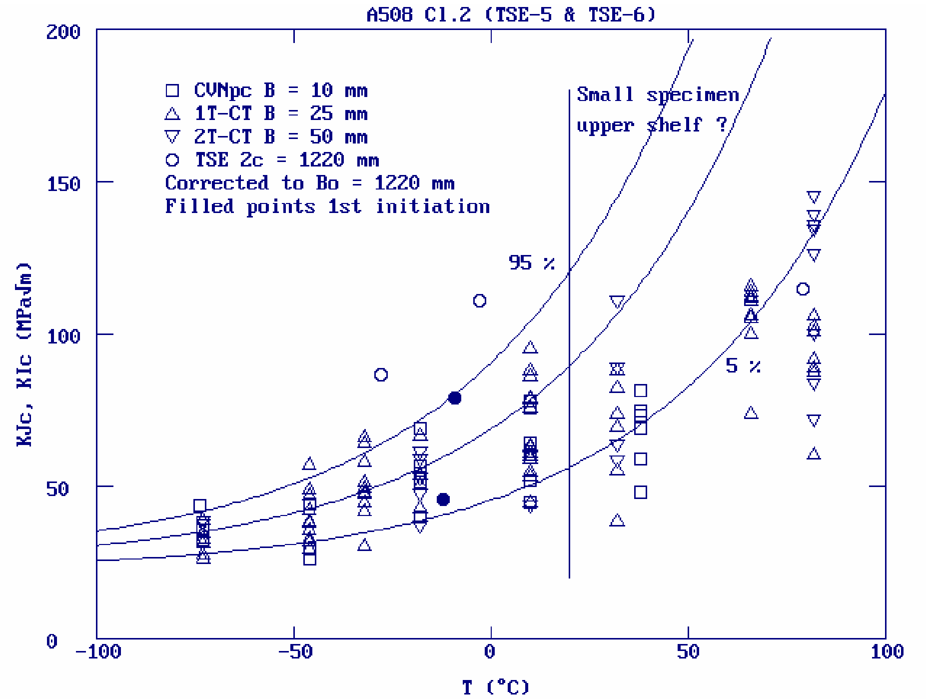

(b) Size corrected TSE-5 and TSE-6 data.

Fig. 6.3: Un-corrected and size-corrected data of the TSE-5 and TSE-6 (the two lowest temperature results) tests. The Master Curves are based on T<20°C data.

6.5. Experiment TSE-FR at Framatome

TSE-Fr is a thermal shock experiment on a thick-walled pressure vessel with a wall thickness of 230 mm [Pellissier-Tanon et al, 1983, 1986]. The cylinder had a long crack of 1000 mm (Table 6-1). The material characterization was performed with comparatively large specimens (75 mm and 100 mm thickness) producing valid K_{IC} values. The material characterization program was not very large, but since the program was designed to model as closely as possible the situation at the TSE crack tip, it appears adequate in size. The actual un-corrected data is presented in Fig. 6.5a. Three initiation events occurred in the experiment. The trend is the same as before, with the subsequent initiations being a higher level than the previous toughness. The temperature along the crack front was comparatively even for the first initiation, but somewhat uneven for the subsequent initiations. Even though the material characterization consist of valid K_{IC} data, the TSE results (especially the first initiation) go below the experimental lower bound from the material characterization tests. Already in the original analysis of the test results, this behaviour was attributed to the statistical size effect.

The outcomes of this test are analysed by Wallin [1995] based on the Master Curve methodology. The data, size corrected to 1000 mm according to the statistical size effect, together with the Master Curve is presented in Fig. 5.5b. The first initiation event in the TSE lie close to the median (50 %) failure probability as determined from the material characterization tests. Also the subsequent initiation events are well within the Master Curve scatter bands. The reason for this is believed to be that the WPS effect arising from the crack arrest events was quite weak, because the arrest and initiation temperatures were quite close to each other.

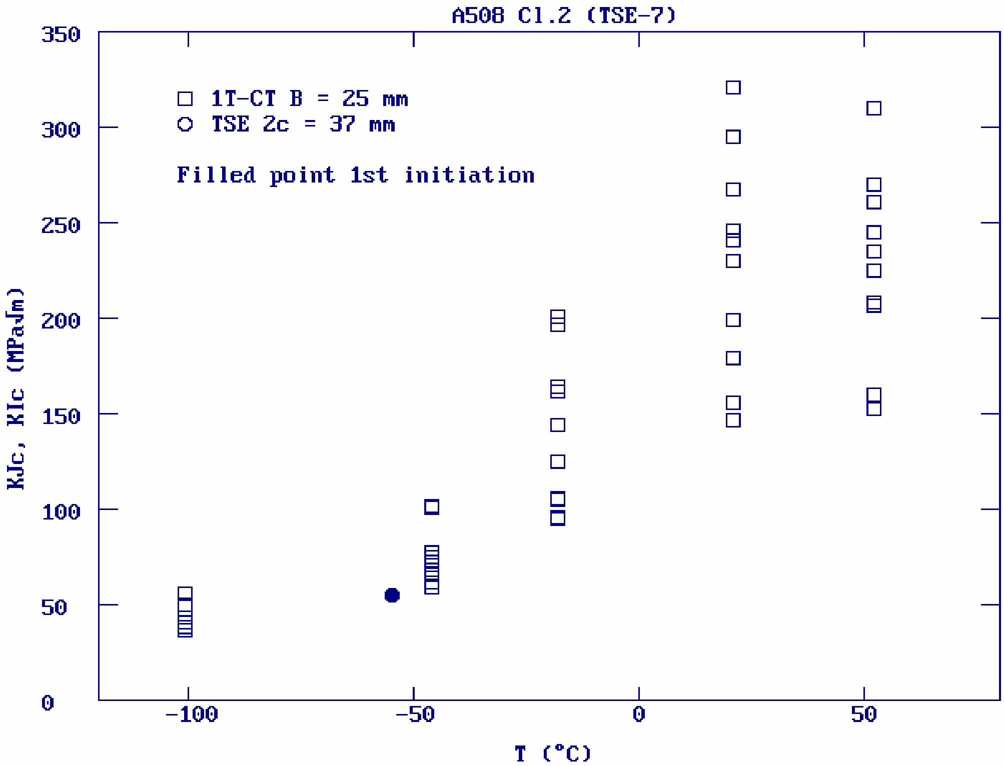

(a) Un-corrected TSE-7 data.

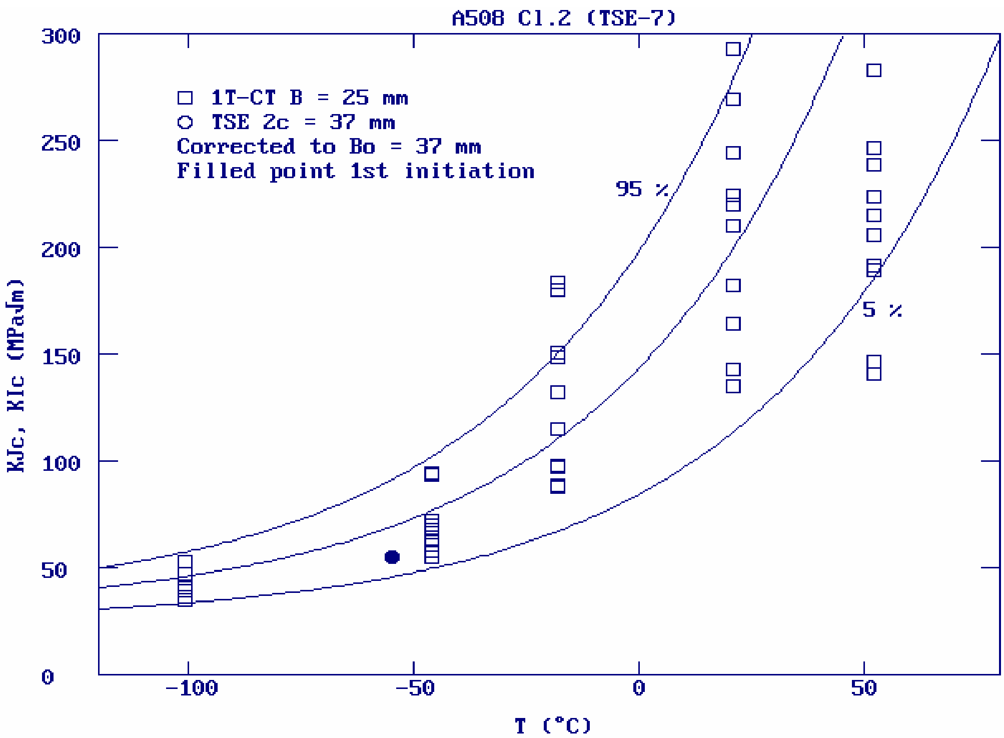

(b) Size corrected TSE-7 data.

Fig. 6.4: Un-corrected and size-corrected data of the TSE-7 test together with Master Curves.

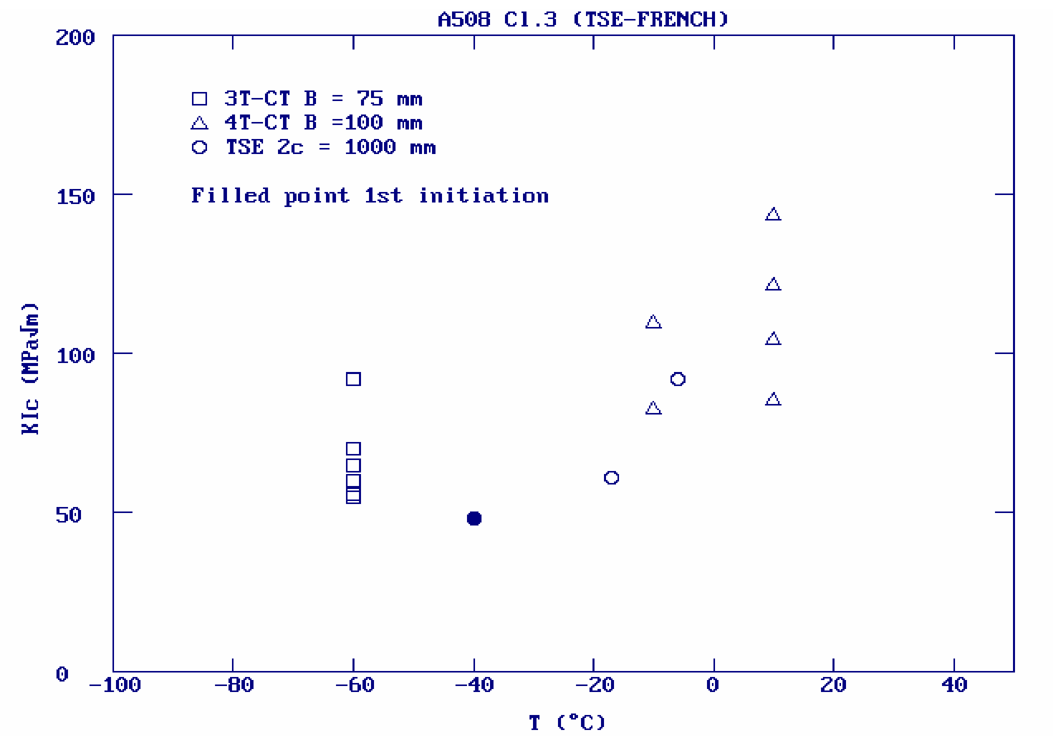

(a) Un-corrected TSE-Fr data.

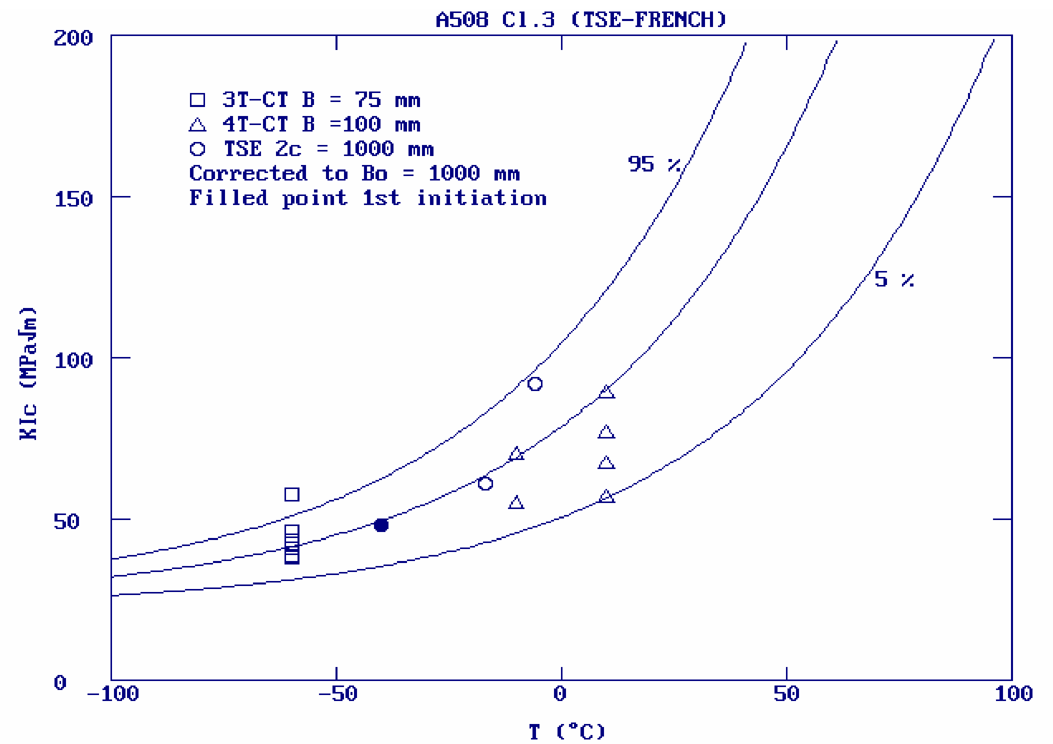

(b) Size corrected TSE-7 data.

Fig. 6.5: Un-corrected and size-corrected data of the TSE-Fr test together with Master Curves.

6.6. Experiment NESC-I at AEA

The NESC-I test is a thermal shock experiment on a thick-walled cylinder with a wall thickness of 170 mm [Bass et al, 2000]. A number of defects were inserted in the cylinder. The cylinder was subjected to high primary and secondary stresses produced by a combined rotation and thermal shock loading. Here we consider only crack R of the test. This is a large through-clad surface crack with a depth of 76.5 mm and a length of 205 mm. The NESC-I cylinder specimen was fabricated from A508 Class 3 steel subjected to a non-standard heat treatment to simulate radiation embrittlement of an RPV steel, resulting a yield strength of about 750 MPa. The cladding thickness was 4 mm, giving a HAZ thickness of 5-10 mm.

Fracture toughness testing was carried out using the ESIS-92 and ASTM E1152-87 standards using CT and 3PB specimens with thickness varying from 10 to 25 mm. The fracture toughness results data were evaluated in order to provide the Master Curves. The reference temperature T_0 for the base metal and the cladding HAZ were determined to be 68 ^oC and 16 ^oC, respectively, based on size-corrected specimen thickness of B = 25 mm. Tests were also conducted on the base material using 3PB specimens with a/W ratio of 0.1 and 0.5 to study shallow crack effects on cleavage fracture toughness in the transition region. The shallow crack data generated from the a/W = 0.1 specimens resulted in a transition temperature T_0 to be 32 ^oC.

The test cylinder was subjected to simulated pressurized-thermal shocks. The cylinder temperature prior to the quench was 293 ^oC and the temperature of the quench water was 2.0 ^oC. The rotation of the cylinder went up to the target speed of 2600 rpm. Crack R experienced crack arrest event after a relatively small amount of ductile tearing and cleavage extension, as shown in Fig. 6.6. The largest crack growth was found close to the cladding HAZ.

The outcomes of this test are analysed by Rintamaa et al [2000] based on the Master Curve methodology and using finite element analyses. Fig. 6.7 Shows the assessment results concerning crack R of this experiment. In general, the fracture mode of this case, i.e. ductile initiation and tearing followed by cleavage, was successfully predicted by three-dimensional finite element based fracture assessment combined with Master Curve description of fracture toughness. It was also observed that analysis based on the ASME RT_{NDT} reference temperature did not provide consistent description of the fracture event of the test.

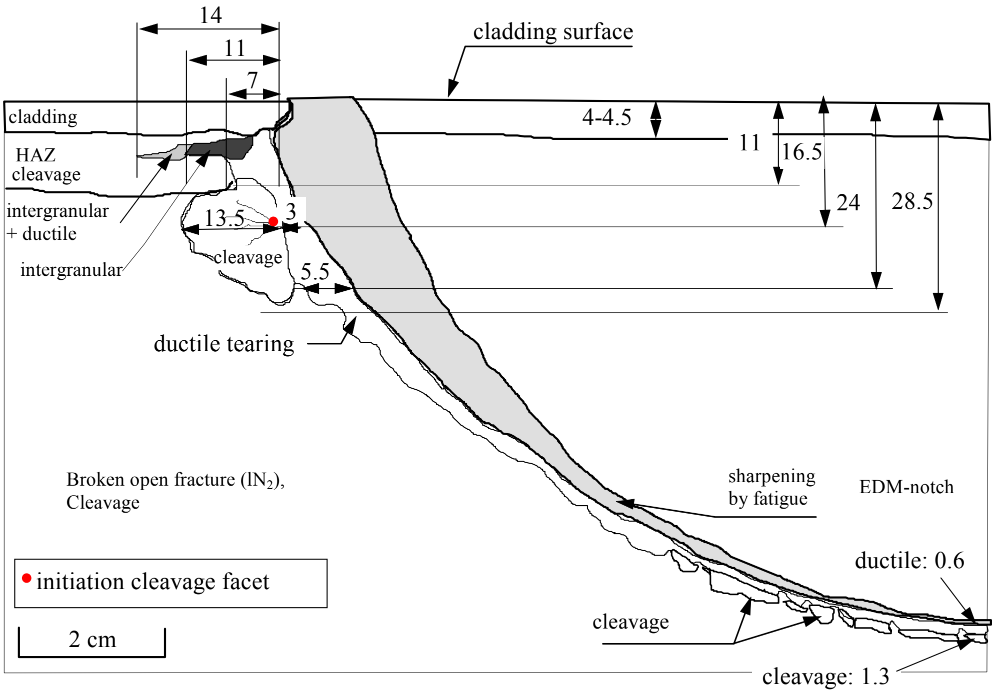

Fig. 6.6: Crack growth of crack R in the NESC-I experiment [Bass et al, 2000].

6.7. Experiment NESC-II at MPA

The NESC-II tests are thermal shock experiments on thick-walled cylinders [Stumpfrock et al, 2003]. Two experiments denoted as NP1 and NP2 are conducted within the project. The test cylinders have an inner radius of 202.5 mm, a wall thickness of 188.6 mm (including 8 mm cladding) and a length of 580 mm. The NP1 cylinder contained two through-clad semi-elliptical cracks, denoted as crack A and crack B. These were inserted in the circumferential plane on the inner surface of the test piece at mid section on opposite sides. The depth and length of these defects were a = 23.8 mm and 2c = 63 mm for crack A and a = 19.6 mm and 2c = 59 mm for crack B. The NP2 cylinder contained only one fully circumferential crack under the cladding. The crack depth varies between 5.5 mm and 10.5 mm along the crack front, giving an averaged crack depth of 8.0 mm. The base material used for the NP1 and NP2 components was type “17 MoV 8 4” (similar to A508 Class 2) steel subjected to a non-standard heat treatment to simulate radiation embrittlement of an RPV steel, resulting in a yield strength of about 680 MPa.

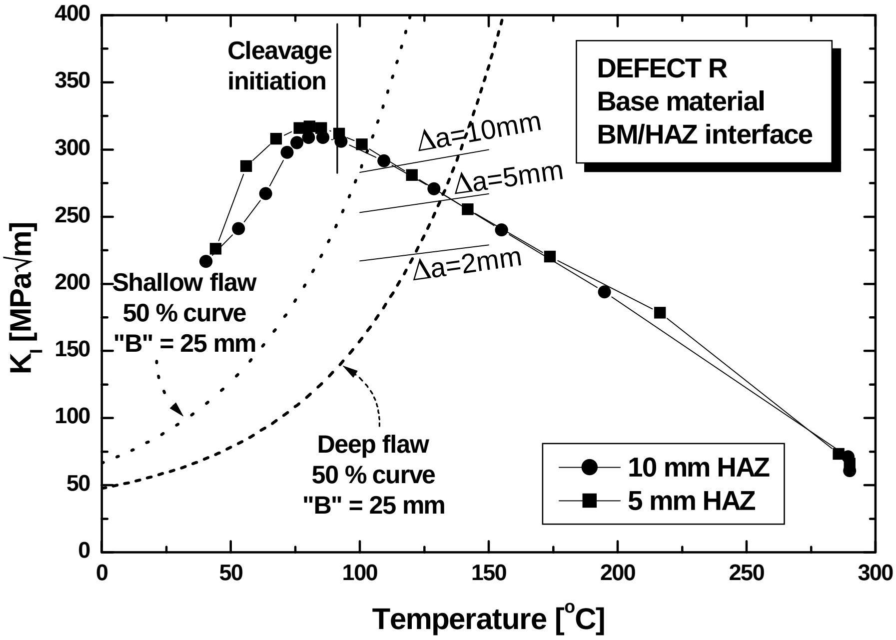

(a) Crack front position close to HAZ.

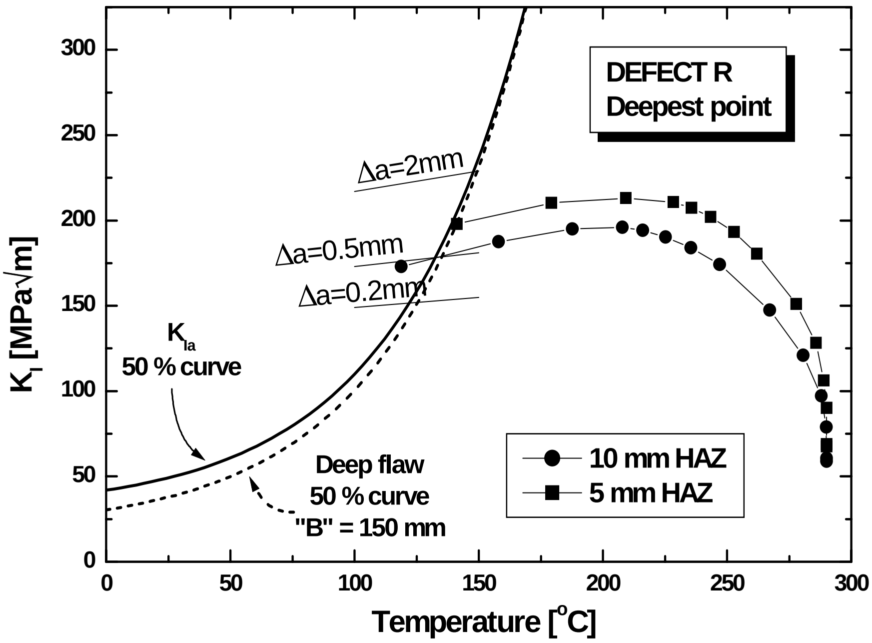

(b) Crack front position at the deepest point.

Fig. 6.7: Crack driving force and material fracture resistance of the surface defect R of the NESC-I test [Rintamaa, 2000].

An extensive test program was conducted for evaluation of the fracture toughness properties of the base material. A series of fracture test on both shallow and deep-notched SEN(B) specimens of section 10x10 mm^2 was conducted at VTT prior to the NP1 and NP2 tests. Also a series of fracture test was conducted on single edge notched bend specimens, SEN(B), with a/W= 0.55 at MPA. The fracture toughness results have been evaluated in order to provide the Master Curves and RT_{NDT} of the base material, resulting in the following results.

- The reference temperature RT_{NDT} was estimated to be 140°C.
- Estimations on the Master Curve reference temperature T_0 are made considering the size corrections to a reference thickness. This leads to the following results:

T_0 = 60 °C	For standard SEN(B) with B_0 = 25 mm.
T_0 = 76 °C	For surface cracks A and B in the NP1 test, with crack front length of 70 mm in the base material.
T_0 = 137 °C	For the subclad crack in the NP2 test, with crack front length of 1373 mm in the base material.

The test cylinders were subjected to simulated pressurized-thermal shocks. The cylinders were also subjected to external axial loads. For the NP1 test, the initial temperature on the inner surface of the cylinder was 155 °C and 200 °C on the outer surface. The internal pressure in the test loop was constant at 78 bar during the test and the axial force was constant at 20 MN. For the NP2 test, the initial temperature on the inner surface of the cylinder was 234.8 °C and 287.1 °C on the outer surface. The internal pressure in the test loop was constant at 58 bar during the test and the axial force was constant at 43 MN. The NP1 test produced no crack growth event, while the NP2 test experience a crack growth and arrest event with a maximum extension of approximately 15 mm.

The outcomes of these tests are analysed by Sattari-Far [2000] based on the Master Curve methodology and using detailed finite element analyses. Fig. 6.8 Shows the assessment results of the NP1 and NP2 tests. It was observed that the Master Curve methodology can satisfactorily predict the experimental outcomes of these tests. For the surface defects in the NP1 cylinder the loading did not become critical for a cleavage fracture event. For the subclad defect in the NP2 cylinder a cleavage fracture event could be predicted by the analysis. While assessments based on the fracture toughness data size-corrected for the actual crack front length lead to good predictions, using fracture toughness data without size correction in the Master Curve methodology may lead to non-conservative fracture assessments. The test predictions are very conservative if fracture toughness values based on the reference temperature RT_{NDT} (i.e. the ASME K_{1a} curve) are used.

6.8. Experiment O1 at KTH

The O1 tests are brittle fracture experiments on thick-walled plates under mechanical loads [Sattari-Far, 2001]. The main objective of this study was to simulate the fracture conditions of the beltline region of an aged reactor during a cold over-pressurization loading. The main features of the fracture conditions to be simulated were material properties (mechanical, physical and fracture toughness), loads (internal pressure, residual stresses) and defect geometry (surface shallow crack through the cladding).

A base material having features of $RT_{NDT} \approx 80$ °C and $\sigma_Y \approx 480$ MPa was considered appropriate the experimental objectives of this study. Thus, test plates of A508 Class 3 reactor material were specially heat treated to introduce the required embrittlement properties corresponding to the aged reactor material. The special heat-treatment consisted of heating-up the material blocks to 1250 °C, holding at this temperature in 1.5 hours, and cooling down by spraying nitrogen gas on all surfaces of the block. This resulted in $RT_{NDT} = 72$ °C and a yield strength of 495 MPa for the base material.

A basic functional requirement for the configuration of the test specimen was that the stress conditions in the ligament would be equivalent to the conditions in the reactor beltline region. Accordingly, five cruciform-shaped fracture specimens of sizes 800x800x80 mm having a cross section dimension of 120x80 (including 7 mm cladding) were chosen for this study. The longitudinal and transverse dimensions of the specimens were chosen to be able to impose a biaxial ratio of 1:0.5 (corresponding to the internal pressure biaxial ratio in the reactor pressure vessel). In addition, four clad beams with dimension 800x120x80 mm were also tested under uniaxial loading. Shallow surface cracks of different depths were introduced in the clad beams by notching and pre-fatigue bending.

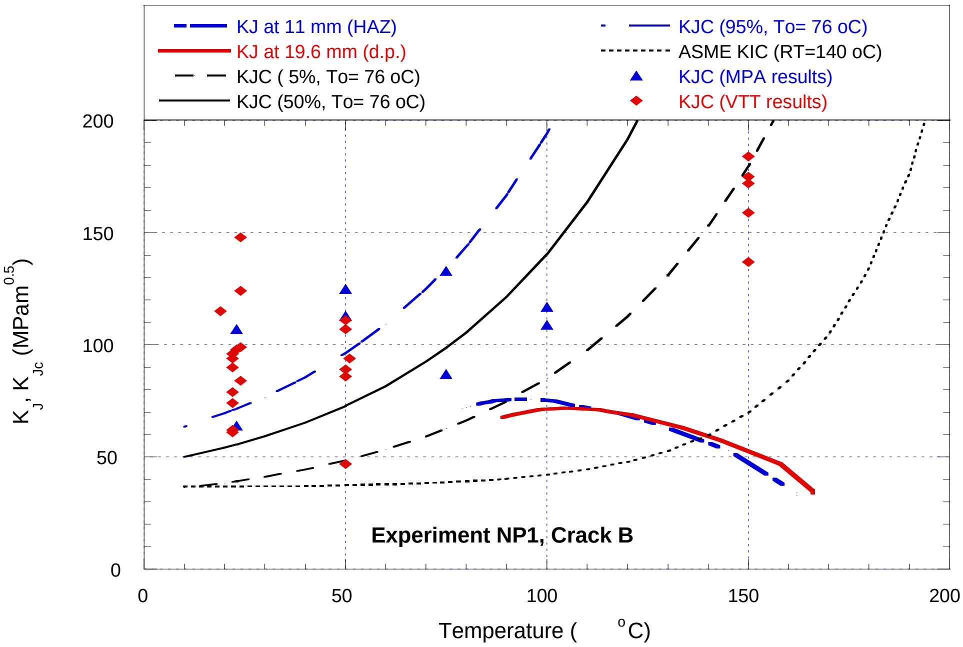

(a) Two positions along the surface crack in the NP1 test.

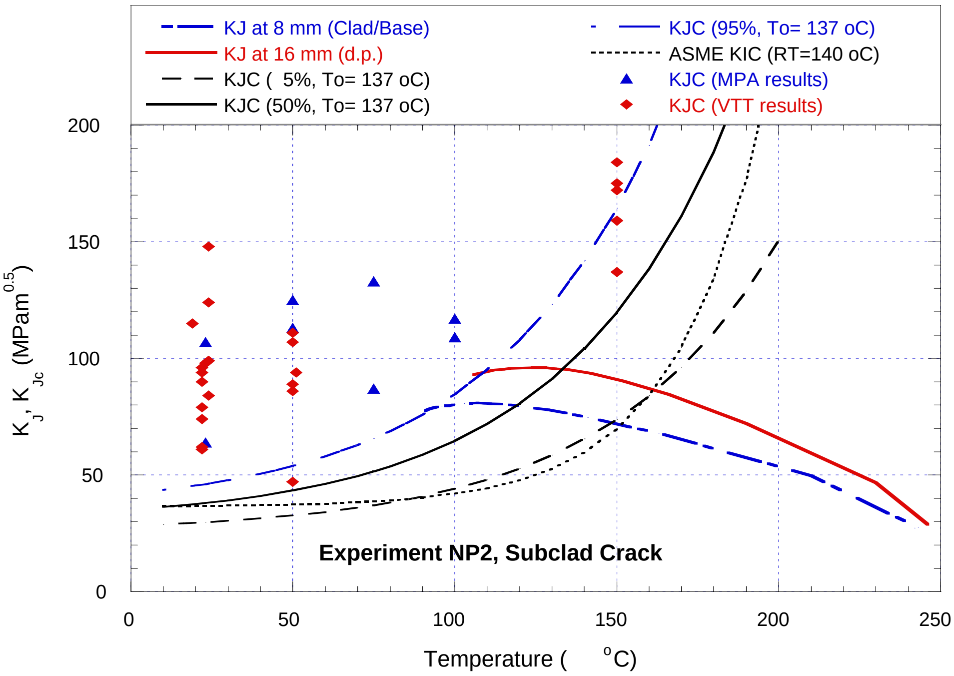

(b) Two crack tips of the subclad crack in the NP2 test.

Fig. 6.8: Crack driving force and material fracture resistance of the NESC-II tests based on the size-corrected Master Curves [Sattari-Far, 2000].

The fracture test program within this study consisted of tests on single-edge notched SEN(B) specimens under 3-point bending and tests on clad beams containing surface cracks subjected to uniaxial and biaxial loading. The SEN(B) specimens were used to evaluate fracture toughness values according to ASTM Standard E399 and also to develop different Master Curves according to ASTM Standard E1921-97. The objective of the tests was to obtain cleavage fracture toughness under conditions similar to those in the reactor.

The outcomes of these tests are analysed by [Sattari-Far, 2004b]. Fig. 6.9 shows the assessment results based on the Master Curve methodology. Fig. 6.9a shows the fracture toughness data from different test specimens compared with a standard Master Curve (B = 25 mm). The corresponding results when the size-corrected Master Curves regarding the actual crack front were used are shown in Fig. 6.9b. It is observed that all tests experienced fracture in the lower shelf region. The analyses of the O1 tests indicated that the K_{Jc} values at fracture in the uniaxial and biaxial bend tests correlated well with the standard Master Curve for the material. No significant effects of shallow crack and biaxial loading were observed in the clad beams tested in the experimental program of this study. It could be concluded that for temperature corresponding to the lower shelf region, the crack-tip constraint conditions in the clad beams, having shallow cracks under uniaxial and biaxial loading, are effectively similar to the conditions in a standard SEN(B) specimen.

6.9. Experiment NESC-IV at ORNL

The NESC-IV tests are brittle fracture experiments on thick-walled plates under mechanical loads [Bass et al, 2002]. The NESC-IV project consisted of two parts, A and B, that were focused on fracture toughness testing and model development for shallow surface flaws and for embedded flaws, respectively. The target temperature for the testing program was the lower transition temperature range for the selected material. The test specimens were fabricated from A533 GB with a stainless steel clad overlay. The yield strength of the base and weld materials were 500 MPa and 625 MPa at room temperature.

A total of six clad cruciform specimens containing shallow surface flaws were tested in Part A. The cruciform specimens have a nominal thickness of 102 mm and an austenitic cladding of 6 mm.

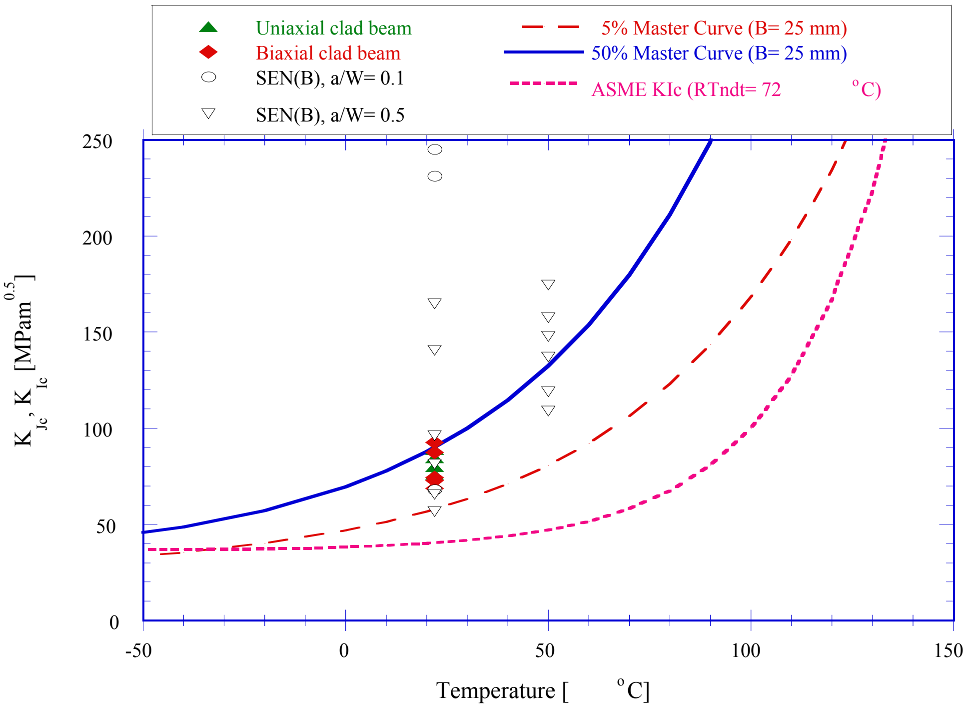

(a) Master Curves based on standard bend specimens with *B*= 25 mm.

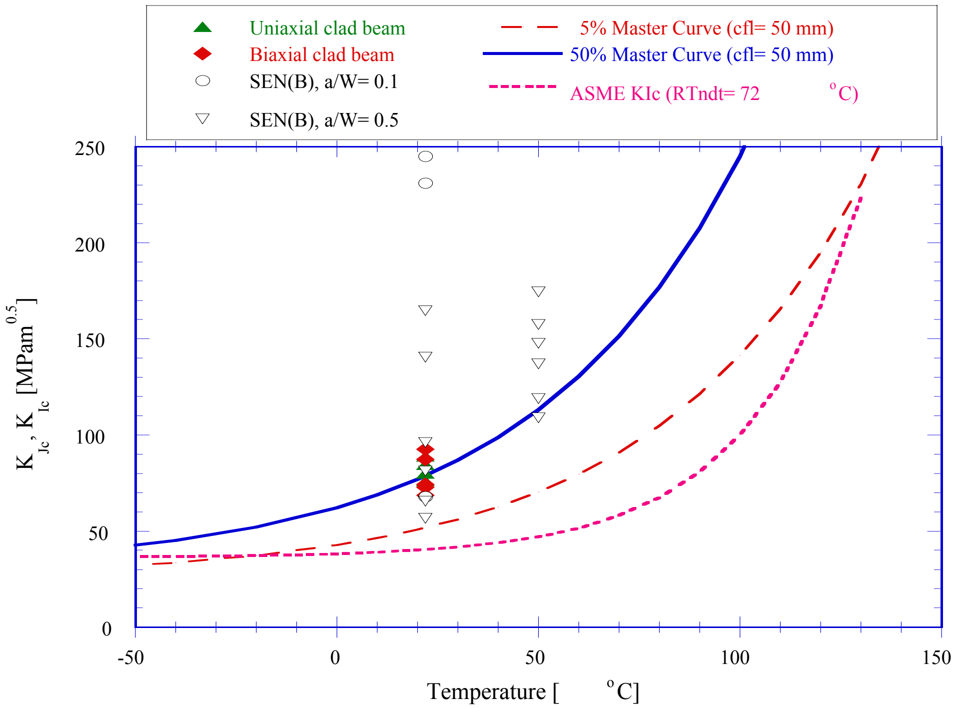

(b) The Master Curves size-corrected for crack front length of 50 mm.

Fig. 6.9: Cleavage fracture toughness of the O1 test compared with the Master Curves and ASME K_{Ic} curve [Sattari-Far, 2001].

The test section for the cruciform beams contained weld material below clad layer, in which the surface flaw was inserted. The length orientation of the flaw was parallel to the longitudinal weld and it extended in the weld through-thickness direction. After pre-cracking the final nominal dimensions of the flaw were 53.3 mm long and 19.1 mm deep (including the cladding). Part B concentrated on uniaxial (configuration and loading) beam bend specimens. A total of four uniaxial specimens containing embedded flaws were tested. Two of the test sections included the surface clad layer, while the remaining two were without cladding. The test section for the uniaxial beams contained only plate material below the clad layer (i.e. no weld material). The embedded flaw was a 2D sharp notch extending through the entire specimen with a flaw depth of about 20 mm located 14 mm under the surface. The uniaxial specimens had a nominal thickness of 102 mm.

The key experimental variable was the test temperature of the beam, the objective being to achieve cleavage failure in the non-linear region of the load-versus-CMOD curve. Furthermore, each set of specimens should be tested at a single temperature to facilitate statistical analysis of the results. However selection of a suitable temperature was not straightforward. In the first test of the cruciform specimen with a target crack-tip temperature of -60˚C the specimen failed well within the elastic region of the load-versus-CMOD curve. As a consequence, the subsequent tests were performed at slightly higher temperatures, in the range –40 to –33 ^{o}C.

The post-test fractography confirmed that the failure mode in the cruciform specimens was pure cleavage fracture, without prior ductile tearing. Two different labs investigated the position of the cleavage initiation points, indicating that this tended to occur towards the surface of the specimen (in the cladding HAZ) and not at the deepest point of the defect. The outcomes of these tests are analysed by [Sattari-Far, 2004b]. Fig. 6.10 shows the assessment results of these tests based on the Master Curve methodology. Size-corrected toughness curves considering the actual crack front sizes are used in the analysis. Fig. 6.10a gives the assessment results of two uniaxial specimens, one with and one without a clad layer. Tip-S and Tip-D are the surface and deep crack-tip, respectively. Note that the cleavage fracture occurred at the deep crack-tip in the uniaxial specimens. Fig. 6.10b gives the assessment results of the five tests of the cruciform specimens. The results are for the cladding HAZ, where most of the tests experienced the cleavage fracture initiation.

The preliminary results of the post-test analyses of the NESC-IV tests indicated that the K_{Jc} values at fracture in the biaxial bend tests correlated with the standard Master Curve for the weld material. Evaluation of the constraint parameters T and Q in the sub-surface region supported the hypothesis that at low loads the loss of constraint expected for shallow surface-breaking flaws would be offset by a biaxial loading effect.

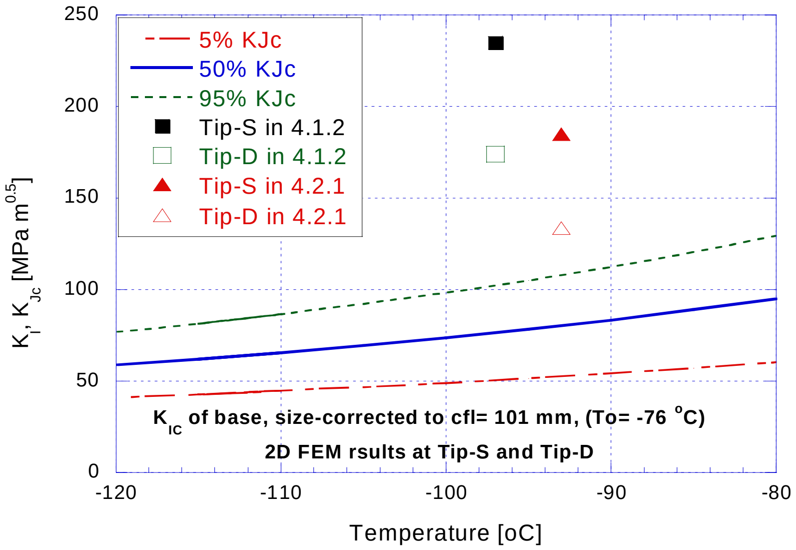

(a) Analysis of embedded flaws under uniaxial loading.

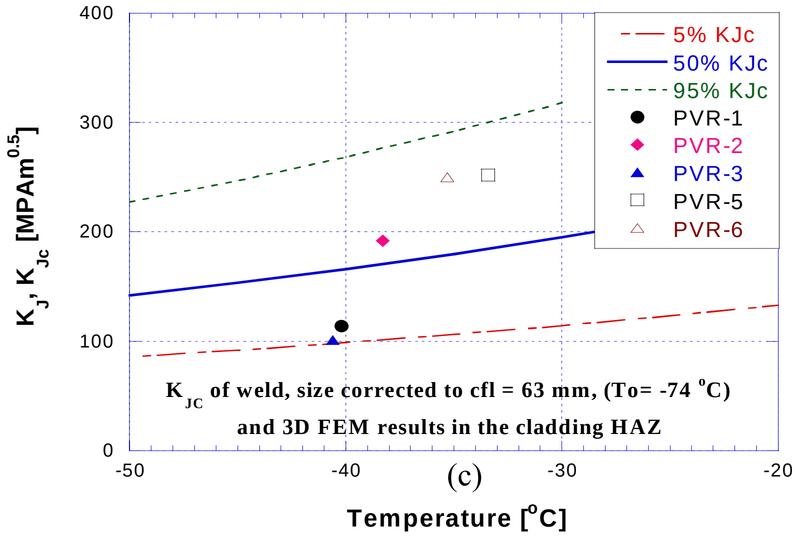

(b) Analysis of surface flaws under biaxial loading.

Fig. 6.10: Cleavage fracture toughness of the NESC-IV tests compared with the size-corrected Master Curves [Sattari-Far, 2004b].

6.10. Experiments PTSE-1 and PTSE-2 at ORNL

Two large pressurized thermal shock experiments, PTSE-1 and PTSE-2, were conducted at ORNL [Bryan et al, 1985 and 1987]. The tests were performed on two large scale pressure vessels with a wall thickness of 150 mm and using very long surface cracks (about one meter). The initial flaw depth was in both cases close to $a/W = 0.1$. PTSE-1 experienced three different transients and PTSE-2 two transients. In both tests, both brittle crack initiation and arrest occurred. These tests are very interesting, since they are most closely mimicking a real PTS transient in a nuclear pressure vessel. These experiments are analysed according to the Master Curve methodology [Wallin, 2004c].

The material for PTSE-1 was a SA-508 class 2 steel with a yield stress of 625 MPa, ultimate stress of 785 MPa, NDT of +66ºC and RT_{NDT} of +91ºC. The cleavage fracture initiation properties of the steels turned out to be strongly inhomogeneous. This required a non-standard inhomogeneous bimodal Master Curve analysis of the material [Wallin et al, 2004d]. The resulting Master Curve analysis of this material is presented in Fig. 6.11. The fracture toughness was measured using 25 mm CT specimens. The material can be divided into two different fracture toughness populations; one with a T_0 of +65ºC with an occurrence probability of 34 % and another with a T_0 of 12ºC with an occurrence probability of 66 %. Since the flaw in the experiment was 1000 mm in length, a value of +65ºC was taken as descriptive of the material. Similarly, the crack arrest test results were analysed with a similar but simpler log-normal distribution having the same temperature dependence as the MC.

The material for PTSE-2 was an A 387 grade 22 class 2 steel (2 ¼ Cr-1 Mo). In the test, the lower yield strength of this material caused the steel to flow plastically, and this affected the mechanical properties. The post-test values of the material properties were; yield stress of 470 MPa, ultimate stress of 625 MPa and NDT of +75ºC. The resulting post-test Master Curve analysis of this material is presented in Fig. 6.12. Also here, the fracture toughness characterisation used 25 mm CT specimens. There is a clear difference between the two material states. However, the PTSE-2 material does not show the same inhomogeneity as PTSE-1. This enabled a standard Mater Curve analysis of the data.

The resulting Master Curve analysis of these two tests is presented in Fig. 6.13. These tests were also evaluated for constraint considerations in using the Master Curve methodology, as will be discussed in section 7.3 of this report.

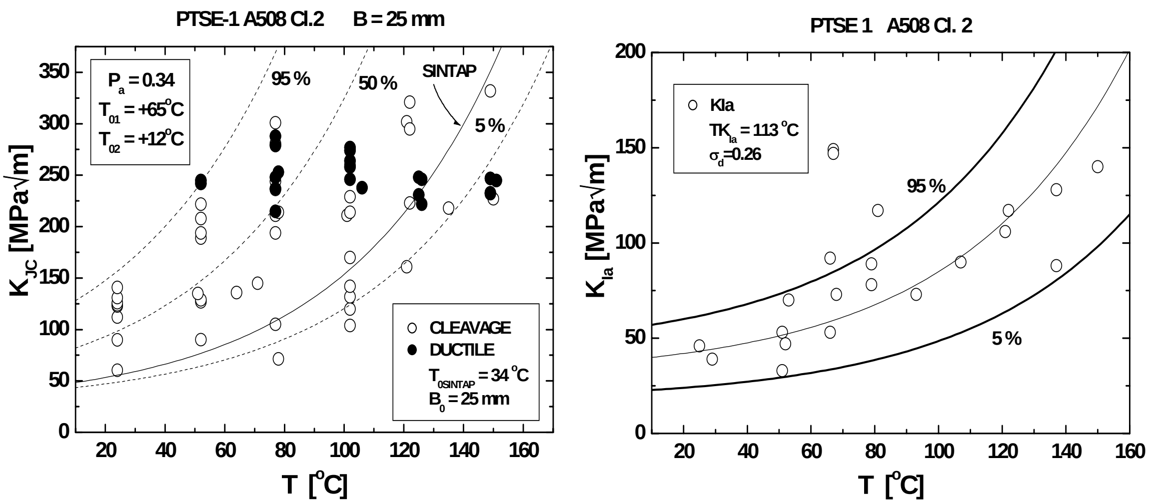

Fig. 6.11: Initiation and arrest fracture toughness of the PTSE-1 material [Wallin, 2004c].

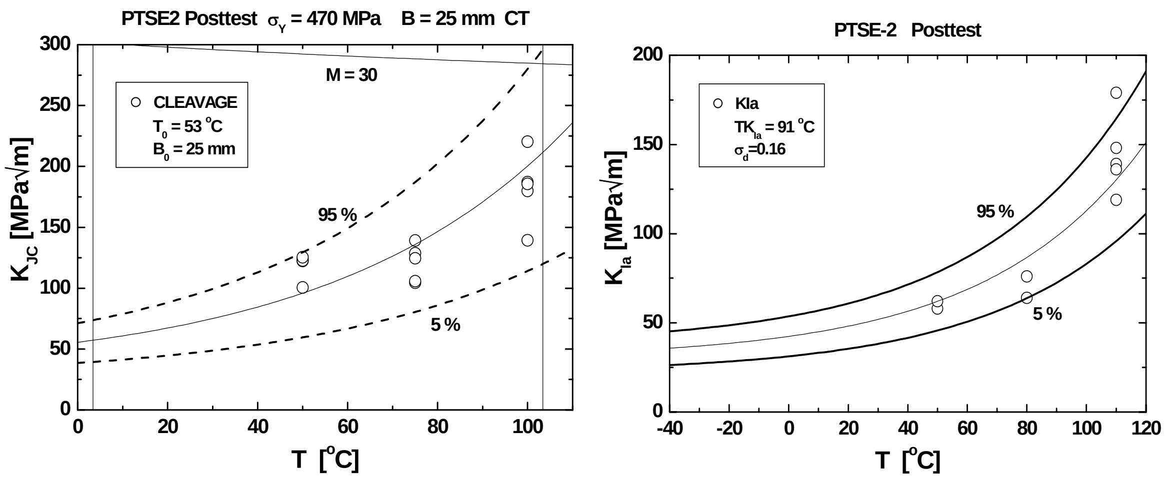

Fig. 6.12: Initiation and arrest fracture toughness of the PTSE-2 material [Wallin, 2004c].

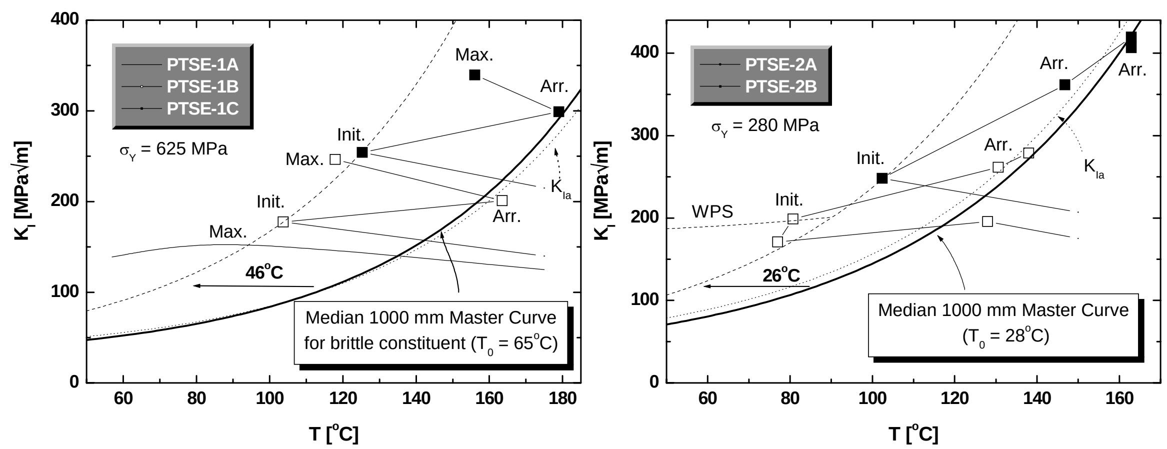

Fig. 6.13: Master Curve analysis of the PTSE-1 and PTSE-tests [Wallin, 2004c].

7. CONSTRAINT EFFECTS

The commonly used fracture mechanics methods are based on a single-parameter description. This means that the crack-tip field in a cracked body is described by a single parameter provided that certain conditions are satisfied. However, the crack-tip field and the fracture toughness are only geometry independent within a limited range of loading and geometric conditions, which ensures similar crack-tip stress triaxiality (constraint) in the laboratory specimen and the structure under consideration. The size and geometry requirements restrict the application of different fracture mechanics disciplines. Under small scale yielding (SSY) conditions, the single parameter K, J and $CTOD$ characterize the crack-tip conditions, and thus each one can be used as a geometry-independent fracture criterion. At increasing loads in finite cracked bodies, the SSY field gradually diminishes as the plastic zone senses nearby traction free boundaries. Consequently, the single-parameter fracture mechanics disciplines break down, and the fracture toughness depends on the size and geometry and type of loading of the fractured body. A number of approaches have been proposed to extend fracture mechanics applications beyond the limits of the single-parameter assumptions. Most of these new approaches involve the introduction of a second parameter to characterize the crack-tip constraint conditions.

One important question arising in application of the Master Curve methodology is how the method accounts for the constraint effects. The original Master Curve methodology describes the cleavage fracture toughness of the material under high constraint conditions for which the single parameter characterization of the material toughness (K_{Jc}) holds. Indeed, adoption of a three parameter Weibull distribution to describe measured K_{Jc}-values, with a geometry independent value of K_0, theoretically requires that SSY conditions prevail at fracture in each of replicate test specimens used to compute the statistical estimate for K_0 and thereafter T_0, Eqs. (4-5) and (4-7). Moreover, the ASTM E1921 standard does not require testing of 1T size specimens. It is allowed to use Charpy size fracture specimens (W= B= 10 mm, a/W= 0.5) and convert the results to 1T equivalent values according to Eq. (4-3). The ASTM procedure includes limits related to specimen size and K_{Jc}-values through Eq. (4-2). Indeed, the M= 30 value has been selected largely on the basis of experimental data sets to ensure the existence of the SSY condition at fracture of the replicate test specimens. The connection between T_0

and the crack-tip constraint become exceedingly complex once SSY conditions begin to breakdown under increasing load. There are very limited studies reported on this subject. Ruggieri *et al* [1998] studied the difference in reference temperature T_0 for the SSY and SEN(B) specimens under LSY. They showed, by performing very detailed non-linear 3-D finite element analysis, that the Weibull stress σ_w may emerge as a crack-front parameter which can couple remote loading with a micromechanics model. Based on the argument that the Weibull stress is the single crack characterizing parameter, fracture occurs at equal values of σ_w in different crack configurations even if K_J-values may vary widely due to constraint loss. They also found that loss of constraint leads to decrease in the T_0 temperature, and the shift of T_0 due to constraint loss occurs only in one direction (lowering T_0, thus enhancing the fracture toughness value at a given temperature). Questions such as how to quantitatively consider effects of in-plane constraint (shallow cracks) and out-of-plane constraint (biaxial loading) are still open in the Master Curve concept. Despite this, application of this methodology in predictions of experimental results has shown promising results, see for instance Bass *et al* [2000], Sattari-Far [2000 and 2004] and Wallin [2004c].

In this Chapter, some basic ideas in the description of crack-tip fields and constraint parameters are discussed.

7.1. Stress field around a crack tip

The crack tip stress field for a given material, in a cylindrical coordinate system (r, θ) centred at the crack tip, can in general be given by:

$$\frac{\sigma_{ij}}{\sigma_0} = f_{ij}\left[\frac{r}{(J/\sigma_0)}, \theta, \kappa, \frac{J}{L\sigma_0}; \text{geometry}\right]. \tag{7-1}$$

Here the stress components σ_{ij} are normalised with σ_0 that is a reference value (usually equal to the yield strength), and the distance from the crack tip is normalised by the value J/σ_0. The near-tip stress triaxiality is denoted by κ which depends on the remote load and the crack geometry. L is a characteristic length scale of the finite geometry (for instance the uncracked ligament length) and J the applied J-integral, defined by Rice [1968]. For three-dimensional cases, the local J-value at a point on the crack front can be obtained from:

$$J = \lim_{ds \to 0} \frac{1}{ds} \int_A (w\delta_{1j} - \sigma_{ij} u_{i,1}) n_j \mathrm{d}A, \tag{7-2}$$

where w is the deformation work density, δ_{ij} the Kronecker delta, σ_{ij} and u_i the Cartesian components of the stress and displacement. A is a simply connected surface enclosing the crack front segment of length ds and n_j the outward unit normal to A.

Within the linear elastic fracture mechanics (LEFM) concept, it is assumed that the near-tip field can be fully described by the single-parameter K (the stress intensity factor). This is provided that certain conditions are satisfied, e.g. the conditions for applicability of the ASTM Test Method for Plane-Strain Fracture Toughness of Metallic Materials (ASTM E399). In the application of LEFM, it is understood that the crack-tip plastic zone is much smaller than any relevant specimen dimension. In such a case, K uniquely characterizes the stress and strain states in a region outside the plastic zone but well away from the specimen boundary.

At increasing load and breakdown of LEFM, the elastic-plastic fracture mechanics (EPFM) may be invoked. For a power law hardening material and for applications beyond the LEFM limits, asymptotic expansions of Eq. (7-1) for the Mode I stress components around a crack tip my be developed in the following form:

$$\sigma_{ij} = \sigma_{ij}^{\mathrm{HRR}} + Q\sigma_0 \left(\frac{r\sigma_0}{J} \right)^q \hat{\sigma}_{ij}^{(1)}(\theta, n) + \text{higher order terms.} \tag{7-3}$$

The first term in Eq. (7-3) is the asymptotic HRR solution, after Hutchinson [1968] and Rice and Rosengren [1968]. If the HRR term in Eq. (7-3) can be considered to dominate over a significantly large region that encompasses the fracture process zone, the single-parameter J uniquely and autonomously characterizes the local stresses and strains ahead of a stationary crack in a power law strain hardening material.

However, observations from large-scale yielding tests indicate that the relationship between the single-characterizing parameter (K or J) and the near-tip fields looses the one-to-one correspondence when the plastic zone size ahead of the crack tip is significant compared to the characteristic dimensions of the cracked body. The loss of this single-parameter uniqueness results in different fracture toughness properties in different types of specimen of a given material. A number of researchers have attempted to extend the limits of the J-integral description by introducing a second parameter to characterize the crack-tip conditions. According to these two-parameter approaches, the crack driving force J scales the extent of deformation ahead of the crack tip, while the second parameter κ (often termed as constraint parameter) scales the stress triaxiality ahead of the crack-tip. Accordingly, the fracture toughness is described by a J-κ locus in such an approach. Fig. 7.1 shows critical J-values for cleavage fracture as a function of the constraint parameter Q obtained from tests on SEN(B) specimens with different a/W-values. It is observed that the critical J increases, as Q becomes more negative (loss of constraint). This indicates that fracture toughness tends to increase as constraint decreases, for instance in shallowly cracked bodies under dominantly tension loading.

Despite the fact that the crack-tip constraint effects are qualitatively well understood, still no single measures that are generally agreed upon exist to quantify these effects. In the following, two constraint parameters that have got the most considerations in the literature are briefly discussed.

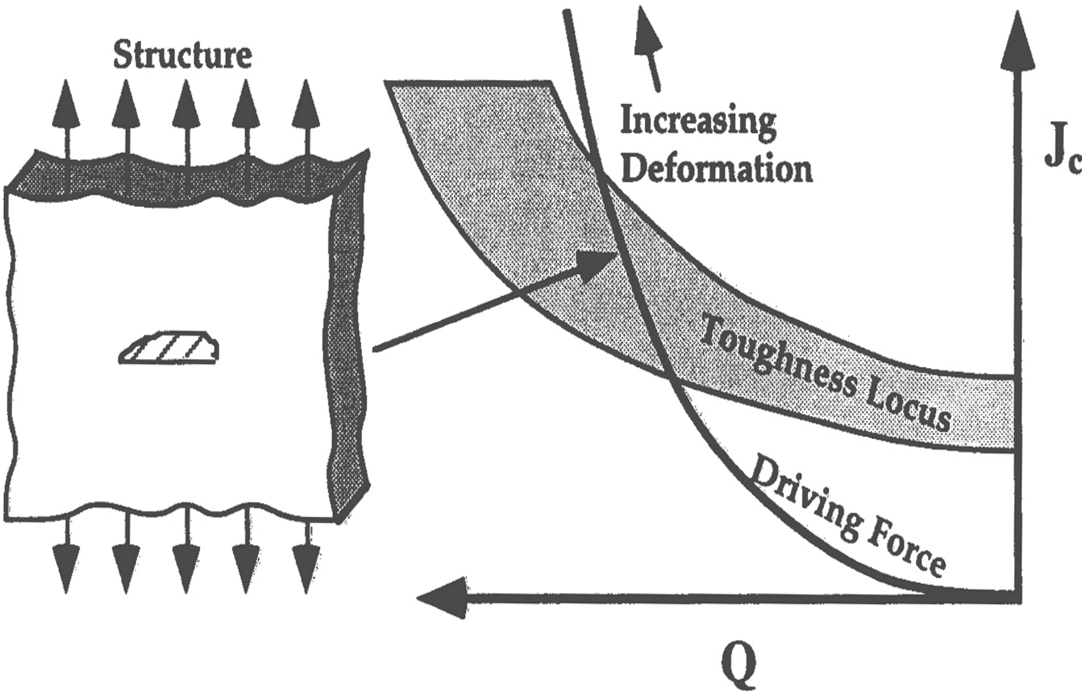

Fig. 7.1: Application of a *J-Q* toughness locus. Failure occurs when applied J-Q curve passes through the toughness locus.

7.2. Constraint parameters

The T_{stress} and the Q stress are the most cited constraint parameters in the literature. These two parameters are briefly described here.

The elastic T_{stress}

For a crack in an isotropic elastic material subject to plane strain Mode I loading at a load level that is sufficiently small that crack-tip plasticity is well-contained, the crack-tip field can be characterized by the two-term Williams [1957] solution as:

$$\sigma_{ij} = \frac{K_I}{\sqrt{2\pi r}} f_{ij}(\theta) + T\delta_{1i}\delta_{1j} \,. \tag{7-4}$$

Using different combination of the two loading parameters, K_I and T, different near crack-tip fields can be generated. Note that T has dimension of stress and is a function of geometry and loading conditions. Thus $(K_I/\sigma_0)^2$ or equivalently J/σ_0 (using $K_I^{\ 2} = JE/(1\text{-}\nu^2)$) provides the only length scale in the two-parameter formulation. Fields of different crack-tip stress triaxialities can be induced by applying different levels of T/σ_0. Thus, the near-tip field depends on distance only through the $r/(J/\sigma_0)$, and Eq. (7-1) can be written as:

$$\frac{\sigma_{ij}}{\sigma_0} = f_{ij}\left[\frac{r}{(J/\sigma_0)},\theta;T/\sigma_0\right] \tag{7-5}$$

This implies that the stress parameter T provides a convenient means to parameterize specimen geometry effects on crack-tip stress triaxiality (constraint) under condition of well-contained yielding, see for instance Betegon and Hancock [1991]. The T_{stress} can be used as a constraint parameter under SSY conditions. The T_{stress}, compared with others constraint parameters, has the advantage of simplicity, requiring only a linear-elastic analysis of the cracked body. Sherry et al [1995] presented a compendium of T_{stress} solutions for different cracked geometries. Fig. 7.2 gives T_{stress} values in 3PB and CT specimens as a function of the crack-depth, indicating a significant difference of T_{stress} (positive values) in deeply cracked 3PB and CT. Note that the T_{stress} values in Fig. 7.2 are normalized by the remote applied stresses.

A simple equation for the T_{stress} at limit load was developed for the CT specimen by Wallin [2001]. He combined the constraint solutions of Kfouri [1986] with the standard K_I and limit load solutions for the CT-specimen, resulting in the polynomial Eq. (7-6) giving $T_{\text{stress}}/\sigma_Y$ for $a/W \leq 0.7$.

$$\frac{T_{stress}^{CT}}{\sigma_Y} = -2.15 + 15.07\cdot\frac{a}{W} - 27.02\cdot\left(\frac{a}{W}\right)^2 + 15.08\cdot\left(\frac{a}{W}\right)^3 \tag{7-6}$$

The corresponding expression for the 3PB specimens using the T_{stress} solutions of Sham [1991] is given in Eq. (7-7), which is valid for $a/W \leq 0.9$:

$$\frac{T_{stress}^{3PB}}{\sigma_Y} = -1.13 + 5.96\cdot\frac{a}{W} - 12.68\cdot\left(\frac{a}{W}\right)^2 + 18.31\cdot\left(\frac{a}{W}\right)^3 - 15.7\cdot\left(\frac{a}{W}\right)^4 + 5.6\cdot\left(\frac{a}{W}\right)^5 \quad (7\text{-}7)$$

For a test specimen with a/W = 0.50, Eqs. (7-6) and (7-7) yield the T_{stress} /σY = 0.51 and 0.16 for the CT specimen and the 3PB specimen, respectively. The average T_0 difference between CT- and 3PB-specimens, based on the full range of material properties is 7.3ºC with a standard deviation of 2.3ºC [Gao and Dodds, 2000]. These values are amazingly similar to the experimental findings presented in section 5.3, and provides a theoretical validation of the experimental result.

Hancock et al [1993] used a fracture mechanics approach based on the J-T theory to characterize the crack-tip conditions in different cracked geometries. Note that the field of Eq. (7-5) and the applicability of the J-T approach is increasingly violated as the plastic zone under LSY conditions progresses beyond well-contained yielding. For more discussion on applications and limitations of the J-T approach see Hancock et al [1993], Parks [1992] and Kirk and Dodds [1992].

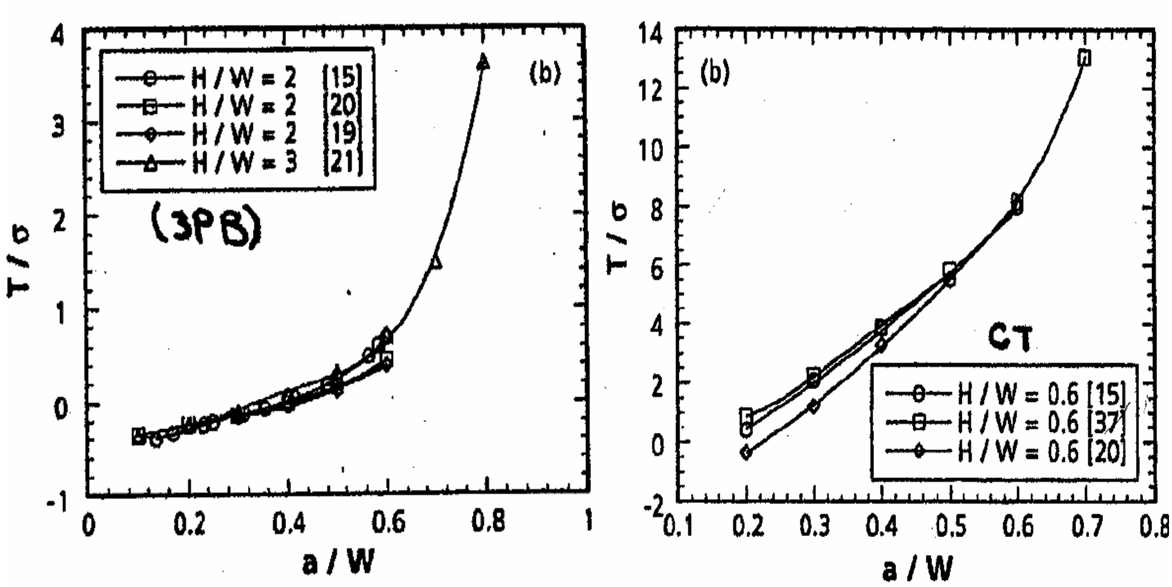

Fig. 7.2: T_{stress} solutions for 3PB and CT specimens [Sherry, 1995].

***The Q* parameter**

O'Dowd and Shih [1991, 1992] studied the crack-tip fields in different geometries at a wide range of load levels by performing detailed finite element analyses. They found that when the crack-tip fields are represented by the first two terms in Equation (7-3), the exponent q is small, indicating that the second term is effectively independent of r. They suggested that the crack-tip stress field can be approximated by:

$$\sigma_{ij} \approx \sigma_{ij}^{\mathrm{Ref}} + Q\sigma_0\delta_{ij}\,. \tag{7-8}$$

Here, $\sigma_{ij}^{\mathrm{Ref}}$ is a reference field with high stress triaxiality, which can be the HRR solution or the SSY solution assuming plane strain conditions. Thus, the constraint factor Q corresponds to a uniform hydrostatic shift in the stress field. Note that Equation (7-8) is valid only in the forward sector $(|\theta| \leq \pi/2)$ within the annulus $J/\sigma_0 \leq r \leq 5\,J/\sigma_0$, which is significant for both brittle and ductile fracture. A definition of Q in elastic-plastic materials using the opening stress component $\sigma_{\theta\theta}$ is proposed as:

$$Q = \frac{\sigma_{\theta\theta} - \sigma_{\theta\theta}^{\mathrm{SSY}}}{\sigma_Y} \qquad \text{at } \theta = 0 \text{ and } \frac{r}{(J/\sigma_Y)} = 2\,, \tag{7-9}$$

where, $\sigma_{\theta\theta}$ is the opening stress taken from the analysis of the actual geometry, $\sigma_{\theta\theta}^{\mathrm{SSY}}$ the opening stress from the SSY analysis (with zero T_{stress}), and σ_Y the yield strength.

Another definition of Q consistent with its interpretation as a triaxiality parameter is proposed as:

$$Q_m = \frac{\sigma_h - \sigma_h^{\mathrm{SSY}}}{\sigma_Y} \qquad \text{at } \theta = 0 \text{ and } \frac{r}{(J/\sigma_Y)} = 2\,, \tag{7-10}$$

where σ_h is the hydrostatic stress. In Eqs (7-9) and (7-10) the SSY solution under plane strain conditions is chosen as the reference field. The *J*-*Q* theory in combination with a micromechanical model has been successfully applied in description of *cleavage fracture* in different geometries, see for instance Dodds *et al.* [1993a, 1993b], Shih *et al.* [1993], Kirk *et al.* [1993], Faleskog [1995] and Bass *et al.* [1999]. Solutions of Q and Q_m in different cracked geometries are given by Sattari-Far [1998]. Fig. 7.3 gives the solutions of these parameters for single-edge notched specimens under pure bending and tension using a material hardening of n = 10. The variations of these constraint parameters along the crack front of a surface crack in a cylinder subjected to internal pressure are shown in Fig. 7.4, where ϕ = 90 degrees is the location at the deepest point.

It is worthy to note that for the SSY condition, one may develop a one-to-one correspondence between Q and T. O'Dowd and Shih [1993] studied this mater, and their results for different hardening exponents are shown in Fig. 7.5.

Factors influencing the crack-tip constraint include specimen thickness, crack depth relative to the specimen thickness, loading type (tension or bending) and loading level. Specimen thickness and crack geometry influences *in-plane* crack-tip constraint, while biaxial loading influences *out-of-plane* crack-tip constraint. Most of the studies reported in the literature consider in-plane constraint effects (for instance shallow-crack effects) and the beneficial effects of the loss of in-plane constraint (T or $Q < 0$) in elevating cleavage fracture toughness, see for instance Towers and Garwood [1986], Theiss *et al* [1992], Kirk *et al* [1993] and Sattari-Far [1995]. Out-of-plane constraint has the potential to influence the crack-tip field in a manner that could alter the cleavage fracture toughness. Experimental evidence is limited, but some data seem to indicate that a significant reduction in fracture toughness is associated with out-of-plane biaxial loading when compared with values from uniaxial loading conditions, see for instance Theiss *et al* [1993], Shum and Bass [1993a, 1993b], Bass *et al* [1999] and Sattari-Far [2004]. There is still no generally validated constraint parameter which can cover effects due to in-plane and out-of-plane constraint in both the cleavage and ductile regimes.

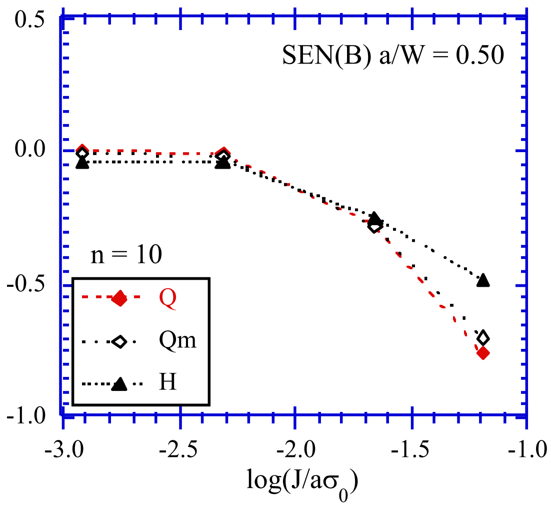

Fig. 7.3: *Q*- parameter solutions in single-edge notched specimens under pure bending and tension using a material hardening of *n* = 10 [Sattari-Far, 1998].

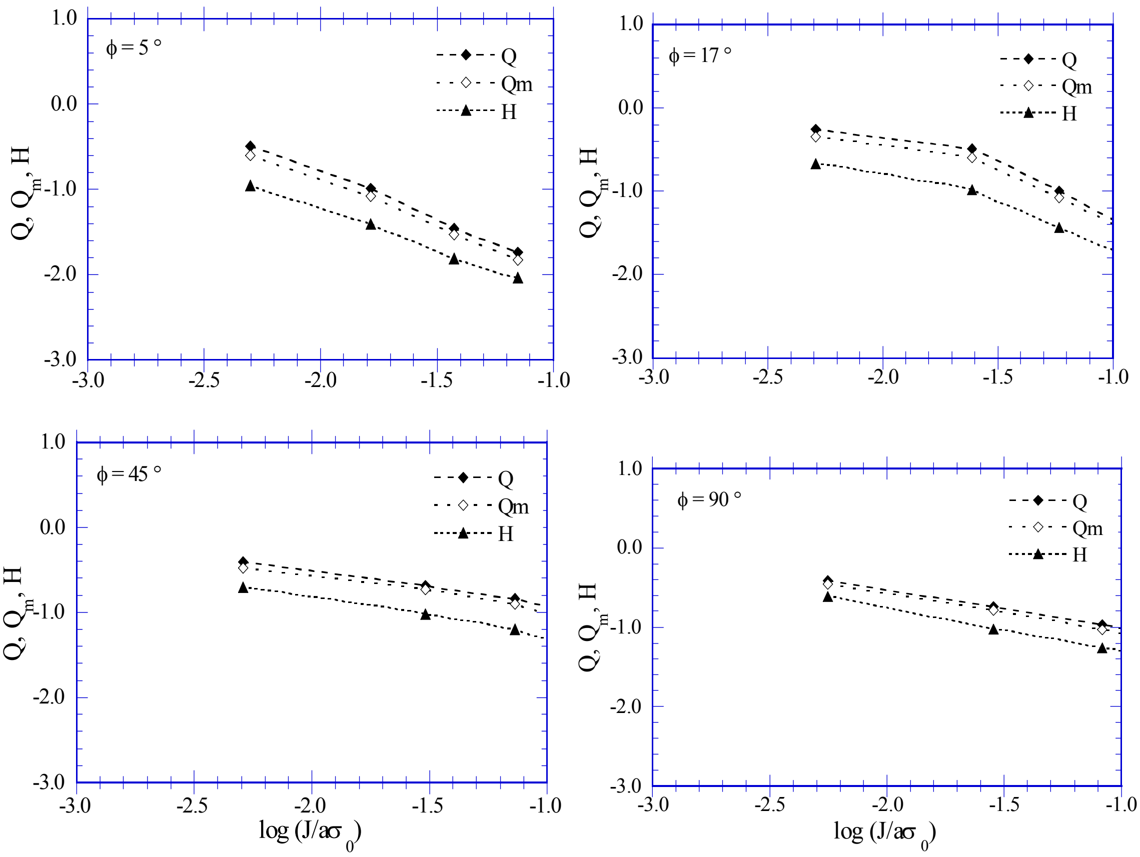

Fig. 7.4: Variations of the constraint parameters at four positions along the crack front of an axial internal surface crack of *a/t* = 0.10 in a cylinder subject to internal pressure using a material hardening of *n* = 10 [Sattari-Far, 1998].

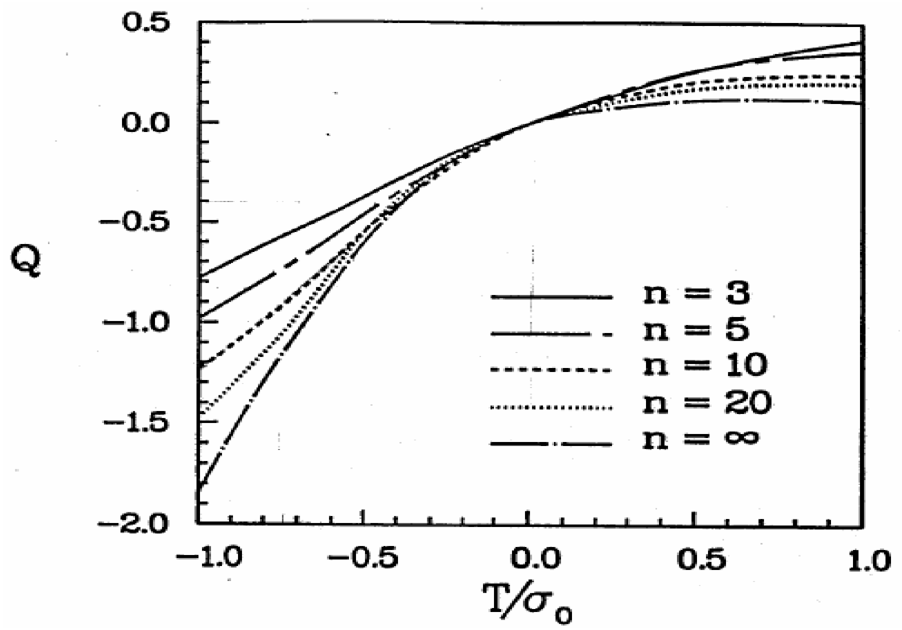

Fig. 7.5: Variations of the constraint parameters *T* and *Q* for different hardening exponents according to O'Dowd and Shih [1993].

7.3. Constraint considerations in the Master Curve Methodology

The use of fracture mechanics in design and failure assessment is to some extent impeded by the difficulties of quantifying the structural constraint as a function of geometry and loading. It is well known that specimen size, crack depth and loading conditions may affect the materials fracture toughness. In order to safeguard against these geometry effects, fracture toughness testing standards prescribe the use of highly constrained deep cracked bend specimens having a sufficient size to guarantee conservative fracture toughness values. The "base line" fracture toughness characterization for brittle fracture given in the Master Curve standard ASTM E1921-03 is such an approach. These "base line" toughness values have one weakness. When applied to a structure having low constraint geometry, the standard fracture toughness estimates may lead to strongly over-conservative estimates. In some cases this may lead to unnecessary repairs or even to an early "retirement" of the structure.

7.3.1. Constraint considerations of small specimens

To improve the Master Curve application in cases with loss of constraint, connections between the constraint parameters (T_{stress} or Q) and the Master Curve transition T_0 are needed.

Such a connection is based on the assumptions presented in Fig. 7.6. It is assumed that, if the constraint can be described by the T_{stress}, then the shape of the fracture toughness temperature dependence is not significantly affected and the constraint differences can be effectively described as a shift in the transition temperature T_0. If the constraint is described by the Q-parameter (large scale yielding), then also the shape of the fracture toughness temperature dependence is affected and a more detailed analysis is required. However, even then, quantifying the constraint in term of T_{stress} will be conservative. This means that if the assumptions made here can be verified and the T_{stress} can be connected with the Master Curve transition temperature T_0, a new tool to assess low constraint geometries with respect to brittle fracture is obtained.

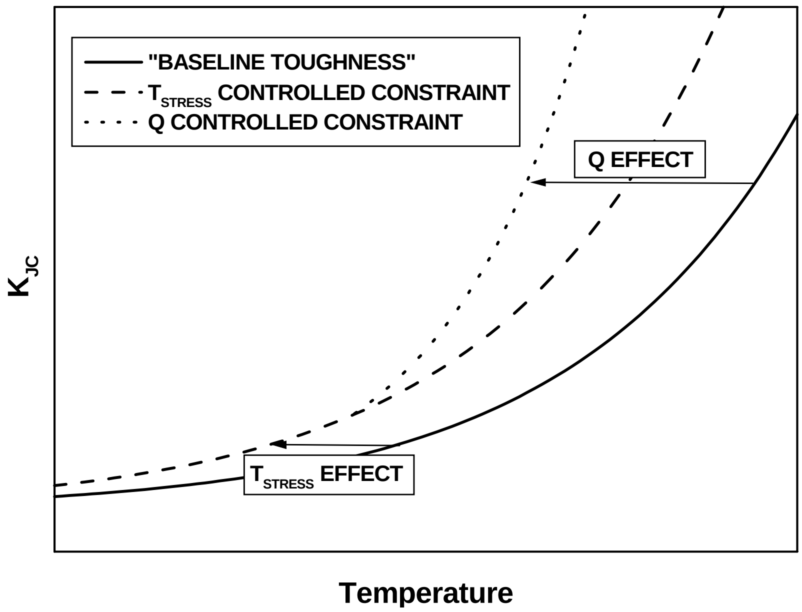

Fig. 7.6: Schematic representation of assumed effect of T_{stress} and Q.

It is imperative that the verification of the assumptions and quantification of the constraint is performed with a well-characterized test geometry. One such geometry is the shallow cracked bend specimen, where both the K_J analysis and the T_{stress} results are well known. The bend geometry remains also in contained yielding to comparatively high K_J-values, thus indicating a T_{stress} controlled constraint description. For this specimen geometry there is also a considerable amount of data available in the literature, omitting the need for any further experimental work. A typical result, showing the trend of increasing fracture toughness with decreasing crack depth is presented in Fig. 7.7, where Mild Steel data by Sumpter [1992] is presented. It is seen that, in the case of bend specimens, for crack sizes above a/W = 0.3 the fracture toughness remains practically constant. In this region the T_{stress} is small or has a positive sign. At smaller crack depths, the fracture toughness starts to increase rapidly. This is connected with the T_{stress} becoming increasingly more negative. Wallin [2001] quantified this increase in toughness in terms of a shift in the Master Curve T_0 transition temperature. His work is briefly described below.

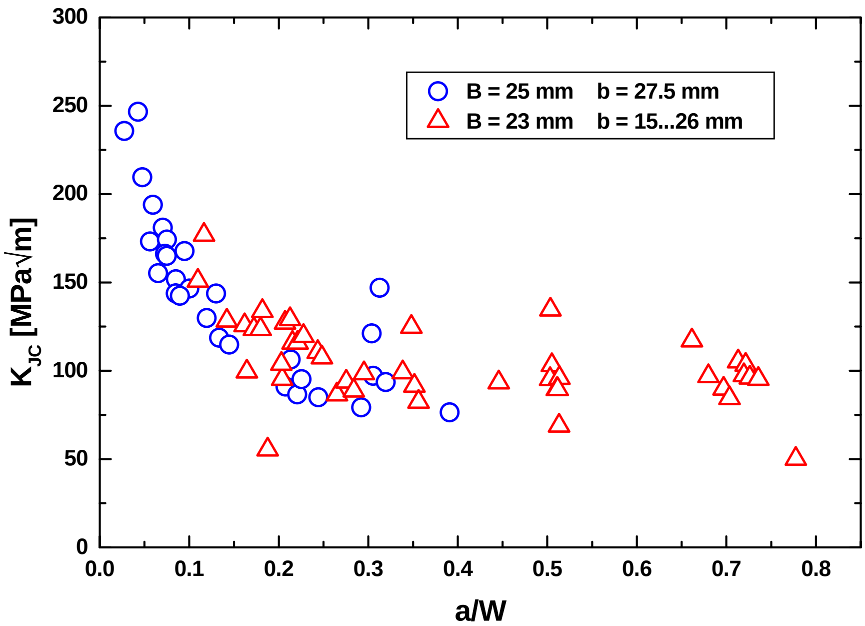

Fig. 7.7: Mild Steel data by Sumpter [1992] showing typical effect of crack depth on brittle fracture toughness.

Materials

The data for the analysis was collected from different literature sources, focussing on fracture toughness results from three-point bend specimens with varying *a/W* values. One pre-requisite for the data was that it should be possible to analyze with the Master Curve method. The list of materials and specimen dimensions is given in Table 7.1.

Master Curve analysis

The Master Curve analysis followed, in principle, the ASTM E1921-03 standard, but the nature of some of the data sets required a more flexible analysis method. The specimen size validity criterion, Eq. (4-2), is used using the size criterion constant M = 30. The limit of contained yielding, which is the parameter that is assumed to determine the measuring capacity of the specimen, is controlled by the ligament. As a check of the assumption above, the shallow crack specimens were also evaluated using crack length a as the controlling dimension. Since this is equivalent to increasing the size criterion M, with respect to b, also the deep flaw specimens were analysed using $M = 120$.

Table 7.1: Materials and specimen sizes used in development of constraint-based Master Curves [Wallin, 2001].

Material	σ_Y [MPa]	a/W	B [mm]	b [mm]
Mild Steel	235	0.05 - 0.7	23 & 25	15 - 28
A533B Cl.1	580	0.1 - 0.55	25 & 89	23 - 74
A36 Steel	248	0.15 & 0.5	13 & 32	6 - 32
A533B Cl.1	400	0.1 & 0.5	51 - 153	48 - 90
A533B Cl.1	432	0.1 & 0.5	101	60 - 91
A533B Cl.1	432	0.1 - 0.5	20 - 32	8 - 22
BS4360 G50C	360	0.2 & 0.5	25	13 - 25
15X2MFA	530	0.1 - 0.5	50 & 100	25 - 50
SAF 2205	548	0.22 - 0.5	25	23 - 25
HY80 W [TS]	650	0.1 & 0.3	35	25 - 31
HY80 W [TL]	650	0.1 & 0.3	35	49 - 63
A508 Cl.3	570	0.1 & 0.5	25	13 - 22
A533B Cl.1 D	5801	0.03 - 0.49	10	5.1 - 9.7
A517 G70	300	0.13 - 0.53	10 - 51	5 - 45
H.S. Steel	663	0.1 - 0.5	15	7 - 13
HY80 W D	7602	0.2 & 0.3	50	35 & 40
HY80 W D	8003	0.15 - 0.32	50	34 - 43
10MnMoNi 55	630	0.1 & 0.55	25	22 - 45

Analysis results

Making the quite realistic assumption that the test specimens usually failed close to plastic limit load, T_{stress} solutions for the three point bend specimen given i Eq. (7-7) were used in this analysis. The use of Eq. (7-7), requires knowledge about the materials yield strength at the test temperature. For simplicity only one yield strength value was used for each data set. For consistency, in all cases, the estimated yield strength at the T_0 temperature was used, regardless of the actual test temperature (or temperatures). This is bound to produce some uncertainty in the results, but this is considered only to be of a second order significance. Some results of this Master Curve analysis are presented in Figs. 7.8 to 7.11. More results and details of this study are found in Wallin [2001].

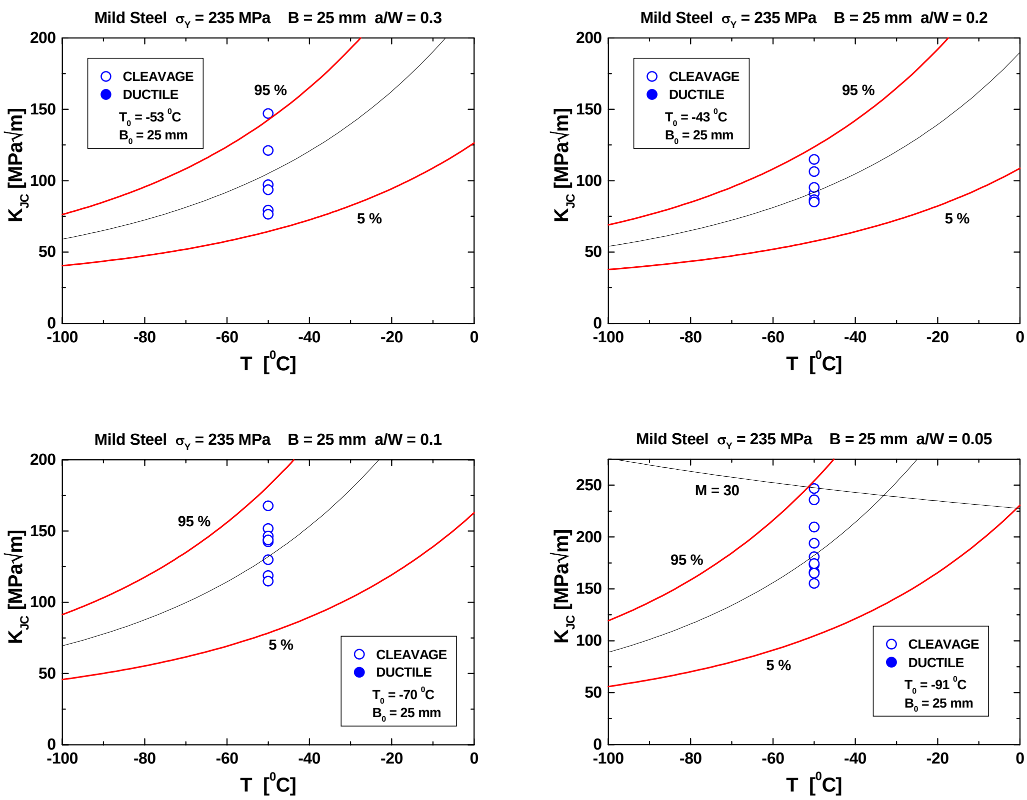

Fig. 7.8: Master Curve analysis of Mild Steel data presented by Sumpter [1992].

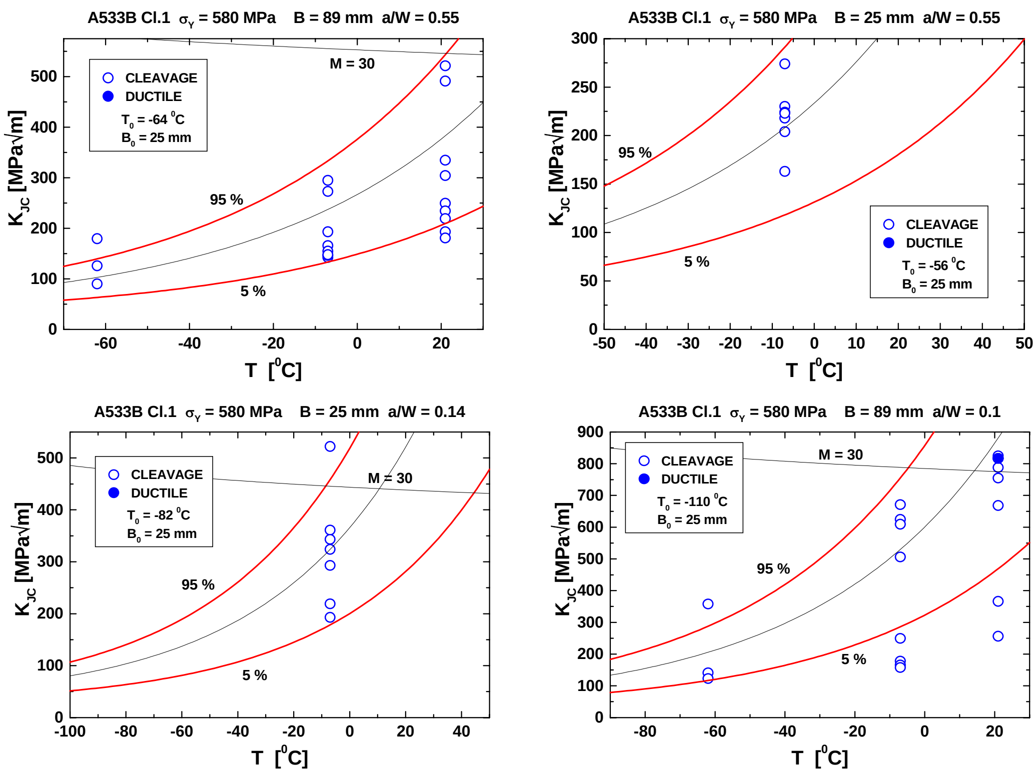

Fig. 7.9: Master Curve analysis of A533B Cl 1 data presented by Link & Joyce [1995].

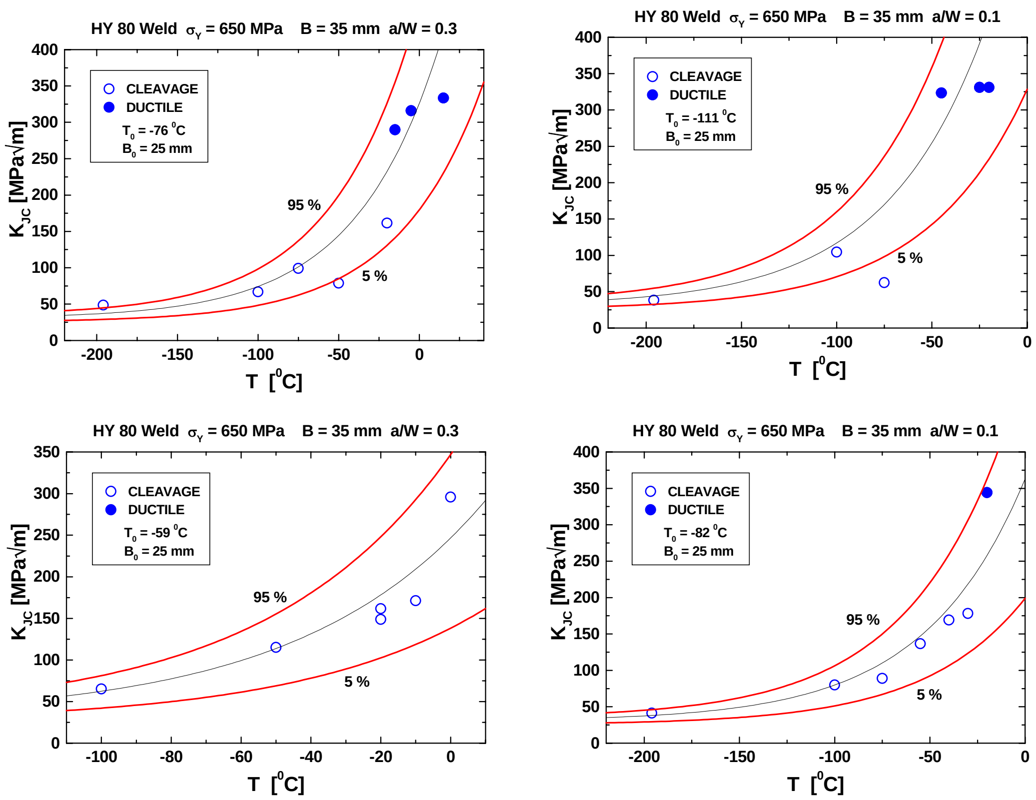

Fig. 7.10: Master Curve analysis of HY 80 weld data presented by Sumpter [1982].

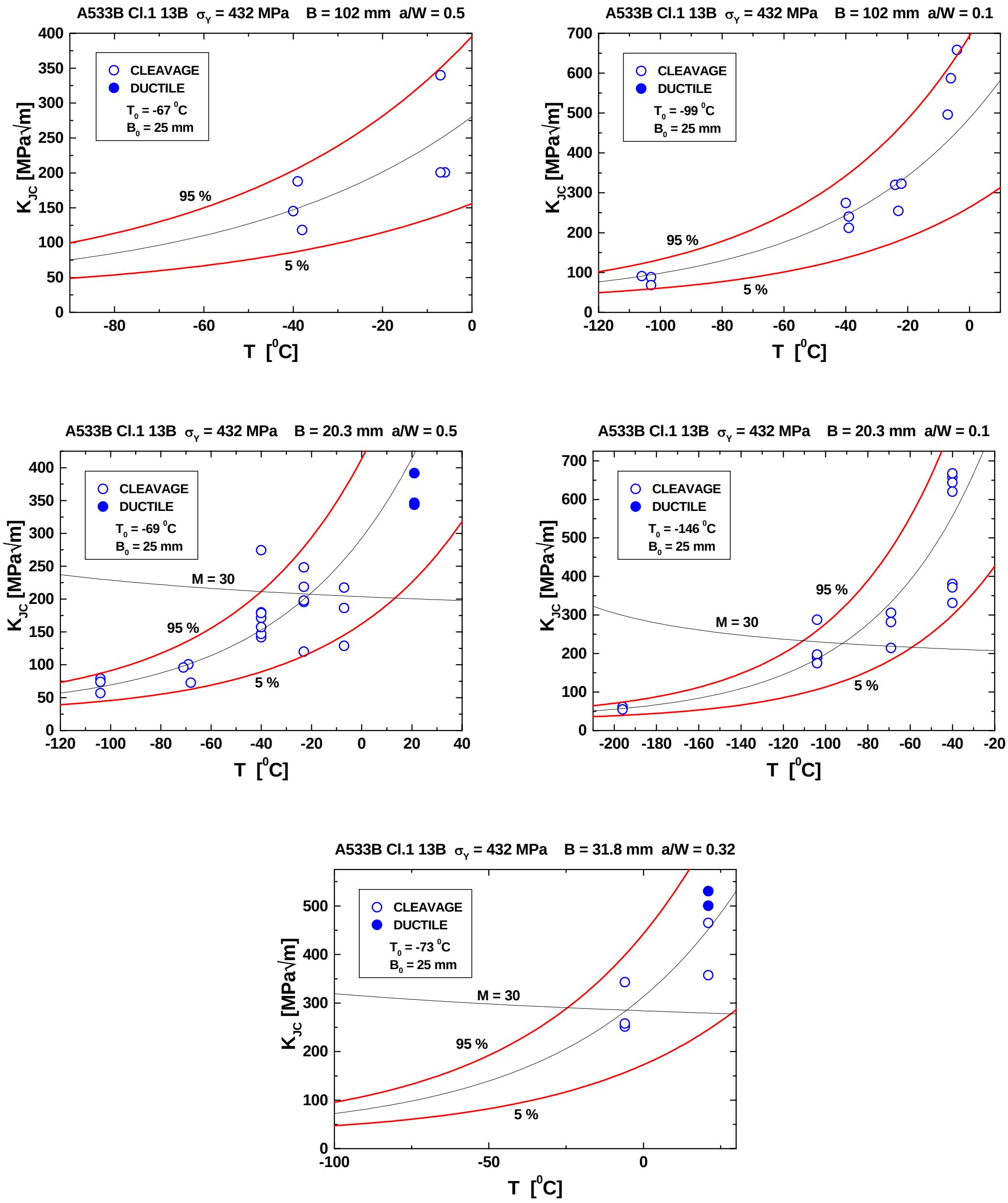

Fig. 7.11: Master Curve analysis of A533B Cl.1 Steel data presented by Theiss & al. [1992] and Smith & Rolfe [1994].

The Master curve analysis of these data supports the assumption that the shape of the Master Curve remains essentially unaffected by T_{stress}. If the shape would change, the more severe censoring criteria should produce systematically different T_0 values. Since this did not occur, the shape must have remained the same. The issues of the shape and scatter are further studied in Figs. 7.12 and 7.13 with different T_{stress} values. Fig. 7.12 contains a composite plot of all the "valid" deep flaw data (having positive T_{stress}), limited to the temperature range of interest in ASTM E 1921 (-50ºC<T- T_0 <+50ºC). Fig. 7.13 contains a similar plot for all the valid shallow flaw data having estimated T_{stress} in the range -500 - -300 MPa. Even though the shallow flaw data is more scarce than the deep flaw data, it is quite clear, that no significant differences between the two sets are visible. In both cases, the Master Curve temperature dependence and scatter assumption are well verified. Since the figures contain only valid data, some censored values from the upper part of the scatter band are not plotted, but this does not affect the overall picture.

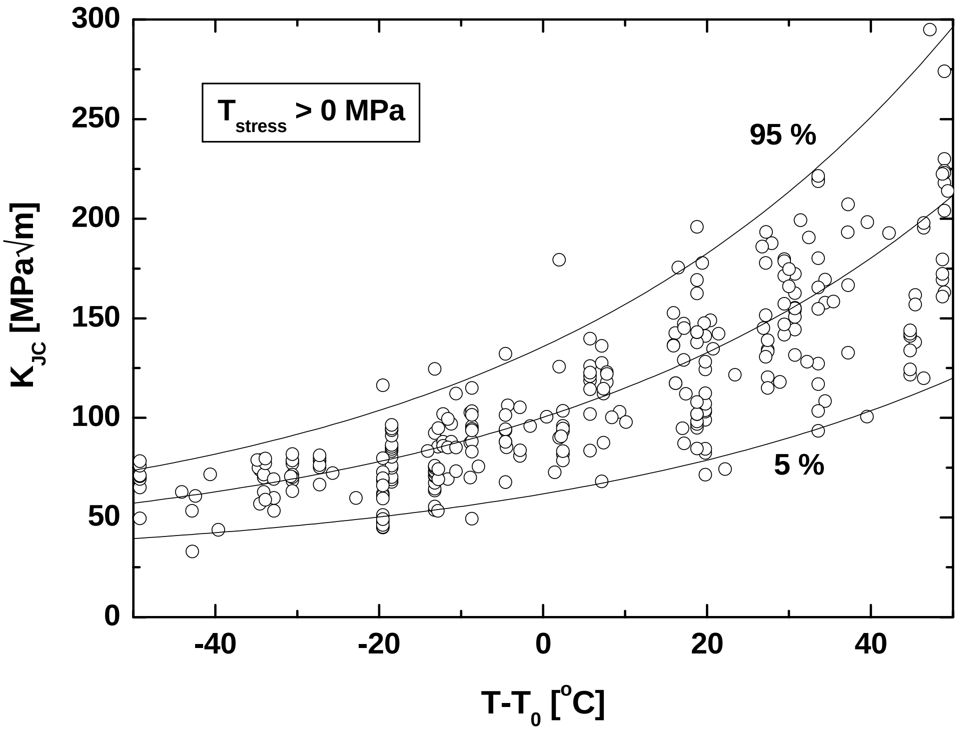

Fig. 7.12: Composite plot of all deep flaw data. Censored data not included.

Generally, it can be stated that the crack depth does not have a significant effect on the temperature dependence, nor the scatter of the brittle fracture toughness. This seems to verify the assumption that the T_{stress} related constraint affects only the transition temperature T_0 and not the shape of the toughness curve. If the assumption would be wrong, a clear change in the temperature dependence and scatter of the shallow cracked data should be visible at lower fracture toughness values than predicted by the size criterion.

The study indicates that positive T_{stress} has an insignificant effect on fracture toughness, whereas for negative values of T_{stress}, the Master Curve T_0 changes nearly linearly with T_{stress}, as shown in Fig. 7.14.

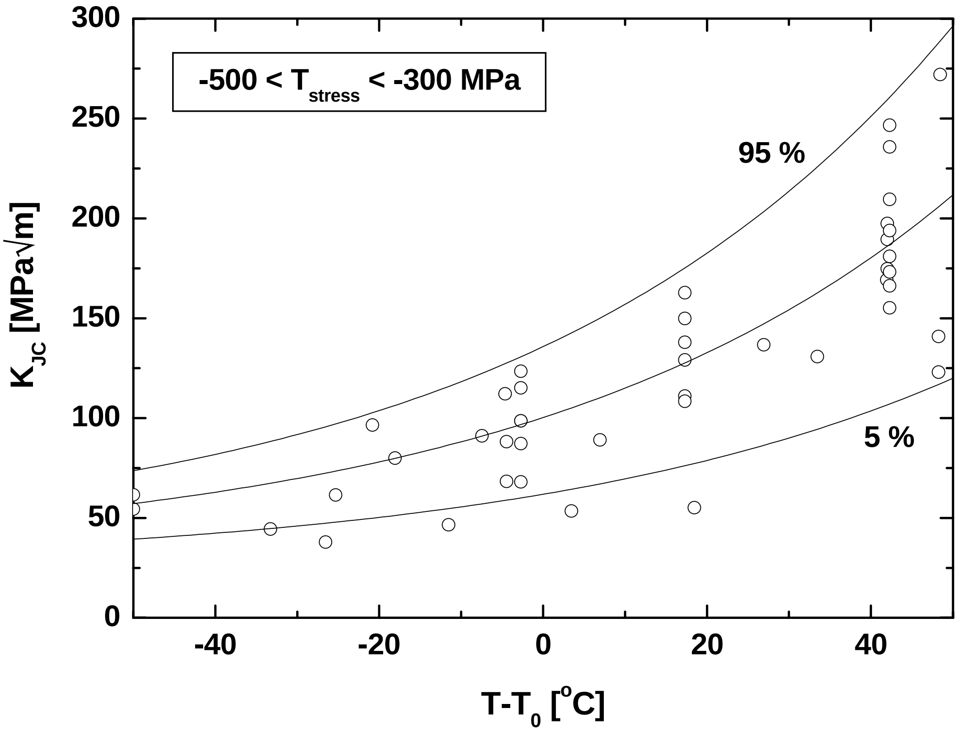

Fig. 7.13: Composite plot of shallow flaw data with -500 < T_{stress} < -300 MPa. Censored data not included.

Since the effect of large scale yielding related loss of constraint (described with Q), probably also affects the results in Fig. 7.14 to some degree, it is better to not define a mean T_{stress} dependence for T_0, but to make it a little conservative. This results in a simple linear relation giving the effect of T_{stress} on T_0 as:

$$T_0 \approx T_{0deep} + \frac{T_{stress}}{10\,MPa/°C} \quad : \textit{for } T_{stress} < 0 \tag{7-11}$$

The above equation provides a simple tool for the application of the Master Curve technology also to low constraint geometries. The fracture toughness of the structure will normally be conservatively estimated by Eq. (7-11), so the integrity of the safety assessment is not in jeopardy even when the structure specific constraint is accounted for.

The present result can also be transformed into a simple approximate constraint correction directly for K_{JC}. Combining Eq. (7-11) with the Master Curve temperature dependence, and specifying a general failure probability and also making the equation compatible with the size adjustment, a constraint correction for a single value fracture toughness can be approximated as:

$$K_{JC} \approx 20 + \left(K_{JCdeep} - 20\right) \cdot \exp\left(0.019 \cdot \left[\frac{-T_{stress}}{10}\right]\right) \qquad for\ T_{stress} < 0 \qquad (7\text{-}12)$$

Here, K_{JC} in MPa√m and T_{stress} in MPa. The validity of Eq. (7-12) is checked in Fig. 7.15, where its predictions are compared with the mean behaviour of a data set performed at single temperatures.

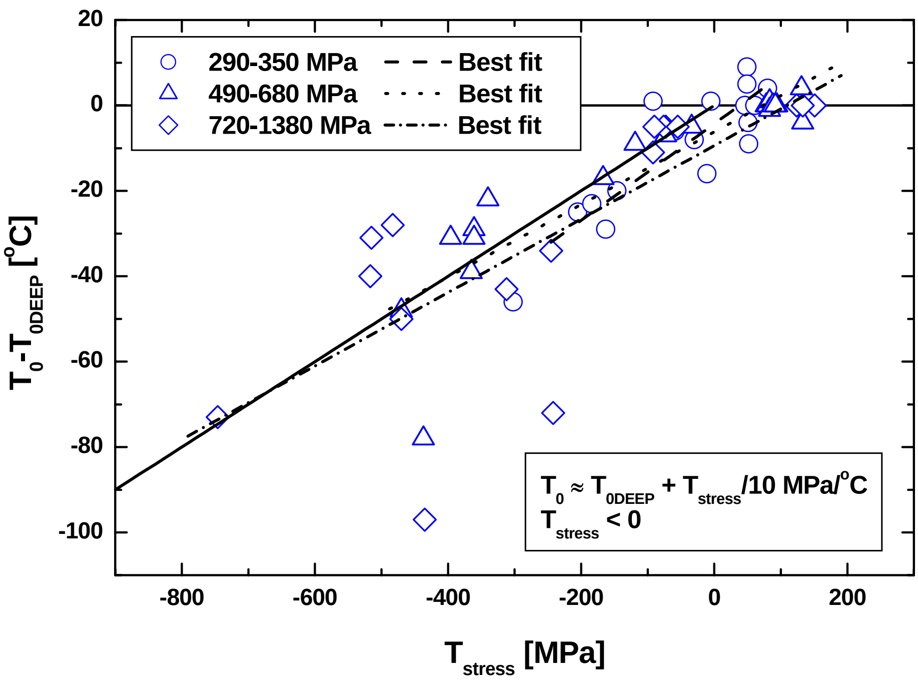

Fig. 7.14: Effect of T_{stress} on the T_0 transition temperature. Materials separated based on yield strength at T_0 temperature.

Even though only bend geometries were included in the present study, the results should be equally applicable for tension geometries. These loose contained yielding earlier than bend specimens and the effect will just be to make Eqs. (7-11) and (7-12) more conservative for these geometries. A more precise description of tension geometries and bend specimens in large scale yielding requires the use of the *Q*-parameter or some similar method capable of describing large scale yielding effects. This appears to be a natural next step in the development of the Master Curve technology.

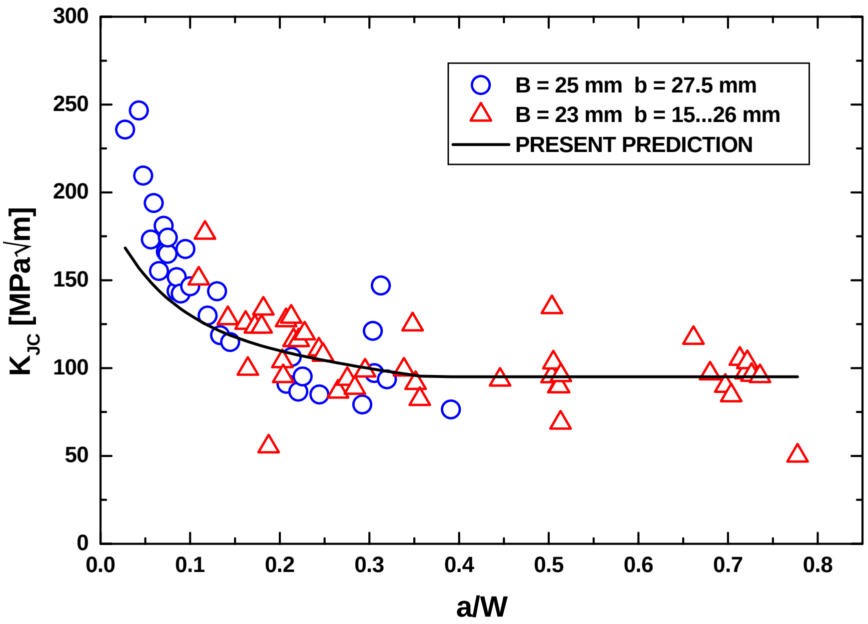

Fig. 7.15: Comparison of the constraint correction prediction given by Eq. (7-12) with Sumpter's Mild Steel data [1992].

7.3.2. Constraint considerations of large scale experiments

(a) Application of MC on the PTSE-1 and PTSE-2 tests

Application of the T_{stress} based Master Curve, Eq. (7-11), was attempted by Wallin [2004c]. Two large scale experiments were analysed based on the Master Curve methodology and considering the constraint effects by using T_{stress}. The experiments studied were the pressurised thermal shock experiments PTSE-1 and PTSE-2, which are described in section 6.10 of this report.

The material for PTSE-1 was a SA-508 class 2 steel with a yield stress of 625 MPa. The fracture toughness was measured using 25 mm CT specimens, so their T_{stress}/σ_{YT} is about 0.4. Since the flaw in the experiment was 1000 mm in length, a value of +65ºC was taken as descriptive of the material. Similarly, the crack arrest test results were analysed with a similar but simpler log-normal distribution having the same temperature dependence as the MC. The analysis indicated a transition temperature of +113ºC for the median crack arrest toughness of 100 MPa√m. The material for PTSE-2 was an A 387 grade 22 class 2 steel (2 ¼ Cr-1 Mo) with a yield stress of 470 MPa. Also here, the fracture toughness characterisation used 25 mm CT specimens. There is a clear difference between the two material states.

The MC analysis of the three transients of PTSE-1 is presented in Fig. 7.16, and for the two transients of PTSE-2 in Fig. 7.17. The first transient in PTSE-1 did not lead to fracture, but the other transients caused both crack initiation and arrest. The figures include the median MC predictions for a 1 m long crack and the median crack arrest predictions. The median MC predictions have not been adjusted for constraint. It was found that the median crack arrest curves, describe very well the crack arrest events in the tests. This means that standard crack arrest toughness is directly applicable to describe crack arrest of a component. This is not the case for the initiation fracture toughness.

In both tests, the CT specimen based median MC has to be shifted to lower temperatures to provide a description of the average initiation toughness. The PTSE-1 requires a shift of approximately 46ºC to make the MC describe the initiation events and the PTSE-2 requires a shift of approximately 26ºC. The shifts are a direct consequence of the different constraint in the tests and in the CT specimens. The behaviour of PTSE-2 is additionally affected by a warm pre-stress effect in transient 2A. The T_{stress} for the CT specimens is approximated based on Eq. (7-6) and the yield stress at +100ºC as approximately 230 MPa for the PTSE-1 material and 100 MPa for the PTSE-2 material. The T_{stress} values for the pressure vessels were estimated from the measured K_I values together with crack depth and β-values for a SE(T) specimen given by Shery et all [1995]. The shallow flaw SE(T) specimen is expected to provide a good estimate of the pressure vessel constraint in these tests. The estimate for PTSE-1 is approximately -350 MPa and for PTSE-2 approximately -270 MPa. This means that the T_{stress} difference between the Ct specimen and the pressure vessel is of the order of 580 MPa for PTSE-1 and of the order of 370 MPa for PTSE-2. When these values are put into Eq. (7-11), the resulting expected shift in T_0 is for PTSE-1 48ºC and for PTSE-2 31ºC. These predictions comply extremely well with the shifts estimated directly from the tests (46ºC for PTSE-1 and 26ºC for PTSE-2). This "blind" estimation provides strong proof for the validity of Eq. (7-11) and the simple use of T_{stress} to quantify constraint.

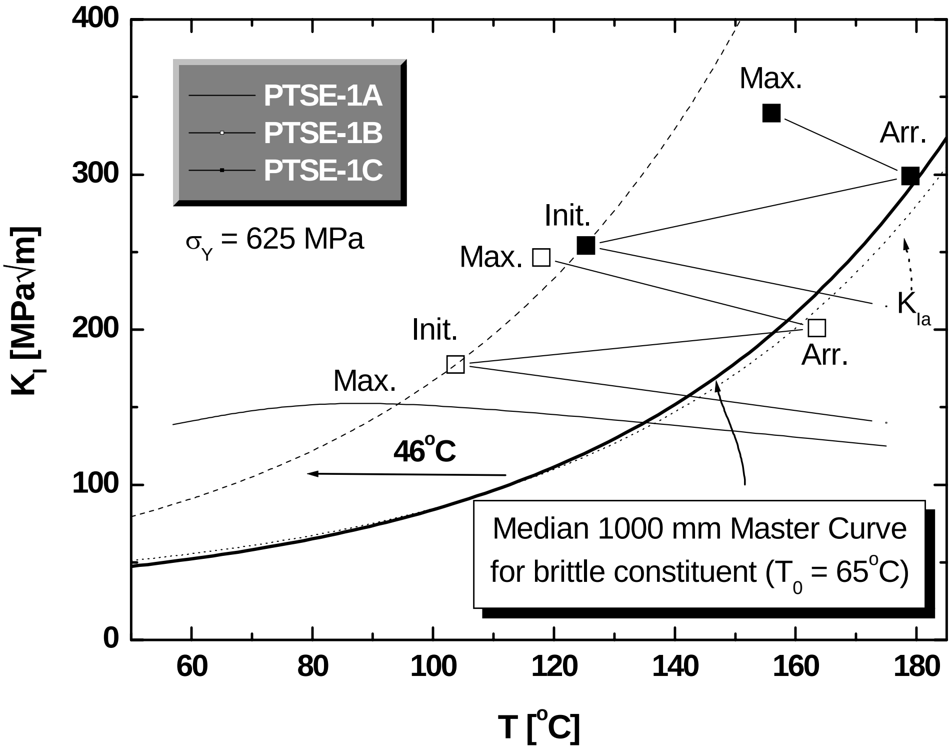

Fig. 7.16: Master Curve analysis of the PTSE-1 test [Wallin, 2004c]. Note that the median MC is not adjusted for constraint.

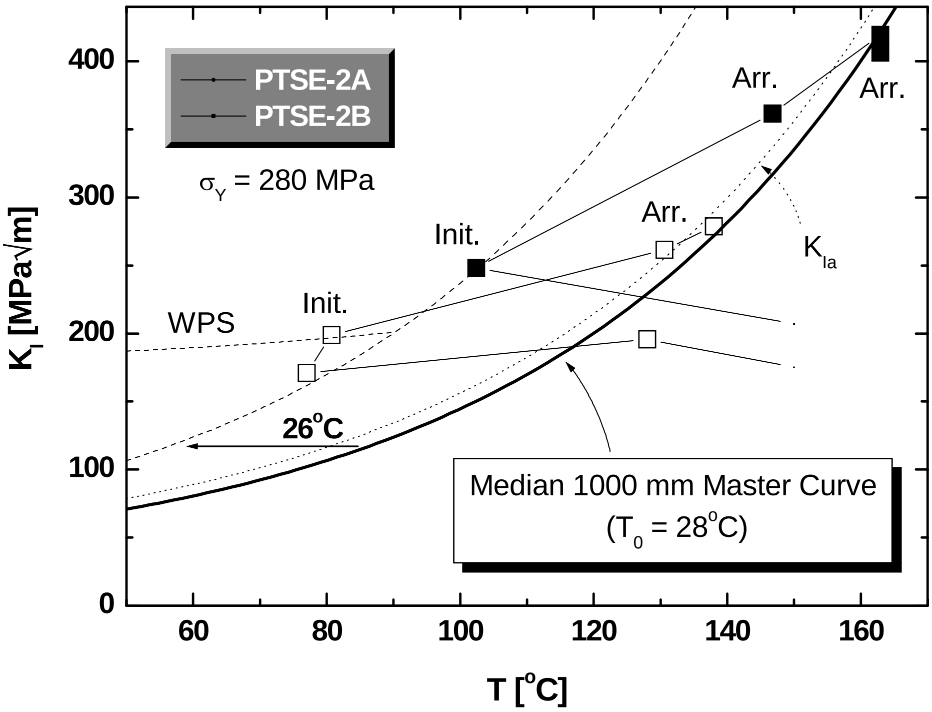

Fig. 7.17: Master Curve analysis of the PTSE-test [Wallin, 2004c]. Note that the median MC is not adjusted for constraint.

(b) Application of MC on the NESC-IV tests

Application of the constraint based Master Curve was attempted by Sattari-Far [2004b] on the NESC-IV tests. Seven large scale experiments were analysed based on the Master Curve methodology and considering the constraint effects by using Q_{stress}. The experiments studied were cruciform clad specimens containing surface cracks under biaxial loading, and beams containing embedded defects under uniaxial loading. The test specimens were fabricated from A533 GB with a stainless steel clad overlay. The yield strength of the base and weld materials were 500 MPa and 625 MPa at room temperature. The fracture toughness was obtained by testing on both shallow and deep SEN(B) specimens. The tests were conducted at low temperatures to ensure the occurrence of brittle fracture events. The crack growth in the cruciform specimens mainly occurred in the cladding HAZ (close to the free surface), while it occurred at the deepest points in the beams with embedded flaws. These tests are described in section 6.9 of this report.

Table 7-2 gives the results of calculations of the crack-tip constraint in the different crack geometries of the performed tests. The results are for SEN(B) specimens of shallow and deep cracks, and interesting locations in the cruciform and beam specimens. It is observed that the shallow SEN(B) specimens and the beams with embedded flaws under uniaxial loading give substantial loss of constraint compared with the constraint state in a standard SEN(B) of a/W $\approx$ 0.50 ($Q_{stress} \approx 0$). However, the cruciform specimens with shallow surface cracks under biaxial loading demonstrate higher constraint state than those in a standard SEN(B) of a/W $\approx$ 0.50.

Fig. 7-18 shows the Master Curve analysis of two beam tests with embedded flaws. The crack driving force and constraint state at the deepest points, where brittle fracture initiations occurred, are selected for the analysis. K_J values at fracture are compared with the size-corrected median Master Curves, both without accounting for constraint, and also with a constraint consideration according to Eq. (7-11). The constraint consideration resulted in a shift of the Master curve approximately 30 ^oC towards the left. It is observed that the constraint consideration significantly improves the Master Curve predictions of the tests.

Fig. 7-19 shows the Master Curve analysis of five cruciform tests with surface cracks. The crack driving force at the mid-point of the cladding HAZ (close to the surface, where brittle fracture initiations occurred) are selected for the analysis. As constraint consideration according to Eq. (7-11) does not cover positive constraint ($T_{stress} > 0$), no constraint corrections are conducted on the Master Curves. It is observed that the fracture events are within the 5% and 95% Master Curves. As the constraint states in the tests are higher than those in a standard SEN(B), the Master Curves would be shifted to the right if the positive constraint would be considered. This would shift the points close to 5% curve towards the 50% curve. However, the quantitative consideration of positive constraint ($T_{stress} > 0$) is not studied yet, and this is an open question for future research.

Table 7.2: Crack-tip constraint values in different crack geometries at a load level of K = 100 MPa√m in the NESC-IV tests [Sattari-Far, 2004b].

Crack geometry	Q
SEN(B)	
a/W = 0.10	-0.45
a/W = 0.50	-0.05
Cruciform tests	
At deepest point	+0.10
In the cladding HAZ	+0.25
Unclad and clad embedded flaws	
Surface tip, Tip-S	-0.80
Deep tip, Tip-D	-0.37

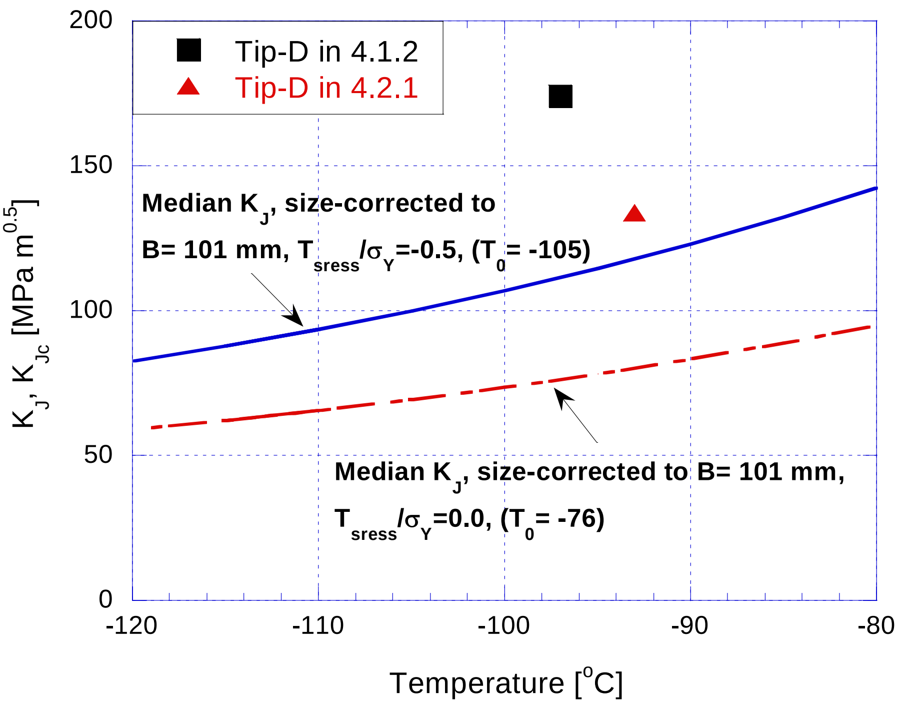

Fig. 7.18: Cleavage fracture toughness of embedded flaws under uniaxial loading in the NESC-IV tests [Sattari-Far, 2004b]

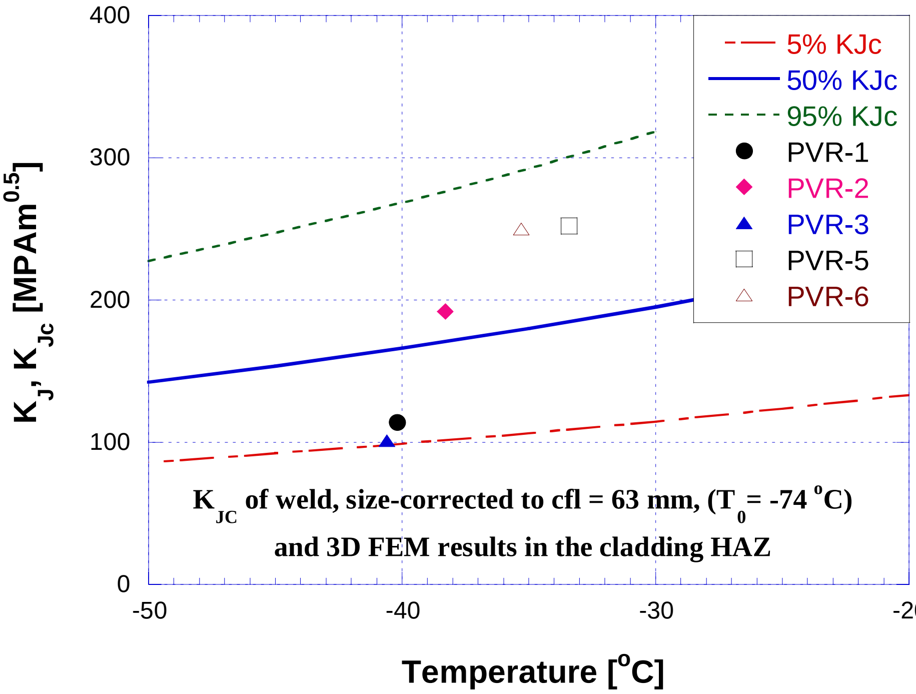

Fig. 7.19: Cleavage fracture toughness of surface flaws under biaxial loading in the NESC-IV tests [Sattari-Far, 2004b]

7.4. Constraint correction for surface cracks

Normally, the Master Curve parameters are determined using test specimens with "straight" crack fronts and comparatively uniform stress state along the crack front. This enables the use of a single K_I value and single constraint value to describe the whole specimen. For a real crack in a structure, this is usually not the case. Normally, both K_I and constraint varies along the crack front and in the case of a thermal transient, even the temperature will vary along the crack front. Generally, real cracks are given in the form of ellipses in order to simplify the analysis. An example of an elliptic surface crack is shown in Fig. 7.20.

The standard Master Curve cumulative failure probability expression is of the form:

$$P_f = 1 - \exp\left\{ \frac{B}{B_0} \cdot \left(\frac{K_I - K_{\min}}{K_0 - K_{\min}} \right)^4 \right\} \qquad (3\text{-}24\text{rep})$$

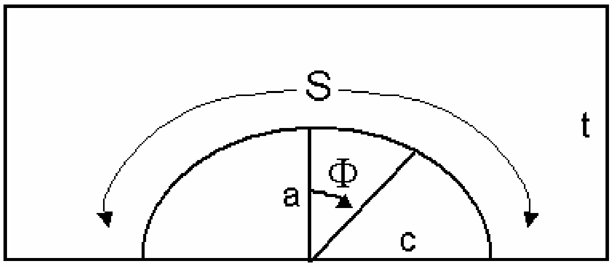

Fig. 7.20: Definition of dimensions of elliptic surface crack.

where B is the specimen thickness, B_0 is the normalisation thickness 25 mm, K_{min} is the minimum fracture toughness (20 MPa√m), K_I is the crack driving force and K_0 is the fracture toughness corresponding to failure probability of 63.2 %.

For a real three dimensional crack, both K_I and K_0 may vary as a function of location (Φ) along the crack front. This leads to the need of a more general expression for the cumulative failure probability, which is given in Eq. (7-13), Wallin [2004d].

$$P_f = 1 - \exp\left\{ \int_0^s \left(\frac{K_{I\Phi} - K_{\min}}{K_{0\Phi} - K_{\min}} \right)^4 \cdot \frac{ds}{B_0} \right\} \tag{7-13}$$

This equation is not suited for a simple visualisation of the results. A visualisation of this equation can be achieved by defining an effective stress intensity factor K_{Ieff}. The procedure is to determine an effective driving force, which would give the same failure probability as Eq. (7-13), in the context of a standard Master Curve presentation. This means essentially a combination of Eqs (3-24) and (7-13), which is presented in Eq. (7-14).

$$K_{IeffT\min} = \left\{ \int_0^s \left(\frac{K_{I\Phi} - K_{\min}}{K_{0\Phi} - K_{\min}} \right)^4 \cdot \frac{ds}{B_0} \right\}^{1/4} \cdot \left(K_{0T\min} - K_{\min} \right) + K_{\min} \tag{7-14}$$

$K_{I\Phi}$ is obtained from the stress analysis as a function of location (ϕ). K_{0Tmin} is the standard (high constraint) Master Curve K_0, corresponding to the minimum temperature along the crack front (T_{min}). It has the form:

$$K_{0T\min} = 31 + 77 \cdot \exp\left[0.019 \cdot \left(T - T_{0T\min}\right)\right] \tag{7-15}$$

$K_{0\Phi}$ is the local K_0 value, based on the local temperature and constraint. It can be expressed as:

$$K_{0\Phi} = K_{0T,Tstress} = 31 + 77 \cdot \exp\left[0.019 \cdot \left(T - T_{0deep} - \frac{Tstress}{10\ \mathrm{MPa/°C}}\right)\right] \tag{7-16}$$

This equation is also directly applicable with the ASME Code Case N-629 fracture toughness reference curve, since it is written in terms of the standard deep specimen T_0.

Eqs. (7-14) to (7-16) give the effective crack driving force K_{Ieff}, normalised to represent a standard Master Curve (with crack front $B_0 = 25$ mm) and the minimum temperature along the crack front. Note that K_{Ieff} accounts for the local stress and constraint state and temperature along the crack front. For cases with constant temperature and no loss of constraint along the crack front, the maximum effective stress intensity factor K_{Ieff} expressed in Eq. (7-14) may be simplified to be equal to the maximum K_I value along the crack front.

In conducting fracture assessment of a surface crack, the effective crack driving force K_{Ieff} should be compared with the fracture toughness. The fracture toughness can be expressed either with the 5 % lower bound Master Curve, which can be expressed in the form:

$$K_{5\%,T\min} = 25.2 + 36.6 \cdot \exp\left[0.019 \cdot \left(T_{\min} - T_{0deep}\right)\right] \tag{7-17}$$

or by using the fracture toughness reference curve from ASME Code Case N-629 (or N-631). This can be expressed in the form:

$$K_{IC,ASME,T\min} = 36.5 + 3.084 \cdot \exp\left[0.036 \cdot \left(T_{\min} - T_{0deep} + 56\right)\right] \tag{7-18}$$

The resulting visualisation is presented in Fig. 7.21. The difference to the presently used visualisation is that the fracture toughness is not directly compared to the crack driving force estimated from stress analysis. Instead, the fracture toughness is compared to an effective driving force, which accounts for the local stress and constraint state and temperature along the crack front, as well as the crack front length. In this way, it is possible to combine the classical fracture mechanical analysis and the state of the art of the Master Curve analysis, and presenting the analysis result in a conventional format.

However, it should be noted that postulated flaws often contain unrealistically long crack fronts. A quarter thickness flaw assumption may be justified, purely from a driving force perspective (as originally has been the intention). From a statistical size adjustment point of view, the assumption is over-conservative. If such postulated flaws are analysed using K_{Ieff}, an additional size adjustment is recommended. A more realistic maximum crack front length is 150 mm. This value is also in line with the original K_{IC} data and therefore justifiable in terms of the principle of functional equivalence. Thus, the form of K_{Ieff} for an excessively large postulated flaw (s > 150 mm) becomes:

$$K_{effT\min} = \left\{ \int_0^s \left(\frac{K_{I\Phi} - K_{\min}}{K_{0\Phi} - K_{\min}} \right)^4 \cdot \frac{150 \cdot ds}{B_0 \cdot s} \right\}^{1/4} \cdot \left(K_{0T\min} - K_{\min} \right) + K_{\min} \tag{7-19}$$

where the postulated crack front length (*s*) is replaced by a maximum crack front length of 150 mm. If NDE can guarantee a smaller value of *s* than 150 mm, it can be reduced further.

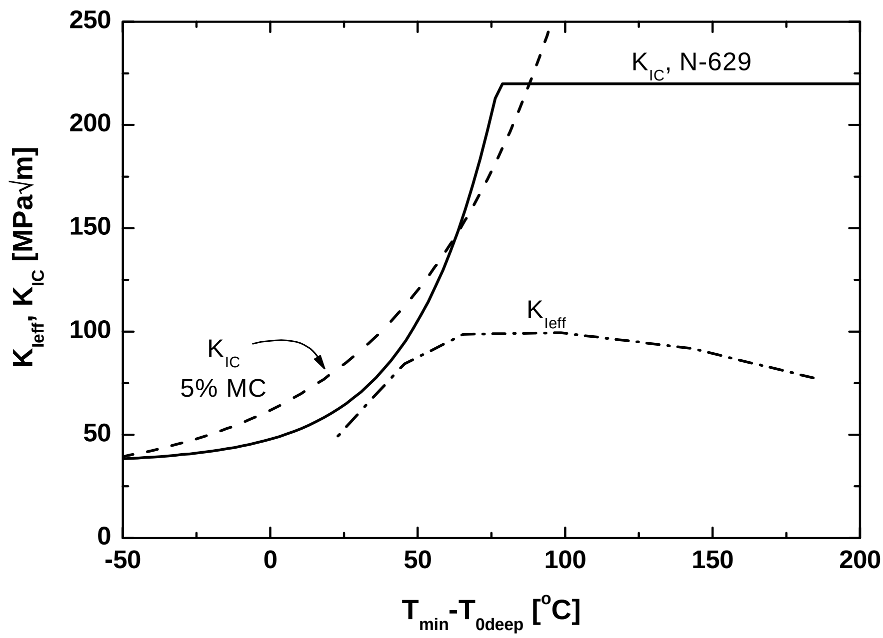

Fig. 7.21: Principle of visualising Master Curve analysis of real flaws.

8. CORRELATION BETWEEN CHARPY IMPACT CVN AND T0

In an ideal situation in structural integrity assessments, fracture toughness data are generated through the use of appropriate fracture mechanics-based toughness tests. However, in the case of existing nuclear power plants, such data are often not available and can not be easily obtained due to the lack of testing material or impracticability of removing material from the actual structure. For such cases, the available material information is often limited to Charpy-V test results. The Charpy impact test was patented by Mr. Charpy, at the beginning of 1900. The test is known to use several different notch configurations, but the most common geometry today is the V-notch. Thus, the test is known as the Charpy-V impact test (CVN). In the test, the energy required to fracture the specimen is recorded. Since the test is dynamic, it measures the materials dynamic properties. However, the use of a shallow notch, reduces to some extent the conservatism introduced by the impact rate. The biggest weakness in the test is that it measures the total "energy" required to fracture the specimen. Thus, the test does not separate between fracture initiation, crack propagation and arrest. This decreases the significance of the test and makes it more qualitative in nature.

A consistent use of the Master Curve method for the assessment of nuclear reactor pressure vessels, require that an estimate of the Master Curve transition temperature T_0 is obtained from the Charpy-V information. This issue is complicated by the fact that the quality and quantity of Charpy-V test data varies from case to case. Sometimes the whole Charpy-V transition curve may be available, while in the other cases only part of the transition curve, or even only a single temperature, is included. There must be a consistent method of applying such different quality data to estimate T_0. The method must be self awarding so that better data quality provides less conservative T_0 estimates than poor data quality. This is the goal of the work presented in this Chapter. The work is limited only to western nuclear grade pressure vessel steels and their welds.

8.1. Charpy-V – T_0 correlations for nuclear grade pressure vessel steels

Two different Charpy-V correlations have been published, specifically developed for the Master Curve T_0, Wallin [1989] and Sokolov and Nanstad [1999]. The first one is a correlation between T_0 and the 28J CVN transition temperature that is also used in the SINTAP structural integrity assessment procedure [1999] and the standard BS 7910. The original correlation is presented in Fig. 8.1.

The second correlation was developed by ORNL between T_0 and the 41J CVN transition temperature, which is the transition temperature most commonly used in nuclear surveillance work, shown in Fig. 8.2.

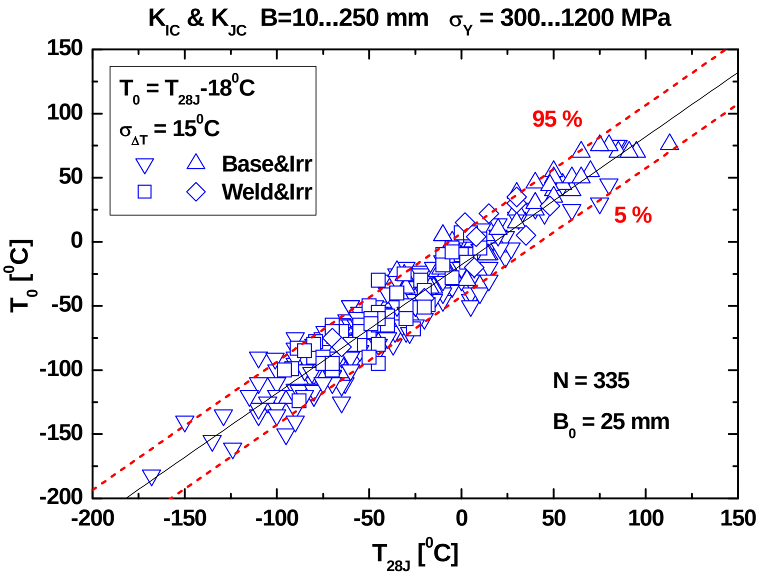

Fig. 8.1: Original Master Curve correlation for T_{28J} transition temperature [Wallin, 1989].

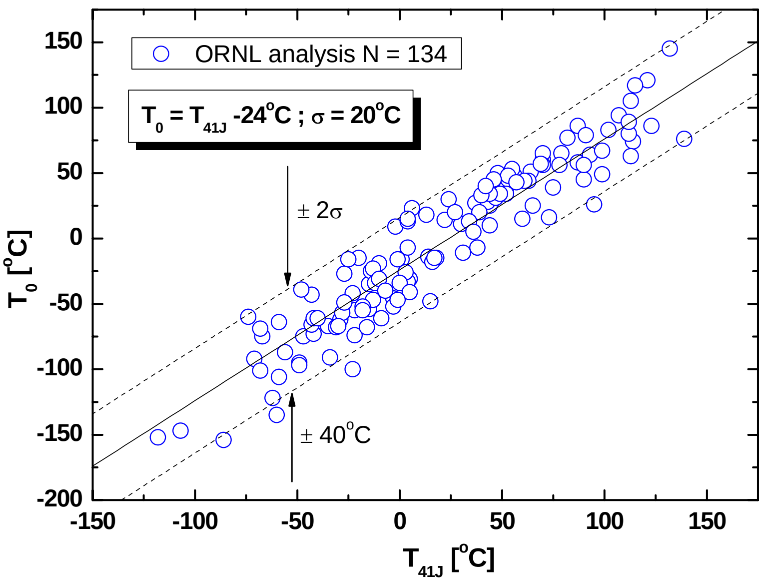

Fig. 8.2: ORNL correlation for T_{41J} transition temperature [Sokolov and Nanstad, 1999].

The first correlation was developed at a time when the Master Curve methodology was still under development. Therefore, the old T_0 estimates cannot be regarded as fully rigorous. Also, the T_{28J} transition temperatures were based on free hand estimates, containing possibly some subjectivity. This raises the need to re-evaluate the original correlation with a more rigorous procedure, using the state of the art definition of T_0 contained in ASTM E1921-03 and a consistent determination of the T_{28J} transition temperature. The second correlation, by ORNL, is newer, but also here the T_0 estimates are not based on the present state of the art. Thus also the second correlation needs re-evaluation. For the re-evaluation, a total of 229 data sets representing only western nuclear grade pressure vessel steels and their welds, were collated from various sources. In all cases, both fracture toughness as well as CVN data were available. The fracture toughness data were analysed in accordance with ASTM E1921-03 and all the CVN data were analysed using an algorithm described in section 8-3. Out of these data sets, 105 provided valid T_0 estimates in accordance with ASTM E1921-03. The usual reason for invalidity was too few data within the temperature validity window of ±50ºC of T_0.

The resulting correlation for T_{28J} is presented in Fig. 8.3. The re-evaluation using a more rigorous analysis did not effectively affect the average difference between T_0 and T_{28J} which only changed by 1°C form 18°C to 19°C. The scatter, however, increased from 15°C to 22°C. This indicates that there may have been some subjectivity included in the original analysis. An 85 % confidence level, represented by 1 standard deviation, is an adequate level of safety for the correlation, since the T_{28J} transition temperature to be applied, when using the correlation, is not directly the average value, but a value that also contains a inhomogeneity margin. The corresponding correlation for T_{41J} is presented in Fig. 8.4. Also here, the average difference between T_0 and T_{41J} changed only by 2°C, but the scatter increased from 20°C to 25°C. The same confidence value as earlier was used to establish a conservative relationship.

The obtained relations between T_0 and T_{28J} and T_{41J} was compared to the whole data set of 229 materials, including also the invalid T_0 values. The effect of this should be to increase the overall scatter in the correlations, since the invalid data have a larger statistical uncertainty. The results are shown in Figs. 8.5 and 8.6. Surprisingly, the scatter is less than for the only valid data. This indicates that the valid data is affected by a few outliers and the actual scatter is normally less than 20°C. For the whole data set, the conservative relation from just the valid data, represents even a higher confidence level than 85 %.

Overall, the re-evaluation confirms to a large extent the previous correlations, but provides a more rigorous result, enabling confident estimation of T_0 from either T_{28J} or T41J.

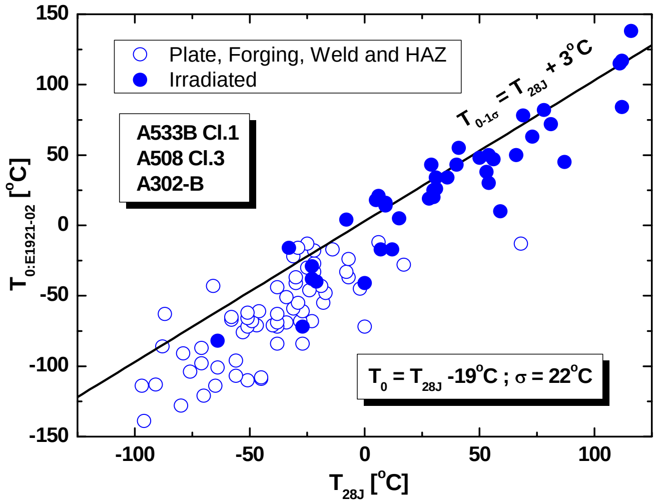

Fig. 8.3. New updated correlation for T_{28J} transition temperature including only western nuclear pressure vessel materials with valid T_0 values.

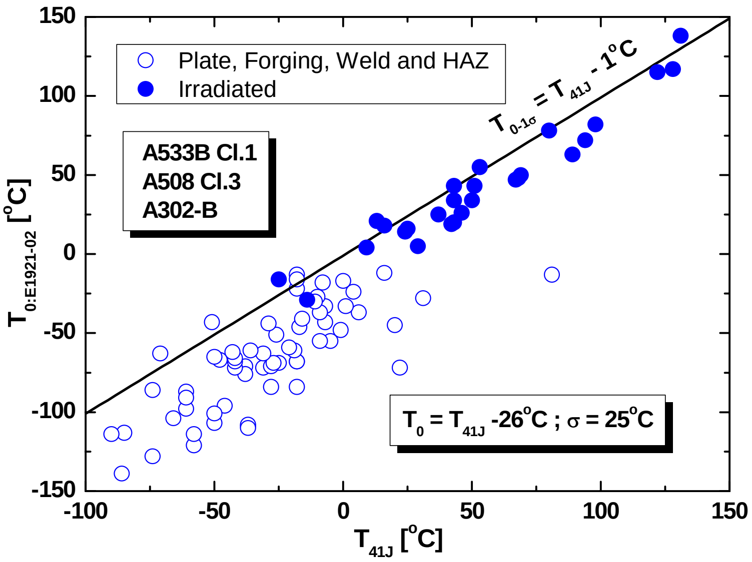

Fig. 8.4. New updated correlation for T_{41J} transition temperature, where only western nuclear pressure vessel materials with valid T_0 values are included.

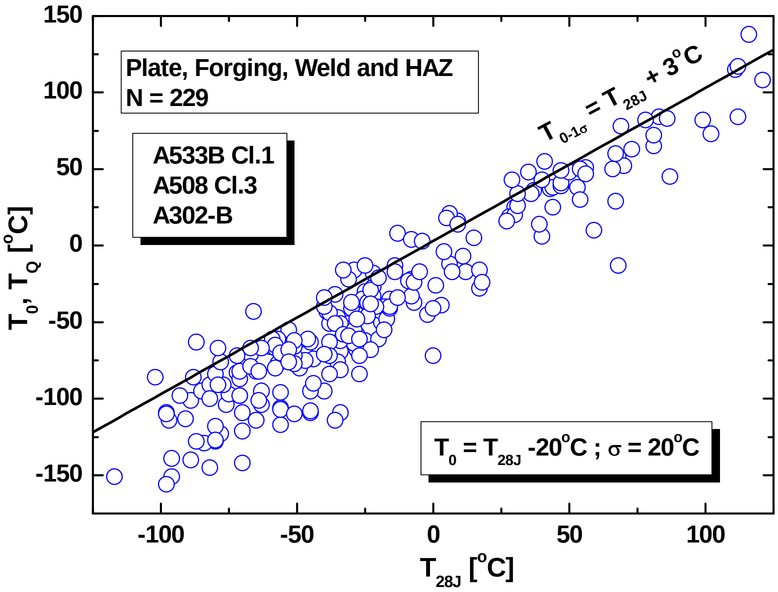

Fig. 8.5: New updated correlation for T_{28J} transition temperature including western nuclear pressure vessel materials with valid and invalid T_0 values. The 1σ line corresponds to the correlation based only on valid T_0 data.

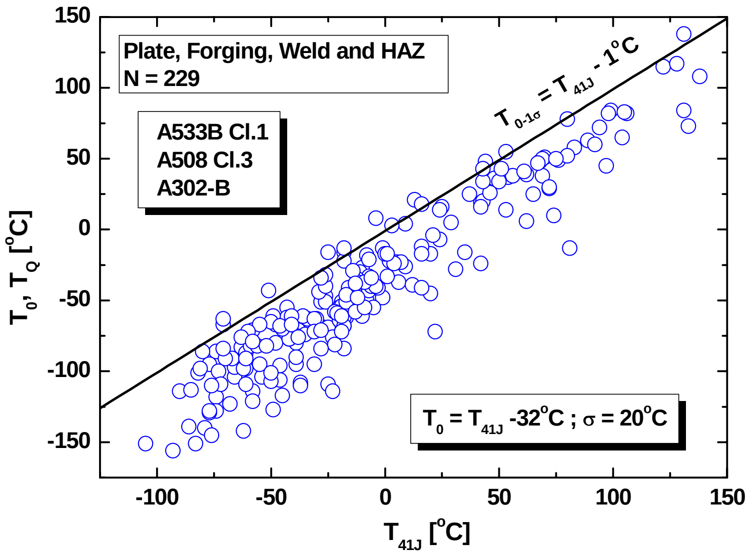

Fig. 8.6: New updated correlation for T_{41J} transition temperature including western nuclear pressure vessel materials with valid and invalid T_0 values. The 1σ line corresponds to the correlation based only on valid T_0 data.

Including the invalid T_0 data into the correlation has a small affect on the mean relation between T_0 and T_{28J}, but there is a large effect on the relation between T_0 and T_{41J}. This indicates that the T_{41J} based correlation is more material specific than the T_{28J} based correlation. The reason for this is considered next.

8.2. Relation between T_{28J} and T_{41J}

The discrepancies in the two correlations between CVN transition temperatures and T_0 indicate that the relation between T_{28J} and T_{41J} is material dependent. The steepness of the CVN transition curve is often connected to the brittle fracture temperature dependence and frequently the Master Curve invariant temperature dependence is challenged with reference to CVN behaviour. It is often forgotten, that the energy increase in a CVN test with temperature is mainly due to an increased portion of ductile crack growth. This means that, the steepness of the CVN transition curve is mainly controlled by the ductile fracture properties of the material. The material dependence is thus mainly related to the upper shelf toughness of the material. The steepness of the CVN transition curve changes as a function of the upper shelf toughness. For the steels studied here, the effect of upper shelf energy on the transition curve steepness is as shown in Fig. 8.7, where the difference in T_{28J} and T_{41J} are presented as a function of upper shelf toughness. Based on Fig. 8.7, one can conclude that the T_{41J} based correlation has a tendency to be more conservative than the T_{28J} based for materials with low upper shelf toughness. For materials with high upper shelf toughness, the reverse is the case. Beside upper shelf toughness, also the yield strength and microstructure affect to some extent the transition curve steepness, but the major parameter is the upper shelf toughness.

8.3. Analysis of complete CVN transition curves

When CVN data is available over the whole transition region, the data can be fitted by a sigmoidal function. In practice, most sigmoidal functions yield equivalent descriptions of CVN transition curve data. As an example four different functions are compared in Fig. 8.8, fitted by a least square fit with relation to KV. In principle, the choice of function is less important than the selected fitting algorithm.

The tanh description of Charpy-V impact data is in its most simple form expressed as:

$$KV = \frac{US - KV_{min}}{2} \cdot \left(1 + \tanh\left(\frac{T - T_{50}}{C}\right)\right) + KV_{min} \quad (8\text{-}1)$$

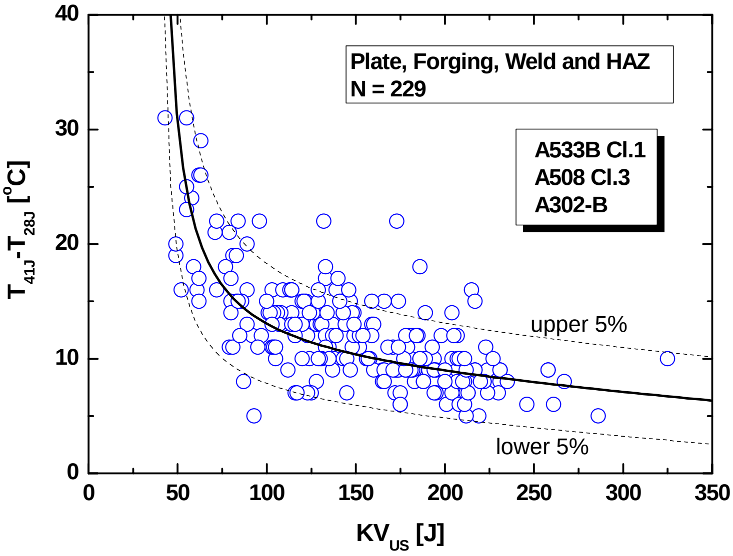

Fig. 8.7: Effect of upper shelf energy on the relation between T_{28J} and T_{41J} transition temperatures for western nuclear pressure vessel steel.

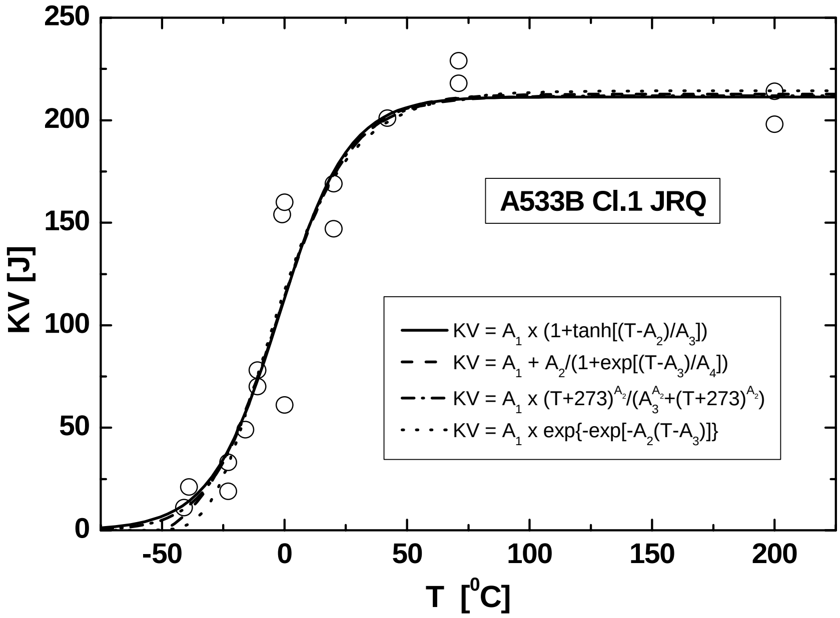

Fig. 8.8: Comparison of different sigmoidal functions ability to describe CVN transition curve data.

In this description, a constant, temperature independent, upper shelf toughness (US) and a fixed lower shelf toughness KV_{min}, are assumed. The relation can also be expressed in the form:

$$KV = \frac{(US - KV_{min}) \cdot \exp\left(\frac{2 \cdot (T - T_{50})}{C}\right)}{1 + \exp\left(\frac{2 \cdot (T - T_{50})}{C}\right)} + KV_{min} \tag{8-2}$$

The inverse form of the relation being:

$$T = T_{50} + \frac{C \cdot \ln\left(\frac{KV - KV_{min}}{US - KV}\right)}{2} \tag{8-3}$$

Where, T_{50} is the temperature at which $KV = (US+KV_{min})/2$.

Sometimes, also temperature dependent upper and lower shelf descriptions are used, but their confidence is not very good, and they should be used only when large data sets covering these toughness regions are available. An example of a typical transition curve for a homogeneous forging is presented in Fig. 8.9.

Most often, the tanh function is fitted by a least square fit with relation to KV. This is the method described in different surveillance procedures, but the method is not optimal for CVN fitting. The drawback with this method is the fact that the scatter in terms of KV (LE, SA) is not constant, but varies over the transition region, being biggest in the centre of the transition region and smallest at the lower and upper shelves (Fig. 8.10). For steep transition curves, this fitting method is thus not very suitable. The scatter in terms of temperature is much more uniform over the whole transition region (Fig. 8.10). Thus, a more proper analysis method requires a modified fitting algorithm to be used. The fitting can be performed with respect to temperature. This ensures the correct weighing of each data point regardless of test temperature. For well behaved transition curves, the different fitting procedures generally produce comparative results, but in some cases there may be significant differences. In such cases the more proper fitting algorithm is preferred. The principle of the fitting algorithm is presented in Fig. 8.11. The fitting is divided into two parts. First, the upper shelf energy, and its standard deviation is determined with the toughness values showing 100 % ductile fracture surface.

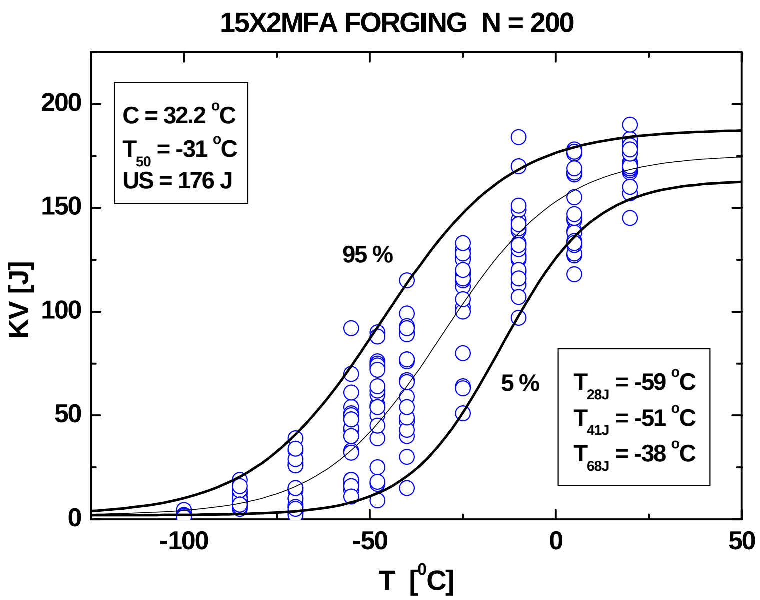

Fig. 8.9: Typical CVN transition curve for nuclear grade forging based on 200 tests.

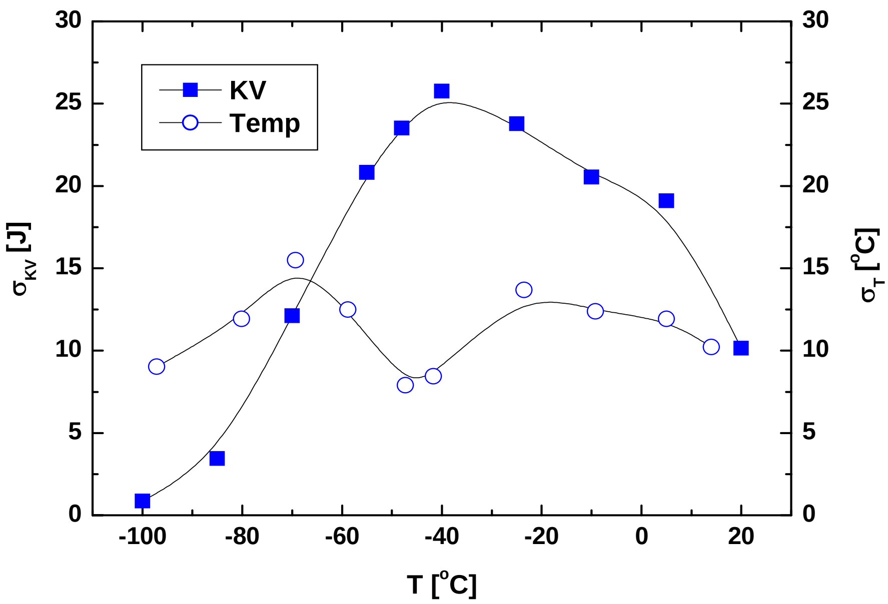

Fig. 8.10: Standard deviation of data presented in Fig. 8.9, showing difference in scatter behaviour in terms of energy and temperature.

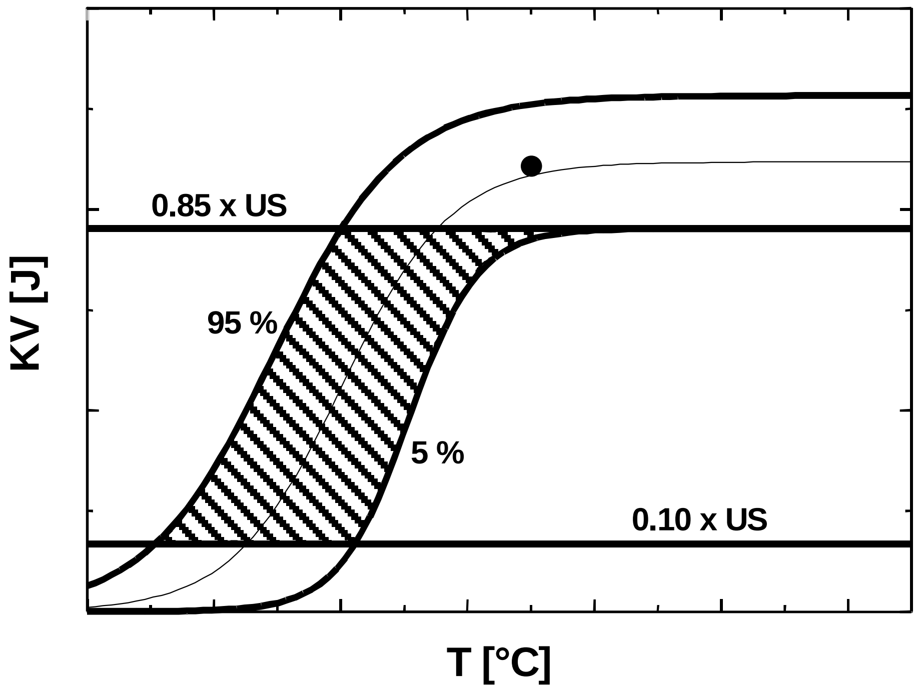

Fig. 8.11: Schematic presentation of modified fitting algorithm.

The calculations are simply

$$\overline{US} = \frac{\sum_{i=1}^{n_{US}} US_i}{n_{US}}$$
$$\sigma_{US} = \sqrt{\frac{\sum_{i=1}^{n_{US}} US_i^2}{n_{US}} - \overline{US}^2} \qquad (8\text{-}4)$$

where n_{US} is the number of results corresponding to upper shelf and US_i is the upper shelf energy for each individual result. The lower shelf impact energy is fixed as 2 Joules. Eq. (8-4) leaves two parameters (T_{50} and C) to be estimated for Eq. (8-1). The fitting makes use of the data points corresponding to the temperature region where the variation in terms of temperature is close to uniform. This region is defined as approximately $0.1\cdot\overline{US} \le KV_i \le 0.95\cdot\overline{US}$. If there are no data in this region, the limits may be changed to include data. In addition to the data belonging to this region, one additional dummy data is added. The dummy data is fixed as having the toughness KV = $0.95\cdot\overline{US}$ and corresponding to the lowest temperature where upper shelf data has been obtained (T_{US}^{MIN}). The role of the dummy parameter is to ensure that the tanh function reaches upper shelf in the right temperature region. This is especially important for steep transition curves.

$$C = 2\cdot\frac{n\cdot\sum_{i=1}^{n}T_i\cdot\ln\left(\frac{\overline{US}-KV_{\min}}{KV_i-KV_{\min}}-1\right)-\sum_{i=1}^{n}T_i\cdot\sum_{i=1}^{n}\ln\left(\frac{\overline{US}-KV_{\min}}{KV_i-KV_{\min}}-1\right)}{\left(\sum_{i=1}^{n}\ln\left(\frac{\overline{US}-KV_{\min}}{KV_i-KV_{\min}}-1\right)\right)^2-n\cdot\sum_{i=1}^{n}\ln\left(\frac{\overline{US}-KV_{\min}}{KV_i-KV_{\min}}-1\right)^2} \quad (8\text{-}5)$$

$$T_{50} = \frac{\sum_{i=1}^{n}T_i+\frac{C\cdot\sum_{i=1}^{n}\ln\left(\frac{\overline{US}-KV_{\min}}{KV_i-KV_{\min}}-1\right)}{2}}{n} \quad (8\text{-}6)$$

where n is the number of data values between $0.1\cdot\overline{US} \leq KV_i \leq 0.85\cdot\overline{US}$ plus the dummy data.

An even more sophisticated fitting algorithm consists of minimizing the least square sum of the distance from each point to the local tangent of the tanh equation. In order to be optimized, this method requires further a weighing of the y-axis by the multiplier, US/(2C). Here, also the upper shelf as well as the lower shelf is fitted simultaneously. This method is however quite cumbersome to use and normally it is sufficient to use the simpler fitting with respect to temperature. The more complicated fitting algorithm serves mainly as a verification tool.

Fig. 8.12 contains a comparison of the accuracy of the different fitting algorithms for the typical nuclear grade material shown in Fig. 8.9. When the data set is large, the choice of algorithm is not important. They all provide similar descriptions of the data. However, if the data set is comparatively small, the fitting algorithm will affect the outcome of the analysis. This is shown in Fig. 8.13, where a number of subsets with 10 specimens each have been taken from Fig. 8.11 and fitted by the different algorithms. The figure shows the cumulative distribution of T_{41J} transition temperatures determined with the different algorithms. The smallest scatter is shown by the temperature based and the sophisticated fitting algorithms, but the temperature based one, is less likely to show large statistical outliers. Overall, the standard deviation of the CVN transition temperature, for this kind of material, for a small data set, is around 6ºC. The energy based fitting algorithm has a tendency to be biased by about 2-3ºC to lower transition temperatures than the temperature based fitting algorithm. Since the correlations in section 8-1 are based on the temperature based fitting algorithm, a bias term of 2°C should be added to the energy based transition temperatures. The correlations already include the uncertainty of both the CVN transition temperature as well as the uncertainty of T_0. Therefore, homogeneous materials do not require additional margin terms, when complete CVN transition curves are available. However, homogeneity of a material cannot be known in advance. This means that an account for possible in-homogeneity must be made. A scheme for this is given next.

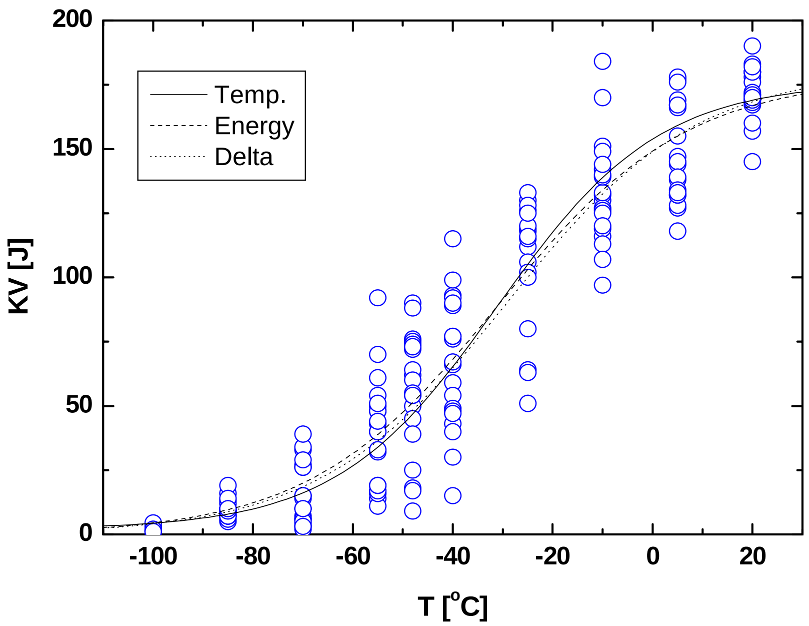

Fig. 8.12: Comparison of the different fitting algorithms for a large data set showing very small differences between the methods.

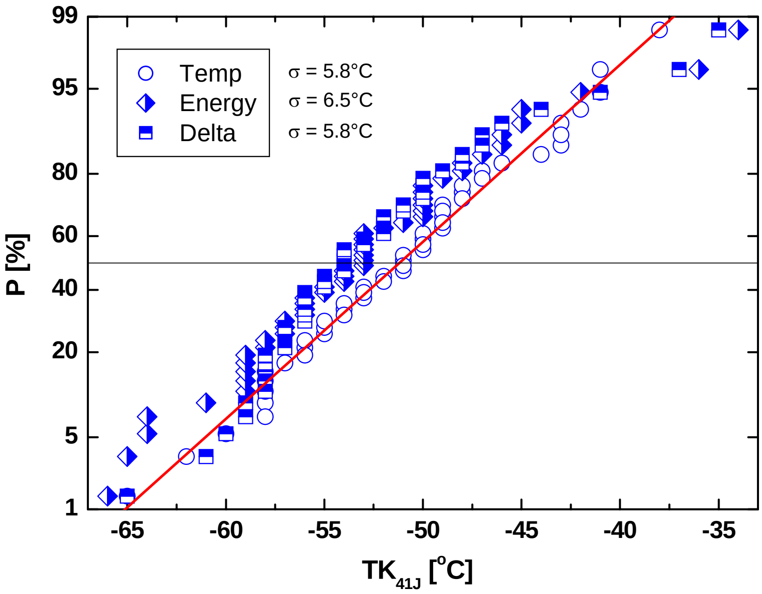

Fig. 8.13: Comparison of the reliability of different fitting algorithms for small data sets.

Accounting for material inhomogeneity

For single materials that can be taken as homogeneous, the scatter of the CVN data in terms of temperature is about 10°C (Fig. 8.10). This estimate is base on the analysis of a multitude of different data sets. Small data sets are not capable of describing the materials homogeneity correctly. One must therefore use simpler methods by which to judge the homogeneity of the material. A simple method is described below (Fig. 8.14):

- Make a mean fit to the data using e.g. the method described above. Fitting with respect to energy is likewise possible.
- Determine a provisional temperature T_{50LB} so that the mean curve becomes a lower limiting curve to the data.
- If $T_{50LB} < T_{50}$ +15 °C then T_{50} remains unchanged (15°C is approximately 1.5 times the standard deviation for a homogeneous steels and corresponds closely to a 96 % confidence level).
- If $T_{50LB} > T_{50}$ +15 °C then $T_{50} = T_{50LB}$ -15 °C.

This assessment of in-homogeneity is applicable if the data set contains at least 10 results covering the whole transition region. Fewer results or incomplete temperature coverage causes the data set to describe an incomplete transition curve. The methodology to assess these is presented next.

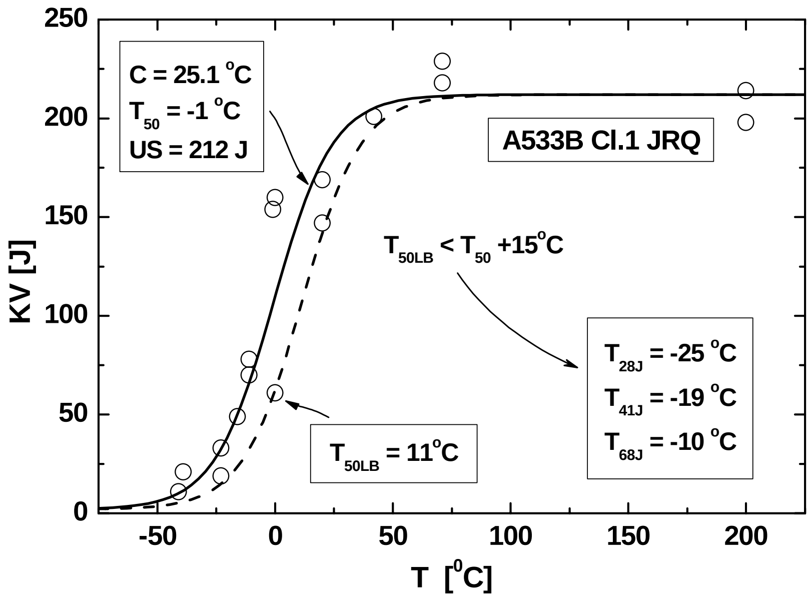

Fig. 8.14: Principle of in-homogeneity assessment. In this example, T_{50} remains unchanged.

8.4. Analysis of incomplete CVN transition curves

Incomplete CVN transition curves are data sets, which do not cover the whole transition region and/or consists of less than 10 test results. The incomplete transition curves can be divided into three categories depending on temperature range covered by the data. Two of the cases require extrapolation of the CVN transition curve. The analysis is based on the recognition that the transition temperature can be deduced from CVN data at a different temperature, provided the parameters *C* and KV_{US} are known in Eqs. (8-7) and (8-8).

$$T_{28J} = T_{KV} - \frac{C \cdot \ln\left(\frac{KV(KV_{US} - 28)}{28(KV_{US} - KV)}\right)}{2} \tag{8-7}$$

$$T_{41J} = T_{KV} - \frac{C \cdot \ln\left(\frac{KV(KV_{US} - 41)}{41(KV_{US} - KV)}\right)}{2} \qquad (8\text{-}8)$$

Since, in the case of incomplete CVN transition curves the parameters *C* and KV_{US} are normally not known, there has to be a conservative procedure to estimate them. Based on an analysis of the data sets presented in Fig. 8.7, a simple methodology for such estimation has been developed. Next the three different cases are addressed separately.

Data below the transition temperature

If the materials upper shelf energy is known, that value may be used to estimate a conservative estimate for the parameter *C* from Eq. (8-9), which corresponds to a 5% upper bound fit to the materials used in Fig. 8.7.

$$C = 69 - 0.06 \cdot KV_{US} \qquad (8\text{-}9)$$

If the upper shelf energy is not known, *C* must be taken as 66°C and an upper shelf energy of 100 J shall be used in connection with Eq. (8-8). The estimation is as follows (Fig. 8.15):

- Determine estimates for the 41J transition temperature for all individual results using Eq. (8-8).
- Seek the highest transition temperature estimate from minimum three specimens corresponding to the closest test temperature of the transition temperature estimate.
- Use this estimate as representative of the material for the T_0 correlation.

Data around the transition temperature

If the materials upper shelf energy is known, that this value may be used to estimate a best estimate for the parameter *C* from Eq. (8-10), which corresponds to a median fit to the materials used in Fig. 8.7.

$$C = 51 - 0.06 \cdot KV_{US} \tag{8-10}$$

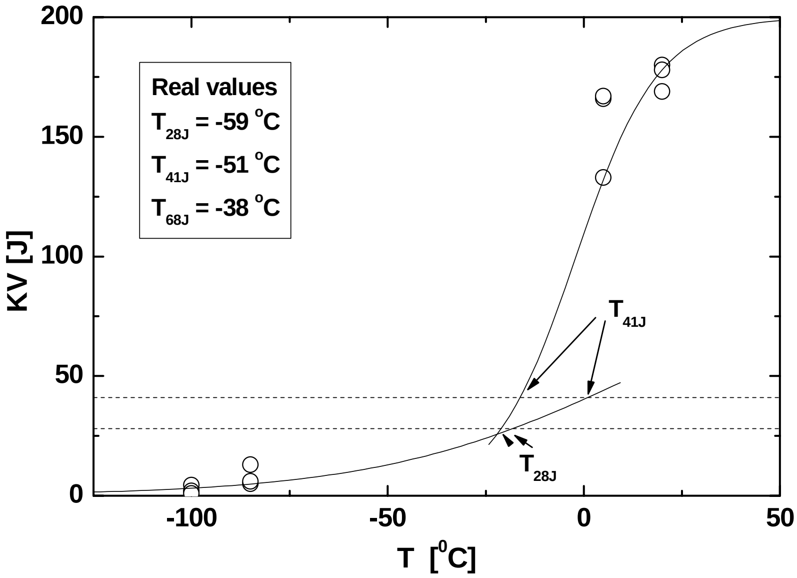

Fig. 8.15: Principle of CVN transition temperature estimation for cases with data below and above the transition temperature.

If the upper shelf energy is not known, C must be taken as 43°C and an upper shelf energy of 200 J shall be used in connection with Eqs. (8-7) and (8-8). The estimation is as follows, and is shown in Fig. 8.16:

Determine estimates for the desired transition temperature for all individual results using Eqs. (8-7) and (8-8).

- Use the highest transition temperature estimate as representative of the material for the T_0 correlation and select the transition temperature definition providing the higher T_0 estimate.

Data above the transition temperature

If the materials upper shelf energy is known, that value may be used to estimate a conservative estimate for the parameter C from Eq. (8-11), which corresponds to a 5% lower bound fit to the materials used in Fig. 8.7.

$$C = 33 - 0.06 \cdot KV_{US} \tag{8-11}$$

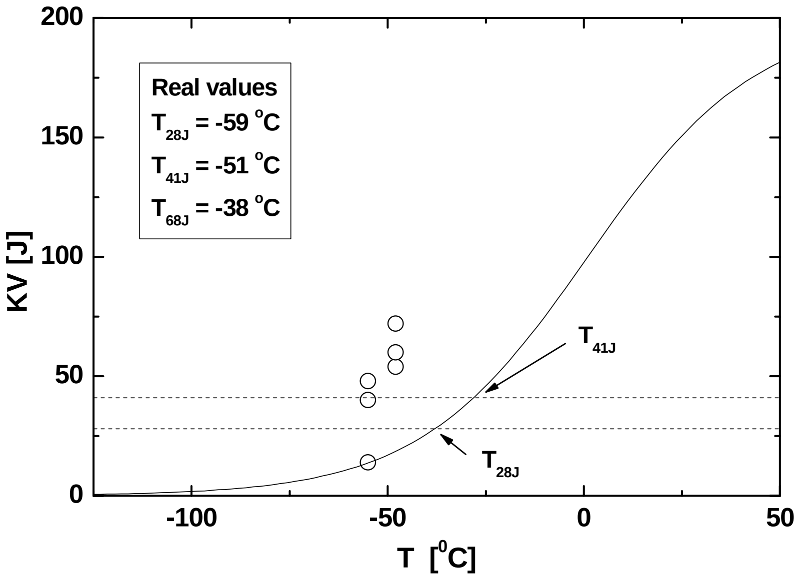

Fig. 8.16: Principle of CVN transition temperature estimation for cases with data around the transition temperature.

If the upper shelf energy is not known, C must be taken as 21°C and an upper shelf energy of 200 J shall be used in connection Eq. (8-7). The estimation is as follows (Fig. 8.15):

- Determine estimates for the 28J transition temperature for all individual results using Eq. (8-7).
- Seek the highest transition temperature estimate from minimum three specimens corresponding to the closest test temperature of the transition temperature estimate.
- Use this estimate as representative of the material for the T_0 correlation.

If only upper shelf energy data is available, then the lowest test temperature, combined with the corresponding upper shelf energy, shall be used for the transition temperature determination. In this case, the transition temperature is estimated from Eq. (8-12), basing parameter C on Eq. (8-11).

$$T_{28J} = T_{US} - \frac{C \cdot \ln\left(\frac{19 \cdot (KV_{US} - 28)}{28}\right)}{2} \quad (8\text{-}12)$$

8.5. CVN-T_o relationships

The methodology developed here aims specifically at deriving conservative Master Curve T_0 estimates from varying quality CVN data. The method is specifically designed for western nuclear grade pressure vessel steels and their welds. The principle of the methodology is applicable also for other steels showing a ductile to brittle transition, but the correlations used are specific to western nuclear grade pressure vessel steels and their welds. Other steels may require changes to these correlations.

Based on an evaluation of the generic behaviour of Charpy-V transition curves, a simple conservative methodology to assess inhomogeneity and incomplete Charpy-V transitions curves has also been drafted. The procedure enables consistent estimation of the T_0 transition temperature from varying quality Charpy-V information. The procedure can be used even when only upper shelf Charpy-V data is available.

Based on the evaluated data, presented in Figs. 8.3 to 8.7, and estimations of T_{28J} and T41J, presented in Eqs. (8-7) and (8-8), the following expressions are recommended in using for western nuclear grade pressure vessel steels and their welds:

$$T_0 = T_{28J} + 3 \ [^{o}C] \quad (8\text{-}13)$$

$$T_0 = T_{41J} - 1 \ [^{o}C] \quad (8\text{-}14)$$

The higher T_0 value from Eqs. (8-13) and (8-14) may be used as the representative T_0 of the material in estimation of the cleavage fracture toughness of the material from the Master Curve.

8.6. Significance of ASME Code Cases N-629 and N-631

The ASME K_{IC} reference curve was originally drawn as a free hand lower bound curve to a specific set of K_{IC} data, [Marston, 1978]. In practice the K_{IC} reference curve is limited by only one material, the HSST 02 plate (Fig. 8.17). Historically the ASME reference curves have been treated as representing absolute deterministic lower bound curves of fracture toughness. In reality, this is not the case. They represent only deterministic lower bound curves to the specific set of data, which represent a certain probability range. The safety level of the curve can be determined based on all available fracture toughness data sets, or it can be limited to the original data sets used for the construction of the curve. If the original data sets would constitute a good description of all materials, the resulting safety levels would be the same. However, if they do not constitute a good description of all materials the resulting safety levels may differ considerably. In this case the intended safety level of the reference curve is established by the original data, for which the reference curve was constructed. When it became evident that the Master Curve based T_0 transition temperature is clearly superior to the old RT_{NDT} definition used in the ASME Code, there rose a need to implement the Master Curve concept also into ASME [Server et al, 1998]. A Master Curve analysis of the original data, as shown in Fig. 8.18, showed that the ASME K_{IC} reference curve corresponds practically to the same degree of confidence as a 5 % Master Curve, with respect to the original data used to establish the K_{IC} curve [Wallin, 1999].

Besides knowledge of the confidence level represented by the reference curve, two other important aspects affect the combination between the ASME Code and the Master Curve. First, the Master Curve "shape" differs clearly from the ASME K_{IC} curve. Second, the ASME Code does not recognise the statistical size effect. The long term goal is to implement the Master Curve in full into the ASME Code [Server et al, 1998]. This, however, requires significant changes to the ASME procedure and is therefore a slow process. In order to introduce a quicker way of introducing T_0 into the Code, a simple relation between T_0 and RT_{NDT} was pursued [Server et al, 1998]. This new definition of reference temperature became known as RT_{To}. The reference temperature is defined in ASME Code Case N-629 for Section XI and N-631 for Section III. The definition is based on a functional equivalence between the RT_{To} and RT_{NDT}. In both cases, the result should be similar to the lower bound estimates of the original data used to define the ASME K_{IC} curve. The definition of RT_{To} was taken as:

$$RT_{To} = T_0 + 19.4 \quad [^{\circ}C] \tag{8-15}$$

The reference temperature RT_{To} may be used as an alternative indexing reference temperature to RT_{NDT} for determination of K_{Ic} and K_{Ia}.

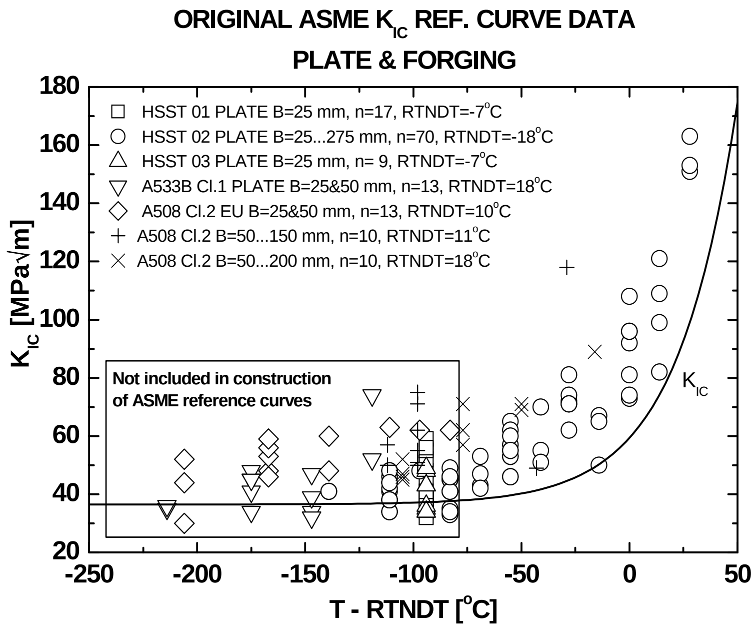

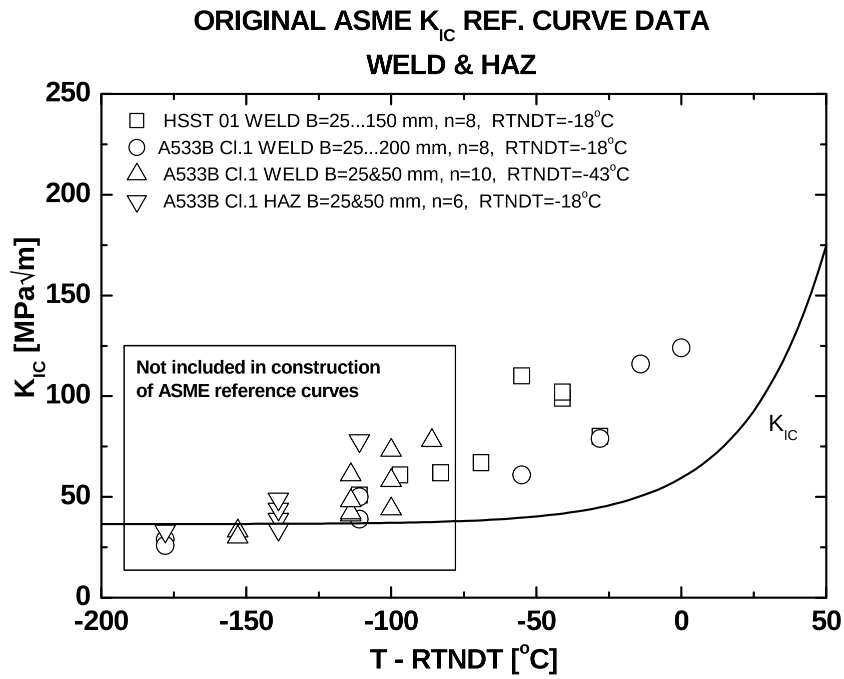

Fig. 8.17: Original data used to establish ASME K_{IC} reference curve [Marston, 1978].

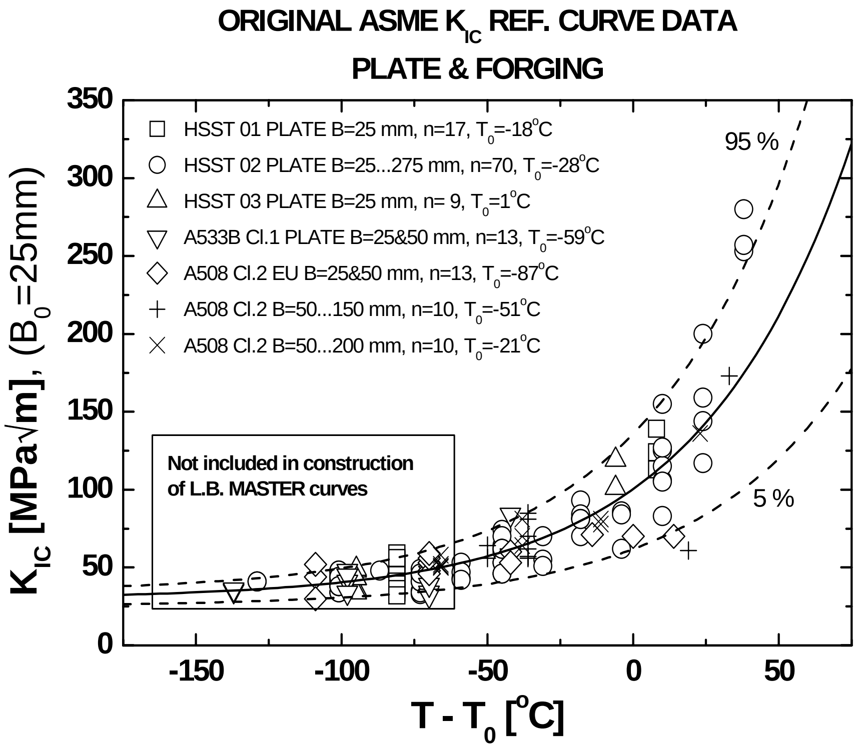

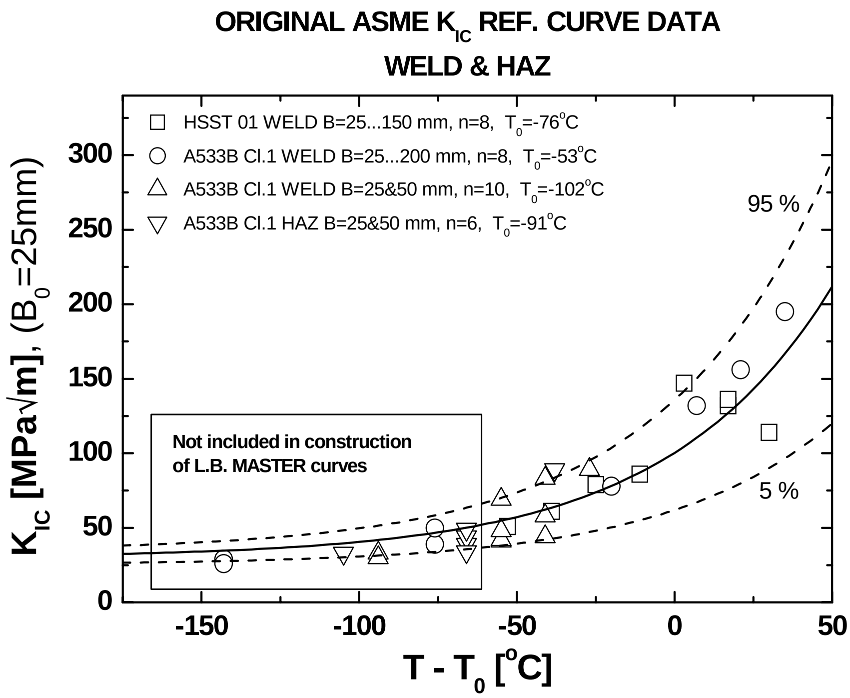

Fig. 8.18: Master Curve analysis of original data used to establish ASME K_{IC} reference curve [Wallin, 1999].

This causes the ASME Code Case K_{IC} curve to be located below the 5 % Master Curve in the temperature region: -55ºC < T-T_0 < +63ºC. Above and below this temperature region, the Code Case curve is less conservative than the 5 % Master Curve. This is, however not of major concern, since below -55ºC the application will be on the lower shelf and above +77ºC the Code Case curve corresponds to upper shelf. The upper crossover of the curves occurs close to 150 MPa√m.

The definition of RT_{To} leads to an artificial size adjustment. I.e. in the temperature region where the Code Case curve lies below the 5 % Master Curve, the Code Case curve corresponds effectively to larger specimens than 25 mm. This effective thickness can be calculated by size-adjusting the 5 % Master Curve to coincide with the Code Case curve. The result is shown in Fig. 8.19. In a temperature region of approximately -40ºC < T-T_0 < +50ºC the Code Case curve corresponds to a specimen thickness larger than 50 mm and within a temperature region of approximately : -20ºC < T-T_0 < +30ºC it corresponds to a specimen thickness larger than 100 mm.

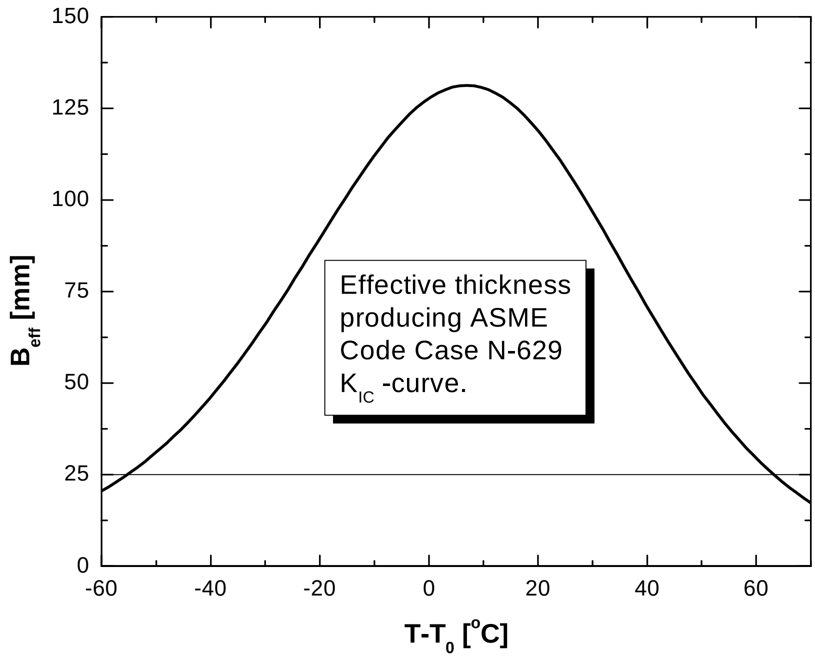

Fig. 8.19: Size adjustment required to make 5 % Master Curve coincide with Code Case N-629 K_{IC} reference curve.

The artificial size adjustment that results from the combined use of RT_{To} and the ASME K_{IC} reference curve causes the Code Case to become essentially a lower bound curve also for the uncorrected original K_{IC} data as seen in Fig. 8.20. It is observed that the 5 % Master Curve without size adjustment is not a lower bound curve to the original K_{IC} data. Thus, the use of the Master Curve as such, would require a size adjustment in connection with the safety assessment. However, since the Code Case curve includes this artificial size adjustment and it forms a lower bound curve for large specimens yielding linear-elastic K_{IC} values, no additional size adjustment is considered necessary in connection with the Code Case curve.

Thanks to the artificial size adjustment, it is possible to determine T_0 (RT_{To}) based on small specimens using the elastic-plastic K_{JC} parameter and to use the Code Case curve to describe the behaviour of postulated "valid" K_{IC} data.

Extremely large specimens may yield K_{IC} values that are not bounded by the Code Case curve, but such specimens have crack front lengths that are much larger than is realistic for a real nuclear pressure vessel. This means that if the uncorrected 500 mm thick specimens shown in Fig. 2.4 would be used to define RT_{To}, a much larger margin than 19.4ºC would be required. This is, however, unrealistic since the pressure vessel does not contain 500 mm long crack fronts. The same is the case for a postulated quarter thickness flaw where the crack front length is much larger than found in reality. The crack front length implied by the Code Case definition of RT_{To} is fully acceptable for the application to nuclear pressure vessels. Additional requirements on the definition of RT_{To} only lead to unnecessary over-conservatism.

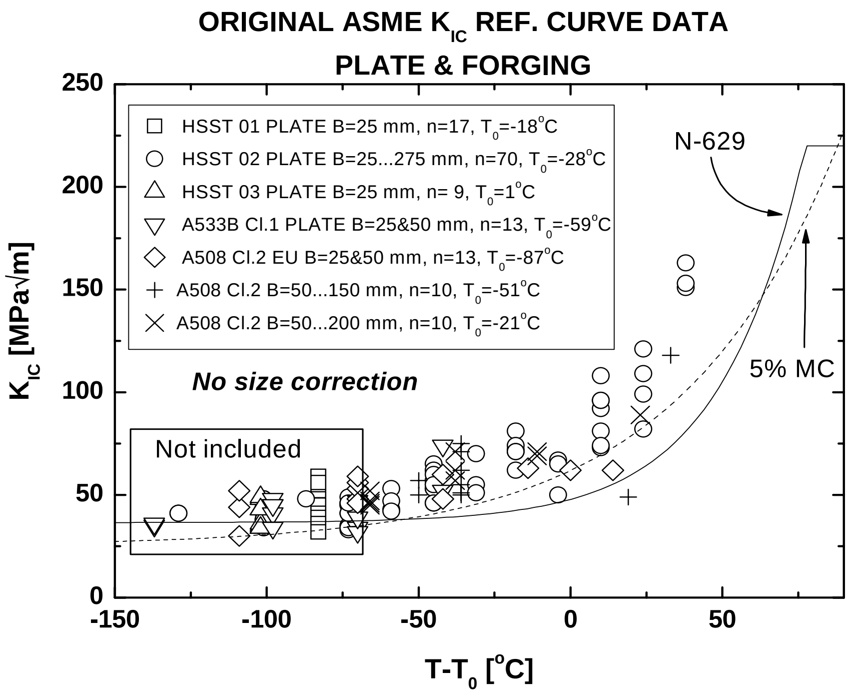

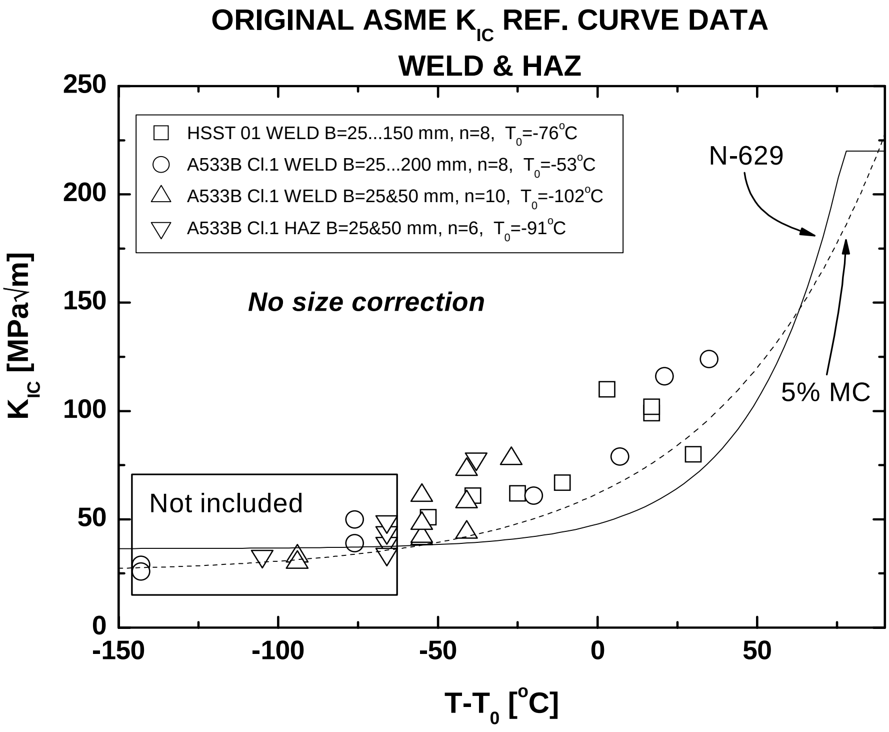

Fig. 8.20: Justification for ASME Code Cases N-629 and N-631.

A comparison between the Master Curves and the ASME K_{Ic} reference curve is shown in Fig. 8.21. Here, Eq. (8-15) is used in converting RT_{NDT} to T_0. It is observed that the ASME K_{IC} reference curve corresponds practically to the same degree of confidence as a 5% Master Curve. It is also observed that sing the 50% Master Curve gives substantially higher value of fracture toughness than what ASME K_{IC} reference curve gives. Thus, using 50% Master Curve in fracture assessment releases some of the overconservatism observed when the ASME K_{IC} reference curve is used.

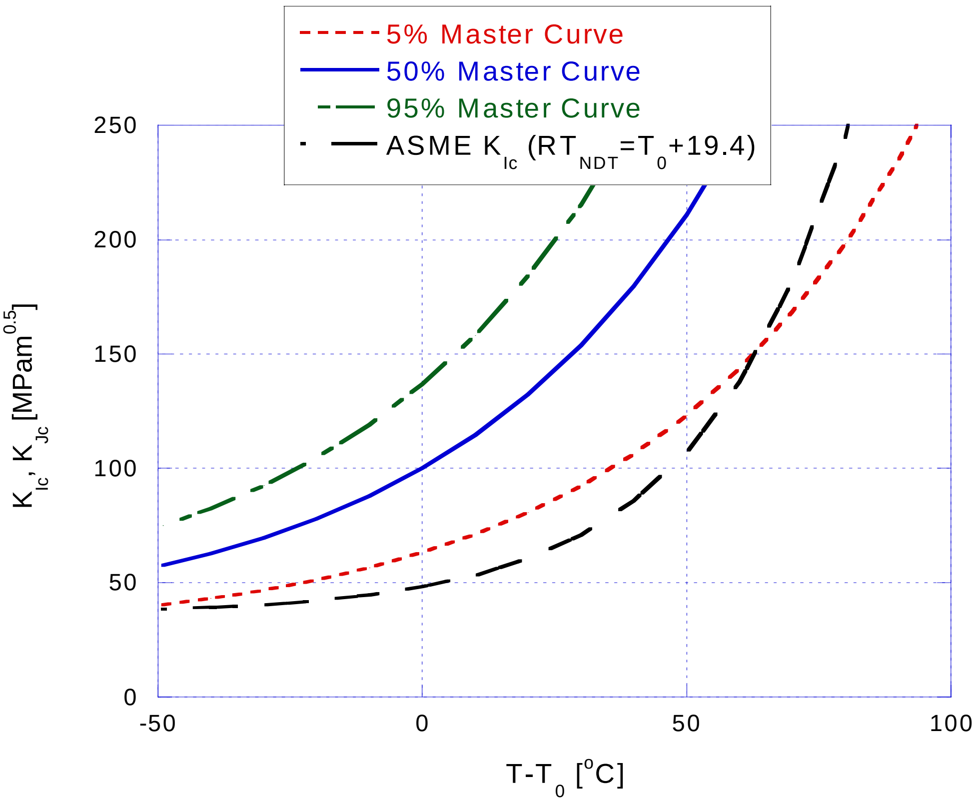

Fig. 8.21: Comparison of fracture toughness of the Master Curves and the ASME K_{Ic} reference curve considering Code Cases N-629.

9. APPLICATION OF THE MC METHOD IN OTHER COUNTRIES

Presently, several countries have adopted or are in the process of adopting the Master Curve method into their brittle fracture safety assessment procedures. These include e.g. the following:

Finland:

The Radiation and Nuclear Safety Authority guide YVL 3.5/5.4.2002, allows the use of the MC for all brittle fracture assessments of nuclear structures. For the pressure vessel materials the MC method is specifically required. Either the full MC evaluation or a simplified applying e.g. RT_{To} can be used.

USA:

The ASME code cases N-629 and N-631 define the RT_{To} reference temperature based on the MC method. Other developments in USA await the handling of Babcock and Wilcox owners Group efforts to gain acceptance for a generic MC based RT_{To} definition for Linde 80 welds.

Germany:

A proposal to include the MC based RT_{To} definition into the KTA rules as a non-mandatory annex is in preparation. Case by case applications of the MC (both full and simplified) have been accepted by German authorities.

UK:

The MC based CVN correlation, including size adjustment, scatter and temperature dependence are included in BS7910.

Czech Republic:

Authorities accepted the new code developed in VERLIFE FP5 EURATOM project, based on full MC evaluation.

Slovakia & Hungary:

VERLIFE procedure is under consideration.

Belgium:

Case by case applications of the MC (both full and simplified) have been accepted by the Belgian authorities.

Russia:

New code based on the MC, but containing a modification to the temperature dependence expression, is under preparation.

IAEA:

Recently finished document on IAEA Master Curve Guidelines that cover both material characterisation and safety assessment based on the MC.

10. ASSESSMENT PROCEDURE BASED ON THE MC METHOD

As shown in the preceding sections, fracture assessments based on the Master Curve methodology give promising predictions on the outcomes of tests on small and large specimens presented in the literature. This gives good confidence on the usage of this methodology for fracture assessments of components in nuclear power plants.

Here, a procedure based on the Master Curve methodology is proposed for fracture assessment of cracked components. The defect is assumed to be an elliptical surface crack in a cylinder subjected to thermal and mechanical loads. Of course, other types of defects and loads can also be treated in the same way. This procedure together with the fracture mechanics Handbook [Dillström et al, 2004] can be used in determination of the acceptable and critical defect sizes in the nuclear components.

The procedure consists of two levels, Simplified and Advanced, depending upon the information available for the fracture assessment. The procedure is valid for the following cases:

(1) Ferritic steels (base and weld)

(2) Fracture in the transition and lower-shelf regions

(3) Actual temperature within: T_0 - 50 °C ≤ T ≤ T_0 + 50 °C

10.1. Simplified assessment procedure

When it is desired to conduct a conservative assessment without performing any complicated calculations, one can use the following simplified procedure. In using the simplified procedure, it is assumed that:

- The crack driving force is constant along the whole crack front, having a magnitude equal to the maximum calculated value along the crack front.
- The temperature is constant along the whole crack front, having a magnitude equal to the minimum calculated or measured value along the crack front.
- The crack-tip constraint is high along the whole crack front, having a magnitude equal to the constraint value in the standard 1T specimen.

I: Determination of the standard fracture toughness K_{JC}^{1T}

(a) If test material is available and fracture mechanics testing is possible:

Perform fracture mechanics tests according to ASTM E1921-03 to determine T_0:

$$T_0 = T - \frac{1}{0.019}\ln\left[\frac{K_{Jc(\mathrm{med})} - 30}{70}\right]. \qquad (4\text{-}7\mathrm{rep})$$

Note that the test should be performed at a temperature close to T_0. Thus, a prior estimate on T_0 is needed before testing. Otherwise some fracture toughness tests at different temperatures should be conducted to find a prior estimate on T_0, see Section 3 of this report for more details.

Based on the obtained T_0 value, determine the standard fracture toughness K_{JC}^{1T} from 50% Master Curves for the desired temperature from:

$$K_{JC}^{1T} = 30 + 70\exp\left[0.019(T\text{-}T_0)\right]. \qquad (4\text{-}9\mathrm{rep})$$

(b) If a valid K_{IC} (plane-strain fracture toughness) result is available at a given temperature T^*:

Evaluate T_0 by using Eq. (4-7rep) and setting $K_{JC(med)} = K_{IC}$ to get Eq. (4-7b):

$$T_0 = T^* - \frac{1}{0.019}\ln\left[\frac{K_{IC} - 30}{70}\right] + C \qquad (4\text{-}7\mathrm{b})$$

Here, the constant C is added as a safety margin related to uncertainties in data, and may be set to 5 ^{o}C.

Determine K_{JC}^{1T} for the desired temperature from Eq. (4-9rep).

(c) If only Charpy impact data are available:

Follow the procedure outlined in Section 8 of this report to determine T_{28J} and/or T_{41J}, thereafter determine T_0 according to the following expressions:

$$T_0 = T_{28J} + 3\ [^{o}\mathrm{C}] \qquad (8\text{-}13\mathrm{rep})$$

$$T_0 = T_{41J} - 1 \text{ [}^{o}\text{C]} \tag{8-14rep}$$

Use the higher value of T_0 from the above equations, and determine K_{JC}^{1T} for the desired temperature from Eq. (4-9rep).

(d) If T_0 is available and use of the ASME K_{JC} curve is desired:

Calculate the reference temperature RT_{To} from:

$$RT_{To} = T_0 + 19.4 \quad \text{[}^{o}\text{C]} \tag{8-15rep}$$

Apply the calculated RT_{To} as RT_{NDT} to the ASME reference curve to determine fracture toughness K_{IC} for the desired temperature using:

$$K_{Ic} = 36.5 + 3.084 \exp\left[0.036(T\text{-}RT_{NDT} + 56)\right] \tag{4-12rep}$$

More details are given in section 8.6 of this report.

II: Size-correction for crack front length

Based on the evaluated standard fracture toughness K_{JC}^{1T}, determine the size-corrected fracture toughness K_{JC}^{cfl} related to the crack-front-length (cfl) of the actual crack geometry using:

$$K_{JC}^{cfl} = 20 + \left[K_{JC}^{1T} - 20\right]\left(\frac{25}{cfl}\right)^{1/4} \tag{4-3rep}$$

Use $cfl = 2c$ (crack length).

III: Determination of crack driving force

(a) If a detailed 3D finite element calculations of the crack driving force K_J along the whole crack front are available, use the maximum value of K_J. The crack driving force K_J is equal to the stress intensity factor K_I, when K_I is directly available. If the J-integral is available, K_J is obtained from the following equation:

$$K_J = \sqrt{\frac{EJ}{1-\nu^2}} \quad \left[\text{MPa}\sqrt{\text{m}}\right] \tag{4-1rep}$$

(b) The engineering assessment approaches, for instance the fracture mechanics Handbook, are commonly used in calculation of the crack driving force in cracked components. They usually give K_I values at the deepest point of the crack and at the intersection with the free surface. When such an approach is invoked, use the maximum value of these two as K_J.

Note that for surface cracks under thermal-mechanical loads, for instance thermal transients, the crack driving force K_J has its maximum value at the intersection with the free surface. Also note that the crack driving force can be due to primary and secondary stresses. These two types of stresses can be treated separately as described for instance in the fracture mechanics Handbook.

IV: Determination of the acceptable and critical defect sizes

By obtaining values of the fracture toughness K_{JC}^{cfl} and the crack driving force K_J for the actual crack geometry, as described through parts I to III above, and using a relevant safety margin, one can determine the acceptable and critical defect sizes for the actual crack case.

The fracture mechanics Handbook can be used for this purpose. It gives a procedure for evaluation and treatment of primary and secondary stresses in calculation of the crack driving force K_J. It also gives guidelines for selection of the safety margins in determination of the acceptable and critical defect sizes.

10.2. Advanced assessment procedure

In assessment of real cracks, normally both the crack driving force and crack-tip constraint vary along the crack front. In thermal transient loading, even the temperature varies along the crack front. A simplified assessment may therefore yield to overly conservative results. Thus, when a detailed finite element result is available, one can use the following more advanced procedure. The procedure considers that:

- The crack driving force and the crack-tip constraint vary along the crack front. The point-wise values of these parameters are used in the fracture assessment.

- The temperature may also vary along the crack front, and the point-wise values are used in the fracture assessment.

I: Determination of fracture toughness

The fracture toughness used in the advanced fracture assessment of a surface crack can be expressed either with the 5 % lower bound Master Curve. This can be expressed in the form:

$$K_{5\%,T\min} = 25.2 + 36.6.\exp\left[0.019(T_{\min}\text{-}T_{0deep})\right] \qquad (7\text{-}17\text{rep})$$

or by using the fracture toughness reference curve from ASME Code Case N-629 (or N-631). This can be expressed in the form:

$$K_{IC,ASME,T\min} = 36.5 + 3.084 \cdot \exp\left[0.036 \cdot \left(T_{\min} - T_{0deep} + 56\right)\right] \qquad (7\text{-}18\text{rep})$$

Here, T_{min} is the minimum temperature along the crack front, and T_{0deep} is the T_0 evaluated for 1T specimen. These follow the guidelines stated in part I of the simplified assessment procedure to determine T_0.

II: Determination of crack driving force and constraint

3D finite element calculations are used to give the crack driving force along the crack front. The crack driving force expressed as a stress intensity factor is thus available for each point along the crack front, dented as $K_{I\Phi}$. The local constraint values along the crack front are also obtained by conducting a 3D finite element analysis using a very fine mesh. Alternatively, *Q*-parameter solutions of Sattari-Far [1998] together with Fig. 7.5 may be used to estimate T_{stress} along the crack front. Based on the obtained values of the crack driving force and constraint, the effective stress intensity factor is calculated, which is described below.

III: Consideration of size effects

Determine the effective stress intensity factor K_{Ieff}, related to the minimum temperature (T_{min}) along the crack front. K_{Ieff} accounts for the local crack driving force $K_{I\Phi}$, constraint state and temperature along the crack front, as well as the crack front length. K_{Ieff} is obtained from the following expression, for details see Section 7.4 of this report:

$$K_{IeffT\min} = \left\{ \int_0^s \left(\frac{K_{I\Phi} - K_{\min}}{K_{0\Phi} - K_{\min}} \right)^4 \cdot \frac{Cds}{B_0} \right\}^{1/4} \cdot \left(K_{0T\min} - K_{\min} \right) + K_{\min} \qquad (7\text{-}14\text{rep})$$

Where, $K_{0\Phi}$ is the local K_0 value that accounts for local temperature and constraint along the crack front. $K_{0\Phi}$ can be expressed as:

$$K_{0\Phi} = K_{0T,Tstress} = 31 + 77 \cdot \exp\left[0.019 \cdot \left(T - T_{0deep} - \frac{T_{stress}}{10\ \text{MPa/°C}} \right) \right] \qquad (7\text{-}16\text{rep})$$

The parameter C in Eq. (7-14rep) considers the crack front size, and has the values; $C = 1$ for $s \leq 150$ mm, and $C = 150/s$ for $s > 150$ mm.

For cases with constant temperature and effectively constant constraint along the crack front, the maximum effective stress intensity factor K_{Ieff} expressed in Eq. (7-14rep) may be simplified to be equal to the maximum K_I value along the crack front.

IV: Fracture assessment of a surface crack

After determination of the effective crack driving force K_{Ieff} and related fracture toughness curve (5% master curve or ASME K_{IC}-N629), one can conduct fracture assessment of the actual crack geometry and loading. Fig. 7.21 illustrates an example of an advanced master curve analysis of a surface crack.

As can be seen, the fracture toughness is not directly compared to the crack driving force estimated from a stress analysis. Instead, the fracture toughness is compared to an effective driving force, which accounts for the local stress and constraint state and temperature along the crack front, as well as the crack front length. If the K_{Ieff} curve does not cross the fracture toughness curve, the case is safe and no fracture event will occur.

By increasing the crack size or magnitude of the loads, the effective driving force K_{Ieff} would be increased. The critical situation is achieved, when the K_{Ieff} curve crosses the related fracture toughness curve.

An alternative rather simple way to conduct a fracture assessment of a surface crack in a reactor pressure vessel is to consider the maximum values of the crack driving force and the constraint parameter. For a semi-elliptical surface crack located at the inner surface of a reactor pressure vessel under thermal-mechanical loads, it has been shown that the maximum values of the crack driving force and the constraint parameter occur near the free surface, as shown in Fig. 10.1. Thus, using the maximum value of the crack driving force along the crack front and the toughness value adjusted for the constraint along the crack front, leads to a conservative fracture assessment.

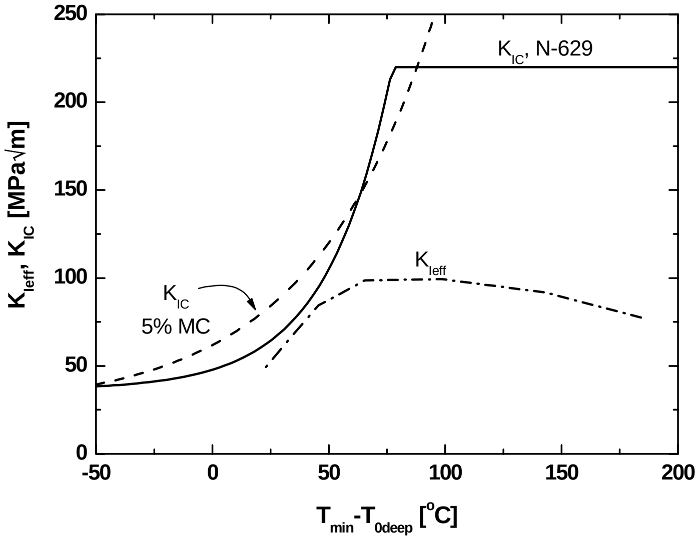

Fig. 7.21rep: Illustration of advanced Master Curve analysis of surface cracks.

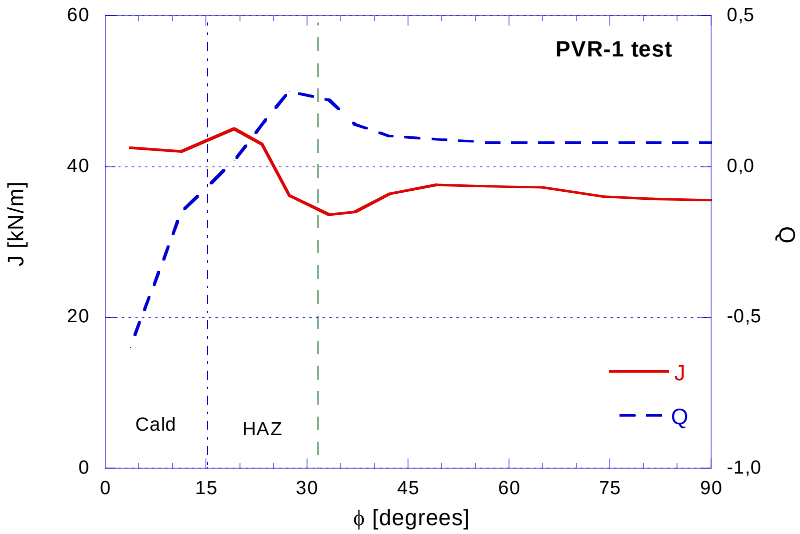

Fig. 10.1: *J* and *Q* along an elliptical surface crack under biaxial loading Sattari-Far [2004b].

11. CONCLUSIONS AND RECOMMENDATIONS

The major motivation for this work is to study the capabilities of the Master Curve methodology for fracture assessments of nuclear components. In performing this task, the theoretical background of the methodology is studied, and its validation on small and large specimens is investigated. Also studied are the correlations between the Charpy-V data and the Master Curve T_0 reference temperature in the evaluation of fracture toughness. The study mainly covers brittle fracture of ferritic steels in the transition and lower-shelf regions. The study supports the following conclusions and recommendations:

1) Cleavage fracture toughness data display normally large amount of statistical scatter in the transition region. The cleavage toughness data in this region is specimen size-dependent, and should be treated statistically rather than deterministically.

2) The Master Curve methodology gives a statistical model to describe the probability of cleavage fracture toughness in mechanical testing of ferritic steels in the transition region. This methodology is described in the ASTM E 1921-03 standard.

3) The ASTM E1921-03 standard describes the determination of the reference temperature T_0, which characterizes the fracture toughness of ferritic steels that experience onset of cleavage cracking at elastic or elastic-plastic instability. By definition, T_0 is a temperature at which the median of the K_{Jc} distribution from 1T size specimens is 100 MPa√m.

4) Determination of T_0 should be based on test results in the temperature range: 50°C ≤ T - T_0 ≤ +50°C. In order to minimise any effects from the master curve temperature dependence, fracture toughness testing should include several test temperatures.

5) If only approximate (lower bound type) information regarding the fracture toughness is required, the master curve can well be extrapolated outside the range -50°C ≤ T - T_0 ≤ +50°C. For an accurate description of the fracture toughness outside this range, tests should preferably be performed at the actual temperature. The Master Curve method can then be used to describe scatter and size effects.

6) Miniature-sized bend specimens are applicable to determine the Master Curve T_0. Material-wise, the most efficient specimen size is 5x5 mm.

7) Specimen size does not affect the T_0 estimate, but there is approximately 8ºC difference between T_0 obtained from the CT- and 3PB-specimens (CT-specimen is more conservative). This difference is due to different constraint levels in these two specimens.

8) Based on the determined Master Curve T_0, fracture toughness curves of different probabilities can be developed. The Master Curve is defined as the median (50% probability) toughness for the 1T specimen over the transition range. The lower-bound (5% probability) and upper-bound (95% probability) curves can also be defined.

9) The crack-tip constraint may be described by both the T_{stress} and the Q-parameter. Positive T_{stress} may have an insignificant effect on fracture toughness, whereas for negative values of T_{stress}, the Master Curve T_0 changes nearly linearly with T_{stress}. The determined relation between T_{stress} and T_0, given in Eq. (5-5), provides a simple tool for the application of the Master Curve technology also to low constraint geometries.

10) Conducting the statistical size correction and applying the Master Curve yield satisfactory descriptions of fracture events both for laboratory specimens and for large scale experiments (Chapters five and six).

11) It is shown that the ASME K_{IC} reference curve is in general over-conservative in describing fracture toughness properties of embrittled materials in the transition region. The Master Curve methodology provides a more precise prediction of the fracture toughness of embrittled materials.

12) Based on this investigation, a straight forward procedure is suggested for application of the Master Curve method in fracture assessments of ferritic steels in the transition and lower shelf regions (Chapter 10). The procedure is valid for the temperatures range: T_0 - 50 $^oC \leq T \leq T_0 + 50$ ^oC.

13) The suggested procedure gives two options, simplified and advanced, depending on the available information. The advanced option accounts for the crack-tip constraint effects. The procedure is illustrated for some examples given in the Appendix of this report.

14) Further study is needed to consider effects of positive constraint ($T_{stress} > 0$) on the brittle fracture toughness.

REFERENCES

ASTM E1921-03, (2003), "Standard test method for determination of reference temperature T_0 for ferritic steels in the transition range", American Society of Testing and materials, Philadelphia.

Andersson, P., Bergman, M., Brickstad, B., Dahlberg, L., Nilsson, F. and Sattari-Far, I., (1996), "A procedure for safety assessment of components with cracks-Handbook", SAQ/FoU-Report 96/08, SAQ Kontroll AB, Stockholm, Sweden.

Bass, B.R., McAfee, W.J., Williams, P.T. and Pennell, W.E., (1999), "Fracture assessment of shallow-flaw cruciform beams tested under uniaxial and biaxial loading conditions", Nuclear Eng. and Design, 188, 259-288.

Bass, R., Wintle, J. and Hurst, R., (2000), "NESC-1 Project Overview", European Commission DG-JRC/IAM, Petten, The Netherlands, 2000.

Bass, R., et al, (2002), "NESC-1V Project: An investigation of the transferability of Master Curve technology to shallow flaws in RPV applications", NESC IV Interium Report No. 4(02), European Commission DG-JRC/IAM, Petten, The Netherlands.

Betegon, C. and Hancock, J.W., (1991), "Two-parameter characterization of elastic-plastic crack tip fields", J. App. Mech. 58, 104-113.

Brickstad, B., et al., (1994), "Analys av skadetåligheten hos reaktortanken Oskarshamn 1", Projekt FENIX, Teknisk Rapport, SAQ Kontroll AB.

Brumovský M, Kryukov A, Gillemot F, Levin V., (1995), "Results from the phase III of the IAEA coordinated research programme: Optimizing of reactor pressure vessel surveillance programmes and their analysis", In. IAEA Specialists Meeting on Irradiation Embrittlement and Mitigation, Espoo, IWG-LMNPP-95/5, Vol. II.

Bryan, R. H., et al, (1985), "Pressurized-Thermal-Shock test of 6-in. thick pressure vessels. PTSE-1: Investigation of warm prestressing and upper-shelf arrest", NUREG/CR-4106, Oak Ridge National Laboratory, 263 p.

Bryan, R. H., et al, (1987), "Pressurized-thermal-shock test of 6-in.-thick pressure vessels. PTSE-2: investigation of low tearing resistance and warm prestressing", NUREG/CR-4888, Oak Ridge National Laboratory.

Chaouadi R., (1998), "Fracture toughness measurements in the transition regime using small size samples" In: Corwin WR, Rosisnski ST, van Walle E, editors. Small Specimen Test Techniques, ASTM STP 1329, pp. 214-237.

Cheverton, R. D., (1976), "Pressure Vessel Fracture Studies Pertaining to a PWR LOCA-ECC Thermal Shock: Experiments TSE-1 and TSE-2", ORNL/NUREG/TM-31, Oak Ridge National Laboratory, Oak Ridge, TN, 201 p.

Cheverton, R. D., and Bolt, S. E., (1977), "Pressure Vessel Fracture Studies Pertaining to a PWR LOCA-ECC Thermal Shock: Experiments TSE-3 and TSE-4 and Update of TSE-1 and TSE-2 Analysis", ORNL/NUREG-22, Oak Ridge National Laboratory, Oak Ridge, TN, 147 p.

Cheverton, R. D., Ball, D. G., Bolt, S. E., (1985), Iskander, S. K., and Nanstad, R. K., "Pressure Vessel Fracture Studies Pertaining to the PWR Thermal-Shock Issue:

Experiments TSE-5, TSE-5A, and TSE-6", NUREG/CR-4249 (ORNL-6163), Oak Ridge National Laboratory, Oak Ridge, TN, 250 p.

Cheverton, R. D., Ball, D. G., Bolt, S. E., Iskander, S. K., and Nanstad, R. K., (1985), ”Pressure Vessle Fracture Studies Pertaining to the PWR Thermal-Shock Issue: Experiment TSE-7”, NUREG/CR-4304 (ORNL-6177), Oak Ridge National Laboratory, Oak Ridge, TN, 133 p.

Dillström, P. et al, (2004), "A combined determination and probabilistic procedure for safety assessment of components with cracks-Handbook", RSE R&D Report No. 2004/01, Det Norske Veritas, Stockholm, Sweden.

Dodds, R.H., Shih, C.F. and Anderson, T.L., (1993a), Continuum and micromechanics treatment of constraint in fracture, Int. J. Fract. 64, 101-133.

Dodds, R.H., Tang, M. and Anderson, T.L., (1993b), Effects of prior ductile tearing on cleavage fracture toughness in the transition region, Structural research, Series No. 583, University of Illinois at Urbana-Champaign, Illinois.

Faleskog, J., (1995), Effects of local constraints along three dimensional crack fronts–A numerical and experimental investigation, J. Mech. Phys. Solids.

Gao X, and Dodds RH., (2000), "An engineering approach to assess constraint effects on cleavage fracture toughness", Engng Fract Mech.

Hancock, J.W., Reuter, W.G. and Parks, D.M., (1993), "Constraint and toughness parameterized by T", In Constraint Effects in Fracture, ASTM STP 1171, American Society for Testing and Materials, Philadelphia, 21-40.

Hutchinson, J.W., (1968), Singular behaviour at the end of a tensile crack in a hardening material, J. Mech. Phys. Solids 16, 13-31.

Issler, L., (1979), "Status of the Research Integrity of Components", 5th MPA-Seminar.

Kfouri, AP., (1986), "Some evaluations of the elastic T-term using Eshelby's method", Int J Frac., Vol. 30, pp.301-315.

Kirk, M.T. and Dodds, R.H., (1992), "Approximate techniques for predicting size effects on cleavage fracture toughness", Report No. NUREG/CR-5970, U.S. Nuclear Regulatory Commission, Washington.

Kirk, M.T., Koppenhoefer, K.C. and. Shih, C.F., (1993), Effect of Constraint on specimen dimensions needed to obtain structurally relevant toughness measures, Constraint effects in fracture, ASTM STP 1171, American Society for Testing and Materials, Philadelphia, 79-103.

Kussmaul, K., Föhl, J. and Roos, E., (1986), "Some conclusions wit regard to the safety assessment of cracked components drawn from the research program Integrity of Components (FKS II) at the present state", 12th MPA Seminar.

Lee B-S, Homg J-H, Yang W-J, Chi S-H., (1999), "Master Curve characterization of the fracture toughness in un-irradiated and irradiated RPV steels using full- and 1/3-size precracked Charpy specimens", In: Irradiation Embrittlement and Mitigation, IWG-LMNPP-99/2. IAEA, Vienna.

Link, RE., and Joyce, JA., (1995), "Experimental Investigation of Fracture Toughness Scaling Models" In: Kirk M, Bakker A, editors. Constraint Effects in Fracture Theory and Applications: Second Volume. ASTM STP 1244, pp. 286-315.

Marston, T.U., (1978). Flaw Evaluation Procedures - Background and Application of ASME Section XI Appendix A, EPRI NP-719-SR. Electric Power Research Institute, Palo Alto, California.

McCabe, D. E., (1993), "A comparison of Weibull and KIC analysis of transition range data", Fracture Mechanics: Twenty-Third Symposiym, ASTM STP 1189.

Merkle J.G., Wallin K., McCabe D.E., (1998), "Technical basis for an ASTM standard on determining the reference temperature T_0 for ferritic steels in the transition range" NUREG/CR-5504, US Nuclear Regularity Commission, Washington, USA.

O'Dowd, N.P. and Shih, C.F., (1991), "Family of crack-tip fields characterized by a triaxiality parameter-I. Structure of fields", J. Mech. Phys. Solids 39, 989-1015.

O'Dowd, N.P. and Shih, C.F., (1992), "Family of crack-tip fields characterized by a triaxiality parameter-II. Fracture applications", J. Mech. Phys. Solids 40, 939-963.

O'Dowd, N.P. and Shih, C.F., (1993), "Two-parameter fracture mechanics: Theory and applications", Report No. NUREG/CR-5958, US Nuclear Regularity Commission, Washington, USA.

Parks, D.M., (1992), "Advances in charaterization of elastic-plastic crack-tip fields", Topics in Fracture and Fatigue, Springer Verlag.

Pellissier-Tanon, A., Sollogoub, P., Houssin, B., and Robisson, F., (1983), "Crack Initiation and Arrest in a SA 508 Cl. 3 Cylinder Under Liquid Nitrogen Thermal Shock Experiment" Transactions of the 7th International Conference on Structural mechanics in Reactor Technology (SMIRT), Vols. G/F 1/8, North Holland Publishing Co. Amsterdam, The Netherlands, pp. 137-142.

Pellissier-Tanon, A., Devaux, J. C., and Houssin, B., (1986), "Application of Statistical Cleavage Criteria to Fracture Control of Pressure Vessels" 6th European Conference on Fracture (ECF 6): Fracture Control of Engineering Structures, Vol. II, H. C. Elst and A. Bakker, Eds., Engineering Materials Advisory Services LTD., Warley, U.K., pp. 903-916.

Rice, J.R., (1968), A path independent integral and the approximate analysis of strain concentration by notches and cracks, J. App. Mech., 35, 379-386.

Rice, J.R. and Rosengren, G.F., (1968), "Plane strain deformation near a crack tip in a power law hardening material", J. Mech. Phys. Solids, Vol. 16, pp.1-12.

Rintamaa, R. et al, (2001), Consistency of fracture assessment criteria for the NESC-I thermal shock test", J. Press vessel & Piping, Vol. 28, pp.125-135.

Ruggieri, C., Dodds, R.H. and Wallin, K., (1998), "Constraint effects on reference temperature T0 for ferritic steels in the transition region", Eng. Fract. Mech., 60, 19-36.

Sattari-Far, I., (1995), Constraint effects on ductile crack growth in cladded components subjected to uniaxial loading, Int. J. Fatigue Fract., 18, 1051-1069.

Sattari-Far, I., (1998), “Solutions of constraint parameters Q, Qm and H in different cracked geometries”, Report No. SINTAP/SAQ/08, SAQ Kontroll AB, Stockholm, Sweden.

Sattari-Far, I., (2000), ”Fracture mechanics analysis of NESC-II experiments”, RSE R&D Report No. 2000/04, Det Norske Veritas, Stockholm, Sweden.

Sattari-Far, I., (2004a), “Fracture assessment of a brittle RPV under cold loading”, Nuclear Engineering and Design, Vol. 228, pp. 143 – 150.

Sattari-Far, I., (2004b), “Post-test analysis of uniaxial and biaxial NESV-IV tests, NESC-IV Progress Meeting, Warrington,.

Server, L. W, Rosinski, S. T., Hoffman, C., Byrne, S., Yoon, K. and Lott, R., (1998), "Application of Master Curve fracture toughness methodology for ferritic steels", EPRI Technical Report TR-108390.

Sherry, A. H., France, C. C. and Goldthorpe, M. R., (1995) "Compendium of T_{stress} solutions for two and three dimensional cracked geometries", Fatigue Fract. Engng. Mater. Struct., (18), pp. 141-155.

Shih, C.F., O'Dowd, N.P. and Kirk, M.T., (1993), “A framework for quantifying crack tip constraint, Constraint effects in fracture, ASTM STP 1171, American Society for Testing and Materials, Philadelphia, 2-20.

Sham, T-L., (1991), “The determination of the elastic T-term using higher order weight functions”, Int J Frac, Vol. 48, pp. 81-102.

Shum, D.K. and Bass, B.R., (1993a),” Analysis of thermal shock data, Heavy-Section Steel Technology Program”, Report No. NUREG/CR-4219, 9, No. 2, Oak Ridge National Lab., USA.

Shum, D.K. and Bass, B.R., (1993b),” Absence of toughness elevation in thermal shock experiment TSE-5A: Preliminary explanation based on crack-tip constraint”, Report No. ORNL/NRC/LTR 92/94, Oak Ridge National Lab., USA.

SINTAP, (1999), “Structural Integrity Assessment Procedures for European Industry- Final Procedure”, Contract No BRPR-CT95-0024, Project No. BE95-1426.

Smith, JA. And Rolfe, ST., (1994), “The effect of crack depth (a) and crack depth to width ratio (a/W) on the fracture toughness of A533-B steel”, J PVT, Vol. 116, pp. 115-121.

Sokolov, M., Wallin, K.and McCabe D. E., (1997), “Application of Small Specimens to Fracture Mechanics Characterization of Irradiated Pressure Vessel Steels,” ASTM STP 1321, J.H. Underwood, B. D. MacDonald and M. R. Mitchell, ed., American Society for Testing and Materials.

Sokolov MA, McCabe DE, Davidov YA, Nanstad RK., (1998), “Use of precracked Charpy and smaller specimens to establish the Master Curve” In: Corwin WR, Rosisnski ST, van Walle E, editors, Small Specimen Test Techniques, ASTM STP 1329, pp. 238-252.

Sokolov, M. and Nanstad, R. K., (1999) “Comparison of irradiation-induced shifts of KJC and Charpy impact toughness for reactor pressure vessel steels”, Effects of Radiation on Materials: 18th International symposium, ASTM STP 1325, R. K. Nanstad, M. L. Hamilton, F. A. Garner and A. S. Kumar, Eds., American Society for Testing and Materials, West Conshohocken, PA, pp. 167-190.

Stumpfrock, L. et al, (2003), “Brittle crack initiation, propagation and arrest of shallow cracks in clad vessel under PTS loading”, Report EUR 20696 EN, European Commission DG-JRC/IE, Netherlands.

Sumpter, J.D., (1982), “The effect of notch depth and orientation on the fracture toughness of multi-pass weldments”, Int J Pres Ves & Piping, Vol 10(3), pp. 169-180.

Sumpter, J.D. and Forbes, AT., (1992), “Constraint-based analysis of shallow cracks in mild steel”, In: Shallow Crack Fracture Mechanics, Toughness Tests and Applications, TWI. Paper 7.

Theiss, T.J., Rolfe, S.T. and Shum, D.K., (1992), “Shallow-crack toughness results for reactor pressure vessel”, Int. Conf. on Shallow Crack Fracture Mechanics, Toughness Tests and Application, Cambridge, UK.

Theiss, T.J. et al., (1993), “Initial results of the influence of biaxial loading on fracture toughness”, Report No. NUREG/CR-6036, Oak Ridge National Lab., USA.

Towers, O.L. and Garwood, S.L., (1986), “Influence of crack depth on resistance curves for three-point bend specimens in HY 130”, ASTM STP 905, , American Society for Testing and Materials, Philadelphia, 454-484.

Valo M, Ahlstrand R, Kohopää J, Planman T, Wallin K., (1999), “Characterisation of the mechanical properties of the WWER 440 weld No. 502 with small specimens”, In. IAEA Specialists Meeting on Irradiation Embrittlement and Mitigation, Madrid. IWG-LMNPP-99/2, pp. 159-171.

Wallin, K., (1989), “A simple theoretical Charpy-V – KIC correlation for irradiation embrittlement”, ASME Pressure Vessels and Piping Conference, Innovative Approaches to Irradiation Damage and Fracture Analysis, PVP-Vol. 170, American Society of Mechanical Engineers, New York.

Wallin, K., (1991), “Fracture toughness transition curve shape for ferritic structural steels”, Proceedings of the Joint FEFG/ICF, Int. Conf. on Fract. of Eng. Materials, Singapore, August 6-8, 83-88.

Wallin, K., (1997), “Re-evaluation of the TSE results based on the statistical size effect”, J. Nucl. Eng. Design, Vol. 174, pp.205-218.

Wallin, K.., (1998), ”Master Curve analysis of ductile to brittle transition region fracture toughness round robin data- the EURO fracture toughness curve”, VTT Manufacturing Technology, Finland.

Wallin, K., (1999), "Statistical re-evaluation of the ASME KIC and KIR fracture toughness reference curves", Nuclear Engineering and Design, Vol. 193, pp. 317 - 326.

Wallin K., (2001), “Quantifying T_{stress} controlled constraint by the Master Curve transition temperature T0”, Engng Fracture Mech, 68(3), pp. 303-328.

Wallin, K., (2004), “Critical Assessment of the Standard ASTM E 399”, Fatigue and Fracture Mechanics: 34th Volume, ASTM STP 1461, S. R. Daniewciz, J. C. Newman and K.-H. Schwalbe, Eds., ASTM International, West Conshohocken, PA.

Wallin, K., Planman, T., Valo, M. and Rintamaa, R., (2004b), ”Applicability of miniature size bend specimens to determine the Master Curve reference temperature T0”, VTT Manufacturing Technology, Finland.

Wallin, K., (2004c), ”Experimental estimation of constraint”, Research Report No. BTU072-041227, VTT Manufacturing Technology, Finland.

Wallin, K., (2004d), ”Significance of RT_{To} and K_{IC}”, Research report No. BTU072-041291, VTT, Finland.

Wallin, K., Nevasmaa, P., Laukkanen, A. and Planman, T., (2004d), "Master Curve analysis of inhomogeneous ferritic steels", Eng. Frac. Mech., Vol 21, pp. 2329-2346.

Williams, M.L., (1957), “On the stress distribution at the base of a stationary crack”, J. App. Mech. 24, 111-114.

APPENDIX: EXAMPLE PROBLEMS

To demonstrate how the Master Curve procedure, presented in Chapter 10, is used in practical cases, the following examples are illustrated in this appendix:

Example A: Determination of the Master Curves from fracture toughness tests

Example B: Determination of the Master Curve T_0 from CVN impact data

Example C: Prediction of fracture in cruciform specimens containing surface cracks

Example D: Determination of the critical crack size in a reactor vessel under cold loading

Example A: Determination of the Master Curves from fracture toughness tests

Material: A533 Grade B, test temperature at 38°C, σ_Y = 480 MPa

The fracture toughness test is conducted on 1/2T SEN(B) specimens at 38°C. The raw test data and size-adjusted data to 1T are presented in Table A1. The procedure to determine T_0 and master curves is described below.

(a) *Censoring data which violate $K_{Jc(limit)}$:*

The test data should fulfill the limit requirement expressed in Eq. (4-2).

$$K_{Jc(\mathrm{limit})} = \sqrt{\frac{Eb_0\sigma_Y}{M(1-\nu^2)}} \qquad (4\text{-}2)$$

For E = 200 GPa, b_0 = 12.5 mm, σ_Y = 480 MPa, M = 30 and ν = 0.3, it yields $K_{Jc(limit)}$ to be 210 MPa√m for these 1/2T data. Thus, any test data exceeding this value should be censored. The censored data are shown in parentheses in Table A1. Accordingly, only the first six test data are used here to evaluate the master curves. The corresponding $K_{Jc(limit)}$ value for 1T data, using b_0 = 25 mm, will be 297 MPa√m. Note that K_{Jc} data that exceed the limit of Eq. (4-2) may be used in a data censoring procedure described in the ASTM E 1921-03 standard, including additional restrictions.

Table A1: Fracture toughness K_{Jc} [MPa√m] from raw data (1/2T) and size-adjusted data.

	Raw data from 1/2T	Size-adjusted to 1T
1	139	120
2	172	148
3	176	151
4	181	155
5	195	167
6	201	172
7	(239)	(204)
8	(268)	(228)

(b) *Size-correction of raw data to standard 1T data:*

For test program conducted on other than 1T specimens, the measured toughness data should be size-corrected to their 1T equivalent according to Eq. (4-3).

$$K_{Jc(1T)} = 20 + \left[K_{Jc(x)} - 20\right]\left(\frac{B_x}{B_{1T}}\right)^{1/4} \quad (4\text{-}3)$$

The size-corrected raw data are also given in Table A1.

(c) *Calculations of K_0 and K_{Jc}(med):*

Equation (4-5) and (4-6) are used to calculate K_0 and the median $K_{Jc(med)}$.

$$K_0 = \left[\sum_{i=1}^{N} \frac{(K_{Jc(i)} - 20)^4}{N}\right]^{1/4} + 20 \quad (4\text{-}5)$$

$$K_{Jc(\text{med})} = 0.9124(K_0 - 20) + 20 \quad (4\text{-}6)$$

Here, $N = 6$ is the number of valid tests. Introducing the 1T data from Table A1 to Eq. (4-5) yields K_0 to be 155 MPa√m, and Eq. (4-6) yields $K_{Jc(med)}$ to be 143 MPa√m.

(d) *Evaluation of T_0:*

The reference temperature T_0 is obtained from Eq. (4-10):

$$T_0 = T - \frac{1}{0.019}\ln\left[\frac{K_{Jc(\text{med})} - 30}{70}\right] \quad (4\text{-}10)$$

Where, T is the test temperature. Eq. (4-10) yields T_0 to be 12.8°C.

Note that the reference temperature T_0 should be relatively independent of the test temperature that has been selected. Hence, only data that are distributed over the restricted temperature range $T_0 \pm 50$°C should be used to determine T_0. For this case, T_0 = 12.8°C and T = 38°C, thus the requirement is fulfilled.

(e) *Evaluation of the Master Curve:*

The Master Curve is defined as the median (50% probability) toughness for the 1T specimen over the transition range for the material. The lower-bound (5% probability) and upper-bound (95% probability) curves can also be set up. These three curves are given by the following expressions:

$$K_{Jc(50\%)} = 30 + 70\exp[0.019(T\text{-}T_0)] \qquad (4\text{-}7)$$

$$K_{Jc(5\%)} = 25.4 + 37.8\exp[0.019(T\text{-}T_0)] \qquad (4\text{-}8)$$

$$K_{Jc(95\%)} = 34.6 + 102.2\exp[0.019(T\text{-}T_0)] \qquad (4\text{-}9)$$

Where, K_{Jc} is in MPa√m and T and T_0 in ^{o}C.

For T_0 = 12.8 ^{o}C, and validation window of T_0 ± 50 ^{o}C, the different toughness curves are shown in Fig. A1. Here, the upper limits of the curves are determined by introducing M = 30 and σ_Y = 480 MPa at T = 38^{o}C and σ_Y = 520 MPa at T = -50^{o}C to Eq. (4-2).

The fracture toughness curves presented in Fig. A1 can now be used to evaluate the fracture toughness of the material at any given temperature inside the validation window, i.e. T_0-50 ≤ T ≤ T_0-50. Normally, the 50% toughness curve is used in fracture assessment of cracked components.

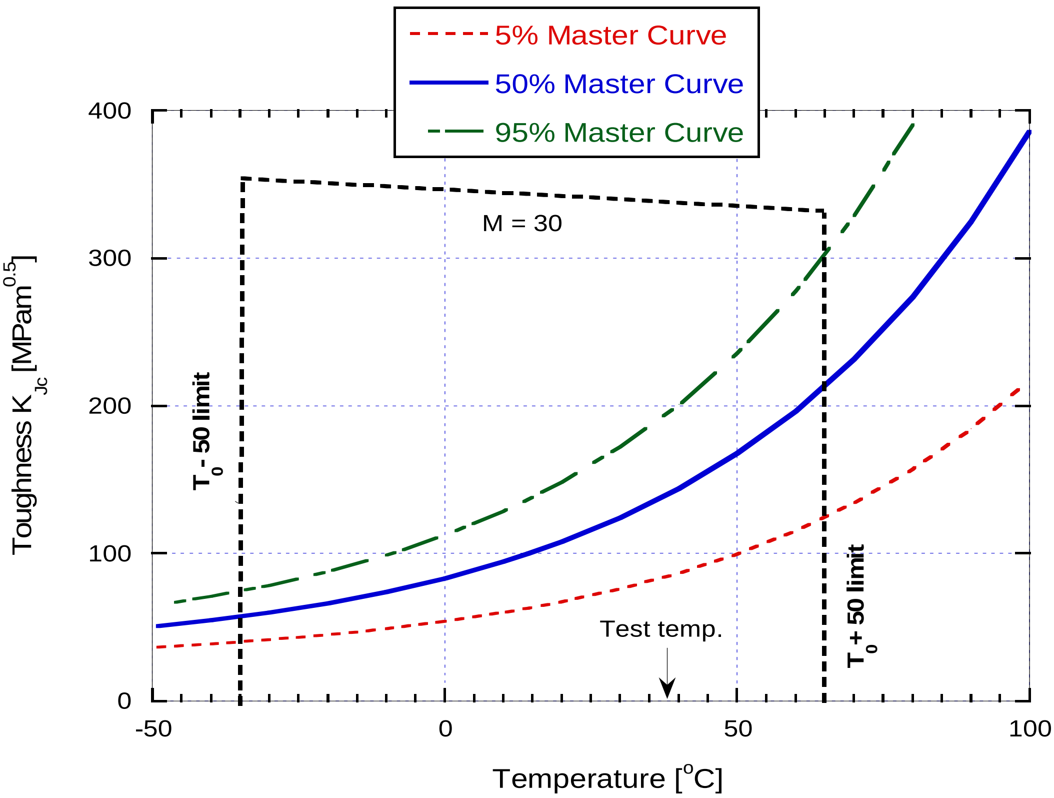

Fig. A1: Master curves and the validation window of the tested A533 GB material.

Example B: Determination of the Master Curve T_0 from CVN impact data

Material: A533B Cl.1 plate (HSST-03)

This is a special steel used as an irradiation monitor material. One set of CVN data available for this material consists of 14 test data. Fig. B1 shows the tanh analysis of these impact data to determine the transition temperatures T_{28J} and T_{41J}. Since the mean curve shifted by 15°C limits all the brittle fracture data, the material is judged to be homogeneous and the mean fit values are representative of the material. This analysis yields T_{28J} and T_{41J} to be -14°C and 1°C, respectively.

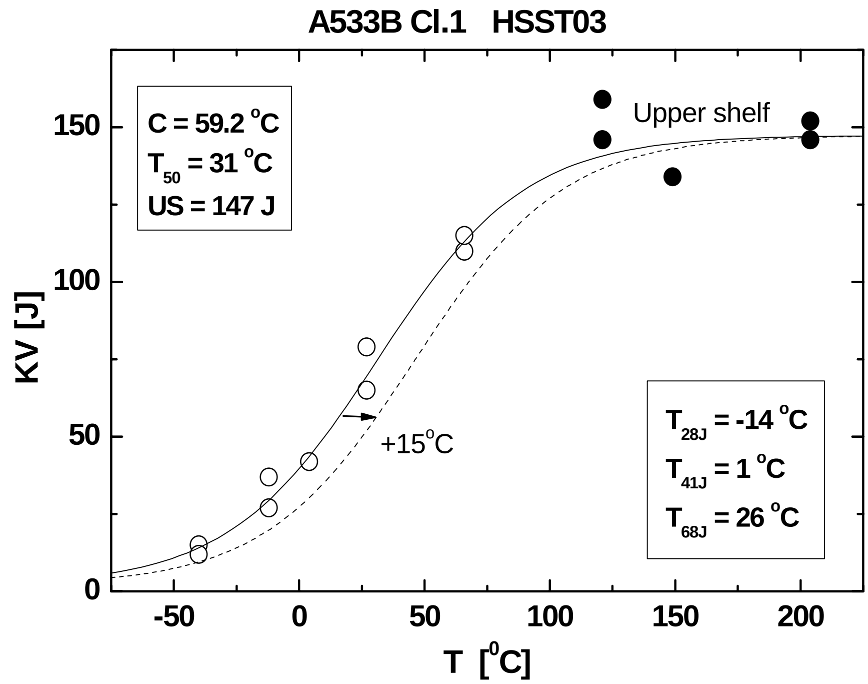

Fig. B1: Tanh analysis of the CVN data of HSST-03 plate.

The T_0 temperature can be estimated with sufficient confidence using either the T_{28J} or the T_{41J} transition temperature. The relevant expressions are given in Eqs. (8-13) or (8-14).

$$T_0 = T_{28J} + 3 \ [^{\circ}\mathrm{C}] \qquad (8\text{-}13)$$

$$T_0 = T_{41J} - 1 \ [^{\circ}\mathrm{C}] \qquad (8\text{-}14)$$

For the HSST-03 plate the values are thus T_0 (T_{28J}) = -11°C and T_0 (T_{41J}) = 0°C. Since the HSST-03 plate has a relatively low upper shelf value, the 41J based estimate is more conservative than the 28J based estimate. Because the whole transition curve is available the less conservative estimate may be chosen as representative for the material.

Table B1 gives actual fracture toughness data for the same material determined with small pre-cracked specimens. When the data is analysed according to the ASTM E1921 standard, a T_0 value of -40°C is obtained, as shown in Fig. B2. The T_0 value corresponds to SE(B) specimen geometry. The higher constraint C(T) specimen would have a T_0 value close to -32°C. This value is 21°C lower than the estimate based on the CVN impact data. This is due to the conservative nature of the correlation used.

Table B1: Fracture toughness data for plate HSST 03.

	B mm	**b mm**	**K_{JC}**	**K_{JC25}**	**δ**
-91	10	4.83	64	55	1
-90	10	4.97	58	50	1
-90	10	4.93	62	53	1
-90	10	4.98	48	42	1
-9	10	4.97	166	136	1
-90	10	4.92	60	52	1
-9	10	5	189	154	1
-30	10	5.11	183	150	1
-28	10	5.16	146	120	1
-50	10	5.07	108	90	1
-48	10	5.03	104	87	1
-31	10	4.73	133	110	1
9	10	4.53	311	251	1
-51	10	4.76	104	87	1
23	10	4.75	348	281	1
-10	10	4.77	173	142	1
-51	10	4.75	92	77	1
-31	10	4.77	118	98	1
9	10	4.73	296	240	1
-10	10	4.72	181	148	1
-51	10	4.75	105	88	1
-10	10	4.72	144	118	1
-31	10	4.76	140	116	1
-51	10	4.77	113	94	1
9	10	4.73	215	175	1
-31	10	4.76	147	121	1
24	10	4.73	379	306	0
-10	10	4.77	178	146	1
23	10	5	383	308	0
21	10	5.05	368	297	0

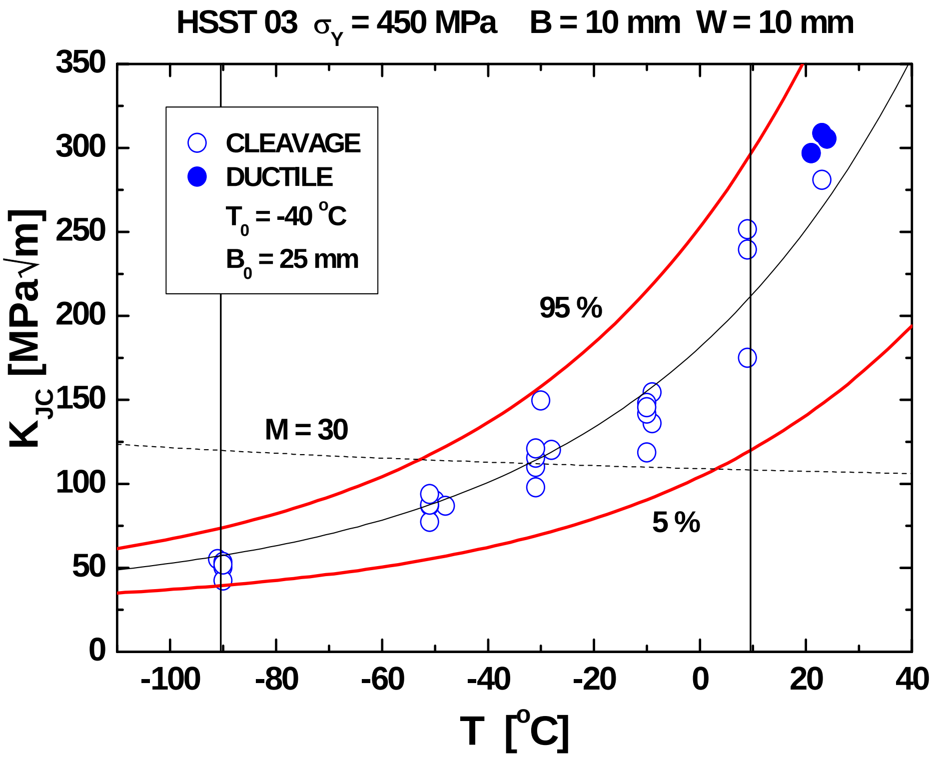

Fig. B2: MC analysis of the fracture toughness data of the HSST-03 plate.

Generally, it can be stated that T_0 can be estimated conservatively from CVN impact data. However, if the result is not acceptable from a structural integrity assessment point of view, the uncertainty can be reduced by performing fracture toughness testing with small specimens.

By knowing the value of the reference temperature T_0, one can determine the MC toughness curves as described in Example A.

Example C: Prediction of fracture in cruciform specimens containing surface cracks

This example illustrates fracture prediction of the PVR-5 test performed within the NESC-IV project [Bass et al, 2002]. The test objective is to obtain a brittle fracture event in a cruciform clad specimen containing surface crack subjected to biaxial loading. A brief description of the NESC-IV tests is given in section 6.9 of this report.

The test specimen is fabricated from A533 GB. The test section contains weld material below the clad layer, in which the surface flaw was inserted. The key parameters needed for the analysis are given below.

Specimen sizes: Shown in Fig. C1

Crack sizes: Depth = 19.1 mm, length = 53.3 mm

Yield stresses: 500 MPa for the base material, 625 MPa for the weld material and 300 MPa for the cladding material (all at room temperature)

Master curve T_0: -88.3^{o}C for the weld material and -96.7^{o}C for the base material obtained from standard 1T specimens

Test temperature: -33.4^{o}C

Loading: Biaxial with 1:1 ratio.

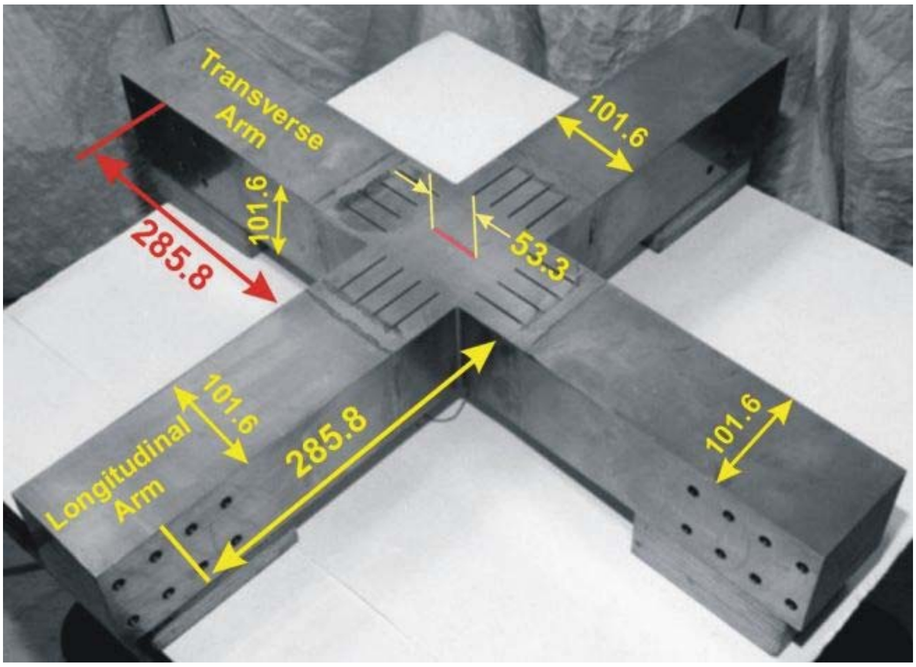

Fig. C1: Cruciform specimen tested under biaxial loading.

The load-CMOD response under loading is available and shown in Fig. C2. The outcomes of this test are analyzed using detailed finite element calculations. Details of this analysis are given by Sattari-Far [2004b].

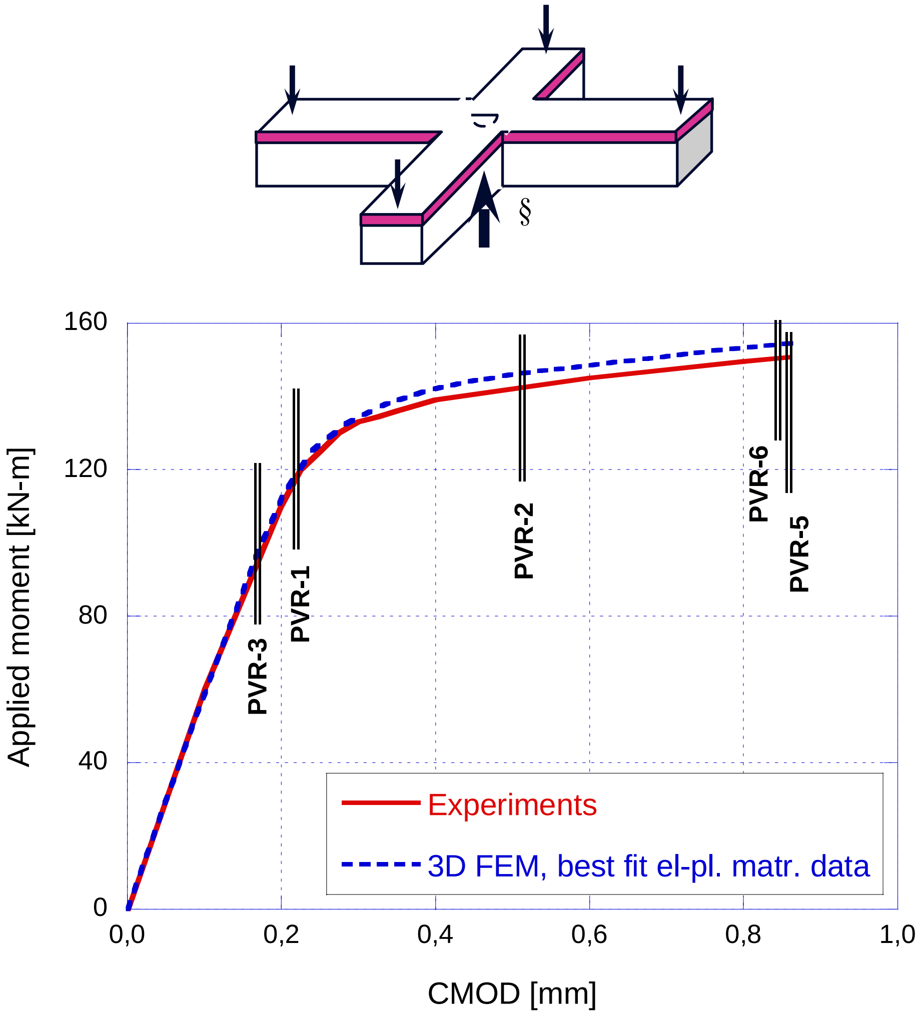

Fig. C2: Load-CMOD responses in the clad cruciform tests under biaxial loading.

Master Curve analysis of the test results

(a) Determine size-adjusted Master Curves

The crack is in the weld material, and T_0 of this material is given to be -88.3°C, obtained from standard 1T specimens. The crack front is semi-elliptical, and its front length in the weld material (below the clad layer) is 63 mm. Using Eqs. (4-3) through (4-7), it yields the size-adjusted T_0 to be -74°C for this crack front length. The corresponding Master

Curves are presented in Fig. C4.

(b) *Determine the maximum crack driving force*

Elastic-plastic three-dimensional finite element analysis is used to calculate the crack driving forces along the whole crack front. Fig. C3 gives the distribution of crack driving force *J* along the crack front at a time under the loading. It is observed that the maximum value of *J* occurs in the cladding HAZ, and not at the deepest point of the crack. Based on the finite element calculations, the maximum *J* value at the fracture event is 252 kN/m in the cladding HAZ. Using Eq. (4-1), it gives K_J to be 241 MPa√m at the fracture event.

(c) *Evaluate the constraint parameter*

Elastic-plastic three-dimensional finite element analysis with very fine mesh is needed to resolve the crack-tip field and determine the constraint parameter *Q*. Fig. C3 gives the distribution of *Q* along the crack front at a time under the loading. It is observed that the maximum value of this parameter occurs in the cladding HAZ, and not at the deepest point of the crack front. The *Q* values do not vary significantly under loading, and has a maximum of +0.25 in the cladding HAZ.

(d) *Master Curve prediction*

The test is conducted at a constant temperature, thus there is no temperature difference along the crack front. The constraint conditin in the cruciform specimen (Q = +0.25) is severer than in the standard 1T specimens ($Q \approx 0$). As there is no fracture toughness data obtained from specimens with high constraint ($Q > 0$), Master Curves based on toughness data from standard 1T specimens are used here. The predicted result of this test is shown in Fig. C4.

The post-test fractography of the fracture surfaces confirms that the failure mode in the cruciform specimens is pure cleavage fracture, without prior ductile tearing. It also reveals that the cleavage initiation sites occur towards the surface of the specimen (in the cladding HAZ), and not at the deepest point of the defect. This is in good agreement with the prediction based on the 3D finite element analysis together with the Master Curve methodology. Presumably, considering the constraint effects by obtaining toughness data for positive constraint ($Q > 0$) could improve the prediction results. Fig. 7.18 illustrates such an analysis.

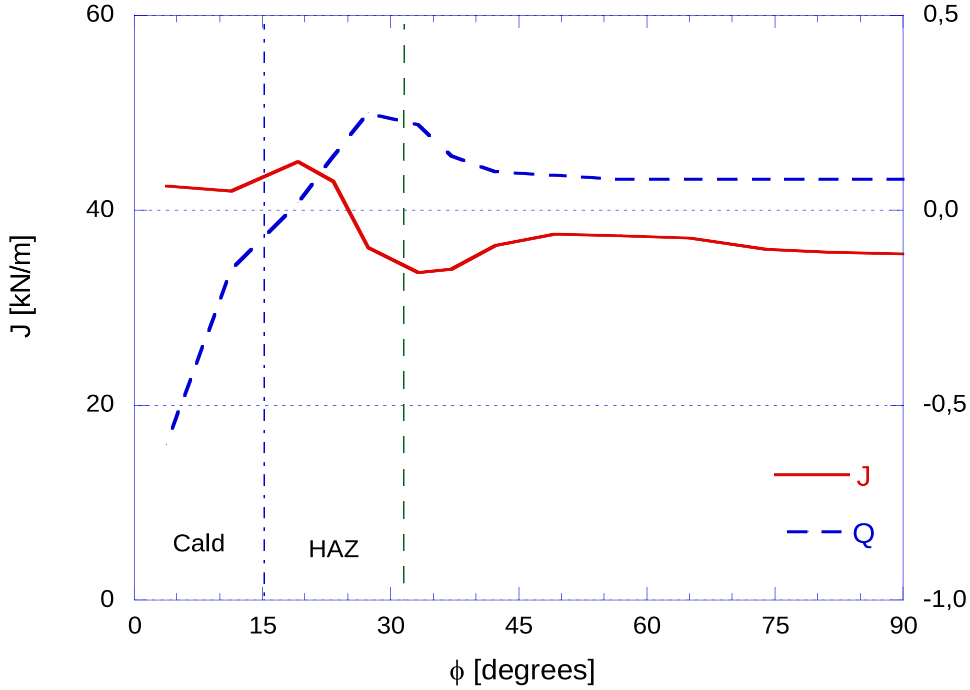

Fig. C3: Distributions of *J* and *Q* along the crack front in test specimen at a time during the loading.

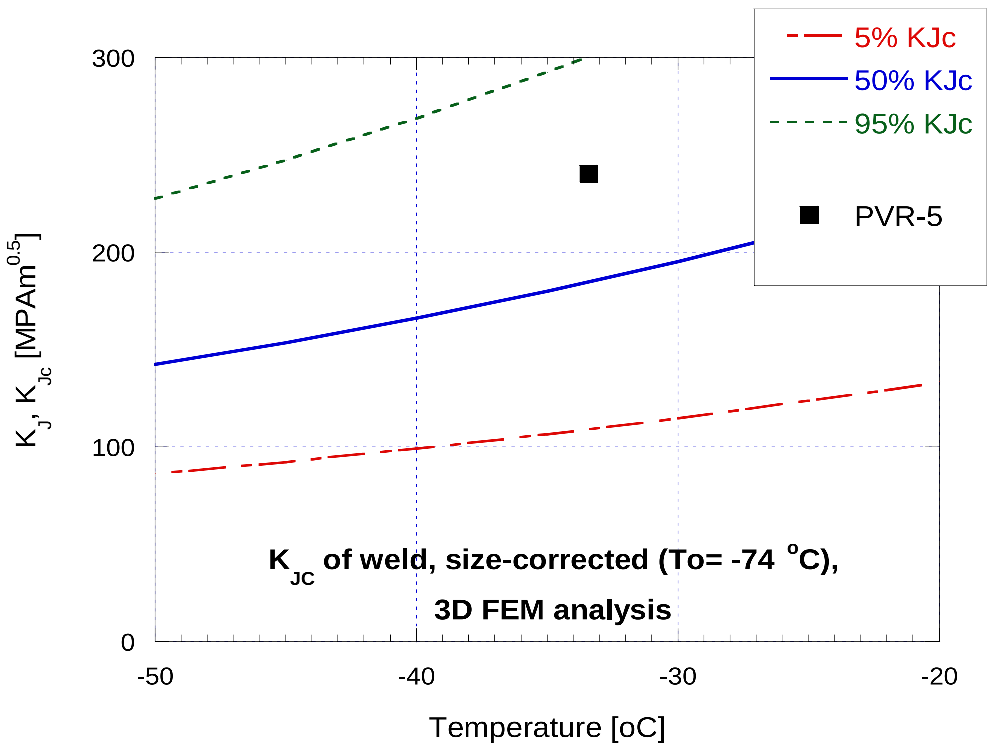

Fig. C4: Master Curve prediction of the cruciform test subjected to biaxial loading.

Example D: Determination of the critical crack size in a reactor vessel under cold loading

This example illustrates fracture assessment of the reactor pressure vessel of Oskarshamn 1 (O1) under a cold over-pressurization event. A preliminary study during the FENIX project [Brickstad et al, 1994] has shown that the cold over-pressurization may be a limiting load case for the O1 reactor. Under a cold over-pressurization scenario, the loading of the reactor occurs at a temperature below RT_{NDT} of the reactor material, which due to neutron irradiation has exceeded the shut-down temperature of the reactor. The ability of the reactor to withstand this kind of loading should also be demonstrated.

In this example the acceptable and critical crack sizes in the beltline region of the O1 reactor under a cold over-pressurization event are determined based on the Master Curve methodology. This assessment is based on a study by Sattari-Far [2004a], in which a specially heat-treated base material was used to simulate material properties of the O1 reactor.

The assessment is based on the following input data:

Reactor inner radius: 2500 mm
Reactor thickness: 131 mm (including a 6 mm cladding layer)
Loading: Internal pressure of 85 bar at40^{o}C
Cladding residual stress of 235 MPa in the cladding layer
Welding residual stress of 50 MPa after PWHT
ASME XI RT_{NDT}: 72^{o}C
Master curve T_0: 30^{o}C, based on tests on standard 1T specimens, Sattari-Far [2004a]
Defect configuration: Surface crack with $2c/a$= 6 in a weld in the beltline region

It should be noted that the value of RT_{NDT} is 72^{o}C here, based on impact tests of the simulated material, compared with the value of 117^{o}C assumed in the FENIX study. The welding residual stresses are applied in the finite element calculations by adding an internal pressure of 26 bars to the actual internal pressure. This pressure gives a circumferential stress of 50 MPa, which is assumed to be present in the welds after post-weld-heat-treatment. Fig. D1 shows the stress distribution in the wall of the reactor during this loading scenario.

Assessment based on the Master Curve methodology

The 50% master curve methodology together with an engineering assessment approach

(SACC) is used here to estimate the acceptable and critical crack sizes in the beltline of the O1 reactor.

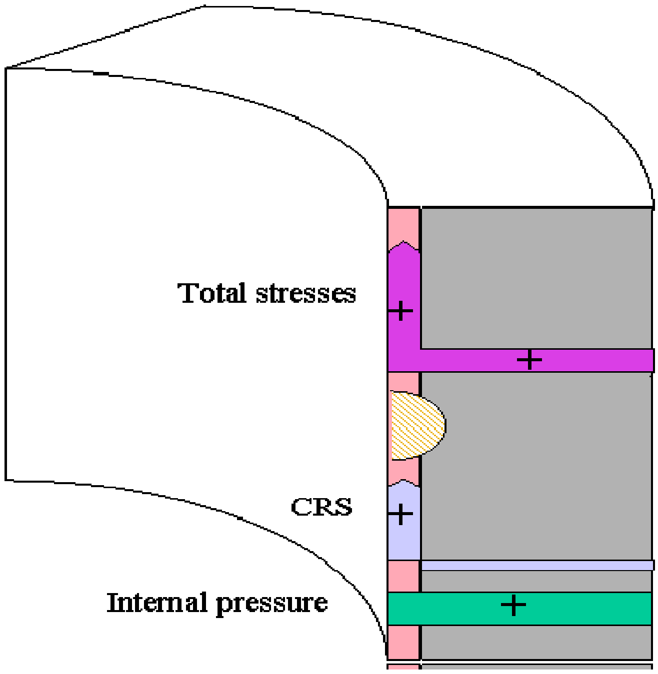

Fig. D1: Stress distribution in the beltline region of the O1 reactor (CRS stands for cladding residual stresses).

(a) Determine the fracture toughness

T_0 of the material (weld) is given to be 30°C, obtained from standard 1T specimens. This should be size-adjusted to the actual crack front size. The crack is semi-elliptical with $2c/a = 6$ located in the axial direction at the inside of the reactor. We begin by assuming a crack front length of 50 mm. Using Eqs. (4-3) through (4-7), it yields the size-adjusted T_0 to be 40°C for this crack front length. Introducing $T_0 = 40$°C and $T = 40$°C to Eq. (4-7), it yields the Master Curve K_{Jc} (50% curve) to be 100 MPa√m.

The corresponding fracture toughness estimation based on the ASME K_{IC} reference curve is 40 MPa√m for RT_{NDT} of 72°C.

(b) Determine the crack driving force

The SACC program, Andersson et al [1996], with its procedure based on the R6-method is used for this assessment. To check the precision of the SACC program in calculation of K_I for the actual case, two detailed 3-D elastic-plastic finite element analyses are performed on crack depths of 12 mm and 20 mm. Fig. D2 compares the crack driving forces obtained from SACC and the detailed finite element calculations. It is observed that the SACC program is conservative in calculation of K_I. The differences between SACC and 3D-FEM are less than 10 % for the studied cases.

For a semi-elliptical surface crack located in the axial direction in the beltline region, the highest K_I value along the crack front in the base material is at the deepest point. Fig. D2 shows the variation of the crack diving force K_I at the deepest point as a function of crack depth for this crack configuration. It is assumed that the crack is in a weld subjected to stresses due to internal pressure, welding residual stresses and the cladding residual stresses.

(c) Evaluate the constraint parameter

Elastic-plastic three-dimensional finite element analysis with very fine mesh is needed to resolve the crack-tip field and determine the constraint parameter Q. According to the 3D finite element calculations along the crack front, presented by Sattari-Far [2004a], the constraint is dominantly positive ($Q > 0$) along the whole crack front in the base material. As there is no fracture toughness data representative for high constraint ($Q > 0$), it is assumed here that $Q \approx T_{stress} \approx 0$, which is similar to constraint conditions in the standard 1T specimens.

(d) Determine the acceptable and critical crack depths

The over-pressurization loading is assumed to be a faulted case, and thus, a safety margin of $\sqrt{2}$ on the fracture toughness is used to determine the acceptable defect depths. The critical defect depths are determined with a safety margin equal to one. The loading occurs at a constant temperature, thus there is no temperature variation along the crack front. No crack-tip constraint effects are considered ($Q \approx 0$). This implies that the fracture toughness can be assumed to be constant along the crack front in the base material.

Assuming that the temperature and constraint are constant along the crack front in the base material, it yields that the maximum effective stress intensity factor K_{Ieff} expressed in Eq. (7-14) may be simplified to be equal to the maximum K_I value at the deepest point. Thus, the critical situation for this crack configuration may occur at the deepest point.

As the size-adjusted MC fracture toughness is dependent on the crack-front-size (crack-depth), the assessment should be conducted in an iterative manner until the evaluated crack depth becomes close to the assumed value (crack depth length) at the start of the assessment procedure.

STEP 1:

We assume a crack-front-length (cfl) of 50 mm for the actual crack. Thus, the size-adjusted MC fracture toughness at the actual temperature (40°C) is 100 MPa√m. This value is used to determine the critical crack size. The toughness value is reduced by a factor of √2 in order to determine the acceptable defect depth. The crack driving forces K_I for different crack depths are shown in Fig. D2, compared with different toughness assumptions. It is observed that K_I is increasing with crack depth in the cladding layer due to the tensile cladding residual stresses. When the crack depth comes into the base material, where the cladding residual stresses are compressive, K_I begins to decrease. For deep cracks, K_I increases with crack depth due to stresses from the internal pressure. Based on Fig. D2, the provisional values of the acceptable and critical crack depths can be determined.

From Fig. D2, it is observed that the ASME K_{Ic} curve gives acceptable and critical defect depths to be less than 7 mm (cladding thickness). The intersections of the K_I-curve with the $K_{Jc}/\sqrt{2}$-line and the K_{Jc}-line give the acceptable respective the critical crack depth based on the MC toughness. This leads to a value of 28 mm for the acceptable and over 40 mm for the critical defect size, also given in Table D1. As a crack of 28-mm depth with $2c/a$= 6 has a crack front length greater than 100 mm in the base material, the used K_{Jc}-value (based on 50 mm crack front length) should be size-adjusted for this value of crack front length, and a new assessment should be conducted.

Table D1: Acceptable and critical crack depths in the O1 reactor under cold pressurization (based on crack-front-length of 50 mm).

Fracture toughness	Acceptable [mm]	Critical [mm]
ASME K_{IC} curve	≤ 6	≤ 6
50% MC with cfl = 50 mm	28	> 40

STEP 2:

We set a crack-front-length (cfl) of 100 mm for the actual crack. Thus, the size-adjusted MC fracture toughness at the actual temperature (40°C) becomes 84 MPa√m. The new assessment results are shown in Fig. D3. This indicates a value of 20 mm for the acceptable and around 40 mm for the critical defect size, as given in Table D2.

Table D2: Acceptable and critical crack depths in the O1 reactor under cold pressurization (based on crack-front-length of 100 mm).

Fracture toughness	Acceptable [mm]	Critical [mm]
ASME K_{IC} curve	≤ 6	≤ 6
50% MC with cfl = 100 mm	20	40

The crack of 20-mm depth with $2c/a$= 6 has a crack front length of about 100 mm in the base material, which is in agreement with the assumption at the start of STEP 2. Thus, the results presented in Table D2 are the final assessment values based on this procedure. Accordingly, from a brittle fracture point of view and based on the 50% master curve methodology with a size-correction related to the crack-front length, a surface crack with depth of 20 mm and $2c/a$= 6 will be acceptable in the O1 beltline region under the cold over-pressurization scenario.

Note that for cases with a temperature variation and/or loss of constraint along the crack front, the maximum effective stress intensity factor K_{Ieff} expressed in Eq. (7-14) should be used to determine the critical defect size.

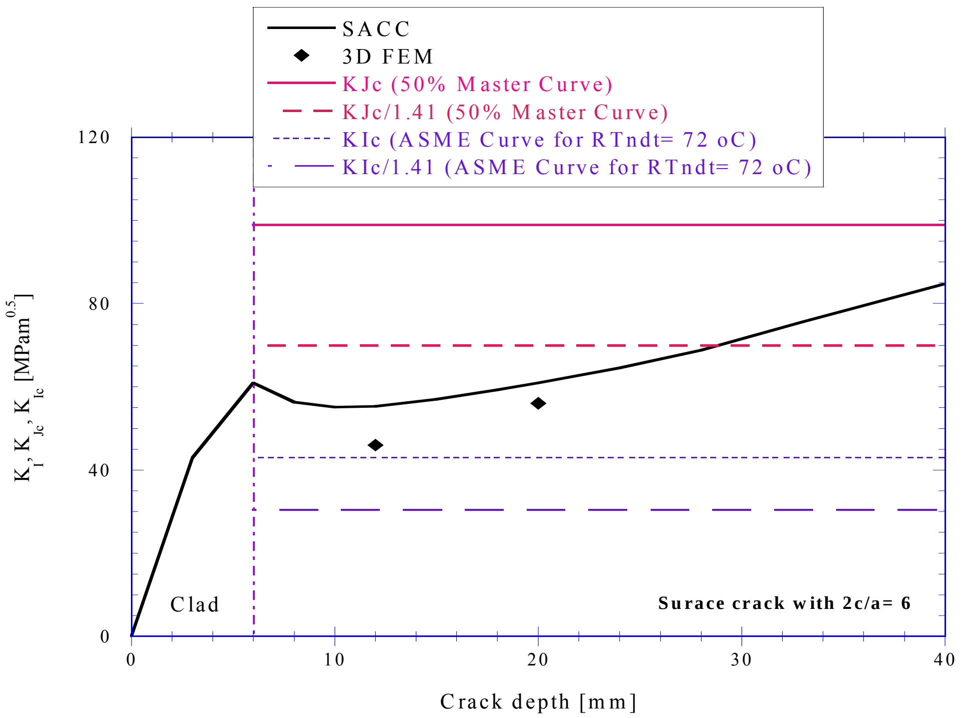

Fig. D2: K_I at the deepest point as a function of crack depth in the O1 reactor under the cold-pressurization. The MC K_{Jc} are size-adjusted for a 50 mm crack front length.

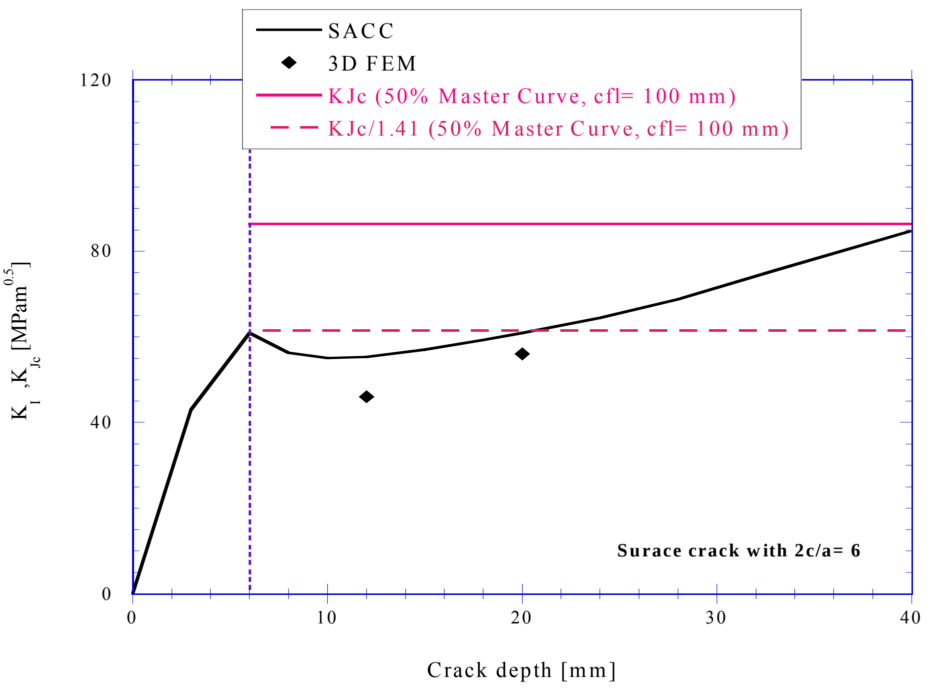

Fig. D3: K_I at the deepest point as a function of crack depth in the simulated O1 reactor under the cold-pressurization. The MC K_{Jc} are size-adjusted for a 100 mm crack front length.

www.ski.se

STATENS KÄRNKRAFTINSPEKTION
Swedish Nuclear Power Inspectorate

POST/POSTAL ADDRESS SE-106 58 Stockholm
BESÖK/OFFICE Klarabergsviadukten 90
TELEFON/TELEPHONE +46 (0)8 698 84 00
TELEFAX +46 (0)8 661 90 86
E-POST/E-MAIL ski@ski.se
WEBBPLATS/WEB SITE www.ski.se